Neuromuscular responses and cost of transport across increasing physiological strain during fatigued running in young adults

Thesis submitted to the University of Ottawa in partial fulfillment of the requirements for the Master of Applied Science in Biomedical Engineering

Zachary Flahaut

Supervisors: Dr. Allison L. Clouthier and Dr. Daniel L. Benoit

University of Ottawa

Ottawa-Carleton Institute for Biomedical Engineering

Faculty of Engineering

General Abstract

Physiological fatigue alters how the neuromuscular system controls movement, with potential implications for performance, injury risk, and the validity of simulation-based energetics assessment. This thesis integrates experimental physiology, EMG, motion capture, and musculoskeletal modelling to examine how oxygen uptake, neuromuscular activity, and energetic cost interact during steady-state running when fatigued. Across two complementary studies, recreationally trained adults completed a 30-minute treadmill run at ~85% VO2 max on a 1% grade while whole-body kinematics, ground-reaction forces, and bilateral surface EMG from key lower-limb muscles were sampled at pre-, mid-, and post-fatigue time points, whilst physiological load was monitored continuously. VO2/kg remained stable (~45 $mL \cdot kg^{-1} \cdot min^{-1}$), whereas heart rate rose by 17.5% and perceived exertion increased significantly across fatigue stages (both $p < 0.01$), confirming progressive internal load despite sagittal-plane joint kinematics remaining stable, with maximum deviations below 3° across the gait cycle. Given that these differences fall within the typical measurement error of marker-based motion capture (~2–5°), this suggests no meaningful alteration in running kinematics. In contrasts, EMG indices (iEMG, RMS) declined in gastrocnemii, rectus femoris, vastus lateralis, and gluteus medius with concomitant median-frequency shifts. Together, these findings indicate fatigue-related alterations in neuromuscular recruitment despite preserved movement patterns.

In the second study, cost of transport (CoT) estimated using three OpenSim metabolic models (*Bhargava2004*, *Umberger2003*, *Umberger2010*) was compared against indirect calorimetry. A two-way repeated-measures ANOVA revealed a strong main effect of estimation method ($F(3,18) = 116.80$, $p < 0.001$), but neither a significant effect of fatigue stage ($F(2,12) = 2.46$, $p = 0.127$) nor a method × stage interaction. *Bhargava 2004* and *Umberger2003* both underestimated CoT relative

to calorimetry (mean biases −6.62 and −6.82 $J \cdot kg^{-1} \cdot m^{-1}$), whereas *Umberger2010* produced a slight overestimation (+2.75 $J \cdot kg^{-1} \cdot m^{-1}$). Correlations with calorimetry were weak and non-significant for all models (r ranging from −0.05 to 0.27), and only indirect calorimetry showed a clear increase in CoT across the fatigue protocol (slope = 0.4349), whereas model-derived CoT remained nearly unchanged.

Collectively, these findings demonstrate a clear decoupling between appearance (stable kinematics) and effort (rising physiological load and metabolic cost) during prolonged high intensity running. When driven by static optimization, commonly used OpenSim metabolic models reproduced the direction of change in metabolic cost across fatigue stages but substantially misestimate absolute energetics and fail to reflect fatigue-driven metabolic drift. The results highlight the need for EMG-informed, personalized musculoskeletal models that incorporate explicit fatigue states.

Acknowledgements

First and foremost, I would like to thank my supervisors, Dr. Allison Clouthier and Dr. Daniel Benoit. Over the past two years, you have shared your knowledge and skills with extraordinary trust, and care. You challenged me to be rigorous, gave me the freedom to explore my ideas, and, above all, taught me to stay curious. No single paragraph can capture my gratitude, but I hope these words convey how deeply I appreciate your guidance.

To Dr. Allison Clouthier: thank you for welcoming me when I needed it most and for supporting my year in Sweden. You didn't have to take me on, let alone encourage such a big leap, but you did, and it changed the course of my training. Your steady mentorship helped me turn broad, sometimes unruly ideas, into focused testable questions. You guided me through the ambitious timelines I set for myself, offering clear, constructive feedback while always making space for my voice. I am profoundly grateful for your balance of kindness and rigor, and for the confidence you placed in me.

To Dr. Daniel Benoit: thank you for taking a chance on me, a football (soccer) player with little to no knowledge on hockey. Your belief opened doors I didn't see at the end of my undergraduate degree. You invited me to Sweden, and that invitation proved genuinely life-changing: it broadened my scientific horizons, introduced me to a new research culture and community, and gave me the independence and confidence to grow as a researcher/scientist. You pushed me to be precise, to ask better questions, and to respect what the data is truly saying. You advocated for opportunities, collaborations, and presentations that helped me grow far beyond what I imagined. I am deeply thankful for the trust you showed and for the high standards you modelled every day.

To both of you, thank you for shaping not only my research, but also the kind of scientist and person I aspire to be. I will carry your lessons on integrity, curiosity, and care for others into the next steps of my career.

To my committee members, Dr. Martin Bilodeau, and Dr. Thomas Uchida thank you for your time, careful review, and constructive guidance as without your guidance and insight this project would not have been possible.

I would also like to acknowledge Dr. Natalie Baddour, who, while not my supervisor or a member of my committee, provided guidance that was immensely impactful, most notably by facilitating my connection with Dr. Benoit, an inflection point that set the last two years of my graduate work in motion.

I would also like to thank all funding agencies, the University of Ottawa, the University of Ottawa Engineering International office, Lund University, CUPE 2626, the Hans K. Uhthoff, MD FRCSC Graduate Fellowship bursary, the Susan Tanner Scholarship, the Huguette-Labelle Scholarship, Canadian Society for Mechanical Engineering/The Ottawa Life Sciences Council Bursary and the International Society of Biomechanics that have helped make my master research possible.

I would also like to thank all my labs mates (Blake, Branimir, Elese, Taylor, Viktor), coworkers (Nicholas (Ryan), Karine, Teresa, Sigrid, Pär) and friends (Célia, Gigi, Griffin, Jake, Jesus, Keely, Kevin, Matteo, Olivia, Rachel, Samy, Sophie, Yuma, Zacharias) along the way whether at uOttawa, Lund or Paris (cataphile et surfacien) for the constant support, guidance and laughs, life may be a huge bowl of pasta with not much flavour but its up to you to find that flavour and you have all truly helped me find that flavour.

Additionally, I wish to express my heartfelt appreciation to my two grandparents. Though they are no longer with us, their wisdom, love, and values continue to inspire me every day. Their

presence in my life has been instrumental in shaping the person I have become, and I often find myself guided by their teachings and memories. I deeply regret that they could not be here to witness this milestone, but I know they are with me in spirit, sharing in this achievement.

To my entire extended family, thank you for being my pillars of strength and for instilling in me the importance of perseverance, resilience, and the pursuit of knowledge. Your collective influence has been immense, and I am forever grateful for the role each of you have played in my life.

I would also like to extend my deepest gratitude to my parents and my brother for their unwavering support throughout this journey. Your steady encouragement through early mornings, late-night calls, and moves across cities and countries has been my guiding light. You believed in me when the path was uncertain, celebrated the small wins, and helped me regain perspective when timelines were ambitious and experiment stubborn. Thank you for the practical help and the intangibles patience, humour, and unconditional love.

From lugging boxes and proofreading drafts to sending meals, tracking flights, and finding apartments at the eleventh hour, you showed up in every way that mattered. You reminded me to rest when I would have pushed through, and to keep going when doubt crept in. The values you instilled, curiosity, grit, kindness shaped how I worked and who I tried to be in the process. I am profoundly grateful for the countless sacrifices you made so I could pursue my dreams; this work is as much yours as it is mine.

And to everyone else who may read this « *Fais de ta vie un rêve et d'un rêve une réalité »* - *Antoine de Saint-Exupéry*

Co-Authorship

This dissertation includes two un-published manuscripts. The authorship is as follows:

Chapter 4: **Flahaut, Z. A**., Ryan, N. S., Halje P, Clouthier, A. L. Benoit, D. L. *Silent Drift: Detecting Fatigue Beyond Kinematics in Constant-Speed Treadmill Running*

Chapter 5: **Flahaut, Z. A**., Ryan, N. S., Halje P, Clouthier, A. L. Benoit, D. L. *Same Pace, Different Price: OpenSim Metabolic Models vs Indirect Calorimetry for Cost of Transport in High-Intensity Running*

For each manuscript, Zachary A. Flahaut completed the tasks of conceptualization and design of the research, acquisition of the data, analysis and interpretation of the data, and writing the manuscripts.

Table of Contents

List of Figures

List of Appendix Figures

List of Tables

List of Appendix Tables

List of Equations

Abbreviations and Definitions

ACL	Anterior Cruciate Ligament
BF	Biceps Femoris
BMI	Body Mass Index
CEINMS	Calibrated EMG-Informed Neuromusculoskeletal Model
CNS	Central Nervous System
CMC	Computed Muscle Control
CoT	Cost of Transport
DOF	Degrees of Freedom
EMG	Electromyography
GRF	Ground Reaction Force
HR	Heart Rate
Hz	Hertz
iEMG	Integrated Electromyography
ID	Inverse Dynamics
JCS	Joint Coordinate System
IK	Inverse Kinematics
K5	COSMED K5 Portable Metabolic System
LG	Lateral Gastrocnemius
MG	Medial Gastrocnemius
MoRe-Lab	Movement and Reality Lab
MT	Musculotendon
MVIC	Maximal Voluntary Isometric Contraction
PF	Patellofemoral
PSIS	Posterior Superior Iliac Spine
RA	Rectus Abdominis
RFT	Random Field Theory
RF	Rectus Femoris
RMS	Root Mean Square
RPE	Rating of Perceived Exertion
RQ	Respiratory Quotient
sEMG	Surface Electromyography
SD	Standard Deviation
SM	Semitendinosus
SPM	Statistical Parametric Mapping
SO	Static Optimization
ST	Semimembranosus
TA	Tibialis Anterior
TF	Tibiofemoral Joint
TRC	Marker Trajectory File for OpenSim
Tegner Scale	Scale rating physical activity from 0 (low) to 10 (high)
VL	Vastus Lateralis

VM	Vastus Medialis
VO2	Volume of Oxygen
VO2 max	Maximal Oxygen Uptake
ZEBRIS	Zebris Capacitance-Based Pressure Treadmill System

*Note that **pre-fatigue** and **pre-exercise**, **mid-fatiguing** and **mid-exercise,** and **post-fatigue** and **post-exercise** have been used interchangeably throughout this dissertation, both referring to standardized time points within the running protocol corresponding to the beginning (0 min), midpoint (15 min), and end (30 min) of the exercise bout.*

Chapter 1: Introduction

1.1 Rationale

Numerous studies have explored maximal oxygen uptake (VO2 max), defined as the highest rate at which oxygen can be taken up, transported, and utilized by the body during maximal exercise (Bassett and Howley, 2000), focusing either on estimating or directly measuring it to examine its impact on physical performance. Research has often addressed its influence on general training outcomes or specific domains such as cognitive performance and physiological adaptation (Bacon et al., 2013; Foster, 1983; Hwang et al., 2017; Olivo et al., 2021; Plini et al., 2024; Scribbans et al., 2016). Separately, extensive work has been done to understand how fatiguing exercise alters neuromuscular activity and joint loading (Quesada et al., 2000), with implications for performance, energy expenditure, and injury risk.

During aerobic activity, metabolic rate and energy cost are tightly coupled with oxygen consumption (Coen et al., 2013; Cramer and Jay, 2016; Jacobs et al., 2012). As oxygen availability declines with fatigue, muscle recruitment strategies and firing patterns shift to compensate, impacting force production, movement coordination, and mechanical efficiency (Amann and Calbet, 2008; Enoka and Duchateau, 2008; Millet and Lepers, 2004). These physiological changes underscore the importance of oxygen uptake as not just a fitness metric, but a central variable in understanding real-time muscular performance.

Despite this, there remains a critical gap: the direct interaction between oxygen uptake, fatigue-induced neuromuscular changes, and their combined effect on joint mechanics has not been fully elucidated. This disconnect is particularly evident in the domain of musculoskeletal modelling (Flaxman et al., 2024). Current biomechanical models often assume consistent neuromuscular input and fail to incorporate real-time physiological adaptations occurring under fatigue. This

simplification can lead to inaccurate estimations of joint loading, muscle forces, and energy expenditure (Hicks et al., 2015; Koelewijn et al., 2019; Seth et al., 2018) which is particularly relevant when interpreting results in athletic or clinical populations where such estimates are often used to support performance or rehabilitation interventions.

To develop musculoskeletal models that reflect real-world conditions, it is essential to account for how fatigue modulates muscle activity and, in turn, alters mechanical loading patterns. Although return-to-activity decisions combine patient-reported outcomes with performance metrics (Flahaut et al., 2024, 2026), these measures rarely capture fatigue or dynamic stability (Romanchuk et al., 2023). Integrating fatigue-sensitive variables like electromyographic data into modelling frameworks has potential for more accurate simulations of movement under varying physiological states (Lloyd and Besier, 2003; Sartori et al., 2013, 2012a).

This study aims to address that need by examining the relationship between oxygen uptake and neuromuscular activity during fatiguing exercise and evaluating their combined effect on knee joint loading and metabolic cost. Using an integrated approach involving electromyography (EMG), VO2 max testing, motion capture, and metabolic analysis, this project seeks to quantify how physiological fatigue translates into biomechanical change. The findings will contribute to the evaluation of commonly used musculoskeletal models, ultimately contributing to improved training design, injury prevention, and rehabilitation strategies grounded in the physiological realities of fatigue.

1.2 Objectives

1. Determine the effect of fatigue during an 85% VO2 max high-intensity test on muscle activation using electromyography in healthy recreational athletes.
    a. Hypothesis: As participants fatigue, keeping their kinematic form at the same speed will require increased neuromuscular effort as aerobic pathways approach their functional

limits, resulting in greater neural drive and the recruitment of additional motor units. We therefore expect within-participant increases in maximum voluntary isometric contraction (MVIC)-normalized EMG root mean square (RMS) as they fatigue, and small shifts in the EMG spectrum toward lower median frequency, consistent with greater recruitment and peripheral fatigue (Enoka and Duchateau, 2008; Farina et al., 2004).

   b. Hypothesis: Within participants, EMG amplitude will increase in association with rising oxygen uptake (VO2) across fatigue stages during high-intensity running at a fixed speed. This relationship is expected to reflect increased neuromuscular effort, manifested as greater neural drive, as metabolic demand progressively increases despite a constant external workload.

2. Implement a statically optimized musculoskeletal model in OpenSim to estimate metabolic cost of running at various fatiguing stages in comparison to experimental data obtained from a portable metabolic system. Study 2 aimed to evaluate the ability of musculoskeletal energy models to estimate cost of transport during prolonged high-intensity running. Study 2 was designed as a validation-oriented investigation to assess whether static optimization–based musculoskeletal models can capture fatigue-related changes in metabolic cost under conditions where neuromuscular adaptations occur without substantial changes in kinematics.

   a. Hypothesis: The statically optimized musculoskeletal model will underestimate the metabolic cost and will not account for fatigue. As such, the error between metabolic costs will increase with increasing fatigue.

1.3 Other Thesis Contributions

This thesis made significant contributions to the data collection protocol development of the Movement and Reality Lab (MoRe-Lab) at Lund University, particularly in refining their research

methodologies and improving the overall workflow of their studies. The specific contributions of this work are as follows:

- A detailed and structured testing protocol was implemented to help guide future studies in the lab. This overarching protocol standardized the procedures for data collection, ensuring that all measurements were obtained in a consistent and reproducible manner across trials. The updated workflow improved clarity in how measurements were taken and processed, supporting more structured and interpretable data collection for the lab's ongoing research.
- Validation of the lab's equipment, ensuring that all devices and sensors worked together seamlessly. This involved verifying the compatibility of different systems used in the studies, such as motion capture, capacitance-based pressure platform, electromyography, and metabolic cart, to ensure that they produced synchronized and accurate data. By confirming that the equipment could function cohesively, the thesis contributed to improving the reliability and efficiency of the lab's experimental setup (Flahaut et al., 2025).
- Instead of relying on the more invasive and physically demanding VO2 max test, a submaximal high-intensity threshold protocol was validated. This alternative method allows for the assessment of an individual's aerobic capacity without requiring them to reach their maximum exertion. The submaximal test is less taxing on participants, making it more suitable for a wider range of subjects, while still providing reliable and meaningful data. This validation represents a significant improvement in terms of participant safety, comfort, and data collection efficiency.
- Further development of coding pipelines to enhance data processing, including filtering marker trajectories and EMG signals for both isometric and dynamic tasks.

Additionally, improvements will be made to optimize the structuring and integration of data from the Zebris FDM capacitance-based pressure platform and the metabolic cart, ensuring more efficient and accurate analysis.

1.4 Thesis outline

This thesis manuscript is organized into six chapters, each providing a detailed exploration of various aspects of the research conducted, from foundational background information to the final conclusions and future directions.

Chapter 2 is a literature review of the physiology and mechanics of the knee level as well as current instrumentation used.

Chapter 3 contains the general methodology used to achieve the objectives of this thesis.

Chapter 4 is a journal manuscript that addresses objective 1.

Chapter 5 is a journal manuscript that addresses objective 2.

Chapter 6 is a general discussion on the entire thesis and presents suggestions for future work based on the conclusions drawn from this thesis.

Computational resources, documenting the hosted repository with configuration files and scripts, software/version information (OpenSim 3.3; MATLAB R2023b), and a checksum manifest to support reproducibility.

Chapter 2: Literature Review

2.1 Anatomy of the Knee

The knee is one of the largest and most complex synovial joints in the human body. It consists of two primary articulations: the tibiofemoral (TF) joint, which connects the tibia and femur, and the patellofemoral (PF) joint, where the patella (kneecap) articulates with the femur (Gupton et al., 2024). The four bones that make up the knee joint are the femur, tibia, fibula, and patella. Together, they form a hinge-like structure capable of supporting the demands of dynamic loads placed on the lower limb.

Functionally, the knee joint permits six degrees of freedom, with its primary movement being flexion and extension (Vaienti et al., 2017). This degree of motion allows for efficient locomotion and is essential in a wide range of physical activities, from walking to high-impact sports. The knee's complex design not only supports movement but also provides stability and load distribution across the joint during weight-bearing activities (Flaxman et al., 2012).

The knee joint is highly vascularized and interconnected with various ligaments, tendons, and muscles, all of which contribute to its stability and function (Astur et al., 2011). On the thigh, two major muscle groups are involved in knee mechanics. The quadriceps, located on the anterior side, is the larger of the two groups and is composed of the vastus lateralis (VL), vastus medialis (VM), rectus femoris (RF), and vastus intermedius (VI). The hamstrings, located on the posterior side of the thigh, consist of the semitendinosus (ST), semimembranosus (SM) and the biceps femoris (BF). These muscle groups work in tandem to control knee extension and flexion, providing both movement and joint stability during physical activities (Solomonow et al., 1987).

From a metabolic perspective, the quadriceps are among the largest muscle groups involved in knee movement (Krishnan et al., 2011), and exhibit high metabolic activity. At maximal aerobic

capacity, the quadriceps have been found to consume approximately 353 mL/kg/min of oxygen (Blomstrand et al., 1997). This highlights the significant metabolic demand placed on the knee joint, particularly during activities that require prolonged or intense physical effort. The large oxygen consumption underscores the importance of muscle strength and endurance in maintaining knee joint health and function (Hepple, 2002), especially in athletic and rehabilitative contexts.

When it comes to structural stability, the knee is primarily governed by four major ligaments: the anterior cruciate ligament (ACL), medial collateral ligament (MCL), lateral collateral ligament (LCL), and posterior cruciate ligament (PCL). These ligaments are critical for maintaining knee stability by preventing excessive motion in different planes. For example, the ACL restricts anterior translation of the tibia, while the PCL resists posterior displacement (Kreder and Hawker, 2010). The MCL and LCL stabilize the knee against valgus and varus forces, respectively (Svantesson et al., 2019). Together, these ligaments ensure that the knee remains stable, even during complex movements. However, the most common way to rupture the ACL, as evident in literature, is valgus knee collapse occurring 50 ms after initial contact with the ground during a change of direction in football (Krosshaug et al., 2007; Quatman and Hewett, 2009).

2.2 Muscle Fibers

Muscle fibers are commonly categorized according to their contractile and metabolic characteristics, which influence performance capacity, fatigue resistance, and energetic efficiency during exercise. Traditionally, skeletal muscle fibers have been described as belonging to two primary groups Type I (slow-twitch) and Type II (fast-twitch), each associated with distinct structural and physiological properties. However, contemporary evidence suggests that muscle fibers exist along a functional continuum, with hybrid phenotypes reflecting adaptations to neural activation patterns, training status, and task demands (Schiaffino and Reggiani, 2011). Human skeletal muscle also contains hybrid fibers co-expressing multiple myosin heavy chain isoforms,

reflecting the dynamic and adaptable nature of fiber-type expression in response to training and functional demands (Schiaffino and Reggiani, 2011).

Type I fibers are highly oxidative and rely predominantly on aerobic metabolism to sustain prolonged, low-intensity activity (Harms and Hickson, 1983; "Muscle Fiber Types," 2012). These fibers are characterized by elevated mitochondrial density, increased myoglobin content, and extensive capillary networks, which facilitate efficient oxygen delivery and utilization. As a result, Type I fibers contribute to endurance performance and are commonly associated with higher maximal oxygen uptake (VO2 max) and delayed onset of fatigue during sustained exercise (Bergh et al., 1978; Coggan et al., 1990). Athletes demonstrating a greater proportion of Type I fibers have been shown to maintain prolonged activity at relatively lower metabolic cost, thereby improving locomotor efficiency and reducing energetic demand during endurance-type tasks (Bacon et al., 2013; Joyner and Coyle, 2008; Pedersen et al., 2002).

Fast-twitch fibers are generally associated with higher contractile velocity and greater force-generating capacity but reduced metabolic efficiency. These fibers can be subdivided into Type IIa (fast oxidative-glycolytic) and Type IIx (fast glycolytic), with Type IIa fibers exhibiting intermediate fatigue resistance and metabolic flexibility ("Muscle Fiber Types," 2012; Schiaffino and Reggiani, 2011). In contrast, Type IIx fibers rely more heavily on anaerobic metabolic pathways and fatigue more rapidly, making them well-suited for short-duration, high-intensity tasks (Bogdanis, 2012; Park et al., 1987). Increased recruitment of fast-twitch fibers during sustained high-intensity exercise has been proposed as a key contributor to the development of the VO2 slow component, whereby oxygen uptake progressively increases despite constant external workload (Barstow et al., 1996; Mero et al., 1991; Poole and Jones, 2017).

While muscle fiber composition contributes to fatigue resistance and performance characteristics, locomotor efficiency cannot be attributed solely to metabolic fiber properties.

According to the size principle of motor unit recruitment, muscle activation progresses from lower-threshold Type I motor units to higher-threshold Type II units as force demands increase (Enoka and Duchateau, 2008). Under fatiguing conditions, alterations in motor unit recruitment strategies, discharge rates, and synchronization patterns may occur, influencing both force production capacity and electromyographic signal characteristics.

In dynamic locomotor tasks such as running, muscle function is further influenced by interactions between muscle fibers and the mechanical behavior of the muscle–tendon unit. Elastic energy storage and return within tendinous structures can reduce active muscle work requirements, thereby modulating metabolic cost independently of fiber-type distribution (Fletcher et al., 2009; Fletcher and MacIntosh, 2017). Consequently, changes in neuromuscular control associated with fatigue may influence movement efficiency and joint loading patterns, rather than fiber composition alone determining performance outcomes.

The relationship between muscle fatigue and joint stability is particularly relevant in tasks involving repetitive loading of the knee joint. While higher aerobic capacity may delay fatigue onset during prolonged exercise, the maintenance of joint stability relies on the coordinated generation of muscular force, rapid neuromuscular responses, and effective motor control strategies. Fast-twitch fibers contribute to rapid force adjustments required for dynamic stabilization, whereas slow-twitch fibers support sustained load sharing during prolonged activity (Besier et al., 2003; Hortobágyi et al., 2011). As fatigue develops, alterations in activation patterns and force-generating capacity may compromise these stabilizing mechanisms, potentially influencing movement mechanics and energetic efficiency.

Overall, muscle fiber characteristics should be interpreted within a broader neuromechanical framework in which metabolic capacity, neural control, and biomechanical demands interact to

determine fatigue responses and locomotor performance (Enoka and Duchateau, 2008; Schiaffino and Reggiani, 2011).

2.3 VO2 max

VO2 max, or maximal oxygen uptake, is a fundamental metric used to assess an individual's aerobic capacity and overall physical fitness. It is defined as the maximum rate at which an individual's body can consume oxygen, reflecting the efficiency of the cardiovascular and respiratory systems in delivering oxygen to the muscles during intense physical activity (Davies and Atkinson, 2013). VO2 max is typically expressed in millilitres of oxygen consumed per kilogram of body weight per minute (mL/kg/min), making it a standardized measure to compare aerobic fitness across different individuals.

The calculation of VO2 max is grounded in the Fick principle (Fick, 1870; Hall and Hall, 2020; Levine, 2008; Wasserman, 2012), which provides a comprehensive formula for understanding oxygen consumption at the cellular level. The Fick equation is expressed as follows:

$$\dot{V}O_2 \max = \dot{Q}(CaO_2 - CvO_2) \quad (1)$$

where $\dot{Q}$ represents the cardiac output, which is the amount of blood the heart pumps per minute. CaO_2 refers to the arterial oxygen content, and CvO_2 represents the venous oxygen content at maximal effort. The difference between CaO_2 and CvO_2, known as the arteriovenous oxygen difference, indicates how much oxygen is extracted by the tissues from the blood. Thus, VO2 max reflects both the cardiovascular system's capacity to deliver oxygen and the muscular system's ability to utilize it during exercise.

VO2 max is typically measured in a controlled laboratory environment using equipment such as treadmills, stationary bikes, or rowing machines (LeMond and Hom, 2015). During these tests, the intensity of exercise is gradually increased until the subject reaches volitional exhaustion, while

respiratory gases are collected and analyzed to determine oxygen consumption. The criterion typically used to determine volitional exhaustion includes a respiratory exchange ratio ≥ 1.10, a heart rate in excess of 90% of age predicted heart rate maximum (220-age), and identification of a plateau (<150 mL/min increase) in V̇O2 max despite a further increase in velocity (Hamlin et al., 2012). This test is considered a gold standard for evaluating aerobic endurance and is widely used in both clinical settings and athletic training.

While VO2 max is a robust indicator of aerobic capacity, it is not without limitations. One significant drawback is its reliance on the subject's motivation, which can affect the test's outcomes. Since the test requires the individual to exert maximum effort until exhaustion, the results may not always represent the true peak functional capacity, particularly if the subject is not fully motivated or familiar with the test protocols. Consequently, VO2 max measurements may sometimes underreport an individual's actual aerobic capacity, leading to potential misinterpretations (Bassett and Howley, 2000; Poole and Jones, 2017).

It is also important to consider the population being studied when looking into VO2 max as depending on their athletic ability, the VO2 max results may differ. In less conditioned athletes VO2 max is limited by oxygen demand as there is less muscle mass and fewer mitochondria, but this can improve over time with training. In contrast, the VO2 max in well-conditioned, high-performing athletes depends more on oxygen delivery through cardiac output and less so on the muscle mass or number of mitochondria available (Bassett and Howley, 2000; LeMond and Hom, 2015).

Another means to measure VO2 max is by completing a sub-maximal VO2 test that can be used to extrapolate the max exertion. This type of testing is typical for individuals who may have physical, mental, or time limitations to complete a VO2 max test. Hence, a submaximal VO2 test provides a practical alternative for estimating VO2 max without requiring the individual to reach

volitional exhaustion. Submaximal VO2 tests involve performing exercise at lower, steady-state intensities while monitoring heart rate response, typically on equipment such as cycle ergometers or treadmills. By extrapolating heart rate data collected during submaximal workloads, these tests can predict maximal oxygen uptake, offering a reliable and non-invasive method for assessing aerobic fitness (Ekblom-Bak et al., 2014; Fitchett, 1985).

The submaximal approach is grounded in the principle that as exercise intensity increases, heart rate and oxygen consumption maintain a near-linear relationship until reaching submaximal levels. This relationship allows the VO2 max to be estimated with reasonable accuracy by applying regression equations or other extrapolation techniques (Åstrand and Ryhming, 1954; Bassett and Howley, 2000). Specific protocols, such as the YMCA submaximal cycle test, use predefined workloads and age-predicted maximal heart rate to produce a VO2 max estimate that is widely used in both fitness assessments and clinical contexts (Jamnick et al., 2016).

Submaximal tests are not only beneficial for avoiding the intense physical demand of maximal testing but also offer greater accessibility in clinical settings or for populations with varying fitness levels. Although submaximal tests may have a higher error margin compared to direct VO2 max measurements, they remain a valid option for estimating aerobic capacity in healthy and athletic populations (Lakomy and Lakomy, 1993).

2.4 Neuromuscular Activity and Muscle Fatigue

Neuromuscular activity during endurance exercise reflects the integrated function of the central nervous system, peripheral musculature, and metabolic processes required to sustain force production and coordinated movement. During prolonged or high-intensity locomotion such as running, the capacity to maintain muscle activation patterns becomes progressively challenged as fatigue develops. Muscle fatigue is commonly defined as an exercise-induced reduction in the ability of a muscle to generate force or power, resulting from both neural and muscular limitations

(Enoka and Duchateau, 2008). This phenomenon is multifactorial, encompassing alterations in motor unit recruitment, metabolic disturbances within muscle tissue, and changes in central motor command (Gandevia, 2001).

Neuromuscular fatigue, a subset of muscle fatigue, refers specifically to impairments in the neuromuscular system that affect both maximal force production and the regulation of submaximal force output required for coordinated movement (Wan et al., 2017). In endurance running, neuromuscular fatigue develops progressively as physiological strain accumulates, potentially influencing muscle activation strategies, movement stability, and injury risk.

2.4.1 Peripheral Fatigue

Peripheral fatigue arises from processes occurring distal to the neuromuscular junction and primarily reflects alterations within the muscle fibers themselves. Mechanisms contributing to peripheral fatigue include metabolite accumulation (e.g., inorganic phosphate and hydrogen ions), impaired excitation–contraction coupling, reduced calcium handling, and diminished energy substrate availability (Allen et al., 2008). These physiological changes collectively reduce the muscle's ability to sustain force production during prolonged exercise.

In running studies, peripheral fatigue has frequently been assessed through changes in surface electromyography (EMG) characteristics. Typical indicators include reductions in signal amplitude, shifts in median or mean frequency of the EMG power spectrum, and altered temporal activation patterns (Farina et al., 2004; Merletti and Parker, 2004). Additionally, decreases in maximal voluntary contraction force or electrically evoked twitch responses following exhaustive running protocols have been used to quantify peripheral contractile impairments (Place et al., 2004). Such measures provide insight into the local muscular limitations that emerge during sustained locomotor activity

2.4.2 Central Fatigue

Central fatigue refers to reductions in the neural drive originating from the central nervous system, leading to decreased motor unit recruitment and firing rates during voluntary contractions (Gandevia, 2001). This form of fatigue involves supraspinal and spinal mechanisms that influence the capacity to maintain intended motor output despite adequate peripheral muscle function.

Experimental assessment of central fatigue has typically involved techniques such as transcranial magnetic stimulation or peripheral nerve stimulation superimposed on maximal voluntary contractions, allowing estimation of voluntary activation deficits (Taylor et al., 2016). In running contexts, direct measurement of central fatigue is less common due to methodological constraints; therefore, indirect indicators such as increased perceived exertion, altered coordination, or the inability to sustain motor performance despite stable external workload are often used to infer central contributions to fatigue (Marcora et al., 2009). These central mechanisms play a critical role in endurance performance, as they influence pacing strategies, movement control, and the regulation of physiological effort.

2.4.3 Measurement of Fatigue in Running

Fatigue during running represents the interaction of central and peripheral mechanisms, making it difficult to isolate specific contributors using a single methodological approach. Consequently, running-based fatigue studies commonly employ integrated assessments combining neuromuscular, physiological, and biomechanical measurements. Surface EMG provides insight into muscle activation patterns and potential peripheral contractile changes, while cardiopulmonary metrics such as heart rate, oxygen uptake, and respiratory exchange ratio reflect systemic metabolic strain (Joyner and Coyle, 2008). Biomechanical analyses, including kinematic and kinetic measurements, offer additional information regarding the functional consequences of fatigue on movement patterns and joint stability (Girard et al., 2012).

Fatigue-induced alterations in neuromuscular control have been associated with reductions in movement accuracy and increased injury risk across various athletic tasks (Antonopoulos et al., 2014; Knicker et al., 2011). For example, fatigue-related decreases in antagonist muscle co-activation during high-demand manoeuvres such as side-cutting have been linked to elevated susceptibility to lower-limb injuries (Zebis et al., 2011). Similarly, exhaustive running has been shown to impair neuromuscular signal propagation and coordination, potentially compromising movement stability during prolonged activity (Girard et al., 2012).

Training status also appears to influence fatigue responses, with more experienced athletes demonstrating greater resilience to neuromuscular deficits due to long-term adaptations in motor unit recruitment and metabolic efficiency (Simoneau et al., 2006). As a result, studying populations with moderate conditioning levels may provide meaningful insights into fatigue-related changes relevant to both athletic and general populations.

2.5 Electromyography (EMG)

Traditional methods for assessing the function and condition of peripheral nerves and muscles often rely on electromyography (EMG) to capture electrical activity during muscle contraction (Silverman et al., 2021). These approaches play a central role in both clinical and research settings, enabling the evaluation of muscle function, the detection of neuromuscular disorders, and the study of motor control.

Surface electromyography (sEMG) is one of the most widely used techniques to evaluate muscle activation. Much of the literature focuses on the amplitude of the sEMG signal, which reflects the electrical potential generated by underlying muscle activity. However, sEMG amplitude is highly sensitive to external and physiological factors such as muscle length, fatigue, electrode placement, and skin impedance that introduce variability into the signal (Farina et al., 2014). This variability complicates interpretation and lowers the precision of amplitude-based measures.

Moreover, although sEMG amplitude provides useful information, it offers only an indirect estimate of neural drive and cannot distinguish between changes in motor unit recruitment, firing rates, or neural fatigue (De Luca et al., 1996; Farina et al., 2004).

Human kinematics occur at relatively low frequencies (approximately 7–20 Hz), whereas the muscle activation signals captured via EMG occupy a much broader higher-frequency bandwidth (approximately 20–450 Hz) (De Luca, 1997; Merletti and Parker, 2004; Winter, 2009). Because joint-level movement unfolds slowly relative to the rapid fluctuations in motor unit activity, kinematic data do not directly reflect the neural processes seen in EMG. This bandwidth mismatch poses challenges when attempting to interpret neuromuscular behaviour or fatigue states from movement alone, particularly during dynamic activities.

Surface EMG is generally used to assess superficial, larger, and easily accessible muscles. One of its advantages is the ability to capture signals from a broad area, representing the combined activity of several motor units. This makes sEMG particularly suitable for studying global activation patterns in large muscles involved in walking, running, or lifting. However, the technique is prone to cross-talk contamination from nearby muscles (Roy et al., 1986). Since the electrode covers a relatively large surface area, it may inadvertently capture signals from adjacent muscles, leading to less precise measurements. That said, modern sensors are increasingly designed to minimize cross-talk, utilizing features like differential amplifiers and improved common-mode rejection ratios to enhance measurement accuracy. Additionally, during dynamic movements, the skin and underlying muscle shift, further distorting the signal, which can compromise the accuracy of the data, especially during exercise (De Luca et al., 2010).

Differences in EMG signal quality and specificity also depend on the recording modality. Early comparative work, such as that reported by Jacobson et al. (1995), demonstrated that surface and intramuscular EMG provide different levels of spatial selectivity, with intramuscular electrodes

offering clearer isolation of individual muscle regions. This distinction is particularly relevant when high-precision or deep-muscle measurements are required.

Intramuscular EMG, on the other hand, involves the insertion of fine wire electrodes directly into the muscle. This invasive technique is primarily used to measure the activity of deep muscles or those with a small cross-sectional area that cannot be assessed with surface electrodes (Andersson et al., 1997; Sutherland, 2001). The major advantage of intramuscular EMG is its ability to selectively detect EMG signals from specific muscles, even during dynamic conditions, while minimizing cross-talk (De Luca and Merletti, 1988; Perry et al., 1981). Intramuscular EMG is also more suitable for studying static and dynamic contractions in isolated muscle regions, making it particularly valuable in research settings that require high-precision measurements (Onishi et al., 2000). However, its invasive nature limits its practical use in clinical or large-scale studies.

In summary, while surface EMG offers a non-invasive and efficient means to study superficial muscle activity, it is prone to cross-talk and signal variability, especially during movement. In contrast, intramuscular EMG, though invasive, provides more accurate, selective measurements of deep muscles, offering greater reliability in dynamic conditions. The choice between these techniques often depends on the specific objectives of the study and the muscles of interest. Both methods provide important insights into nerve conduction, muscle activation patterns, and the amplitude of neural signals, with applications spanning rehabilitation, motor control research, and the diagnosis of neuromuscular disorders.

In high-intensity running performed at a fixed speed, within-participant increases in oxygen uptake (VO2) across stages of a fatigue protocol can reflect rising metabolic demand despite a stable external workload. As this demand increases, EMG amplitude is often expected to increase within individuals, consistent with increased neuromuscular effort (i.e., greater central drive)

required to maintain the task. Accordingly, examining within-subject associations between VO2 and MVIC-normalized EMG amplitude provides a complementary perspective on fatigue-related changes in neuromuscular activation under increasing physiological strain (Enoka and Duchateau, 2008; Farina et al., 2014).

In the context of running, where the primary muscles of interest are superficial and the emphasis is on repeated, whole-body movement patterns under fatigue, surface EMG represents an appropriate and pragmatic methodological choice.

2.6 OpenSim

OpenSim is an open-source musculoskeletal modelling software widely used in biomechanics to simulate and analyze human movement (Delp et al., 2007; Seth et al., 2018). The software provides a robust platform for understanding the interactions between muscles, bones, and joints while playing a critical role in studying the mechanics of human movement in various fields including rehabilitation, sports science, and clinical biomechanics.

In OpenSim, two primary methods for simulating musculoskeletal models are inverse kinematics and forward simulation.

2.6.1 Inverse Kinematics

In OpenSim, inverse kinematics is a critical method that relies on three-dimensional marker data, typically from TRC files gathered through motion capture systems. These data points allow researchers to align predefined markers on a detailed musculoskeletal model with actual marker positions recorded during a subject's movement. Through this alignment, the model can replicate the subject's motion, making it possible to analyze joint angles and movement patterns with high accuracy.

When paired with force plate data from a MOT file, inverse dynamics can be calculated alongside inverse kinematics to provide a deeper analysis of joint moments. Inverse dynamics

leverages the ground reaction force (GRF) vector captured from force plates, which represents the external force exerted on the body at ground contact points. These GRF data are applied within a sequential Newton–Euler framework, starting from distal segments and progressing up the kinematic chain, to compute net joint moments. Importantly, these net moments represent the resultant effect of all internal structures acting about a joint and do not resolve individual muscle or tissue forces, thereby providing necessary context for subsequent muscle-level analyses (Riemer and Hsiao-Wecksler, 2008; Runge et al., 1995).

Within OpenSim, inverse dynamics calculations can be further refined using the Residual Reduction Algorithm (RRA), which is designed to reduce dynamic inconsistencies between measured ground reaction forces and model-based kinematics. RRA applies constrained optimization to adjust the model's mass properties and slightly modify joint kinematics, thereby minimizing residual forces and moments that arise from skin movement artefacts, marker errors, or model–subject mismatch. By improving the dynamic consistency of the motion capture data, RRA enhances the fidelity of joint moment estimates and results in inverse dynamics outputs that better align kinematic measurements with the applied external forces (Faber et al., 2018; Riemer and Hsiao-Wecksler, 2009).

After obtaining joint moments through inverse dynamics, OpenSim can be used to estimate individual muscle forces using a static optimization (SO) algorithm. Static optimization resolves the muscle redundancy problem by identifying the set of muscle forces that can reproduce the joint moments at each time step while minimizing a physiological cost function, typically the sum of squared muscle activations (Thelen et al., 2003). This approach distributes force production across all muscles crossing a joint in a manner consistent with human motor control strategies. The output of SO includes muscle activations, muscle forces, and tendon forces, providing a detailed representation of muscular contributions to movement.

OpenSim also provides colour-coded muscle activation visualizations ranging from blue (inactive) to red (highly active) that can help researchers qualitatively inspect muscle recruitment patterns during simulated motion. Although these visualizations are primarily used in research rather than clinical practice, they can complement quantitative outputs (e.g., muscle activation curves) by offering an intuitive overview of global activation trends. This can be especially useful when communicating findings or when exploring compensatory strategies in complex movements (Delp et al., 2007; Seth et al., 2018). However, detailed interpretation of muscle function typically relies on plotted activation profiles rather than animation alone.

This integration of inverse kinematics, inverse dynamics, and static optimization represents a comprehensive modelling workflow in OpenSim, enabling researchers to derive detailed, model-based insights into joint loading, muscle function, and movement patterns.

2.6.2 Forward Dynamics

In musculoskeletal modelling software forward dynamics is a predictive approach used to simulate musculoskeletal movement by inputting muscle activation data to model how muscles generate force and, subsequently, movement. Unlike inverse kinematics which estimates joint angles by fitting a musculoskeletal model to recorded marker trajectories, forward dynamics computes movement by integrating dynamic equations of motion, though its accuracy depends on model assumptions, muscle parameters, and control strategies. This method is particularly useful in contexts where understanding precise muscle activation patterns and joint dynamics is critical, such as human performance assessment and rehabilitation (Lee and Umberger, 2016; Seth et al., 2018).

OpenSim includes a Forward Dynamics tool that simulates motion by integrating the equations of motion forward in time, given muscle excitations and external forces. A commonly used controller built on top of this tool is Computed Muscle Control (CMC), which computes muscle

excitations that allow the model to track experimentally measured kinematics. CMC therefore requires joint trajectories (from inverse kinematics) and external loads such as ground reaction forces and produces muscle activations that reproduce the observed movement (Delp et al., 2007; S. Shourijeh et al., 2016). While CMC has historically been used for tracking-based simulations, more recent developments such as OpenSim Moco and third-party frameworks like SCONE enable optimal-control–based forward simulations that predict both motion and muscle coordination patterns without requiring motion capture data as input (Dembia et al., 2020; Geijtenbeek, 2019). These forward dynamics approaches allow researchers to study muscle–tendon dynamics and neuromuscular coordination by observing how a biomechanical model behaves when driven by physiologically based muscle models and optimization criteria, providing insight into movement strategies and potential rehabilitation or performance applications.

Forward dynamics in OpenSim provides a powerful research framework for exploring how changes in muscle coordination, strength, or model parameters may influence movement. Although forward dynamics is not used directly in clinical decision-making, its predictive capabilities allow researchers to evaluate hypothetical scenarios such as altered gait strategies, rehabilitation exercises, or changes in muscle activation patterns within a controlled simulation environment. By examining how modifications in muscle force or activation influence overall movement, forward dynamics helps generate mechanistic insights and test intervention concepts that may later be evaluated experimentally or clinically (Mansouri and Reinbolt, 2012; Muñoz-Pepi et al., 2023).

Both methods are integral to understanding movement mechanics. Inverse kinematics is more retrospective, focusing on tracking and analyzing recorded data, while forward dynamics is predictive, aiming to simulate future movement.

2.7 Calibrated EMG-Informed Neuromusculoskeletal Toolbox (CEINMS)

The CEINMS toolbox is an OpenSim-compatible framework designed to estimate muscle forces using EMG-informed modelling rather than relying solely on static optimization. In CEINMS, experimentally recorded EMG signals are processed offline to obtain estimates of neural excitations, which are then combined with joint angles from inverse kinematics and musculotendon dynamics to drive the model (Pizzolato et al., 2017, 2015). Unlike static optimization where muscle forces are obtained by minimizing a cost function at each time step, CEINMS incorporates subject-specific activation patterns and calibrates excitation–activation parameters, allowing it to better represent physiological behaviour during dynamic, non-isometric tasks. Although CEINMS was developed with the potential for real-time applications, it is typically used offline in laboratory settings to provide improved estimates of muscle forces compared with traditional optimization-based approaches (Pizzolato et al., 2015; Sartori et al., 2012a).

By integrating EMG-derived neural excitations with musculoskeletal geometry and musculotendon dynamics, CEINMS produces muscle activation and force estimates that more closely align with experimentally observed physiological behaviour than static-optimization-based approaches (Pizzolato et al., 2015; Sartori et al., 2012a). A key feature of CEINMS is its calibration stage, during which several model parameters are tuned to match the subject's EMG–force relationship. Specifically, CEINMS calibrates excitation–activation parameters (e.g., activation and deactivation time constants), maximum muscle stress, tendon slack length, optimal fibrer length, and EMG–excitation scaling coefficients to improve the match between measured EMG, joint moments, and model-predicted muscle forces (Sartori et al., 2012a).

Another important feature of CEINMS is its ability to simulate excitation patterns for muscles that cannot be directly measured with surface EMG. For example, deep or small muscles, which are often inaccessible due to EMG hardware limitations, can be driven using weighted patterns and

predefined activation structures. This approach expands the model's capability to represent the contributions of muscles beyond the limited number of EMG channels typically available, enabling a more comprehensive reconstruction of neuromuscular coordination (Sartori et al., 2013).

The toolbox has been validated in a variety of contexts, demonstrating its ability to represent neuromuscular interactions across multiple tasks and populations (Assila et al., 2024; Bavil et al., 2024; Romanato et al., 2022). Through its integration of experimentally recorded EMG signals, personalized calibration, and its capacity to estimate the activation of muscles not directly instrumented, CEINMS serves as a robust and adaptable tool for detailed neuromusculoskeletal modelling in research applications.

2.8 Neuromusculoskeletal Modelling (NMSM) Pipeline

The Neuromusculoskeletal Modelling (NMSM) Pipeline is a recently developed MATLAB-based extension to OpenSim designed to enable personalized neuromusculoskeletal modelling and treatment optimization (Fregly, 2021). It comprises two coordinated toolsets, Model Personalization and Treatment Optimization, that together support the computational design of individualized interventions using subject-specific models and predictive simulation. Recent descriptions in the research literature (Fregly, 2021) emphasize the pipeline's aim to facilitate personalized treatments for neuromusculoskeletal impairments by adding model-personalization and optimal-control capabilities on top of OpenSim.

Within Model Personalization, a generic OpenSim model is tailored to a subject by estimating joint model parameters, muscle–tendon properties, neural control properties, and ground-contact characteristics from motion capture, surface EMG, and ground reaction forces, preceded by data preprocessing and muscle–tendon length initialization to align experimental data with the model's kinematics and moment arms.

Treatment Optimization then casts the personalized model into an optimal-control framework that proceeds through tracking, verification, and design phases, with optional surrogate modelling to accelerate solution time. Experimental trajectories are typically represented with splines evaluated at collocation points to enforce tracking and physiological constraints, and the architecture is advertised as applicable to any task that can be sufficiently described by an OpenSim model.

In scope and positioning, however, NMSM is primarily framed as infrastructure for personalized treatment design in neurologic and orthopedic movement impairments rather than as a running-specific analysis pipeline consistently emphasizing clinical use cases and does not provide a running-focused workflow or published validation targeted at endurance running mechanics and energetics. While many components such as ground-contact and neural-control personalization are technically applicable to running, applying NMSM to steady-state or fatigue-state running will require methodological adaptation and careful validation, particularly for foot–ground contact, controller structure, and energy-model calibration, to avoid biased inferences about cost of transport or muscle-level demands in runners.

2.9 Metabolic Cost

Metabolic cost is a key physiological metric used to quantify the energy consumed by the body during a given activity. It provides valuable insight into the efficiency of movement, and it has also been widely adopted as a measure for evaluating the design and operational settings of assistive devices (Collins et al., 2015; Galle et al., 2017; Malcolm et al., 2013). Understanding metabolic cost is particularly critical in fields like biomechanics, rehabilitation, and sports science, where energy expenditure can influence both performance and long-term health outcomes (Boyer et al., 2023; Koelewijn et al., 2019).

Two primary methods are employed to measure metabolic cost: direct and indirect calorimetry. Direct calorimetry involves the use of a calorimeter, a device that measures the total heat produced by the body during physical activity. This method is considered the most accurate approach for assessing metabolic cost as it provides a precise measure of the body's energy expenditure (Kaiyala and Ramsay, 2011). However, despite its accuracy, direct calorimetry is costly, requires highly specialized equipment, and is logistically challenging to implement in many real-world or laboratory settings, as it confines participants to a controlled environment. On the other hand, indirect calorimetry estimates metabolic cost by measuring respiratory gases, specifically the volume of oxygen consumed, and carbon dioxide produced by the body during exercise (Delsoglio et al., 2019). This method, while less accurate than direct calorimetry, is more practical and accessible making it more common in both clinical and research environments. Indirect calorimetry offers a non-invasive and more cost-effective alternative, and it allows for measurements to be taken in a broader range of settings, including dynamic, high-movement environments like sports or rehabilitation scenarios. The trade-off for its affordability and flexibility is a slight reduction in accuracy: indirect calorimetry results typically fall within 1-5% of those from direct calorimetry (Ashcraft and Frankenfield, 2015; Mtaweh et al., 2018; Seale and Rumpler, 1997). Additionally, indirect calorimetry may slightly underestimate energy expenditure, especially during high-intensity activities where anaerobic metabolism plays a more significant role. Nevertheless, this level of accuracy is generally sufficient for most applications, and the method remains a reliable, practical option for measuring metabolic cost in diverse settings.

Both methods have their advantages and limitations, and the choice between them often depends on the specific context and objectives of the study. For instance, indirect calorimetry's lower cost and ease of use make it well-suited for large-scale studies or real-time monitoring in

dynamic situations whereas direct calorimetry is favoured in a controlled, highly precise experiments where accuracy is paramount.

2.9.1 Estimating Metabolic Cost and Cost of Transport in Simulation and Experiment

To evaluate the physiological demands of locomotion, the metabolic cost of movement is often quantified through the cost of transport (CoT) defined as the energy required to move one kilogram of body mass over one meter of distance (J/kg/m). This measure normalizes energy expenditure across participants and movement speeds, making it especially useful in biomechanics research exploring efficiency, fatigue, and performance. Estimating CoT can be accomplished through two principal methodologies: simulation-based musculoskeletal modelling and experimental indirect calorimetry. The software OpenSim provides several metabolic energy models, including (Bhargava et al., 2004; Umberger, 2010; Umberger et al., 2003), that compute muscle-level energetics from joint-level kinematic and kinetic data. Alternatively, indirect calorimetry estimates whole-body energy expenditure by analyzing oxygen uptake and respiratory exchange ratios during physical tasks. Each method comes with inherent assumptions and modelling constraints that influence the resulting CoT values.

The Umberger et al., 2003 model was the first comprehensive metabolic cost model implemented in OpenSim and is grounded in the energetics of Hill-type muscle mechanics. It separates total metabolic cost into four key components: activation heat rate, maintenance heat rate, shortening/lengthening heat rate, and mechanical work rate. These are summed to yield total instantaneous metabolic power. Mathematically, the model's total metabolic energy rate is

$$E_{total} = E_{activation} + E_{maintenance} + E_{shortening/lengthening} + E_{mechanical\,work} \quad (2)$$

Each component corresponds to a different physiological process. Activation heat represents the cost of calcium handling during excitation-contraction coupling; maintenance heat corresponds

to cross-bridge cycling during isometric contraction; the shortening/lengthening term captures concentric or eccentric force production inefficiencies; and mechanical work reflects external work done by muscle-tendon units. Although the model treats eccentric and concentric contractions similarly in terms of metabolic cost, which is a known limitation, it has proven robust for basic walking and running simulations. Studies employing this model have reported CoT values between 3.5–4.0 J/kg/m for running at moderate speeds (~2.5–3.5 m/s), with some underestimation relative to empirical data (Miller, 2014; Uchida et al., 2016b).

In contrast, the Umberger (2010b) model enhances the physiological fidelity of the original version by introducing different mechanical efficiencies for concentric and eccentric contractions, and by adjusting fiber-type distributions at the muscle level. It also refines the thermal components of energy expenditure based on updated muscle thermodynamics. The total energy rate is calculated using the same equation structure as the 2003 model but applies muscle-specific parameters for efficiency and fiber-type recruitment. This model better captures the U-shaped CoT-speed relationship observed in experimental locomotion studies. When applied to running tasks, CoT estimates from Umberger 2010 typically range from approximately 4.0 to 5.2 J/kg/m across commonly studied speeds (Table A 5.1), aligning more closely with values obtained from indirect calorimetry in healthy adults (Koelewijn et al., 2019; van der Zee and Kuo, 2021). Its improved treatment of negative work and fiber recruitment makes it particularly suitable for simulating fatigue, as it accounts for the increasing reliance on fast-twitch fibers under stress.

The Bhargava et al., (2004) model adopts a different formulation by estimating metabolic cost based on excitation and activation states, muscle fiber length, and contraction velocity. Unlike the Umberger models, it is not grounded in mechanical energetics but instead uses a phenomenological approach informed by calcium kinetics and muscle physiology. The total metabolic rate in Bhargava's model is expressed as follows:

$$E_{total} = A_{activation} + A_{maintenance} + A_{shortening} \quad (3)$$

Here, $A_{activation}$ accounts for energy required to activate muscle fibers, $A_{maintenance}$ for the energy consumed to maintain force in isometric conditions, and $A_{shortening}$ for additional energy required during muscle fiber shortening. Notably, this model integrates well with EMG-informed simulations, such as those implemented using the CEINMS toolbox, allowing for subject-specific estimations of energy expenditure that reflect actual neuromuscular control. Bhargava's model tends to generate lower CoT values, typically in the range of 2.8–3.5 J/kg/m for treadmill running because it reflects observed excitations rather than theoretical optima (Pizzolato et al., 2015). Its compatibility with EMG data makes it particularly advantageous when investigating fatigue, where muscle recruitment patterns deviate significantly from baseline.

In contrast to model-based estimates, indirect calorimetry offers an empirical method to determine metabolic cost by measuring respiratory gas exchange. The Péronnet and Massicotte (1991) model is frequently used to convert oxygen consumption (VO2) and respiratory exchange ratio (Respiratory Quotient (RQ)) into metabolic energy. It does so by applying a lookup table of caloric equivalents based on the RQ value, which reflects the proportion of fat versus carbohydrate oxidation. The fundamental equation is

$$Energy\ Expenditure\ \left(\frac{kcal}{min}\right) = VO2 * EE_{O_2} \quad (4)$$

where EE_{O_2} is the energy equivalent of oxygen in kcal/L, varying from 4.69 kcal/L (pure fat oxidation, RQ = 0.7) to 5.05 kcal/L (pure carbohydrate oxidation, RQ = 1.0). For example, at an RQ of 0.95 and a VO2 of 3.2 L/min, the energy expenditure would be approximately 15.88 kcal/min or 66.5 kJ/min. When this value is normalized by body mass and distance travelled, the resulting CoT during submaximal running (~85% VO2 max) typically falls within 4.5–5.5 J/kg/m (Bellenger et al., 2019; Crouter et al., 2019). While indirect calorimetry provides

accurate total energy cost, it lacks resolution regarding individual muscle contributions or joint-specific energetics, making it complementary to simulation-based approaches rather than a replacement.

Together, these models and methods offer a robust framework for interpreting energetic data in biomechanics. The Umberger models are ideal for generalized running simulations where parameter sensitivity is key, while the Bhargava model allows detailed investigation of neuromuscular strategies during fatigue through integration with EMG. Indirect calorimetry, meanwhile, serves as an empirical benchmark for evaluating the accuracy of these models. For the current thesis, the inclusion of multiple CoT estimation techniques, both model-based and experimental, ensures that observed changes in energy expenditure due to fatigue are interpreted with both physiological and mechanical validity. This integrated approach enhances the overall robustness of metabolic cost analyses, particularly when characterizing the interplay between oxygen uptake, neuromuscular activation, and joint loading during prolonged, submaximal exercise.

A summary of CoT values obtained from musculoskeletal models, EMG-informed simulations, and experimental calorimetry is detailed in Table A1. This table offers a comparative perspective across walking and running speeds, modelling approaches, and exercise types, providing essential context for interpreting the simulated and empirical findings presented herein.

Chapter 3: Methods

3.1 General Methodology

This thesis is structured into two primary studies. The first study focuses on investigating the effects of exercise-induced fatigue on neuromuscular activity, while the second study builds on the findings of the first to develop a representative musculoskeletal model of fatigue in the main muscle of interest. This model will be used to estimate the cost of transport, offering insights into the biomechanical implications of fatigue.

The first study aims to examine the relationship between oxygen uptake and neuromuscular activity during a fatiguing task. By analyzing how metabolic demand correlates with muscle activation, this study will provide a deeper understanding of how fatigue is associated with changes in performance and neuromuscular function. Data collection will involve monitoring oxygen consumption, lower-body kinematics, and EMG signals to characterize the relationship between energy expenditure and muscle activation patterns.

The second study will build upon the findings from the first by integrating musculoskeletal modelling techniques to generate subject-specific estimates of metabolic cost using OpenSim. OpenSim, a widely used musculoskeletal modelling software (Delp et al., 2007), will be employed for this purpose due to its ability to integrate subject-specific motion data and estimate muscle activation and metabolic cost within a validated musculoskeletal framework. The aim of this study is to assess the differences between a generic statically optimized OpenSim model (Catelli et al., 2019) and indirect calorimetry cost of transportation values. This comparison is used to evaluate how generic anatomical scaling and optimization-based control assumptions, along with the absence of explicit fatigue modelling, contribute to discrepancies between model-predicted and experimentally measured cost of transport.

This research is part of a larger project approved by the Swedish Ethics Review Authority (Etikprovningsmyndigheten), the diary number for the review at the Swedish Ethics Review Authority is 2024-04208-1. The outcomes of this work are expected to enhance our understanding of the biomechanical effects of fatigue, which can be used to improve rehabilitation strategies and inform the design of assistive devices or interventions targeting knee joint pathologies.

3.2 Participants for the Study

Seven healthy athletes were included in the study based on the data available within the collection timeline, forming a pilot sample for feasibility assessment. Although data were collected from 29 athletes, only seven datasets were fully processed due to the substantial time required for synchronizing, filtering, and modelling.

Prior to data collection, an a-priori power analysis was conducted using G*Power for a repeated-measures ANOVA (within-subject factors) to estimate the recommended sample size for detecting fatigue-related changes across pre-, mid-, and post-fatigue stages. Using an effect size of 0.4, an alpha level of 0.05, and a desired power of 0.80, the analysis indicated that approximately 12 participants would be required. This effect size was selected based on prior fatigue-related neuromuscular studies reporting medium within-subject changes (Borotikar et al., 2008; Chappell et al., 2005; Cohen, 1992; McLean et al., 2007; Quammen et al., 2012).

To be eligible for participation, athletes must have a Tegner activity level score of 5 or higher, indicating that they engage in activities requiring a significant degree of knee stability (Tegner and Lysholm, 1985). This scale helps assess the physical demands placed on the participants' knees during various athletic activities.

However, individuals were excluded from the study if they had sustained an injury to their lower extremities within the past six months that has resulted in missed training sessions or

competitive events. Participants were also excluded from this study if they had sustained any form of cardiovascular incident requiring medical intervention.

3.3 Participant Preparation for Data Collection

Prior to arrival participants were recommended to drink 500 mL of water approximately two hours prior to testing in an attempt to standardize bodily fluid concentration (Li et al., 2024). Upon arrival, participants were introduced to the equipment and protocol and required to read and sign a consent form (*Swedish version of the Consent form* and *English version of the Consent form*) explaining the study as well as the self-reported Tegner activity scale (Tegner and Lysholm, 1985).

After providing informed written consent, participants were provided with tight-fitted spandex shorts and a short-sleeved shirt. Following this, their anthropometric characteristics were measured (height, weight (pre- and post-protocol to account for potential perspiration effects), BMI, distance between their right and left anterior superior iliac spine (ASIS), distance between their left and right posterior superior iliac spine (PSIS), knee and ankle width, leg length (distance from ASIS to medial malleolus), tibia length (distance from tibial condyle to lateral malleolus), and thigh and shank circumference) as well as dominant leg. These metrics were used as reference inputs during the scaling process in OpenSim. The dominant leg of each participant was distinguished by which leg is used to kick a football (soccer ball) a maximum distance (van Melick et al., 2017) and was recorded for descriptive purposes. After anthropometric measurements, participants were provided with a pair of running shoes (Nike Revolution 7, United States).

They were then fitted with surface electromyography (sEMG) electrodes (16-channel Noraxon MyoMotion, Noraxon USA Inc) which were placed on the muscle bellies to determine muscle activation of three quadriceps muscles of interest: rectus femoris (RF), vastus medialis (VM), vastus lateralis (VL), two hamstring muscles (semitendinosus (ST) and biceps femoris (BF)), two gastrocnemius muscles (lateral (LG) and medial (MG)), and the gluteus medialis (Figure A 9.1).

The sEMG were placed following SENIAM guidelines (Hermens et al., 2000) and recommendations from De Luca, (1997) with the EMG data collected at a sampling rate of 2000 Hz.

Participants were then fitted with 56 reflective markers (Figure A 9.2) based on a custom marker set derived from the Qualisys Sport Marker set and the convention used by Mantovani and Lamontagne (2017). Following this, the COSMED K5 (COSMED, Rome, Italy) system was set up in breath-by-breath mode, as this configuration provided the same accuracy and reliability as the mixed chamber mode (Crouter et al., 2019; Guidetti et al., 2018; Perez-Suarez et al., 2018; Winkert et al., 2021, 2020).

Kinematic data were collected using a ten-camera 3D motion analysis system (Arqus A9, Qualisys motion capture system, Gothenburg, Sweden) and captured at 200 Hz. Kinetic data were captured using the embedded force plates at 1000 Hz on the instrumented treadmill (HP Cosmos, Germany) with a capacitance-based pressure platform (FDM-THG, Zebris Medical GmbH, Germany) at a 1% fixed grade (Lourenço et al., 2011) incline to simulate outdoor running.

3.4 Maximum Voluntary Isometric Contractions

To establish baseline muscle activation levels, participants during both visits performed maximum voluntary isometric contractions (MVICs) using an isokinetic dynamometer (System 4 Pro, Biodex Medical Systems, USA) following a three-minute warm-up on a stationary bike (Monark 828E, Vansbro, Sweden) at a self-selected resistance. MVICs were assessed for knee flexion and extension in a seated position with the knee flexed at 65° for extension and 55° for flexion, for plantarflexion in a seated position with knee extended to approximately 145° (range: 140-150°) and the ankle in a neutral position (0°), and for hip abduction in a standing position with the hip maintained at 30° abduction. Each contraction followed a standardized protocol in which participants were instructed to put maximal effort to reaching their maximal contraction, which

they sustained for five seconds. This process was repeated three times for each muscle task, with at least one minute of rest between trials to minimize the effects of fatigue. Prior to testing each participant was given the chance to familiarize themselves with the movement by allowing a practice round before starting the maximal effort trials.

Surface EMG and isometric torque were recorded synchronously using Noraxon MR software (v4.0 Noraxon MyoMotion, Noraxon USA Inc), with EMG data sampled at 2000 Hz while torque was sampled at 1000 Hz. Participants were provided with standardized verbal encouragement and on-screen biofeedback throughout the testing process to maximize effort during each contraction. The collected MVIC data served as a reference for normalizing the dynamic EMG signals obtained during subsequent testing, enabling valid comparisons across participants and fatigue conditions. At the end of each task participants were asked to self report knee pain, difficulty, and perceived exertion using the Borg Scale.

3.5 Visit 1 Running Protocol - VO2 max Testing

To establish an appropriate high-intensity threshold running speed, a VO2 max test was completed to characterize aerobic fitness and to normalize the intensity of the high-intensity running protocol (Aquino et al., 2023; Billat, 2001; Encarnación-Martínez et al., 2023; Kaufman et al., 2006). VO2 max testing was performed with the COSMED K5 on an instrumented treadmill (HP Cosmos, Germany) during an incremental treadmill protocol. Participants were familiarized with the treadmill and equipment (Figure 3.1) and warmed up for 3 minutes at 5 km/h. The test began at an initial speed of 8 km/h, increasing by 0.5 km/h every 2 minutes until exhaustion with ground reaction force (GRF), kinematics, EMG, pressure mat, and metabolic data measured for 30 seconds after the increment in addition to their perceived exertion using the Borg scale.

The test was then stopped when the participant reached their voluntary exhaustion. The criterion used to assess whether $\dot{V}O2$ max was reached was if at the end, two or more of the

following criteria were met: a respiratory quotient ratio ≥ 1.10, a heart rate in excess of 90% at age predicted heart rate maximum (= 220 - age), and identification of a plateau (<150 mL x min−1 increase) in V̇O2 max despite a further increase in velocity (Cortes et al., 2014; Hamlin et al., 2012; Quammen et al., 2012). After the completion of the VO2 max test, participants were given a mandatory five-minute recovery period walking at 5 km/h and then one last one-minute run at 8 km/h prior to being weighed.

Figure 3.1: Experimental setup of HP COSMED with K5

3.6 Visit 2 Running Protocol–High Intensity Submaximal Threshold

Following the first assessment, participants returned to the lab no later then 2 weeks after the initial assessment to complete a submaximal threshold test. Prior to their secondary assessment participants were asked to abstain from vigorous exercise for at least two days prior to the test to reduce the impact of recent training on performance (Aquino et al., 2023; Schneider et al., 2020).

In the secondary assessment participants completed a high-intensity running protocol at 85% of their V̇O2 max running speed on a treadmill set to 1% inclination. This protocol, selected based on previous studies (Aquino et al., 2023; Bellenger et al., 2019; Billat, 2001; De Ruiter et al., 2016; Encarnación-Martínez et al., 2023; García-Pérez et al., 2014; Kaufman et al., 2006; Pollock et al., 1998; Xia et al., 2017), is designed to simulate a high-intensity training session similar to those commonly undertaken by recreational runners and football players (Hespanhol Junior et al., 2013; Quammen et al., 2012). The maximal duration of the protocol is 30 minutes as previous testing has demonstrated that extreme fatigue will onset after 15 minutes of running at 85% VO2 max speed (Aquino et al., 2023; Encarnación-Martínez et al., 2023; García-Pérez et al., 2014; Kaufman et al., 2006).

Throughout the test, metabolic data including heart rate (HR), VO2 max, Respiratory Quotient (RQ) and Borg were measured every 5 minutes to ensure the intended intensity is maintained (Bellenger et al., 2019; Garber et al., 2011; Impellizzeri et al., 2004; Kaufman et al., 2006; Pollock et al., 1998; Vesterinen et al., 2016). Before starting the protocol, participants completed a 3-minute walking warm-up at 5 km/h and then a 2.5-minute light jogging warm-up at 8 km/h (Romagnoli et al., 2018) before being brought up to their 85% VO2 max running speed.

In addition to metabolic data, GRF, kinematics, pressure mat, and EMG data were collected specifically every 5 minutes for 30 seconds, allowing for an evaluation of the evolution of these data as participants fatigue. Once again, after the completion of the test, participants were given a mandatory five-minute recovery period walking at 5 km/h and then one last one-minute stint at 8 km/h prior to being weighed.

3.7 OpenSim Data Preparation

Before creating the OpenSim models, the experimental data collected had to be reformatted into files compatible with OpenSim 3.3 and CEINMS. To accomplish this, a custom Matlab pipeline was used to convert the original. mat files into MOT and TRC formats. OpenSim 3.3 was selected for this workflow because CEINMS is currently only compatible with the OpenSim 3.x architecture, necessitating consistency across the modelling and EMG-driven calibration steps.

3.8 OpenSim model

A generic full-body OpenSim musculoskeletal model (Catelli et al., 2019) will serve as the foundational model for conducting two metabolic cost analyses in this research. This model was selected because it provides a detailed representation of the musculoskeletal system, featuring 40 Hill-type muscle-tendon units per leg and 37 degrees of freedom (DOF). The degrees of freedom include 3 DOF for the hip joints, 1 DOF for the knee joints, and 2 DOF for the ankle joints, offering a comprehensive framework for simulating complex human motion where high hip flexion may occur.

The first step involved scaling the generic model to match the specific dimensions of the subject using the OpenSim Scale Model tool with a MoRe-Lab Scaling Setup File with all model processing performed using the computational resources described in the Computational Resources chapter. This process was informed by data from a static standing trial, ensuring that the musculoskeletal geometry is accurately aligned with the subject's physical characteristics.

Before proceeding to the static optimization or EMG-driven model calibration, we analyzed experimental data from three running trials of the data collection. The marker data from these trials were then analyzed using OpenSim's Inverse Kinematics (IK) tool, following the IK Setup file described in Computational resources, which was used to calculate the joint angle trajectories. The two modelling approaches used to estimate muscle activation, static optimization and EMG-driven

modelling, are described in detail in the subsequent sections, including their underlying assumptions and implementation.

3.8.1 Static Optimization model

Following the computation of joint kinematics via inverse kinematics (IK), the OpenSim Inverse Dynamics (ID) tool was used to estimate net joint moments based on measured ground reaction forces and segment kinematics. These IK-derived joint angles, together with external loads and model dynamics, were then provided to the Static Optimization (SO) tool, which computed muscle forces and activations that best reproduced the joint moments obtained from ID, thereby resolving the muscle redundancy problem.

SO determines a unique solution by minimizing the sum of squared muscle activations while constraining muscle forces to reproduce joint torques within physiological limits (Anderson and Pandy, 2001). This approach was selected due to its computational efficiency, stability, and widespread use in running simulations, enabling consistent estimation of muscle forces across participants.

However, SO relies on several assumptions, including the neglect of activation dynamics, tendon compliance, and history-dependent muscle behaviour, and does not explicitly account for fatigue-related changes in muscle capacity. As a result, estimated muscle activations may not fully reflect true neuromuscular control strategies under fatigue conditions, potentially influencing downstream estimates of metabolic cost. These limitations are important when interpreting the sensitivity of model-derived outcomes to fatigue in the present study.

This process allowed for subject-specific estimations of muscle forces across the running trials, using the scaled *Catelli* musculoskeletal model. After muscle forces were estimated, additional analyses were conducted using the OpenSim Analyze Tool. This included Muscle Analysis, which provided data on muscle fiber length and fiber velocity; Force Analysis, which computed individual

muscle and joint reaction forces; State Analysis, which generated time-varying states for muscle activation, length, and force; and Probe Analysis which calculated the CoT. The results from these analyses were later used to calculate model-based metabolic energy expenditure using three distinct metabolic models.

3.9 Data Processing Analysis

3.9.1 Processing and Normalization of Kinematic, Kinetic, and EMG Signals

To properly analyze the collected data, multiple filtering and processing steps were applied across kinematic, kinetic, and electromyographic (EMG) signals. A schematic overview of the EMG processing pipeline is provided in Figure 3.2.

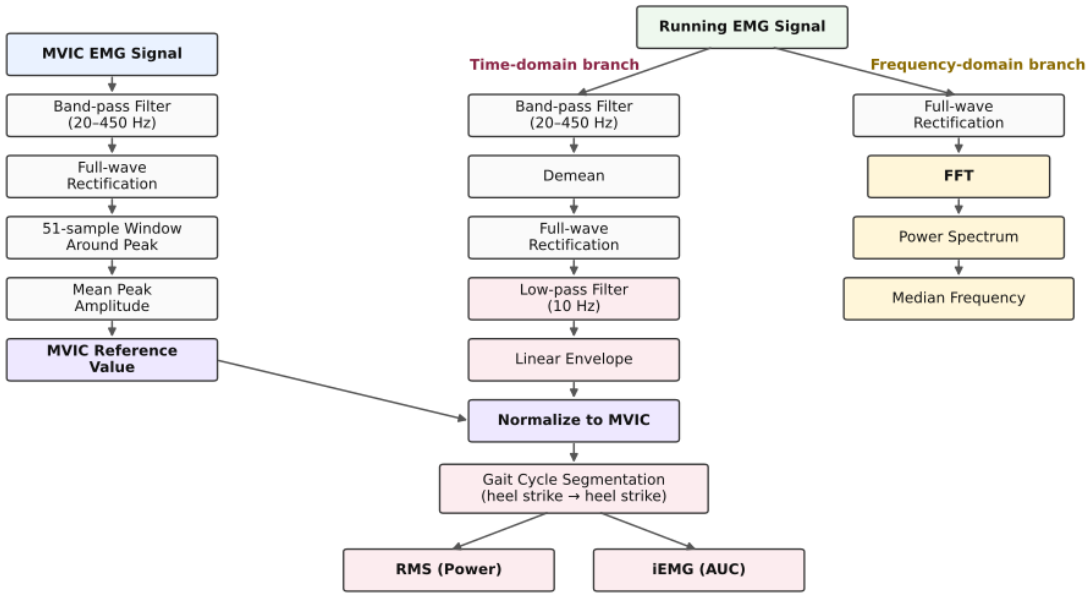

Figure 3.2: EMG signal processing pipeline for time- and frequency-domain analyses.

For kinematic marker trajectories collected during the submaximal threshold test, a 4th-order dual-pass low-pass Butterworth filter (6 Hz cutoff) was applied to remove high-frequency noise while preserving the underlying movement signal. Similarly, kinetic data were filtered using the same 4th-order dual-pass low-pass Butterworth filter. Once filtered, the marker trajectories were used to extract hip flexion, abduction, and rotation; knee flexion angle; and ankle flexion,

abduction, and rotation angles using a MATLAB pipeline based on Wu et al. (2002). Following this, kinematic and kinetic data were segmented into their respective running cycles based upon heel marker trajectory and GRF for further analysis.

Different filtering and processing methods were used for EMG data depending on the specific output being analyzed. For MVIC (Maximal Voluntary Isometric Contraction) EMG signals, the signals were first filtered using a 4th-order band-pass Butterworth filter (20–450 Hz). The filtered signals then underwent full-wave rectification and signal conditioning. The maximal EMG value for each trial was determined by taking a 25-frame window around the peak recorded value as to include 51-frames of which the average was taken, and the average of these values was used as the participant's maximal muscle activation for normalization purposes (Clancy and Hogan, 1999, 1997).

For the high-intensity threshold test, EMG signals were analyzed both filtered and unfiltered. The filtered EMG signals were first band-pass filtered (20–450 Hz), demeaned to remove any residual offset, and full-wave rectified. The rectified signal was then low-pass filtered using a 4th-order Butterworth filter (10 Hz cutoff) to generate a linear envelope representing the time-varying muscle activation. These processed EMG signals were normalized to the maximal muscle activation obtained from the MVIC trials (Burden, 2010; Hermens et al., 2000). Although the primary analyses focused on within-participant comparisons across fatigue conditions, MVIC normalization was applied to reduce inter-muscle and session-dependent variability and to facilitate interpretability of activation levels across time.

For frequency-domain analysis, the unfiltered EMG signals were first rectified and then processed using a Discrete Fast Fourier Transform (DFT; Equation 5) to obtain the frequency-domain representation of the signal (Oppenheim and Schafer, 2010). The resulting spectrum was subsequently used to compute frequency-based metrics, including both mean frequency and

median frequency. Median frequency was defined as the frequency that divides the power spectrum into two regions containing equal total power.

$$\mathrm{X(k)} = \sum_{n=0}^{N-1} x(n) e^{-j2\pi kn/N} \tag{5}$$

In this equation, $x(n)$ represents the time-domain EMG signal, X(k) is the complex-valued DFT at discrete frequency bin k, n denotes the time-sample index, N is the total number of samples in the EMG segment, and $j = \sqrt{-1}$ is the imaginary unit. The exponential term $e^{-j2\pi kn/N}$ maps the time-domain signal into the frequency domain, allowing the spectral content of the EMG signal to be quantified across discrete frequency bins.

Time-domain EMG variables were calculated from the processed and MVIC-normalized EMG envelope. EMG power (Equation 6) (De Luca, 1997; Winter, 2009), equivalent to root mean square (RMS) amplitude, was computed as follows:

$$EMG_{power} = \sqrt{\frac{1}{N} \sum_{n=1}^{N-1} x_n^2} \tag{6}$$

In this expression, x_n denotes the EMG amplitude at sample n, and N is the total number of samples in the analysis window. The term x_n^2 represents the instantaneous power of the signal, and the square-root of the mean of these squared values yields the root-mean-square (RMS) EMG amplitude over the window.

The area under the curve also known as integrated EMG (iEMG) was determined through the trapezoidal rule (Equation 7) (Konrad, 2005; Winter, 2009).

$$\mathrm{iEMG} = \sum_{n=1}^{N-1} \frac{x_n + x_{n+1}}{2} * \Delta t \tag{7}$$

In this equation, x_n and x_{n+1} are successive EMG samples, N is the number of samples in the interval, and Δt is the sampling period. The term $\frac{x_n+x_{n+1}}{2}$ approximates the EMG amplitude using the trapezoidal rule, and summing across all samples yields the integrated EMG (iEMG), representing the total EMG activity over the time window. representing the total muscle activation over the time window. Both RMS (power) and iEMG (AUC) were expressed relative to the MVIC reference value.

After filtering, the processed EMG signals were analyzed to extract key muscle activity features. Average power (RMS) represents the overall energy of the EMG signal, providing insights into the amplitude of muscle activation during the task (Falconer and Winter, 1985; Merletti and Parker, 2004; Winter, 2009). Median frequency, a measure of the frequency content of the EMG signal, is often used as an indicator of muscle fatigue. As fatigue progresses, motor unit recruitment and firing rates change, leading to shifts in median frequency (De Luca, 1984; Kupa et al., 1995; Lindstrom et al., 1970). The iEMG quantifies the total muscle activation over the duration of the contraction, offering a cumulative measure of muscle effort (Hermens et al., 1992; Konrad, 2005; Sushkova et al., 2021; Winter, 2009). These parameters, particularly median frequency and iEMG, are well-established in EMG studies of muscle performance and are crucial for detecting early signs of muscle fatigue during prolonged or high-intensity physical activity (Allison and Fujiwara, 2002; Corvini and Conforto, 2022; Falconer and Winter, 1985; Farina et al., 2002; Hodges and Bui, 1996; Mu et al., 2022; Sun et al., 2022).

Since participants were running during data collection, their muscles underwent continuous length changes due to the dynamic nature of the gait cycle. To ensure consistent EMG analysis, the running trials were segmented into individual gait cycles (heel strike to heel strike), allowing the EMG signals to be time-normalized to a common cycle duration. Time normalization reduces

variability related to differences in stride duration and enables meaningful comparisons of muscle activation patterns across strides and participants. This approach is commonly used to reduce variability associated with differences in stride duration and facilitates meaningful comparisons of muscle activation patterns across strides and participants (Derrick et al., 2002; Winter, 2009).

3.9.2 Cost of Transport Model and Calculation

The cost of transport, defined as the energy required to move one kilogram of body mass over one meter of distance (J/kg/m), was calculated using both experimental and simulation-based methods to assess the metabolic efficiency of running under fatigued conditions. CoT provides a normalized measure of metabolic cost, allowing for comparisons across trials, participants, and modelling approaches, and is particularly useful in studies examining changes in locomotor efficiency during fatigue.

For the experimental approach, metabolic data were collected using the COSMED K5 portable indirect calorimetry system, configured in breath-by-breath mode. Time-synchronized trial segments lasting 30 seconds were isolated using trial-specific markers. For each segment, the average oxygen uptake rate ($\dot{V}O2$, in mL/min) and respiratory quotient (RQ) were extracted. To estimate the energy equivalent of oxygen, the model proposed by Péronnet and Massicotte (1991) was used (Equation 4), which calculates the caloric value per millilitre of oxygen consumed as a function of RQ. The energy expenditure over each trial was then computed by multiplying the VO2 by this energy equivalent, producing a gross energy value in joules per minute. In order to estimate net energy cost, the metabolic energy from a resting walking trial (serving as a gait baseline) was subtracted from the gross trial energy, thereby isolating the energy cost specific to running effort. Both gross and net energy expenditures were then normalized by the participant's body mass and the distance travelled on the treadmill calculated as the product of trial duration and speed to yield gross and net CoT values.

In parallel, simulation-based CoT estimates were derived using output from the OpenSim Static Optimization and Analyze tools. Muscle-level variables such as activation, fiber length, fiber velocity, and active fiber force were exported from three running trials per participant. These outputs were processed using custom Python scripts to calculate energy expenditure according to three established metabolic models: *Umberger2003*, *Umberger2010*, and Bhargava2004 (Equations 2 and 3, respectively). The *Umberger2003* model partitions energy into activation heat, maintenance heat, mechanical work, and lengthening heat, assuming a fixed efficiency for both concentric and eccentric contractions. The *Umberger2010* model builds upon this by incorporating fiber-type distribution and differing efficiencies for eccentric versus concentric muscle actions, allowing for a more physiologically realistic representation of muscle energetics. In contrast, the Bhargava2004 model uses a phenomenological approach grounded in muscle excitation and activation dynamics, without explicitly modelling mechanical work.

For each model, the total estimated energy expenditure across all muscles was integrated over time and then normalized by participant mass and treadmill distance to yield CoT values for each trial. A fixed trial duration of 30 seconds was assumed, corresponding to the experimental protocol.

3.10 Statistics for the studies

3.10.1 First Study

The statistical analysis for the first study was conducted using JASP software (version 0.18.1), a comprehensive, validated tool that supports a wide range of statistical techniques. To assess the effect of fatigue throughout the exercise protocol, a one-way repeated measures ANOVA was conducted across pre-, mid-, and post-exercise conditions. Normality of all variables was verified using the Shapiro–Wilk test, and where Mauchly's test indicated a violation of sphericity, Greenhouse–Geisser corrections were applied. The level of significance was set at $\alpha = 0.05$, allowing for the identification of significant changes in neuromuscular activity over time.

Neuromuscular behaviour was evaluated using three EMG-derived metrics: median frequency, RMS amplitude (power), and integrated EMG (iEMG), all normalized to each muscle's MVIC. Separate repeated-measures ANOVAs were conducted for each variable and each muscle studied to determine whether fatigue induced changes in global activation amplitude, spectral content, or cumulative activation across the session. These analyses captured whether neuromuscular output increased, decreased, or shifted in frequency as physiological strain accumulated.

In addition to neuromuscular activity, joint kinematics were statistically analyzed using Statistical Parametric Mapping (SPM), with a one-way repeated measures SPM ANOVA performed across the gait cycle for each joint degree of freedom including hip flexion–extension, hip abduction-adduction, hip internal-external rotation, knee flexion–extension, ankle plantarflexion–dorsiflexion, ankle inversion-eversion, and ankle internal-external rotation. This approach enabled time-continuous comparisons of kinematic waveforms and allowed the identification of localized gait-cycle regions where fatigue produced changes in movement patterns (Pataky, 2010). By evaluating these parameters alongside neuromuscular activity, we aim to describe how fatigue-related changes in muscle function occur in parallel with alterations in movement patterns.

3.10.2 Second Study

All statistical analyses for the second study were carried out using Python (v3.10), with data processing and inference performed using the pandas, NumPy, SciPy, seaborn, and statsmodels libraries. Prior to running parametric procedures, the normality of all cost-of-transport (CoT) values was verified using the Shapiro–Wilk test. Where appropriate, Mauchly's test of sphericity was examined, and Greenhouse–Geisser corrections were applied when sphericity assumptions were violated.

To evaluate differences in metabolic cost across fatigue stages and estimation approaches, a two-way repeated-measures ANOVA was performed with "Method" (Bhargava 2004,

Umberger 2003, Umberger 2010, and indirect calorimetry) and "Stage" (pre-, mid-, and post-fatigue) entered as within-participant factors. This analysis provided a global assessment of whether the three musculoskeletal models differed from experimental calorimetry and whether any of the approaches detected fatigue-related changes in CoT across the protocol.

Following significant main effects, planned post hoc comparisons were performed using paired-sample t-tests. These pairwise analyses compared each musculoskeletal model with indirect calorimetry at each fatigue stage, compared the three models with each other, and assessed within-method changes from pre- to mid- and pre- to post-fatigue. To minimize inflation of Type I error, Holm–Bonferroni corrections were applied to all families of post hoc tests, and effect sizes (Cohen's d) with 95% confidence intervals were reported alongside exact p-values.

To assess the degree of agreement between model-derived and calorimetry-derived CoT values, Bland–Altman analyses were conducted separately for each metabolic model. Mean bias and the 95% limits of agreement were calculated to quantify systematically under- or over-estimation relative to calorimetry and to visualize whether the magnitude of disagreement increased with higher metabolic cost. Complementary to the agreement analysis, Pearson correlation coefficients were computed between model-based and experimental CoT values, and root-mean-square error (RMSE) was calculated to provide an absolute measure of prediction error for each model.

An additional analysis focused on the ability of each method to capture directional changes in metabolic cost across the session. For each participant and each method, linear regression was used to compute the slope of CoT across the three fatigue stages, providing a concise summary of stage-wise drift. These slopes were used to compare the responsiveness of the metabolic models to fatigue against the experimentally measured drift observed through indirect calorimetry.

To evaluate potential asymmetries in muscle-level energy expenditure predicted by the models, paired-sample t-tests were performed to compare left–right muscle-group energy contributions,

with multiplicity controlled using Holm corrections. This allowed characterization of limb-specific energetic patterns and assessment of whether the models predicted consistent bilateral behaviour.

Because accurate joint kinematics are essential for reliable metabolic estimates, a methodological validation of the inverse-kinematics pipeline was conducted. Joint-angle trajectories computed using OpenSim were compared with those obtained from an independent MATLAB/Quaternion implementation using one-dimensional Statistical Parametric Mapping. A two-way SPM repeated-measures ANOVA with factors "Method" (OpenSim vs MATLAB) and "Stage" (pre, mid, post) was used to identify any time-localized differences across the gait cycle, and when required, SPM paired t-tests were performed. These analyses confirmed that differences between pipelines were small, localized, and not stage-dependent, supporting the validity of the kinematic inputs to the metabolic models.

To examine the temporal relationship between experimental muscle activation and the muscle activation patterns generated by static optimization, an EMG–model timing analysis was performed. For each muscle and each stage, the temporal lag between EMG onset and model-derived activation onset was quantified, and a repeated-measures ANOVA assessed whether these lags differed across the fatigue stages. The absence of systematic drift confirmed that static-optimization activation timing remained stable throughout the protocol and was therefore appropriate for use in the metabolic cost calculations.

Finally, to assess the dynamic consistency of the musculoskeletal simulations, a residual actuator analysis was performed following the recommendations of Hicks et al. (2015). Residual forces and moments were expressed relative to peak net external force and to the product of center-of-mass height and peak external force, respectively, and compared against established thresholds for acceptable simulation quality. This analysis served as a global quality-control step to evaluate whether the simulations were sufficiently dynamically consistent to support interpretation of

model-derived muscle forces and metabolic cost estimates, particularly for relative comparisons across fatigue conditions.

Chapter 4: Manuscript 1

Title: Silent Drift - Detecting Fatigue Beyond Kinematics in Constant-Speed Treadmill Running

Zachary A. Flahaut[1, 2], Nicholas S. Ryan[3], Pär Halje[3], Allison L. Clouthier[1, 4], Daniel L. Benoit[3]

[1] Ottawa-Carleton Institute for Biomedical Engineering, University of Ottawa, Canada

[2]Department of Mechanical Engineering, University of Ottawa, Canada

[3]Department of Health Sciences, Faculty of Medicine, Lund University, Lund, Sweden

[4]School of Human Kinetics, University of Ottawa, Ottawa, Ontario, Canada

4018 words

4.1 Abstract

Background: Fatigue-related alterations in neuromuscular control are thought to underpin the high incidence of non-contact lower-limb injuries that occur in the later stages of football, handball, and other running-dominant sports. Yet few studies have examined how progressive fatigue during high-intensity sessions, similar to those commonly performed by recreational runners and football players, reshapes multi-muscle activation patterns when athletes maintain a constant running speed.

Purpose: Determine the effect of oxygen uptake during an 85% VO2 max high-intensity testing on muscle activation using electromyography (EMG) in healthy athletes.

Methods: Seven recreationally trained adults (24.3 ± 3.2 y) completed the run on an instrumented treadmill. Whole-body kinematics, ground-reaction forces, and bilateral surface EMG of quadriceps, hamstrings, gastrocnemii, and gluteus medius were sampled pre- (0 min), mid- (15 min), and post-exercise (30 min). EMG median frequency (MF), integrated activity (iEMG), and RMS (power) measures, and EMG amplitudes were normalized to maximal voluntary isometric contractions. Physiological load (VO2/kg, heart rate, Borg, Respiratory Quotient) was recorded continuously. Repeated-measures ANOVA, and statistical parametric mapping tested fatigue effects ($\alpha = 0.05$).

Results: VO2/kg remained stable (~45 $mL \cdot kg^{-1} \cdot min^{-1}$), but HR (+17.5%, $p < 0.01$) and Borg (+45.7%, $p < 0.01$) both increased, suggesting progressive fatigue. Sagittal-plane hip, knee, and ankle angles changed <3° relative to baseline, indicating no significant altered running mechanics. In contrast, iEMG, and power declined in the lateral gastrocnemius, rectus femoris, vastus lateralis, and gluteus medius ($\eta^2_p \geq 0.46$), accompanied by MF increase in the gastrocnemii, and semitendinosus.

Conclusion: Thirty minutes of sustained high-intensity running provoked substantial neuromuscular fatigue despite limited kinematic changes. The decoupling of muscle activation from kinematic changes in biomechanics suggests athletes may appear technically sound while operating in a physiologically vulnerable state. Targeted conditioning to improve gastrocnemius, quadriceps, and hip-stabilizer endurance, alongside in-play fatigue monitoring, may reduce late-game injury risk.

291 words

Keywords: neuromuscular fatigue; surface EMG; running biomechanics; injury prevention; VO2 max; statistical parametric mapping

4.2 Introduction

Running is one of the most common and accessible forms of physical activity, serving as a fundamental movement pattern in various sports, and a primary mode of exercise for individuals across all fitness levels. Its popularity stems from its low cost, ease of access, and well-documented benefits for cardiovascular and musculoskeletal health. Regular running has been associated with improved aerobic capacity, enhanced neuromuscular function, and reduced risk of chronic diseases, making it a widely adopted form of exercise for both recreational and competitive athletes (Lee et al., 2014; Pollock et al., 1998).

In team sports such as football (soccer), rugby, and handball, running is a key determinant of performance, requiring athletes to sustain prolonged aerobic efforts interspersed with frequent high-intensity sprints, sudden changes in direction, and rapid accelerations and decelerations (Garrett et al., 2019). These repeated movements impose substantial physiological demands on the body, particularly on the lower limb musculoskeletal system. Among the various joints involved, the knee is particularly vulnerable to overuse, and fatigue-related injuries, which are common in endurance-based and high-intensity sports. In football, for instance, a significant proportion of injuries occur in the later stages of a match, when fatigue becomes a dominant factor, leading to compromised movement mechanics and reduced neuromuscular control (Chahla et al., 2018; Ekstrand et al., 2011; Pangrazio, 2016; Wilke et al., 2016). Understanding how fatigue influences neuromuscular function and joint stability during high-intensity running is therefore crucial for injury prevention and performance optimization.

Although extensive research has examined knee injury biomechanics, far fewer studies have investigated how fatigue-induced neuromuscular alterations affect lower-limb function during sport-specific running. Carvalho et al. (2023) addressed this gap by showing that lower-limb extensor fatigue significantly increases the sample entropy of hip, knee, and ankle joint

kinematics—indicative of reduced movement regularity during treadmill running, with impairments persisting for at least 20 minutes post-fatigue. Fatigue resulting from prolonged high-intensity exercise is known to compromise neuromuscular control, altering muscle activation patterns, joint loading, and movement efficiency (Alba-Jiménez et al., 2022; Paquette and Melcher, 2017). These changes can degrade running mechanics, amplify ground reaction forces (GRF), and heighten susceptibility to non-contact injuries (Gao et al., 2023; Luo et al., 2019). Electromyography (EMG) is widely used to assess neuromuscular fatigue, with typical findings including decreased median frequency (reflecting slower motor unit conduction velocity) and increased amplitude (indicating compensatory motor unit recruitment) derived from isolated muscle tests or controlled treadmill protocols with frequent rest breaks (Collins et al., 2018; De Luca, 1997; Farina et al., 2004; Garrett et al., 2023; Place et al., 2004; Zebis et al., 2011). However, these methodologies may not replicate the dynamic, progressive fatigue conditions athletes experience in real-world competition.

Another limitation of existing research is the tendency to examine fatigue effects on individual muscles rather than considering the coordinated function of multiple lower-limb muscle groups. Running and sport-related movements require a complex interplay between key muscle groups, including the quadriceps, hamstrings, and gastrocnemius, which collectively contribute to knee stabilization, propulsion, and shock absorption (Rimmer et al., 2020). Fatigue-induced disruptions in intermuscular coordination can lead to inefficient movement patterns, increased joint stress, and a greater risk of injury (Enoka, and Duchateau, 2008). For example, reduced hamstring activation relative to the quadriceps can impair knee joint stability, potentially increasing the risk of anterior cruciate ligament (ACL) injuries (Nicol et al., 2006; Zebis et al., 2011). Despite these concerns, few studies have examined how progressive fatigue alters neuromuscular activation across multiple lower-limb muscles during sustained high-intensity running.

VO2 max, as a validated measure of the cardiorespiratory system's maximal oxygen-transport capacity (Hawkins et al., 2007), directly shapes how muscles resist fatigue by governing oxygen delivery for mitochondrial ATP synthesis (Coen et al., 2013; Cramer and Jay, 2016; Miller et al., 2014; Millet, 2011). Athletes with higher VO2 max can sustain oxidative phosphorylation longer, slowing the shift to anaerobic glycolysis, and the build-up of metabolites that impair excitation–contraction coupling and precipitate neuromuscular fatigue (Barstow et al., 1994; Goodall et al., 2015). In practice, this translates to more stable electromyographic patterns, preserving median frequency and moderating amplitude increases thereby maintaining coordinated muscle activation and consistent joint-loading throughout prolonged, high-intensity running (Esteve-Lanao et al., 2007). Yet, despite these mechanistic links, few investigations have directly correlated individual VO2 max profiles with neuromuscular fatigue markers and the associated biomechanical adaptations during high-intensity running, leaving a critical gap in our understanding of how aerobic fitness modulates fatigue resistance and injury susceptibility.

In response to these gaps, this study will determine the effect of oxygen uptake during an 85% VO2 max high-intensity running protocol on lower-limb muscle activation, measured via surface EMG, in healthy, trained athletes. Specifically, we address two research questions: (1) How does increasing VO2 uptake at 85% VO2 max alter EMG amplitude in the quadriceps, hamstrings, and gastrocnemius, and (2) As fatigue develops, what changes occur in joint kinematics, and how are these changes related to concurrent shifts in EMG activity?

We hypothesize that, first, rising VO2 uptake will increase EMG amplitude due to greater motor unit recruitment and increased neural drive in response to escalating metabolic demands. Second, we hypothesize that lower-limb joint kinematics will remain largely preserved across fatigue stages, with only limited changes in joint angles across the gait cycle. Despite preserved kinematic patterns, maintaining running mechanics under fatigue is expected to require

progressively greater neuromuscular effort, potentially increasing metabolic cost and physiological strain. Understanding this dissociation between apparent movement quality and underlying neuromuscular fatigue has important implications for injury risk, training optimization, and performance monitoring during high-intensity running.

4.3 Methods

4.3.1 Participants

Seven uninjured (6 males, 1 female) adults (age =24.29 ± 3.2 years, height = 173.54 ± 5.89 cm, mass = 71.59 ± 6.51 kg, BMI = 23.73 ± 1.26 kg/m^2, Tegner scale = 6.29 ± 1.7). All participants were right-leg dominant. Leg dominance was based upon the foot they would use to kick a football (soccer ball) a maximum distance. Participants were included if they reached a minimum score of 5 on the Tegner scale, had not sustained an injury to their lower extremities within the past six months that resulted in missed training sessions or competitive events, and did not suffer from any form of cardiovascular or neurological conditions. All participants read and signed a letter of informed consent approved by the local Ethics Review Authority, the diary number for the review at the Ethics Review Authority is 2024-04208-1.

4.3.2 Data Collection

Upon arrival, participants were provided with tight-fitting spandex shorts and short-sleeve shirts to allow unobstructed access to anatomical landmarks and reduce sensor movement during running. Anthropometric measurements, including height, weight, leg length, shank length, leg width, ankle width, and anterior/posterior superior iliac spine distances, were recorded to standardize biomechanical modelling.

Surface electromyography (sEMG) electrodes (Ultium, 16 channels, Noraxon, USA) were placed bilaterally on the quadriceps, hamstrings, gastrocnemius, and gluteus medius and collected at 2000 Hz, following the SENIAM guidelines (Hermens et al., 2000) for optimal signal

acquisition. Participants then performed a 3-minute warm-up on a stationary bicycle (Monark 828E, Sweden) at a self-selected resistance. This was followed by maximal voluntary isometric contractions of the hip, knee, and ankle musculature using an isokinetic dynamometer (System 4 Pro, Biodex Medical Systems, USA) to establish reference contractions for EMG normalization.

After the strength assessments, 56 retroreflective markers (14 mm diameter) were placed on anatomical landmarks, and in cluster sets based upon the Qualisys Sports marker set. Kinematic data were collected at 200 Hz using infrared motion capture cameras (Arqus A9, Qualysis, Sweden), while kinetic data from an embedded force plate (Arsalis, Belgium) within an instrumented treadmill (HP Cosmos, Germany) were sampled at 1000 Hz. Physiological data were collected using the K5 metabolic cart (Cosmed, Italy) in the breath-by-breath mode.

Prior to the main running protocol, participants completed a brief familiarization phase, consisting of a short walking trial at 5 km/h and a light jog at 8 km/h. They then proceeded with the 30-minute high-intensity threshold run, performed at 85% of their previously determined VO2 max on an instrumented treadmill set to a 1% incline. Previous VO2 max values were obtained from a first visit which occurred within two weeks of the follow up session to standardize the high-intensity threshold run intensity. This protocol was adapted from the work of Hespanhol Junior et al. (2013) and Quammen et al. (2012) to better replicate the running conditions typically encountered in football and recreational outdoor running.

Data were recorded at 5-minute intervals for 30 seconds, with each recording followed by a self reported exertion level (Borg).

4.3.3 Data Processing

Kinematic marker trajectories collected during the test were low-pass filtered using a fourth-order dual-pass Butterworth filter with a 6 Hz cutoff. Joint angles for the hip (flexion, abduction,

rotation), knee (flexion), and ankle (flexion, abduction, rotation) were then computed using standard joint coordinate system definitions based on the ISB recommendations for the lower limb (Grood and Suntay, 1983; Wu et al., 2002).

Following filtering, gait events were identified using local maxima in the anterior–posterior heel marker trajectory to detect heel strikes. Gait cycles were defined from heel strike to subsequent ipsilateral heel strike and joint angle time series for each cycle were resampled to 101 data points (0–100% gait cycle).

Different processing approaches were applied to EMG signals depending on the analysis context. For maximal voluntary isometric contractions (MVICs), EMG signals were band-pass filtered using a fourth-order Butterworth filter (20–450 Hz), followed by full-wave rectification. A 51-frame window centered on the maximum peak value (25 frames before and after) was used to compute the average peak amplitude, which was then used for normalizing EMG amplitudes collected during running. For time-domain EMG variables (RMS, iEMG), signals followed the same filtering as the MVICs EMG signals. All data were processed using custom MATLAB scripts (vR2023b).

4.3.4 Statistical Analysis

To assess fatigue effects across the exercise protocol (0^{th} min (pre-), 15^{th} min (mid-), and 30^{th} min (post-) exercise), one-way repeated measures ANOVAs were performed in JASP (v0.18.1.0, Amsterdam, Netherlands) with statistical significance set at $\alpha = 0.05$. Significant main effects were followed by pairwise post hoc comparisons, with Holm–Bonferroni corrections.

Dependent variables were grouped into three domains: EMG variables (average median frequency, normalized integrated EMG (iEMG), and normalized RMS (power), with iEMG, and RMS scaled to each muscle's maximal value recorded during its MVIC trial); physiological variables (Borg scale rating, heart rate, respiratory quotient (RQ), and VO2/kg); and kinematic

variables. Kinematic data were analyzed via one-dimensional statistical parametric mapping (SPM) repeated measures ANOVA across the three time points using all valid cycles. When a significant main effect was detected, post hoc SPM paired t-tests were conducted between time points (pre vs. mid, pre vs. post, and mid vs. post). To control for multiple comparisons across these pairwise tests, significance was adjusted using a Bonferroni-corrected threshold (α = 0.05/3). Statistical significance for both omnibus and post hoc analyses was determined using random field theory (RFT)-based thresholds, which account for multiple comparisons across the time-normalized gait cycle. Following time normalization of each stride to 100% of the gait cycle, stride data were averaged within each participant and condition to avoid artificially inflating the sample size. The minimum number of available strides (33) was used to ensure consistent cycle coverage across pre-, mid-, and post-exercise trials before averaging. These participant-level averaged waveforms were then entered into the SPM repeated-measures analysis.

In all analyses, Mauchly's test of sphericity was performed, and a Greenhouse–Geisser correction was applied when sphericity assumptions were violated.

4.4 Results

4.4.1 Physiological parameters

As shown in Table 4.1 participants maintained a consistently high VO2/kg throughout the trial (p = 0.787, η_p^2 = 0.016), along with an elevated RQ (p = 0.45, η_p^2 = 0.123), indicating sustained exertion. Despite this, physiological markers of fatigue were evident. HR increased significantly by 17.5% from baseline (p <0.01, η_p^2 = 0.883), and perceived exertion (Borg scale) rose by 45.7% (p <0.01, η_p^2 = 0.908), confirming an increasing physiological and subjective strain over time.

Table 4.1: Mean (± SD) values of key physiological parameters averaged over 30-second intervals at pre-, mid-, and post-exercise time points during a 30-minute high-intensity running trial. Statistically significant pairwise differences between fatigue stages are indicated by an asterisk (*) for differences from pre-fatigue and a dagger (†) for differences from mid-fatigue, based on Bonferroni-adjusted comparisons ($p < 0.05$).

Parameter	Pre-Fatigue	Mid-Fatiguing	Post-Fatigue
VO2 ($mL \cdot kg^{-1} \cdot min^{-1}$)	44.2 ± 6.9	45.2 ± 8.3	45.0 ± 7.6
RQ	1.03 ± 0.09	1.04 ± 0.11	1.08 ± 0.12
HR (bpm)	161 ± 11	181 ± 6*	190 ± 7*†
Borg	12 ± 1	15 ± 2*	17 ± 2*†

4.4.2 Kinematic parameters

The joint kinematics of the lower limbs were analyzed at three time points: pre-exercise, mid-exercise, and post-exercise. Mean joint angles for hip, knee, and ankle, and their corresponding standard deviations were plotted in Appendix Figures A 4.1-4.13.

4.4.2.1 Hip

In the sagittal plane, hip flexion–extension followed the expected double-peak gait pattern, with peak extension occurring at approximately 45% of the gait cycle (Figure A 4.1). A significant difference was identified in the right hip flexion during late swing (~60–70% of the gait cycle) (p =0.012, η_p^2 = 0.643), corresponding to an increase in hip flexion of approximately 1.8–2.4° in the post-fatigue condition relative to pre-fatigue. No significant differences were observed for the left hip. In the frontal plane, the right hip demonstrated a significant difference during 70–85% of the gait cycle (p =0.001, η_p^2 = 0.831) with greater hip abduction in the mid- and post-fatigue conditions. The magnitude of this difference ranged from ~1.5 to 2.0° compared with pre-fatigue (Figure A 4.3).

In the transverse plane, hip internal–external rotation exhibited greater variability across the gait cycle relative to other planes. A single significant difference was observed at the beginning of stance (~0–10%) (p =0.047, η_p^2 = 0.142) with a mean rotational difference of approximately 1° between conditions. No additional significant changes were detected (Figure A 4.5).

4.4.2.2 Knee

Knee flexion–extension followed a characteristic gait pattern, with peak flexion observed during the swing phase (~60–70% of the cycle; Figure A 4.7). A significant difference was detected in the right leg during late swing (~80–90%), (p =0.017, η_p^2 = 0.681) (Figure A 4.7), corresponding to a mean increase in knee flexion of approximately 2–3° in the post-fatigue condition relative to pre-fatigue. No significant differences were observed for the left knee.

4.4.2.3 Ankle

No statistically significant differences were observed in ankle kinematics across the sagittal, frontal, or transverse planes for either limb throughout the gait cycle (Figures A 4.9–A 4.14).

4.4.3 Lower limb EMG

Figures 4.1 to 4.3 present the results of the neuromuscular analysis for each muscle of interest in both legs, detailing changes in average median frequency, normalized RMS (power), and normalized iEMG across the pre (0 min), mid (15 min), and post (30 min) time points.

4.4.3.1 Biceps Femoris

The right biceps femoris exhibited a significant reduction in iEMG over time (p = 0.01, η_p^2 = 0.55), while the left biceps femoris remained unchanged (p = 0.87, η_p^2 = 0.02). Power decreased on the right side (p = 0.08, η_p^2= 0.41) though the left side remained stable (p = 0.80, η_p^2= 0.04). No significant changes were observed in median frequency for either leg.

4.4.3.2 Gluteus Medius

The right gluteus medius exhibited a significant reduction in iEMG over time (p = 0.04, η_p^2 = 0.51), while the left side showed no significant change (p = 0.40, η_p^2 = 0.14). No significant changes were detected in median frequency or power.

4.4.3.3 Lateral Gastrocnemius

The left lateral gastrocnemius exhibited a significant reduction in iEMG over time (p = 0.01, η_p^2 = 0.58), with a similar, though slightly weaker, trend on the right (p = 0.06, η_p^2= 0.47). Power decreased significantly on both sides (p = 0.02, η_p^2= 0.47 for left, p = 0.02, η_p^2= 0.60 for right). The right leg showed a significant increase in median frequency (p = 0.04, η_p^2 = 0.53).

4.4.3.4 Medial Gastrocnemius

The right medial gastrocnemius median frequency significantly increased (p = 0.038, η_p^2 = 0.68). No significant changes were detected in iEMG and Power.

4.4.3.5 Rectus Femoris

The left rectus femoris iEMG exhibited a significant reduction (p = 0.05, η_p^2= 0.40), while the right side remained unchanged (p = 0.28, η_p^2= 0.19). No significant changes were detected in power or median frequency.

4.4.3.6 Semitendinosus

Power declined bilaterally, though the effect was more pronounced in the left leg (p = 0.02, η_p^2 = 0.50) compared to the right (p = 0.07, η_p^2 = 0.43). The right semitendinosus exhibited a significant increase in median frequency (p = 0.01, η_p^2 = 0.55), suggesting changes in neuromuscular activation patterns.

4.4.3.7 Vastus Lateralis

The left vastus lateralis iEMG exhibited a significant reduction (p = 0.02, η_p^2 = 0.49), as did power (p = 0.03, η_p^2 = 0.46). The right vastus lateralis followed a similar trend, with iEMG reducing (p = 0.01, η_p^2 = 0.69), and power declining (p = 0.03, η_p^2 = 0.58). No significant changes were observed in median frequency.

4.4.3.8 Vastus Medialis

No significant changes were found in iEMG for either left (p = 0.66, η_p^2 = 0.07) or right (p = 0.09, η_p^2 = 0.33) VMO. Power showed a mild decline, though not significant (p = 0.27, η_p^2 = 0.20 for left, p = 0.13, η_p^2 = 0.33 for right). The right VMO median frequency decreased slightly, though not significantly (p = 0.31, η_p^2 = 0.17).

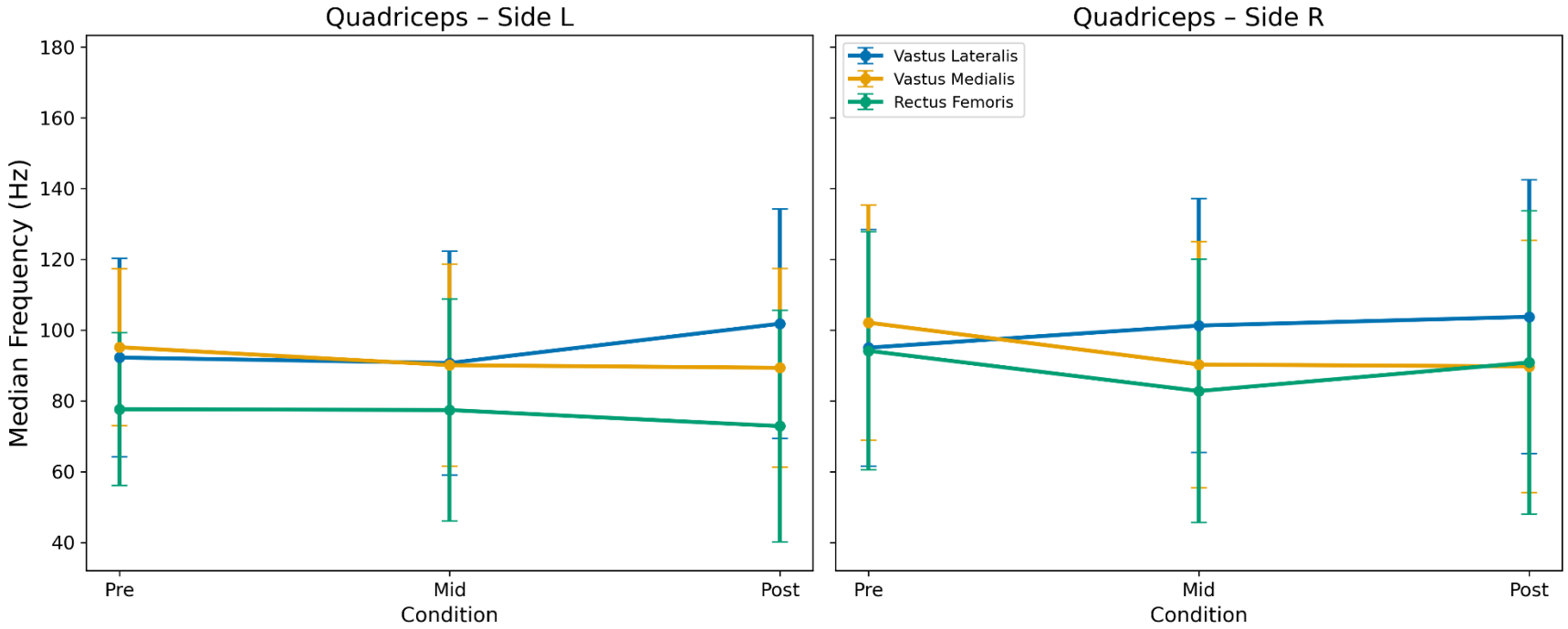
Quadriceps – Side L
Quadriceps – Side R
Median Frequency (Hz)
180
160
140
120
100
80
60
40
Pre
Mid
Post
Condition
Vastus Lateralis
Vastus Medialis
Rectus Femoris

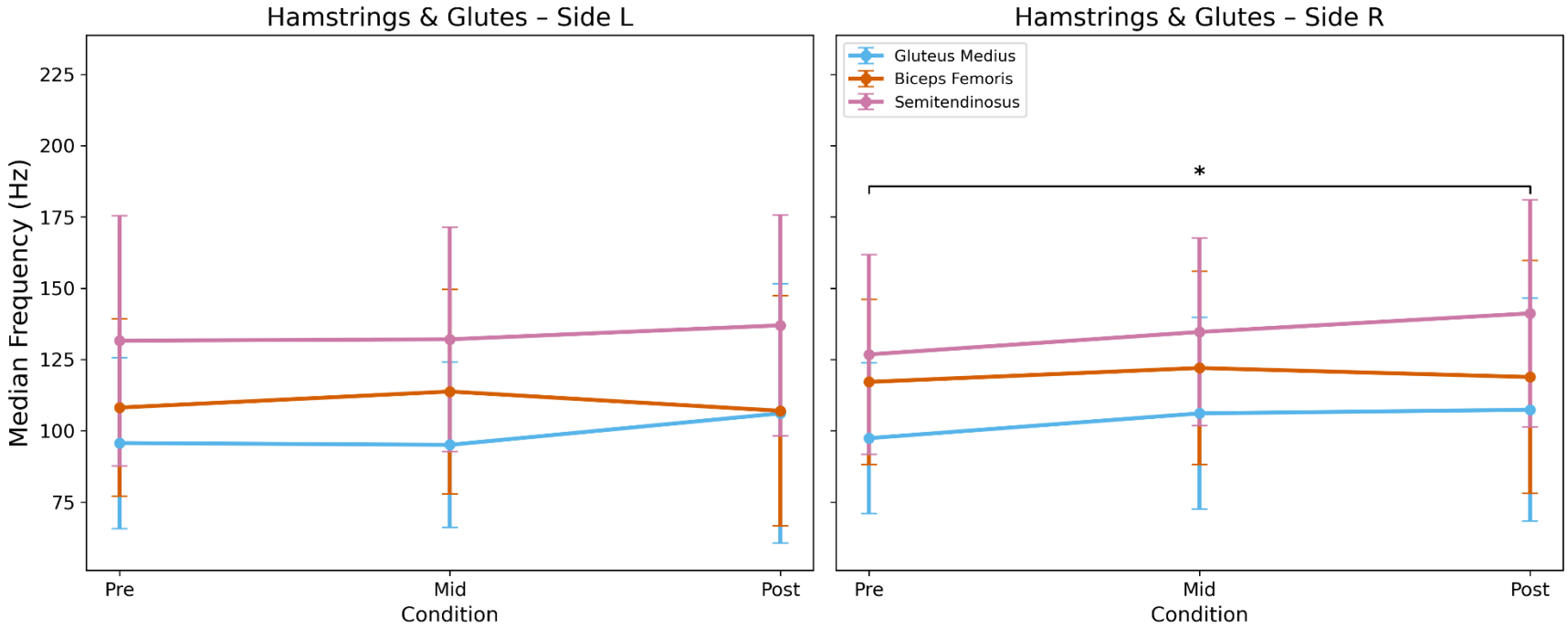
Hamstrings & Glutes – Side L
Hamstrings & Glutes – Side R
Median Frequency (Hz)
225
200
175
150
125
100
75
Pre
Mid
Post
Condition
Gluteus Medius
Biceps Femoris
Semitendinosus
*

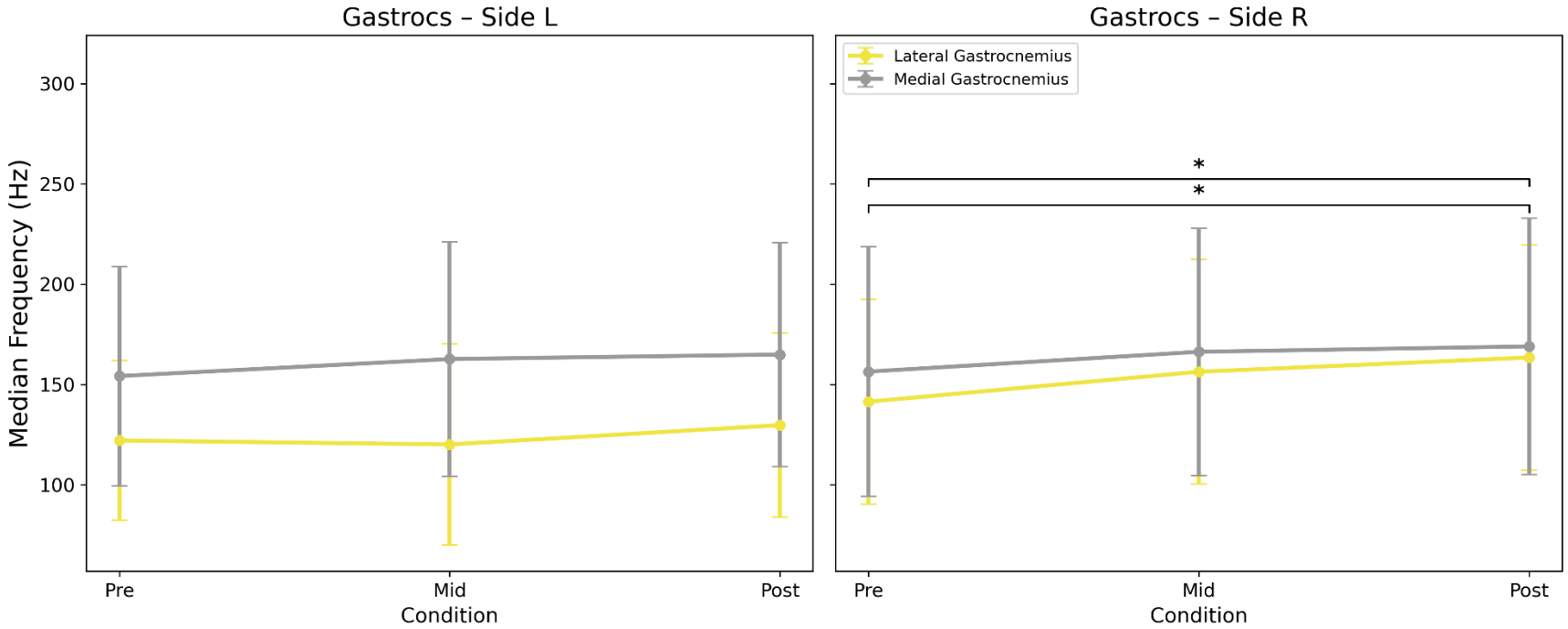

Figure 4.1: Changes in lower-limb muscle electromyography median frequency across stages of a high-intensity treadmill running fatigue protocol. Mean ± standard deviation of surface electromyography (EMG) median frequency, expressed in hertz (Hz), for major lower-limb muscle groups of the left (L) and right (R) legs during a high-intensity treadmill running protocol. Muscles are grouped by anatomical function and presented separately for the quadriceps (vastus lateralis, vastus medialis, rectus femoris), hamstrings and gluteals (gluteus medius, biceps femoris, semitendinosus), and gastrocnemius muscles (medial and lateral heads). Values are shown for three fatigue stages: pre-fatigue (baseline, 0 minutes), mid-fatigue (15 minutes), and post-fatigue (30 minutes) of continuous running performed at a fixed intensity corresponding to the experimental fatigue protocol. Median frequency was calculated from the power spectral density of the processed EMG signals using identical analysis procedures across conditions and participants. Stage-related differences were assessed using repeated-measures analysis of variance (ANOVA). These data summarise within-session changes in the spectral content of muscle activation with progressive fatigue. Statistically significant differences across stages are indicated by an asterisk (*), while trends toward significance are denoted by (†) ($p < 0.05$ and $p < 0.10$, respectively).

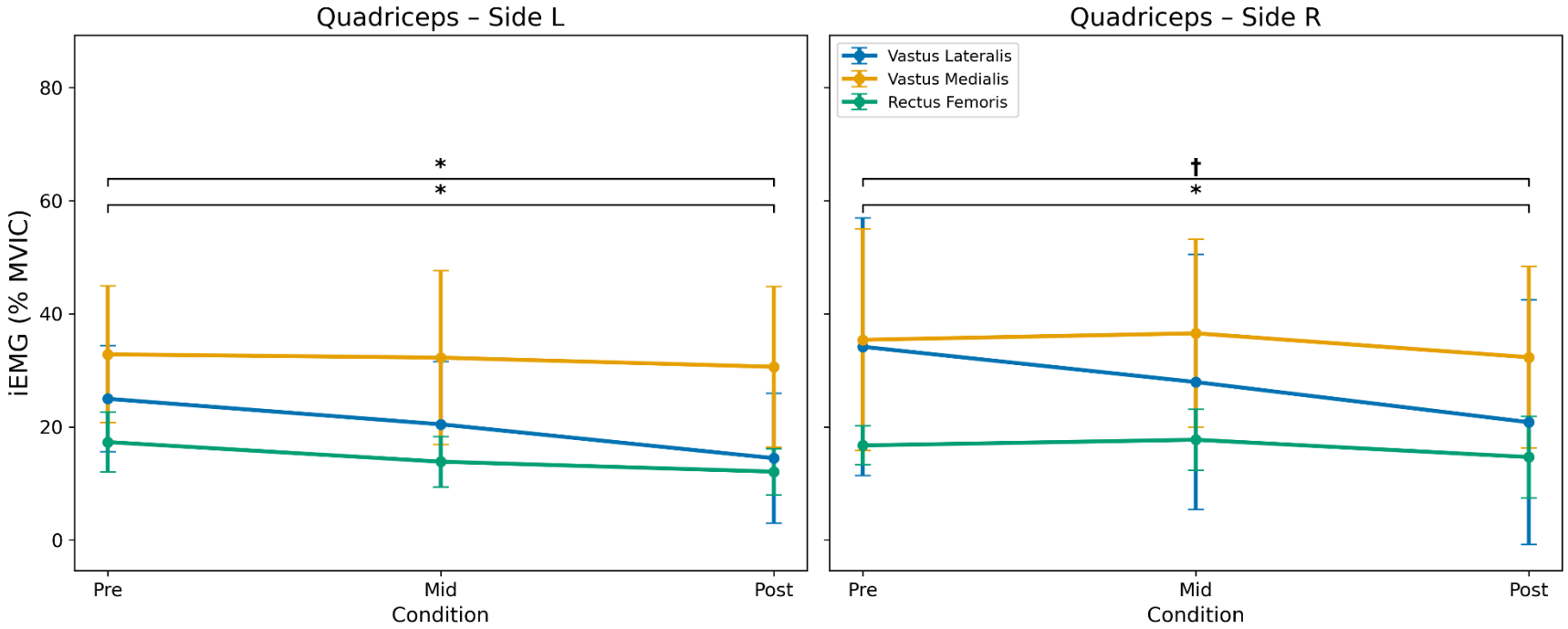
Quadriceps – Side L
Quadriceps – Side R
Vastus Lateralis
Vastus Medialis
Rectus Femoris
iEMG (% MVIC)
0
20
40
60
80
*
*
†
*
Pre
Mid
Post
Condition

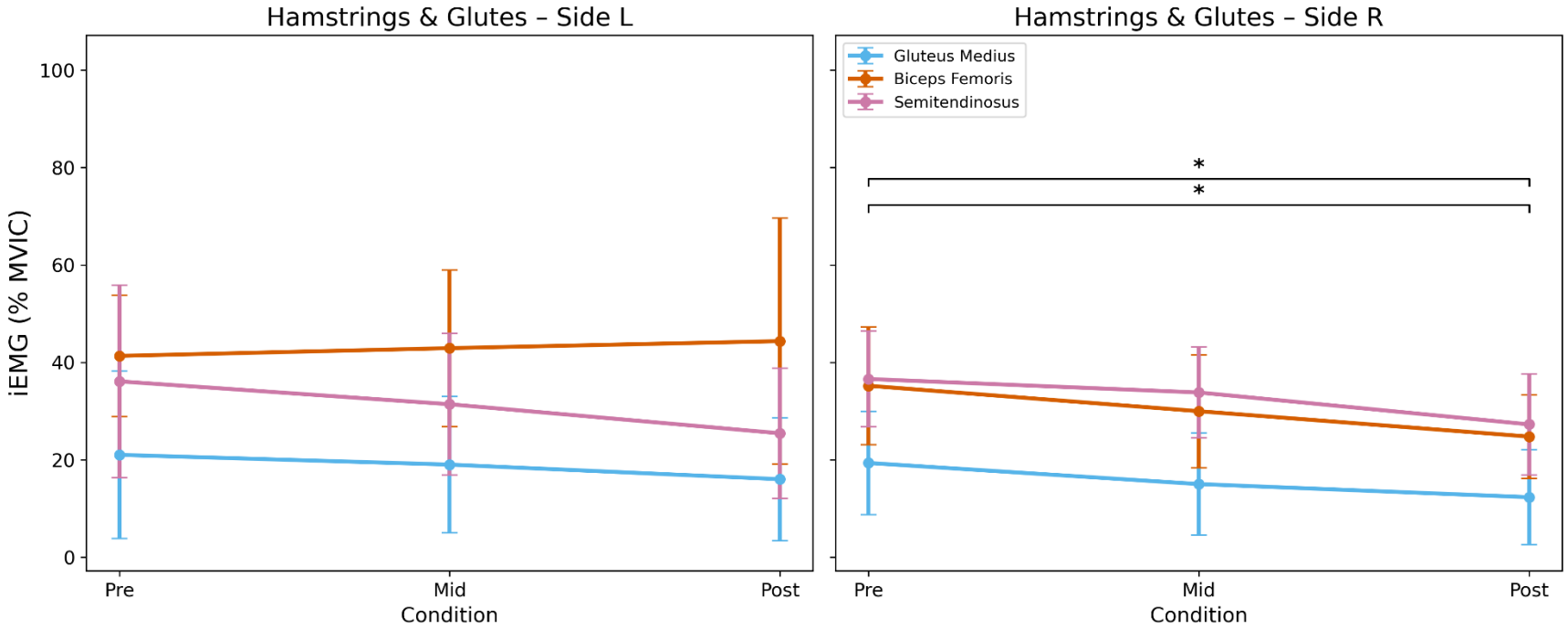
Hamstrings & Glutes – Side L
Hamstrings & Glutes – Side R
iEMG (% MVIC)
100
80
60
40
20
0
Pre
Mid
Post
Condition
Gluteus Medius
Biceps Femoris
Semitendinosus
*
*

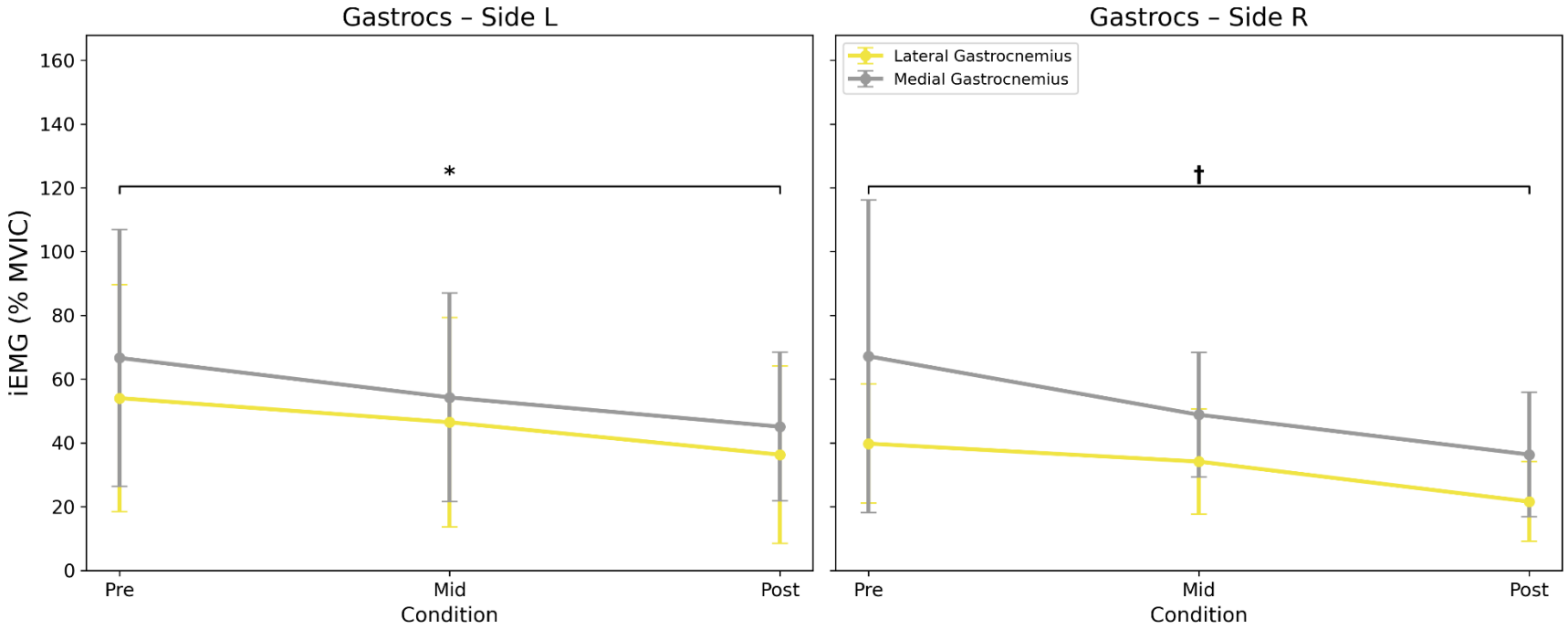

Figure 4.2: Changes in lower-limb integrated electromyography across stages of a high-intensity treadmill running fatigue protocol. Mean ± standard deviation of surface electromyography (EMG) integrated amplitude (iEMG), and expressed as a percentage of maximum voluntary isometric contraction (MVIC), for major lower-limb muscle groups of the left (L) and right (R) legs during a high-intensity treadmill running protocol. Muscles are grouped by anatomical function and presented separately for the quadriceps (vastus lateralis, vastus medialis, rectus femoris), hamstrings and gluteals (gluteus medius, biceps femoris, semitendinosus), and gastrocnemius muscles (medial and lateral heads). Values are shown for three fatigue stages: pre-fatigue (baseline, 0 minutes), mid-fatigue (15 minutes), and post-fatigue (30 minutes) of continuous running performed at a fixed intensity corresponding to the experimental fatigue protocol. Integrated EMG was computed by time-integrating the processed EMG signal over the analyzed gait cycles using identical procedures across conditions and participants. Stage-related differences were assessed using repeated-measures analysis of variance (ANOVA). These data summarise within-session changes in overall muscle activation magnitude with progressive fatigue. Statistically significant differences across stages are indicated by an asterisk (*), while trends toward significance are denoted by (†) ($p < 0.05$ and $p < 0.10$, respectively).

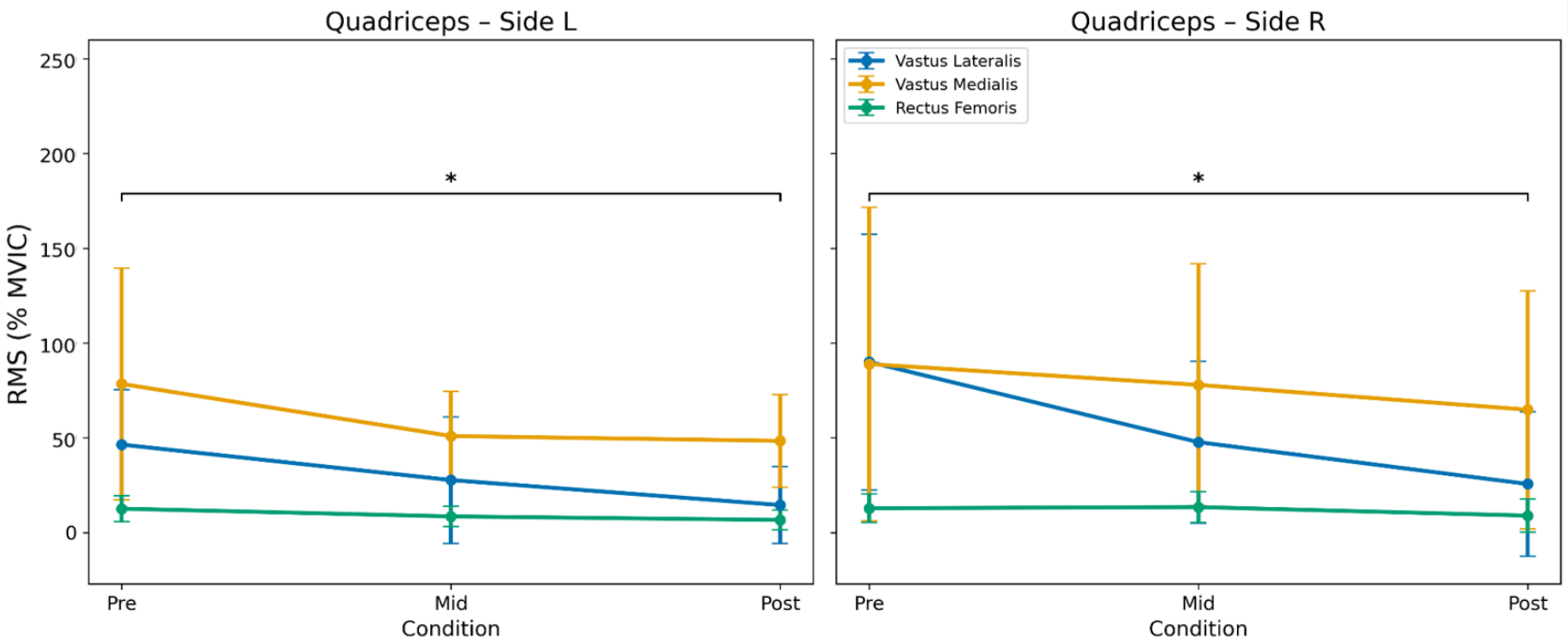
Quadriceps – Side L
Quadriceps – Side R
Vastus Lateralis
Vastus Medialis
Rectus Femoris
RMS (% MVIC)
250
200
150
100
50
0
*
*
Pre
Mid
Post
Condition

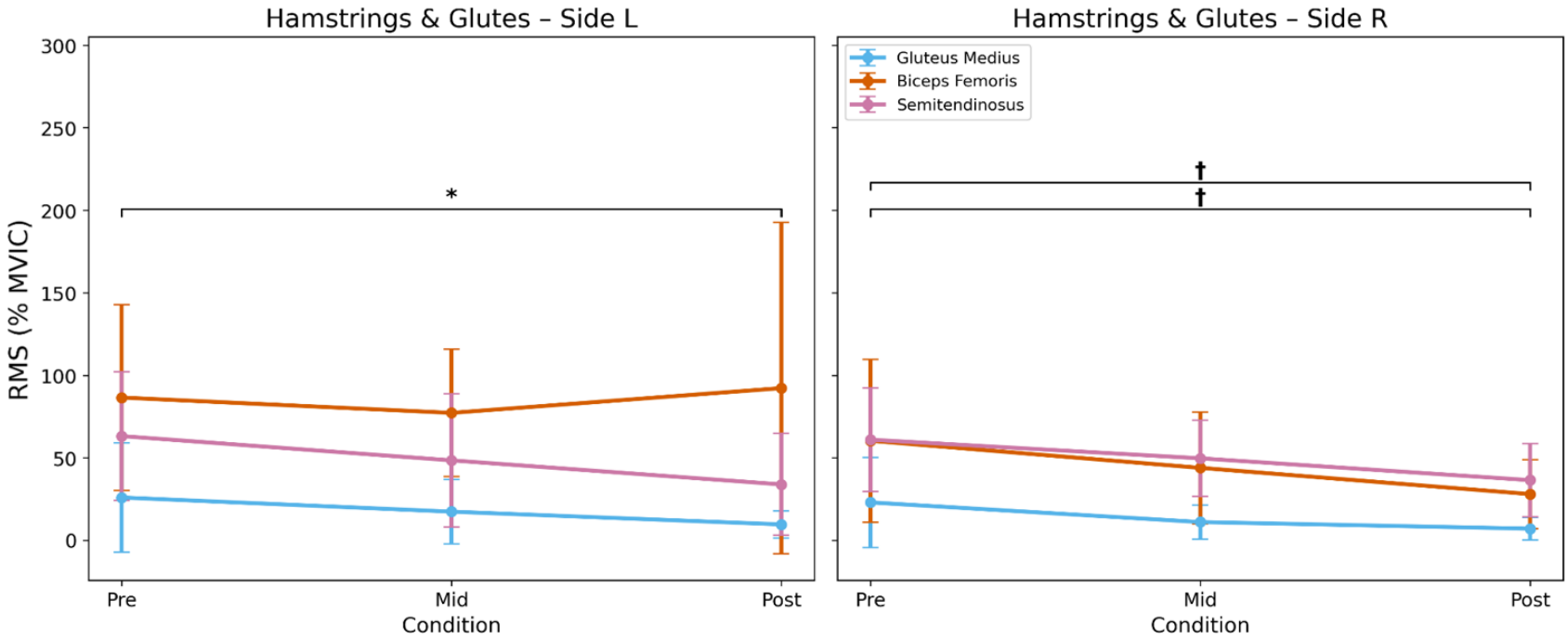
Hamstrings & Glutes – Side L
Hamstrings & Glutes – Side R
RMS (% MVIC)
300
250
200
150
100
50
0
*
†
†
Gluteus Medius
Biceps Femoris
Semitendinosus
Pre
Mid
Post
Condition

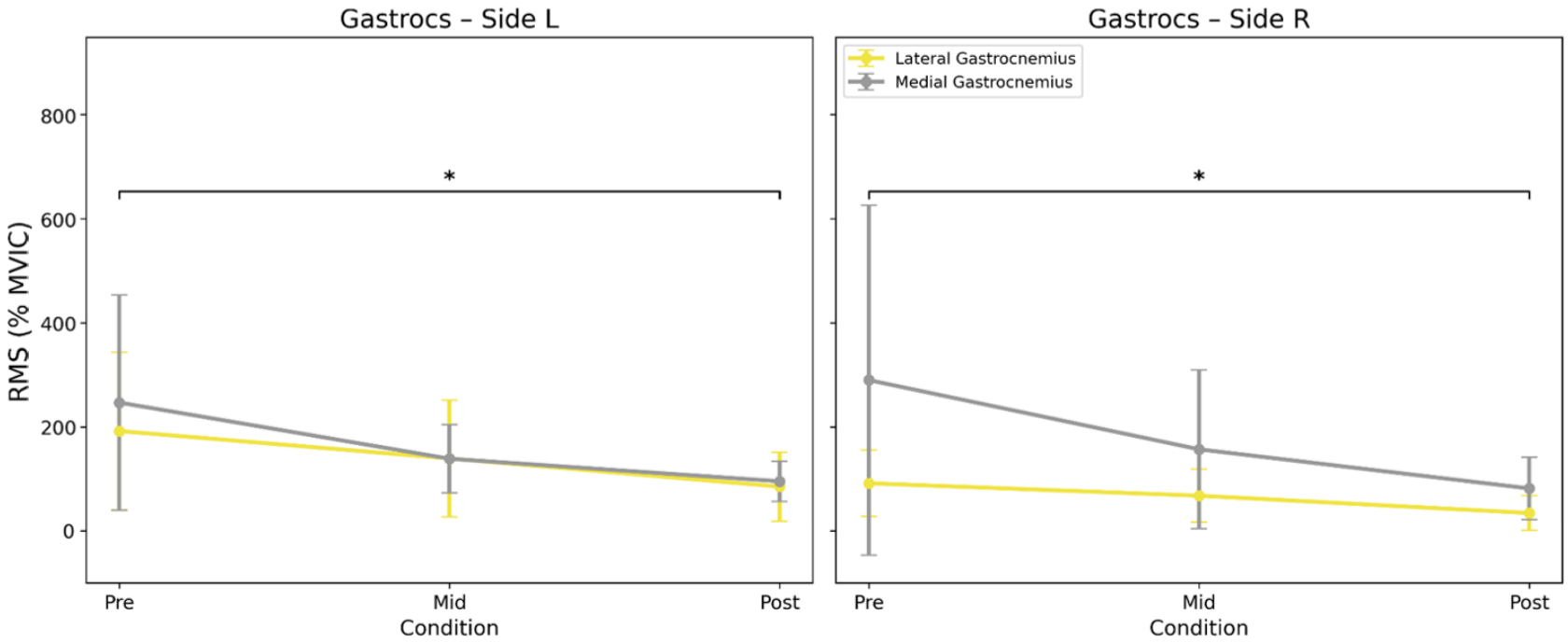

Figure 4.3: Changes in lower-limb electromyography root mean square amplitude across stages of a high-intensity treadmill running fatigue protocol. Mean ± standard deviation of surface electromyography (EMG) signal amplitude, quantified as root mean square (RMS) and expressed as a percentage of maximum voluntary isometric contraction (MVIC), for major lower-limb muscle groups of the left (L) and right (R) legs during a high-intensity treadmill running protocol. Muscles are grouped by anatomical function and presented separately for the quadriceps (vastus lateralis, vastus medialis, rectus femoris), hamstrings and gluteals (gluteus medius, biceps femoris, semitendinosus), and gastrocnemius muscles (medial and lateral heads). Values are shown for three fatigue stages: pre-fatigue (baseline, 0 minutes), mid-fatigue (15 minutes), and post-fatigue (30 minutes) of continuous running performed at a fixed intensity corresponding to the experimental fatigue protocol. RMS values were calculated from the processed EMG signals using identical analysis procedures across conditions and participants and normalized to MVIC. Stage-related differences were assessed using repeated-measures analysis of variance (ANOVA). These data summarise within-session changes in muscle activation amplitude with progressive fatigue. Statistically significant differences across stages are indicated by an asterisk (*), while trends toward significance are denoted by (†) ($p < 0.05$ and $p < 0.10$, respectively).

4.5 Discussion

The objective of this study was to examine the neuromuscular and kinematic response to fatigue induced by prolonged high-intensity steady-state running, with a focus on lower-limb muscle activation patterns and joint kinematics. Across the 30-minute trial, participants exhibited a consistent physiological strain, evidenced by significant increases in heart rate and perceived exertion, without significant changes in respiratory quotient, which remained very close to or above 1, and oxygen consumption. These markers confirm sustained aerobic demand and align with real-world exertion levels seen in competitive sport settings (Schlink et al., 2021; Willer et al., 2021).

Despite this sustained physiological load, joint kinematics remained largely consistent across the running cycle. Only minor, non-clinically relevant deviations, such as a 1–3° difference in right hip flexion and right knee flexion were observed. These small changes are within the expected range of measurement error (Willwacher et al., 2022), given the limitations expected by issues such as soft tissue artefact (Benoit et al., 2006). This stability in movement mechanics underscores that the neuromuscular changes observed in the EMG data are not a byproduct of altered biomechanics running technique but rather reflect genuine fatigue-induced shifts in muscle activation.

Notably, there was a progressive and significant decline in iEMG and mean power across key lower-limb muscles, particularly in the medial gastrocnemius, lateral gastrocnemius, rectus femoris, vastus lateralis, and gluteus medius. These muscles play essential roles in propulsion, stabilization, and shock absorption. The observed reductions in their activation, and therefore likely force-generating capacity, highlight the onset of neuromuscular fatigue as exercise progresses. In several cases, this was accompanied by increases in median frequency particularly in the medial and lateral gastrocnemius and semitendinosus, which may suggest compensatory recruitment of higher-threshold motor units to maintain performance under fatigue (Jewell et al., 2019; Schlink et al., 2021).

Changes in EMG spectral content and amplitude observed in this study may reflect multiple physiological mechanisms beyond simple fatigue-related declines in force production. For instance, increases in muscle temperature during prolonged exercise can elevate muscle fiber conduction velocity, leading to shifts in EMG frequency content independent of fatigue (Farina et al., 2004; Merletti and Parker, 2004). Conversely, metabolite accumulation, alterations in ion gradients, and reduced membrane excitability associated with peripheral fatigue may decrease conduction velocity, producing opposing spectral shifts (Allen et al., 2008; Enoka and Duchateau, 2008). In addition, changes in motor unit recruitment strategies, including increased recruitment of higher-threshold motor units or altered discharge rates and synchronization, may influence EMG amplitude without directly reflecting proportional changes in muscle force output (De Luca, 1997; Farina et al., 2014).

Methodological factors must also be considered when interpreting EMG signals during dynamic tasks such as running. Electrode placement, skin movement artefact, and signal processing choices—including filtering, rectification, and windowing—can introduce variability in both amplitude and frequency-domain measures (De Luca, 1997; Winter, 2009). Furthermore, the non-stationary nature of EMG signals during cyclic locomotion complicates spectral interpretation, particularly under fatigue conditions where motor unit behaviour is continuously evolving.

Taken together, these interacting physiological and methodological factors highlight the complexity of interpreting EMG changes during prolonged, fatiguing exercise. While the observed reductions in iEMG and alterations in frequency content are consistent with the development of neuromuscular fatigue, they should be interpreted within a multifactorial framework rather than as direct proxies of muscle force or fatigue alone.

Collectively, these findings support the idea that physiological fatigue precedes and drives neuromuscular fatigue during high-intensity endurance running (Glover and Chaudhari, 2024;

Willwacher et al., 2022). Since joint angles and overall movement mechanics remained stable, the changes in EMG amplitude and frequency can be attributed to fatigue-induced neural and muscular adaptations rather than mechanical compensations. This distinction is important: if mechanics remain intact while activation patterns deteriorate, athletes may be unknowingly operating in a fatigued, high-risk state without visible kinematic or kinetic red flags.

From a practical standpoint, this has direct implications for late-game injury prevention in sports like football or handball. As fatigue accumulates, neuromuscular function deteriorates while biomechanics appear unchanged, masking vulnerability. Diminished activation in stabilizing muscles such as the gluteus medius and gastrocnemius could compromise joint control, particularly around the knee and ankle. Although hamstring muscles are generally considered protective of the anterior cruciate ligament, fatigue-related alterations in neuromuscular coordination and force-sharing between muscle groups may nonetheless influence joint loading strategies during high-demand tasks.

These results emphasize the importance of conditioning strategies that extend beyond aerobic endurance to include neuromuscular fatigue resistance. Monitoring EMG markers throughout competition or developing in-game substitution and recovery protocols based on physiological fatigue thresholds could help mitigate injury risk. Future research should explore how these EMG trends evolve in actual game conditions, as well as whether targeted interventions, such as resistance training, neuromuscular retraining, or fatigue monitoring technologies, can sustain muscle activation profiles over time.

4.5.1 Limitations

Soft-tissue artefact may have affected the accuracy of joint kinematics, particularly during high-intensity movement where skin and soft tissues undergo greater displacement relative to the underlying bone. This movement can also influence EMG measurements because surface

electrodes deform with the skin, potentially introducing signal variability despite careful placement and standardized preparation procedures. Additionally, the volitional nature of a VO2 max test may have led to not all participants reaching true maximal effort during their first visit VO2 max testing which was used to standardize their steady state speed during the second visit, potentially affecting the uniformity of physiological strain.

Additionally, the relatively small sample size may limit the generalizability of the findings and reduce statistical power to detect subtle effects (Button et al., 2013). Furthermore, participants consisted of recreationally active individuals with similar training backgrounds, which may not fully represent highly trained or elite athletes. Differences in skill level, training history, and fatigue resistance could influence neuromuscular and physiological responses to prolonged running (Joyner and Coyle, 2008), and therefore the present findings should be interpreted within the context of this population.

4.6 Conclusion

This study demonstrated that thirty minutes of sustained, high-intensity running at 85% VO2 max elicited clear signs of neuromuscular fatigue marked by declines in integrated EMG and RMS in the gastrocnemius, quadriceps, and gluteus medius despite virtually unchanged lower-limb kinematics. The concurrent increases in EMG median frequency in the gastrocnemii and semitendinosus suggest compensatory recruitment of higher-threshold motor units as fatigue progressed.

These findings demonstrate that athletes can maintain apparent "technically sound" running mechanics even while critical stabilizing muscles are operating at diminished capacity. From an applied perspective, this decoupling between visible biomechanics and underlying neuromuscular state underscores the need for integrated late-game monitoring and tailored conditioning programs. Specifically, incorporating endurance training for the gastrocnemius, quadriceps, and hip-

stabilizers, alongside in-play fatigue monitoring (e.g., real-time EMG or heart-rate variability), may help identify and mitigate periods of elevated injury risk.

Future work should validate these laboratory findings in ecological game-play settings and explore whether interventions, such as targeted resistance protocols or dynamic substitution strategies, can sustain neuromuscular performance under fatigue. By bridging the gap between physiological load and injury prevention, such approaches have the potential to reduce non-contact lower-limb injuries in running-dominant sports and optimise athlete performance throughout the full duration of competition.

4.7 Appendix

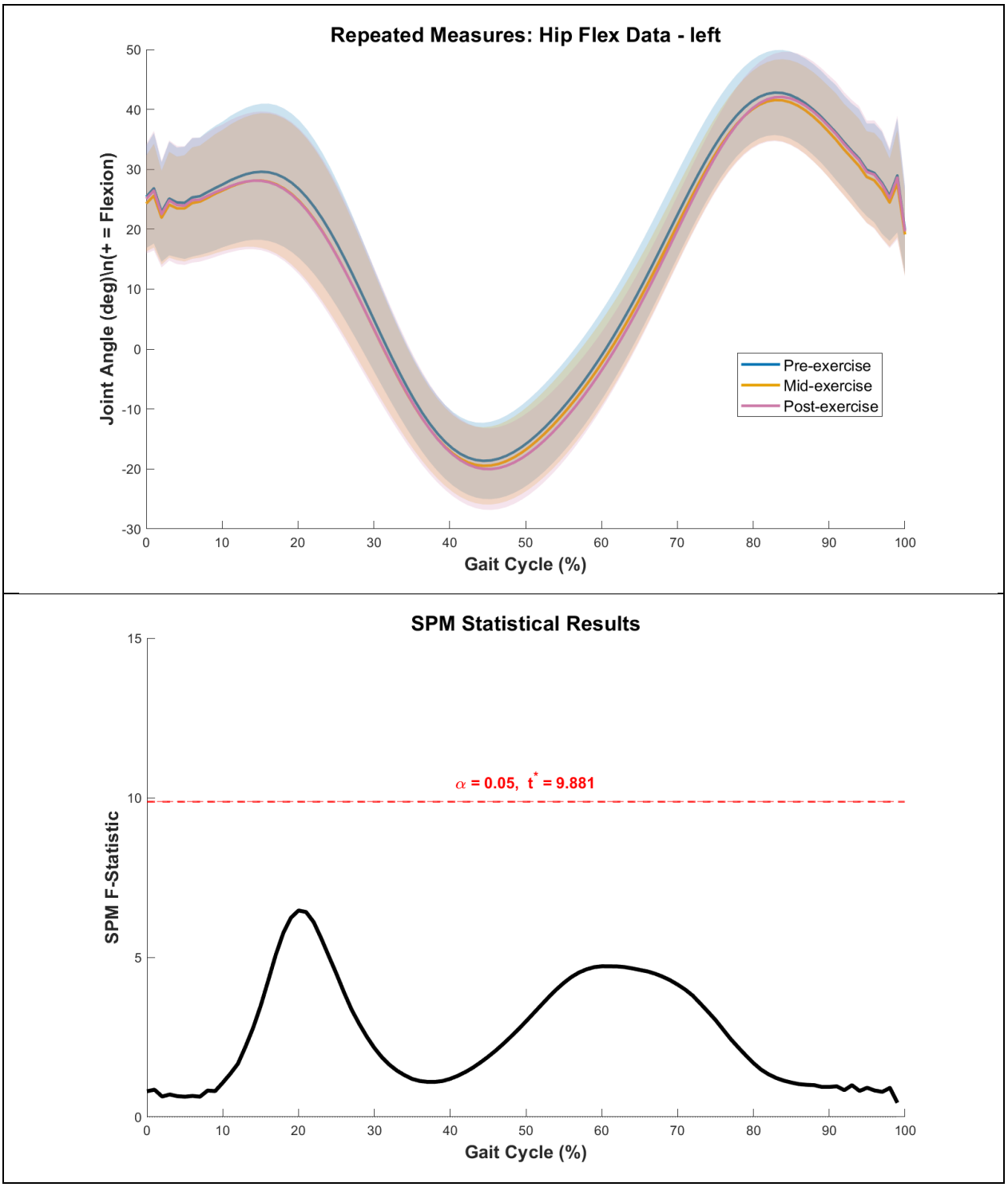

Figure A 4.1: Left-leg hip flexion–extension kinematics and SPM across the gait cycle. Top panel: mean left hip flexion angle (°) time-normalized to 0–100% for three time points: pre-exercise (blue), mid-exercise (red), and post-exercise (green). Shaded regions represent standard deviations. Bottom panel: SPM repeated-measures ANOVA F-statistic (black) for the left leg across the gait cycle with the α = 0.05 critical threshold (red dashed line; Fcrit=9.881). Supra-threshold intervals denote gait phases with significant differences among time points.

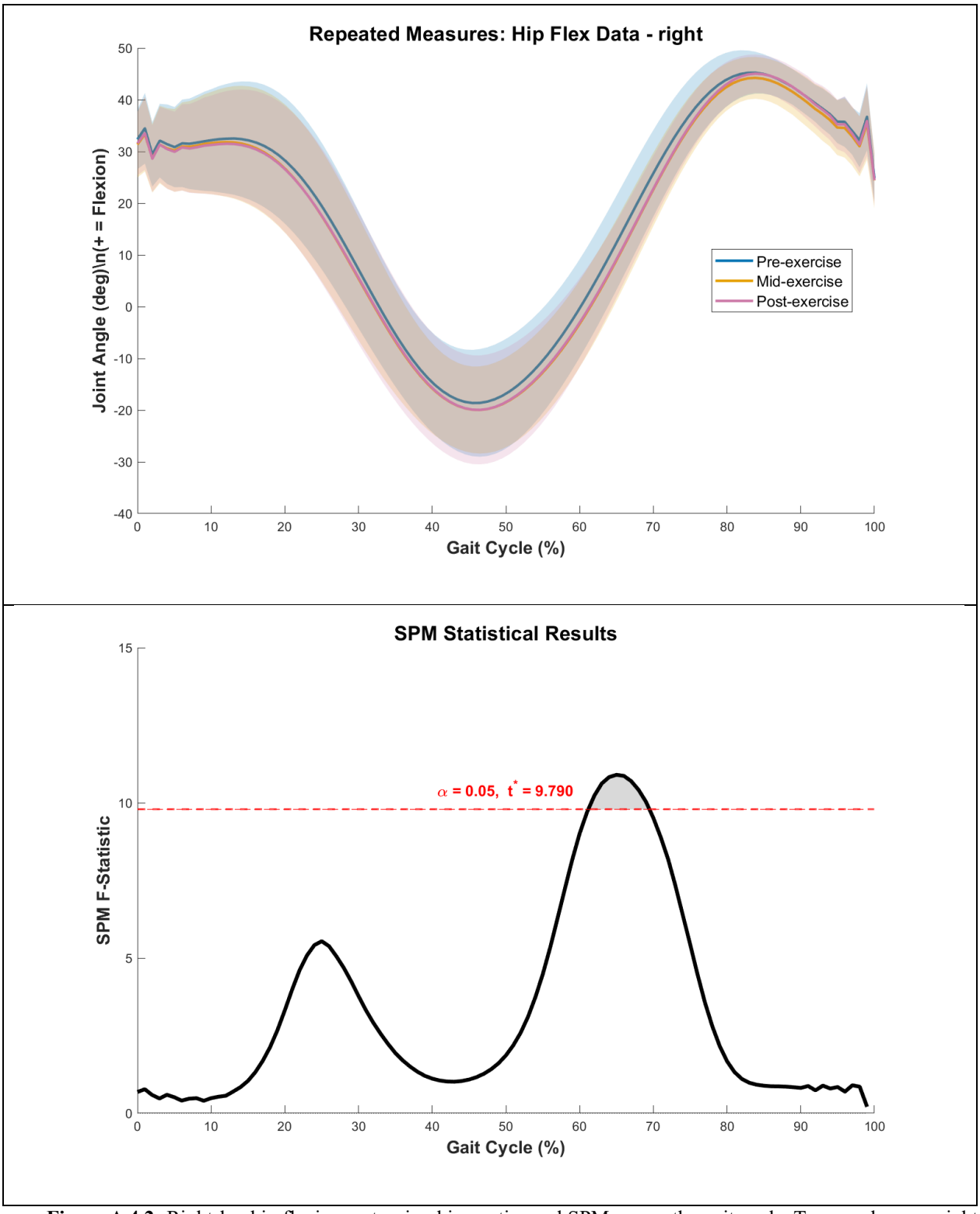

Figure A 4.2: Right-leg hip flexion–extension kinematics and SPM across the gait cycle. Top panel: mean right hip flexion angle (°) time-normalized to 0–100% for three time points: pre-exercise (blue), mid-exercise (red), and post-exercise (green). Shaded regions represent standard deviations. Bottom panel: SPM repeated-measures ANOVA F-statistic (black) for the right leg across the gait cycle with the α = 0.05 critical threshold (red dashed line; Fcrit=9.790). Supra-threshold intervals denote gait phases with significant differences among time points.

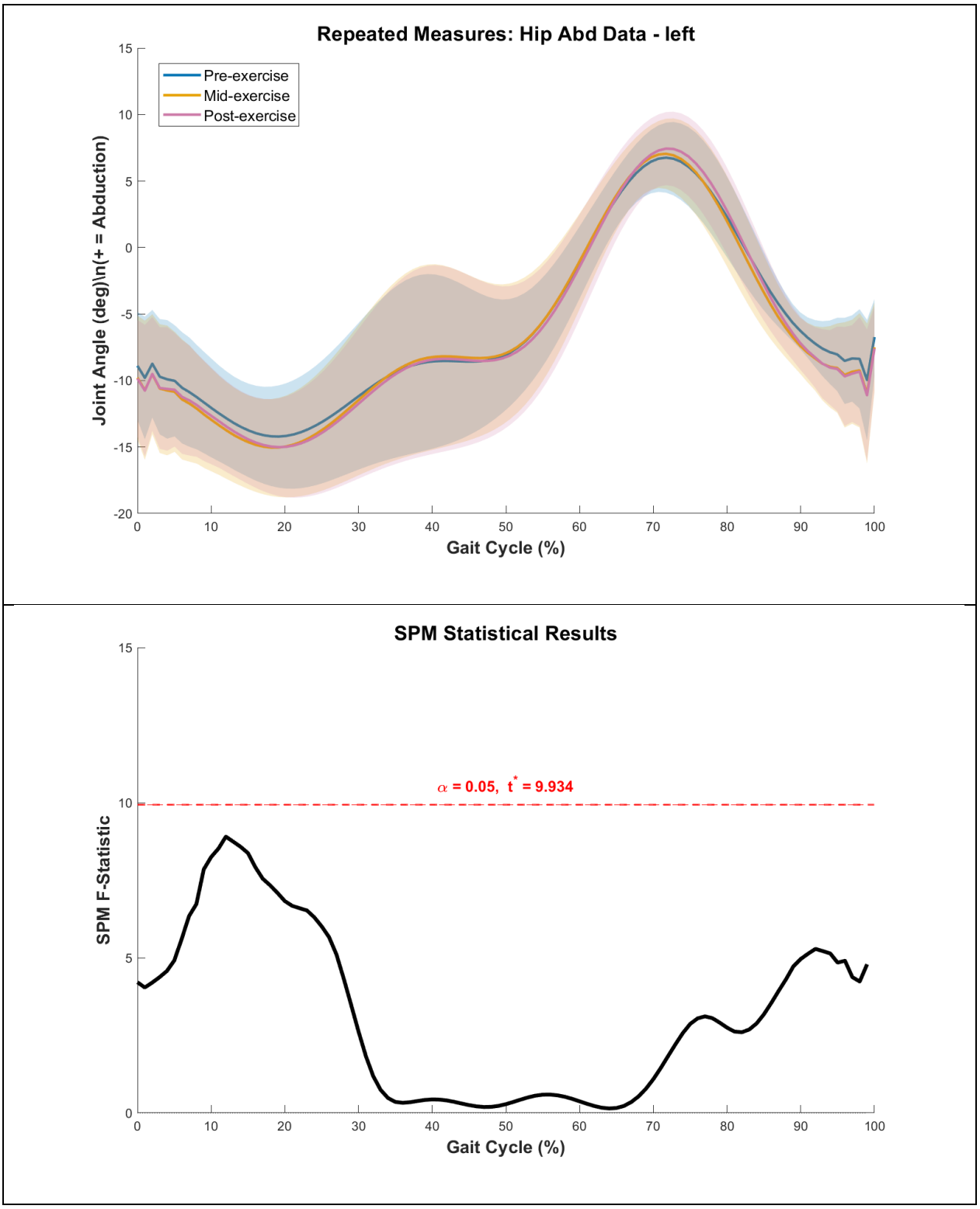

Figure A 4.3: Left-leg hip abduction–adduction kinematics and SPM across the gait cycle. Top panel: mean left hip abduction–adduction angle (°) time-normalized to 0–100% for three time points: pre-exercise (blue), mid-exercise (red), and post-exercise (green). Shaded regions represent standard deviations. Bottom panel: SPM repeated-measures ANOVA F-statistic (black) for the left leg across the gait cycle with the α = 0.05 critical threshold (red dashed line; Fcrit=9.934). Supra-threshold intervals denote gait phases with significant differences among time points.

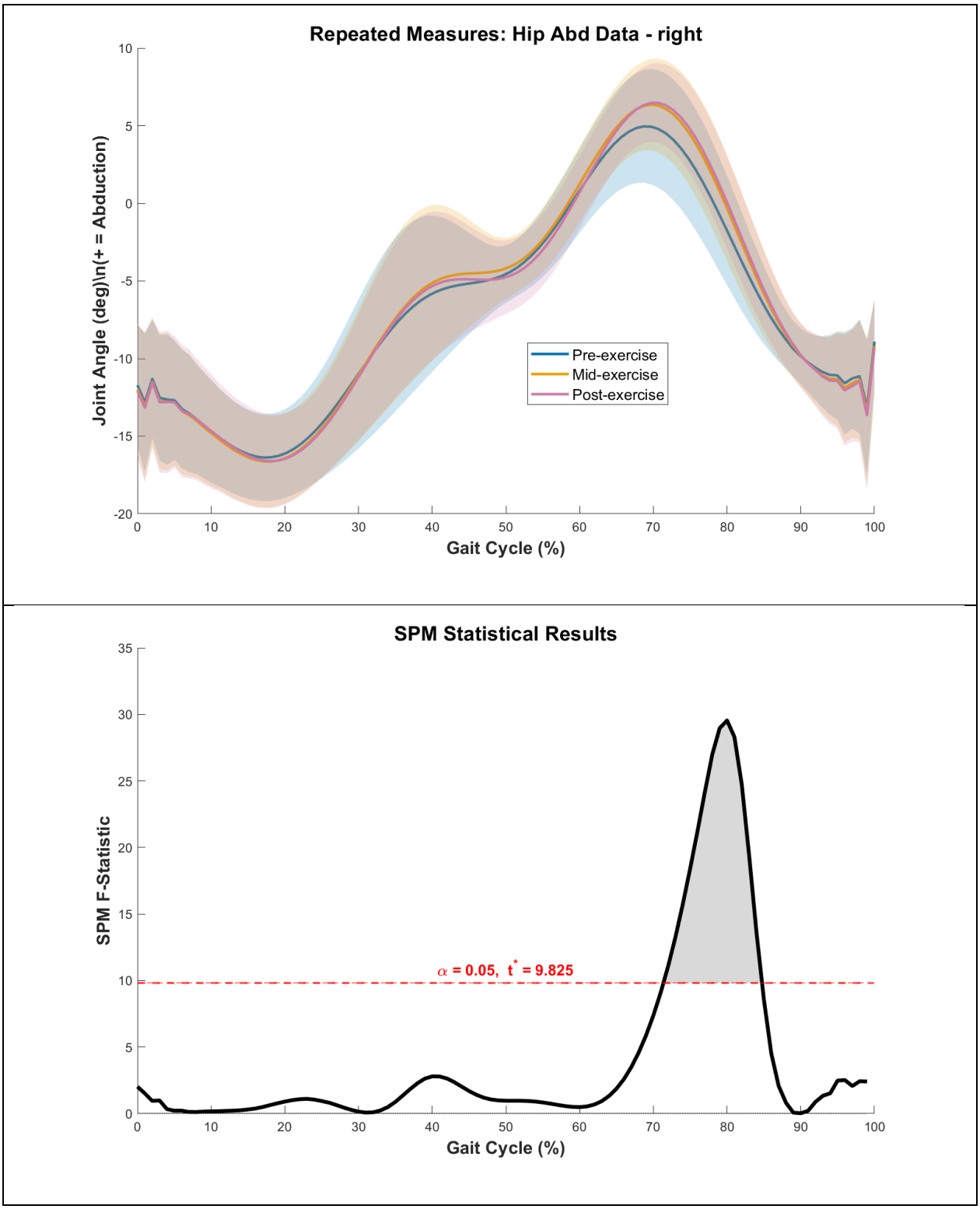

Figure A 4.4: Right-leg hip abduction–adduction kinematics and SPM across the gait cycle. Top panel: mean right hip abduction–adduction angle (°) time-normalized to 0–100% for three time points: pre-exercise (blue), mid-exercise (red), and post-exercise (green). Shaded regions represent standard deviations. Bottom panel: SPM repeated-measures ANOVA F-statistic (black) for the right leg across the gait cycle with the α = 0.05 critical threshold (red dashed line; Fcrit=9.825). Supra-threshold intervals denote gait phases with significant differences among time points.

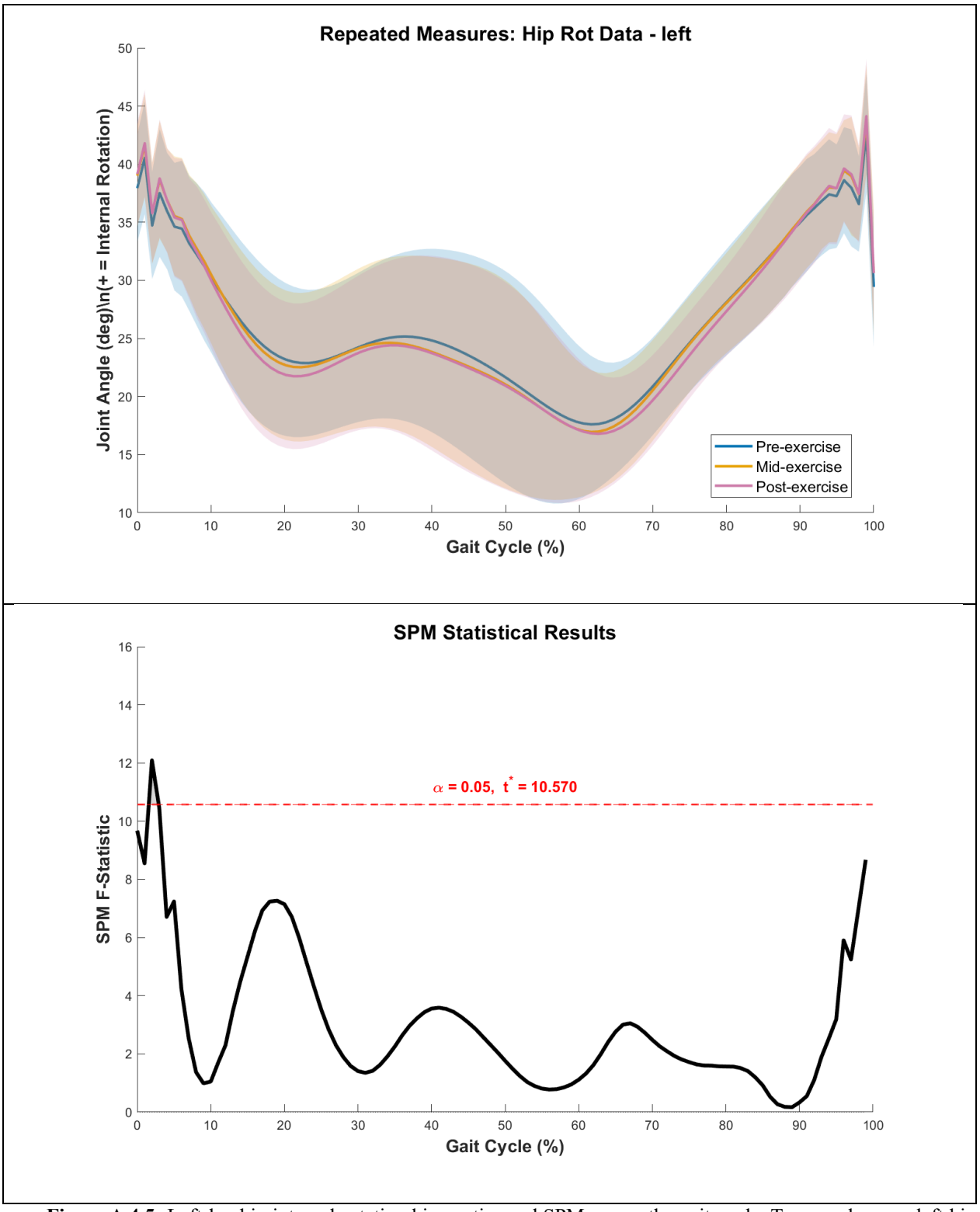

Figure A 4.5: Left-leg hip internal rotation kinematics and SPM across the gait cycle. Top panel: mean left hip internal rotation angle (°) time-normalized to 0–100% for three time points: pre-exercise (blue), mid-exercise (red), and post-exercise (green). Shaded regions represent standard deviations. Bottom panel: SPM repeated-measures ANOVA F-statistic (black) for the left leg across the gait cycle with the α = 0.05 critical threshold (red dashed line; Fcrit=10.570). Supra-threshold intervals denote gait phases with significant differences among time points.

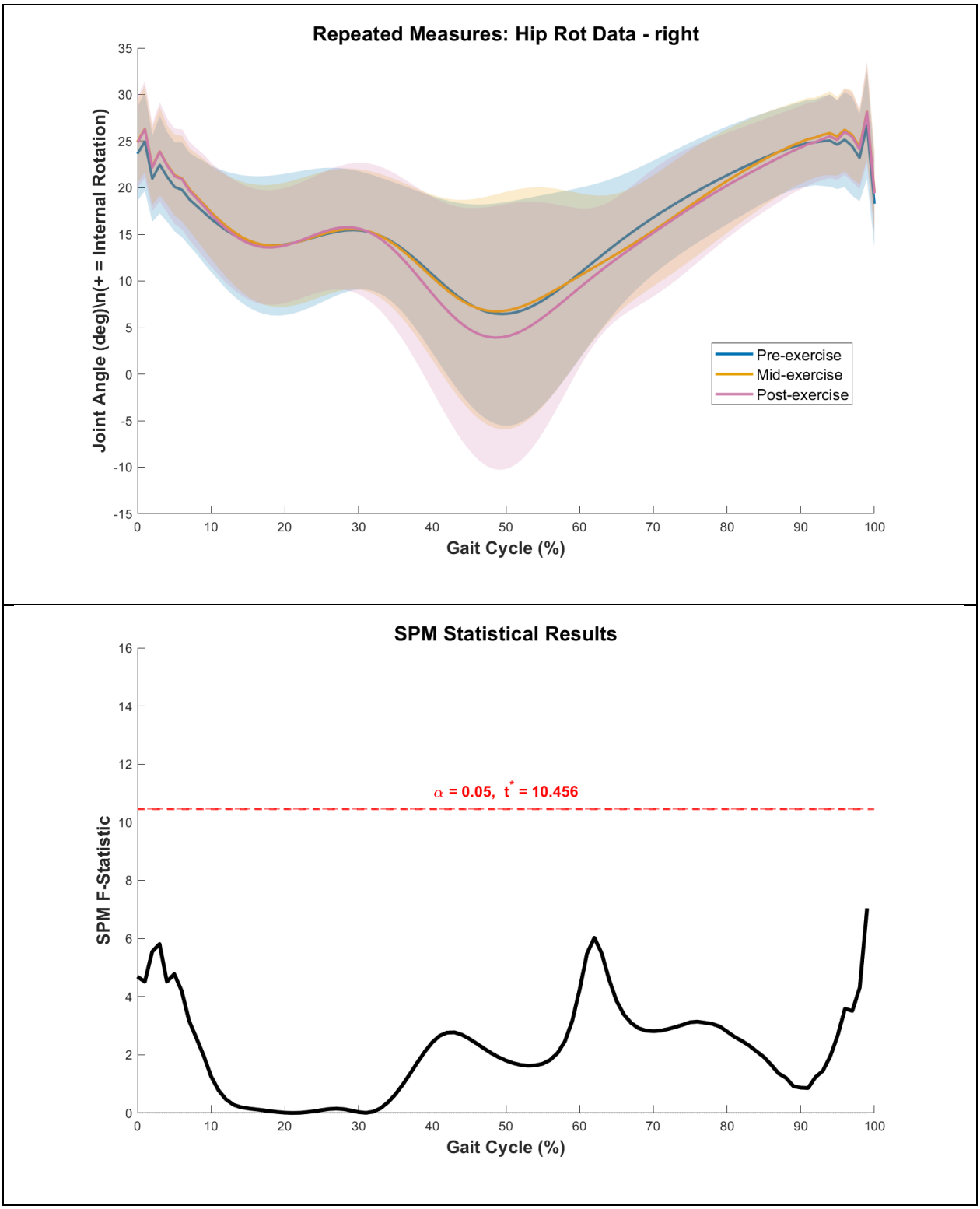

Figure A 4.6: Right-leg hip internal rotation kinematics and SPM across the gait cycle. Top panel: mean right hip internal rotation angle (°) time-normalized to 0–100% for three time points: pre-exercise (blue), mid-exercise (red), and post-exercise (green). Shaded regions represent standard deviations. Bottom panel: SPM repeated-measures ANOVA F-statistic (black) for the right leg across the gait cycle with the α = 0.05 critical threshold (red dashed line; Fcrit=10.456). Supra-threshold intervals denote gait phases with significant differences among time points.

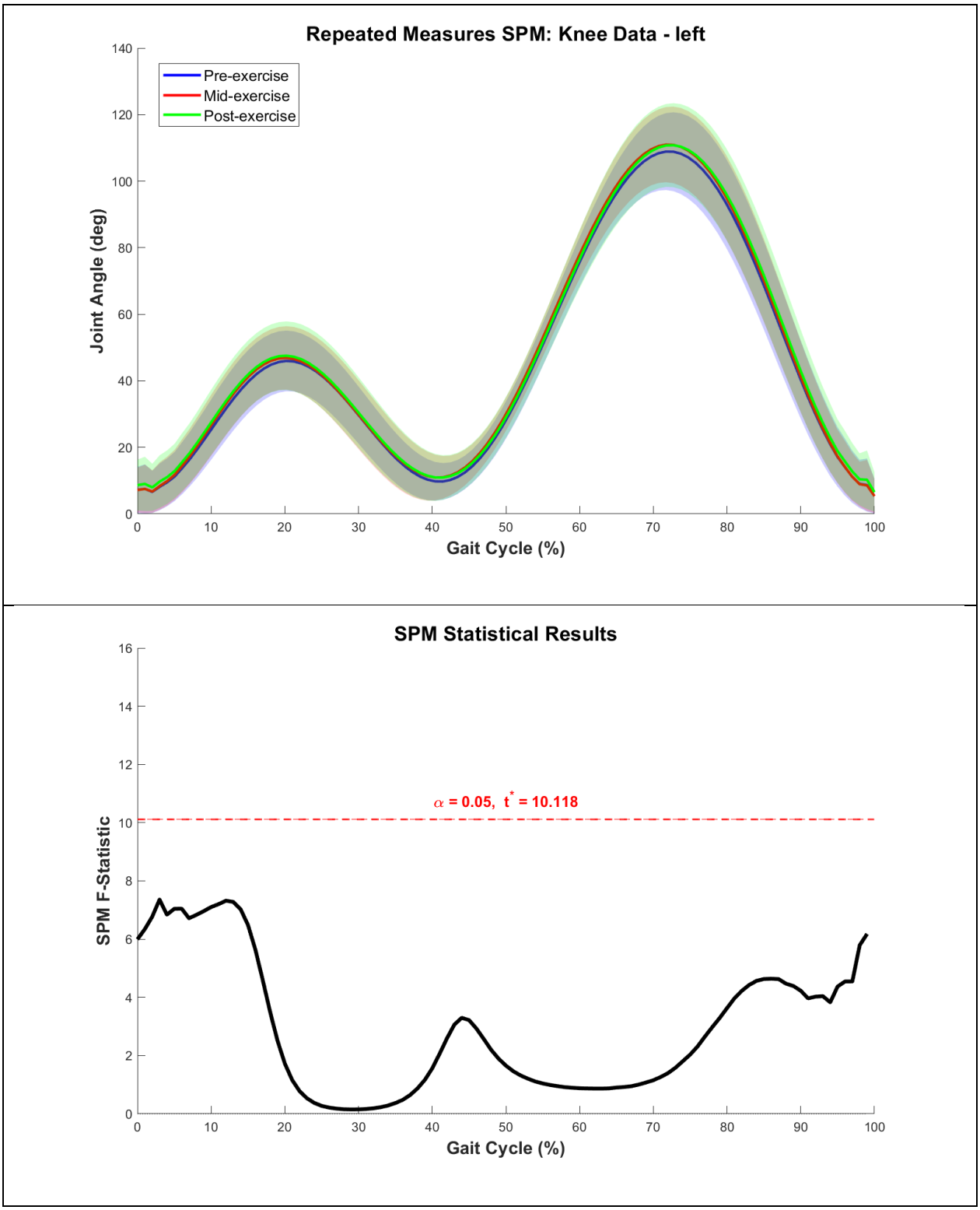

Figure A 4.7: Left-leg knee flexion–extension kinematics and SPM across the gait cycle. Top panel: mean left knee flexion angle (°) time-normalized to 0–100% for three time points: pre-exercise (blue), mid-exercise (red), and post-exercise (green). Shaded regions represent standard deviations. Bottom panel: SPM repeated-measures ANOVA F-statistic (black) for the left leg across the gait cycle with the α = 0.05 critical threshold (red dashed line; Fcrit=10.118). Supra-threshold intervals denote gait phases with significant differences among time points.

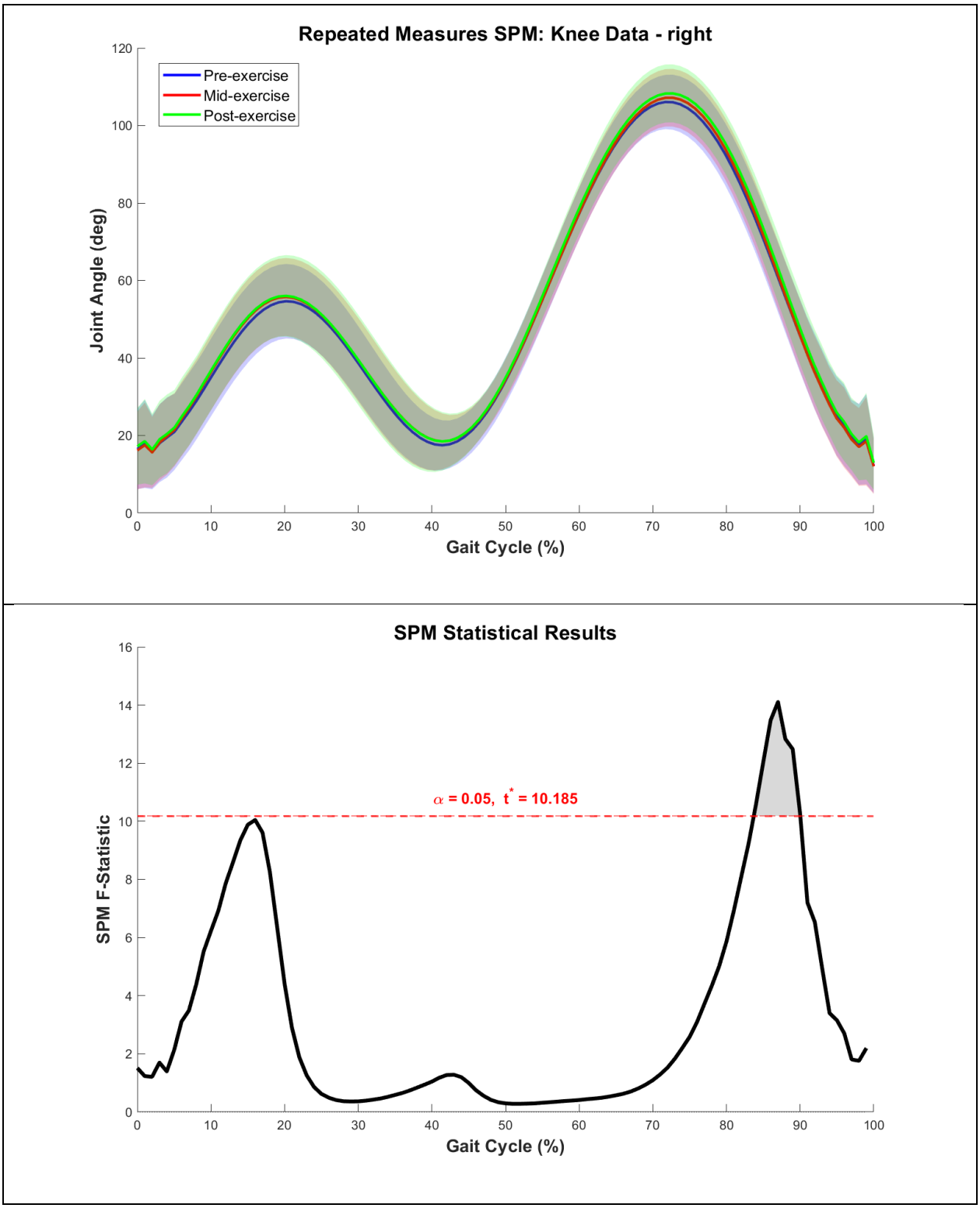

Figure A 4.8: Right-leg knee flexion–extension kinematics and SPM across the gait cycle. Top panel: mean right knee flexion angle (°) time-normalized to 0–100% for three time points: pre-exercise (blue), mid-exercise (red), and post-exercise (green). Shaded regions represent standard deviations. Bottom panel: SPM repeated-measures ANOVA F-statistic (black) for the right leg across the gait cycle with the α = 0.05 critical threshold (red dashed line; Fcrit=10.185). Supra-threshold intervals denote gait phases with significant differences among time points.

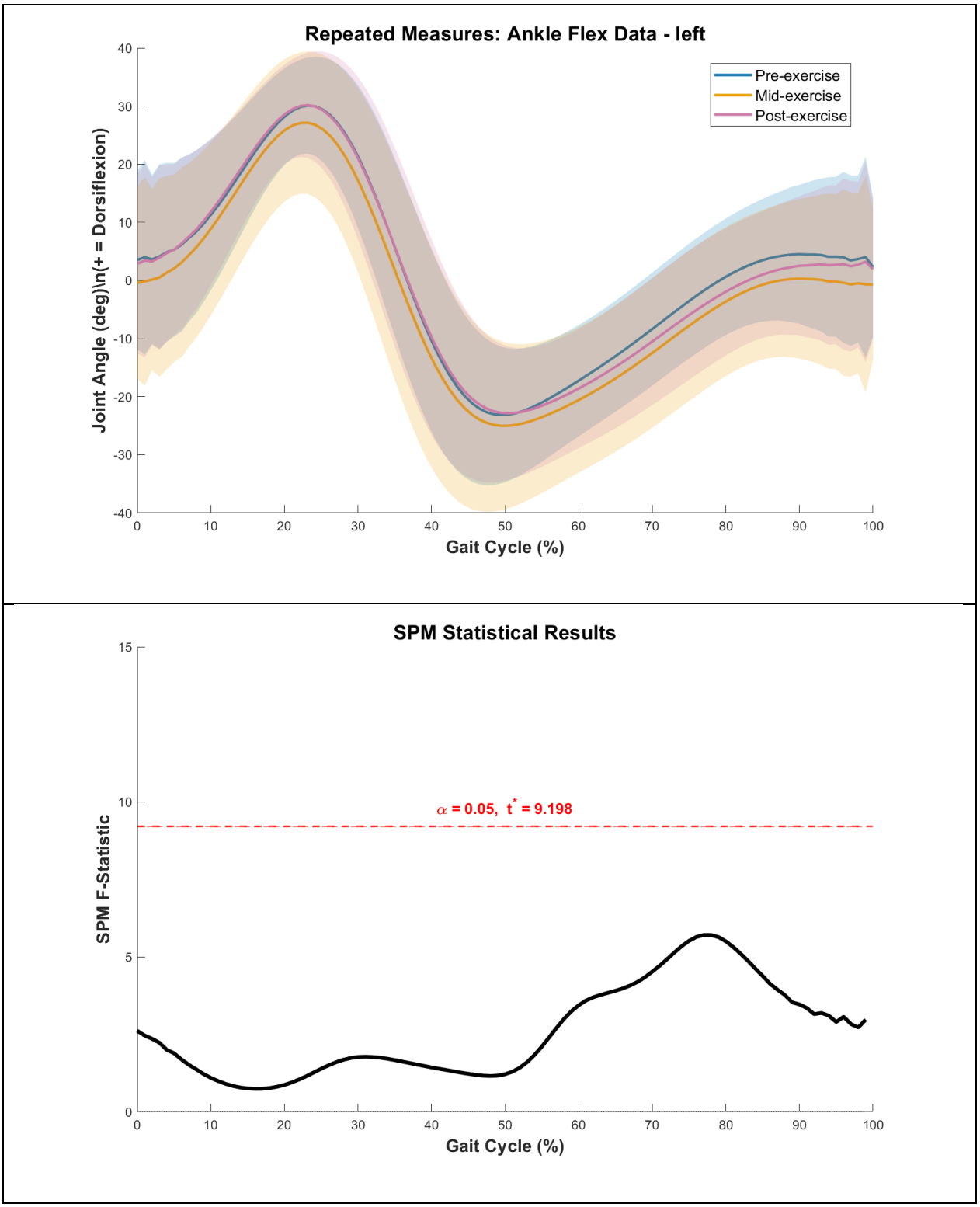

Figure A 4.9: Left-ankle knee flexion–extension kinematics and SPM across the gait cycle. Top panel: mean left ankle flexion angle (°) time-normalized to 0–100% for three time points: pre-exercise (blue), mid-exercise (red), and post-exercise (green). Shaded regions represent standard deviations. Bottom panel: SPM repeated-measures ANOVA F-statistic (black) for the left leg across the gait cycle with the α = 0.05 critical threshold (red dashed line; Fcrit=9.198). Supra-threshold intervals denote gait phases with significant differences among time points.

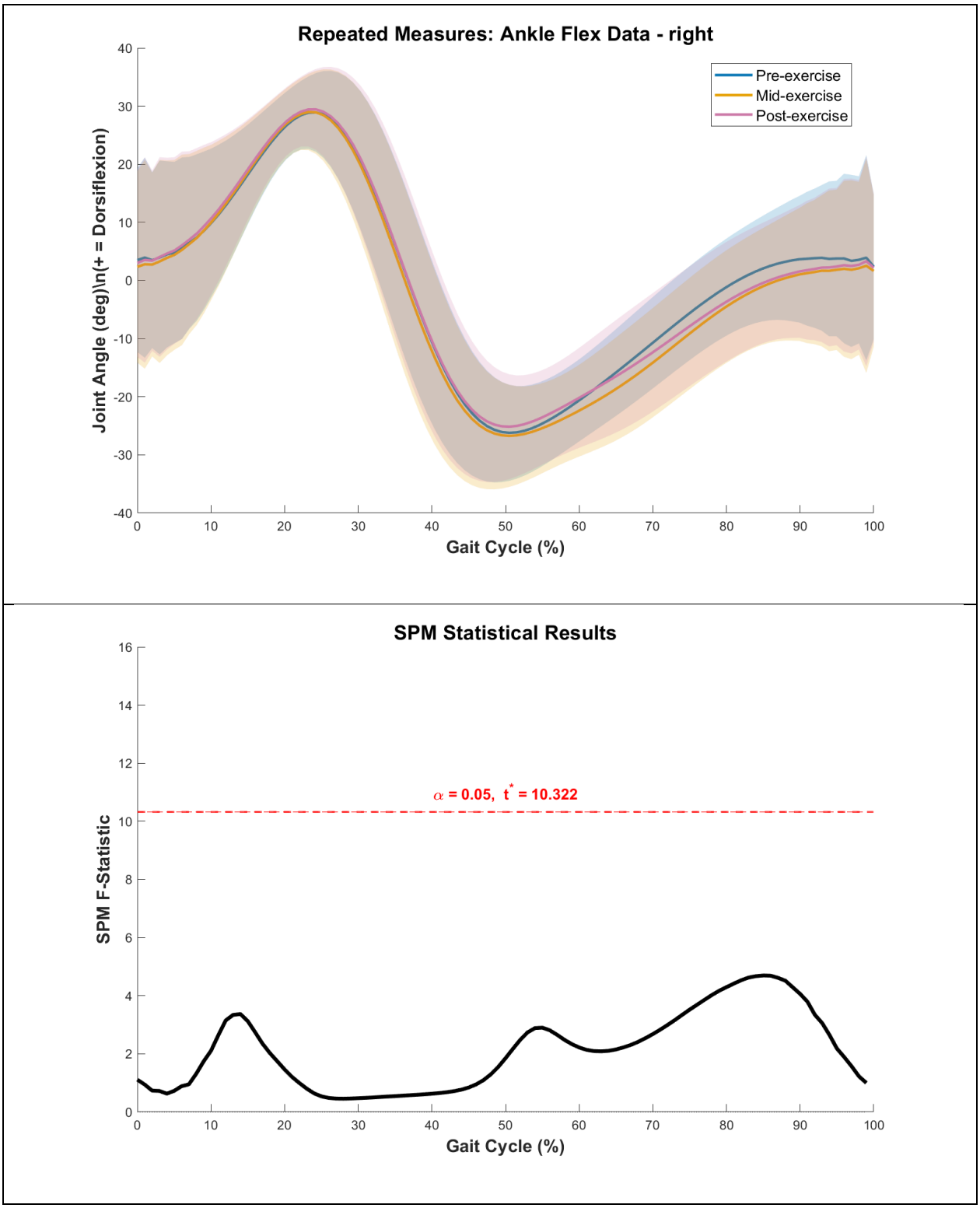

Figure A 4.10: Right-ankle knee flexion–extension kinematics and SPM across the gait cycle. Top panel: mean right ankle flexion angle (°) time-normalized to 0–100% for three time points: pre-exercise (blue), mid-exercise (red), and post-exercise (green). Shaded regions represent standard deviations. Bottom panel: SPM repeated-measures ANOVA F-statistic (black) for the right leg across the gait cycle with the α = 0.05 critical threshold (red dashed line; Fcrit=10.332). Supra-threshold intervals denote gait phases with significant differences among time points.

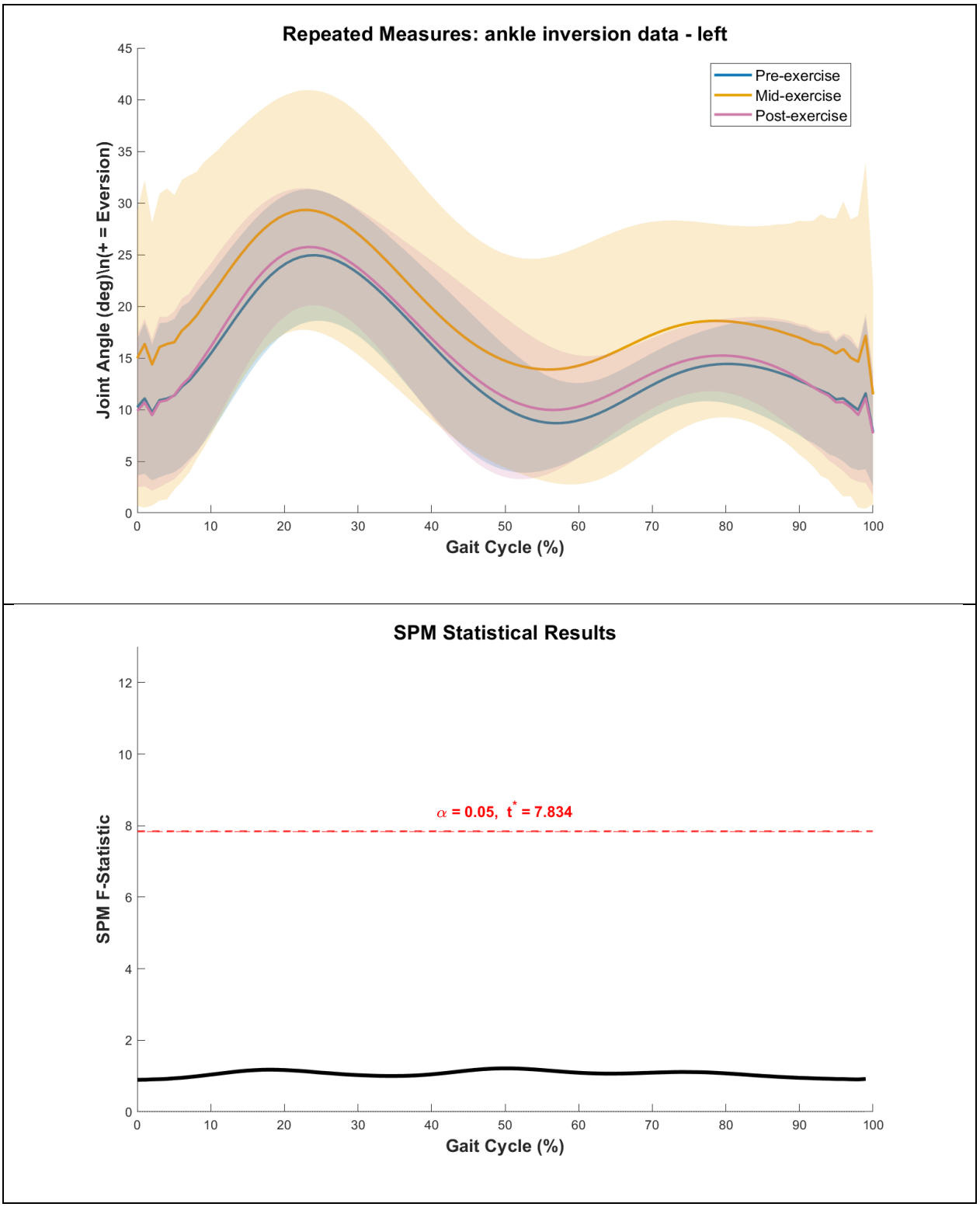

Figure A 4.11: Left-leg ankle inversion-eversion kinematics and SPM across the gait cycle. Top panel: mean left ankle inversion-eversion angle (°) time-normalized to 0–100% for three time points: pre-exercise (blue), mid-exercise (red), and post-exercise (green). Shaded regions represent standard deviations. Bottom panel: SPM repeated-measures ANOVA F-statistic (black) for the left leg across the gait cycle with the α = 0.05 critical threshold (red dashed line; Fcrit=7.834). Supra-threshold intervals denote gait phases with significant differences among time points.

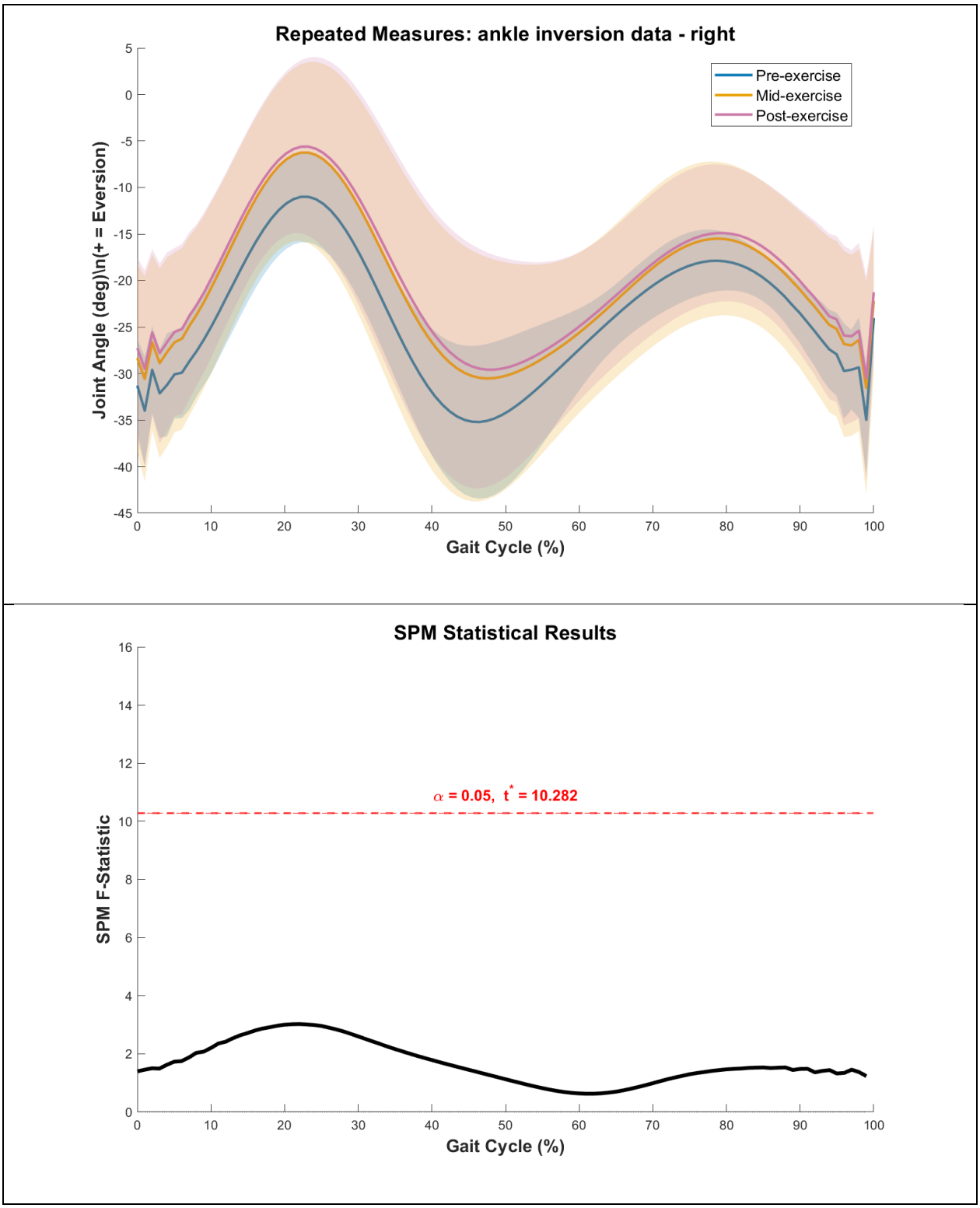

Figure A 4.12: Right-leg ankle inversion-eversion kinematics and SPM across the gait cycle. Top panel: mean right ankle inversion-eversion angle (°) time-normalized to 0–100% for three time points: pre-exercise (blue), mid-exercise (red), and post-exercise (green). Shaded regions represent standard deviations. Bottom panel: SPM repeated-measures ANOVA F-statistic (black) for the right leg across the gait cycle with the α = 0.05 critical threshold (red dashed line; Fcrit=10.282). Supra-threshold intervals denote gait phases with significant differences among time points.

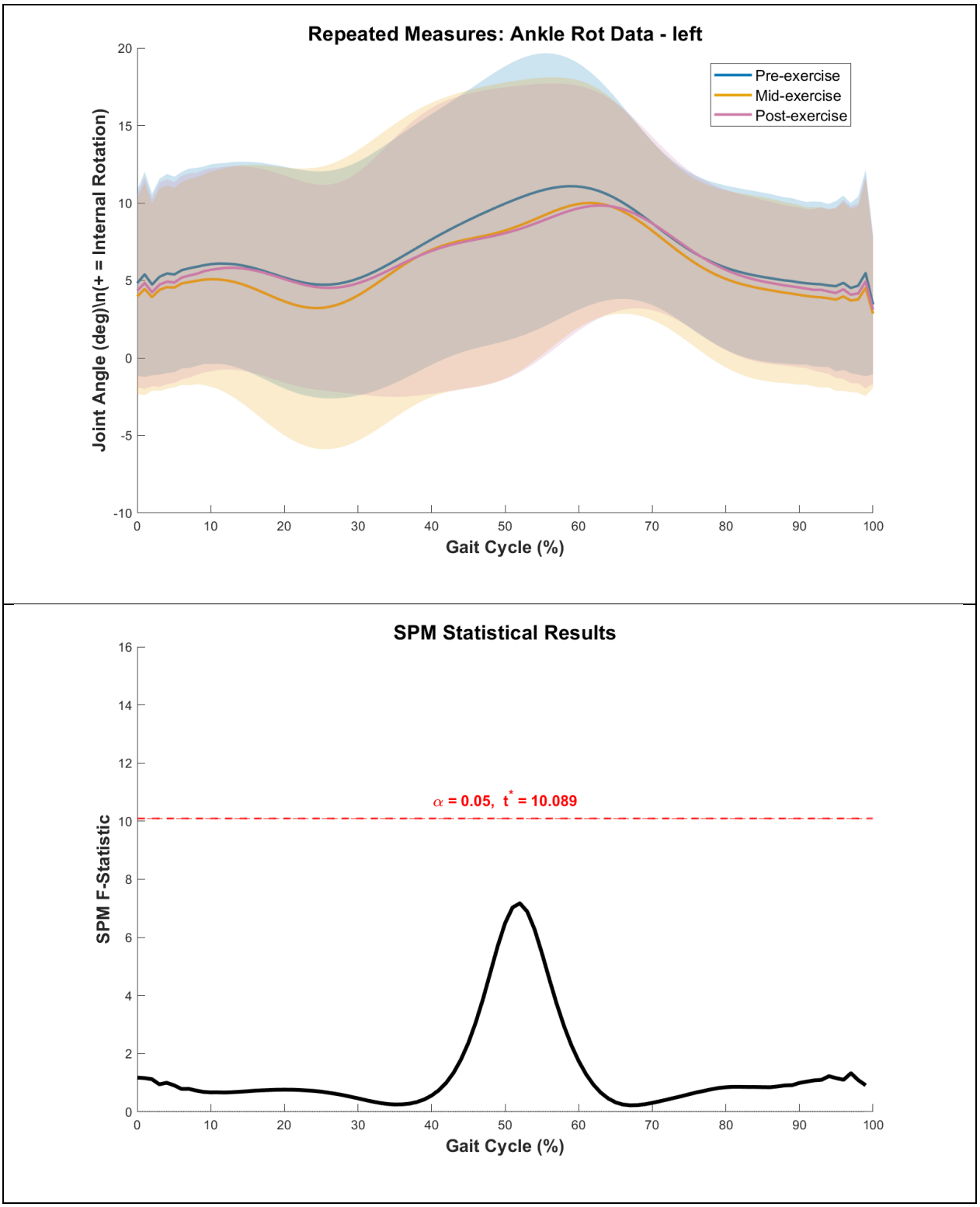

Figure A 4.13: Left-leg ankle internal rotation kinematics and SPM across the gait cycle. Top panel: mean left ankle internal rotation angle (°) time-normalized to 0–100% for three time points: pre-exercise (blue), mid-exercise (red), and post-exercise (green). Shaded regions represent standard deviations. Bottom panel: SPM repeated-measures ANOVA F-statistic (black) for the left leg across the gait cycle with the α = 0.05 critical threshold (red dashed line; Fcrit=10.089). Supra-threshold intervals denote gait phases with significant differences among time points.

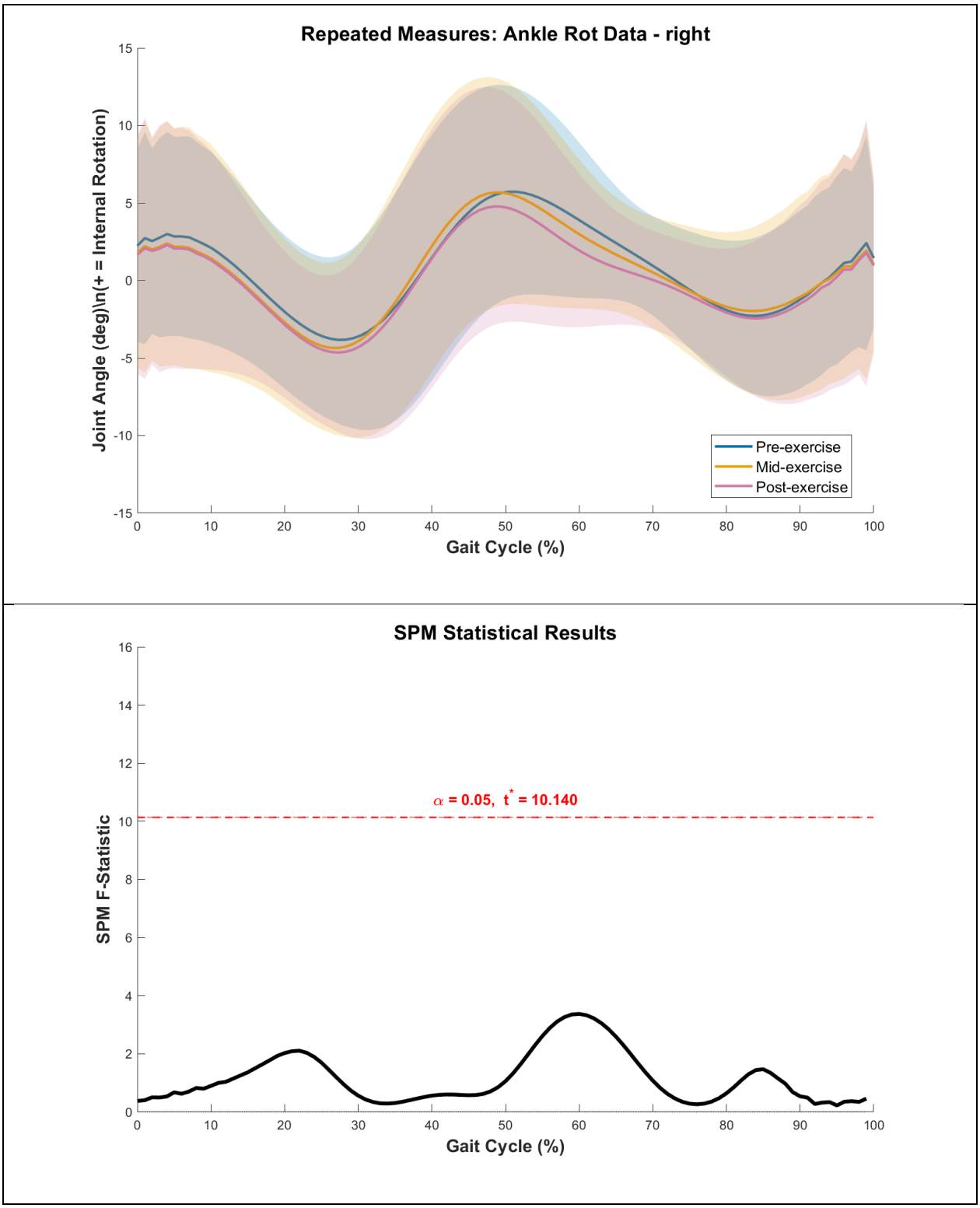

Figure A 4.14: Right-leg ankle internal rotation kinematics and SPM across the gait cycle. Top panel: mean right ankle internal rotation angle (°) time-normalized to 0–100% for three time points: pre-exercise (blue), mid-exercise (red), and post-exercise (green). Shaded regions represent standard deviations. Bottom panel: SPM repeated-measures ANOVA F-statistic (black) for the right leg across the gait cycle with the α = 0.05 critical threshold (red dashed line; Fcrit=10.140). Supra-threshold intervals denote gait phases with significant differences among time points

4.8 References

Alba-Jiménez, C., Moreno-Doutres, D., Peña, J., 2022. Trends Assessing Neuromuscular Fatigue in Team Sports: A Narrative Review. Sports 10, 33. https://doi.org/10.3390/sports10030033

Allen, D.G., Lamb, G.D., Westerblad, H., 2008. Skeletal Muscle Fatigue: Cellular Mechanisms. Physiol. Rev. 88, 287–332. https://doi.org/10.1152/physrev.00015.2007

Barstow, T.J., Buchthal, S., Zanconato, S., Cooper, D.M., 1994. Muscle energetics and pulmonary oxygen uptake kinetics during moderate exercise. J. Appl. Physiol. 77, 1742–1749. https://doi.org/10.1152/jappl.1994.77.4.1742

Benoit, D.L., Ramsey, D.K., Lamontagne, M., Xu, L., Wretenberg, P., Renström, P., 2006. Effect of skin movement artifact on knee kinematics during gait and cutting motions measured in vivo. Gait Posture 24, 152–164. https://doi.org/10.1016/j.gaitpost.2005.04.012

Button, K.S., Ioannidis, J.P.A., Mokrysz, C., Nosek, B.A., Flint, J., Robinson, E.S.J., Munafò, M.R., 2013. Power failure: why small sample size undermines the reliability of neuroscience. Nat. Rev. Neurosci. 14, 365–376. https://doi.org/10.1038/nrn3475

Carvalho, R., Fonseca, S.T., Okai-Nóbrega, L.A., Santos, T.R.T., Araújo, P.A., Quirino, J., Martins, W.R., Prado, L.S., Souza, T.R., 2023. Effects of lower-limb extensors' neuromuscular fatigue on the regularity of running movements: a crossover study. Sports Biomech. 1–18. https://doi.org/10.1080/14763141.2023.2236082

Chahla, J., Sherman, B., Cinque, M., Miranda, A., Garrett, W.E., Chiampas, G., O'Malley, H., Gerhardt, M.B., Mandelbaum, B.R., 2018. Epidemiological Findings of Soccer Injuries During the 2017 Gold Cup. Orthop. J. Sports Med. 6. https://doi.org/10.1177/2325967118791754

Coen, P.M., Jubrias, S.A., Distefano, G., Amati, F., Mackey, D.C., Glynn, N.W., Manini, T.M., Wohlgemuth, S.E., Leeuwenburgh, C., Cummings, S.R., Newman, A.B., Ferrucci, L., Toledo, F.G.S., Shankland, E., Conley, K.E., Goodpaster, B.H., 2013. Skeletal Muscle Mitochondrial

Energetics Are Associated With Maximal Aerobic Capacity and Walking Speed in Older Adults. The Journals of Gerontology: Series A 68, 447–455. https://doi.org/10.1093/gerona/gls196

Collins, B.W., Pearcey, G.E.P., Buckle, N.C.M., Power, K.E., Button, D.C., 2018. Neuromuscular fatigue during repeated sprint exercise: underlying physiology and methodological considerations. Applied Physiology, Nutrition, and Metabolism 43, 1166–1175. https://doi.org/10.1139/apnm-2018-0080

Cramer, M.N., Jay, O., 2016. Biophysical aspects of human thermoregulation during heat stress. Autonomic Neuroscience 196, 3–13. https://doi.org/10.1016/j.autneu.2016.03.001

De Luca, C.J., 1997. The Use of Surface Electromyography in Biomechanics. J. Appl. Biomech. 13, 135–163. https://doi.org/10.1123/jab.13.2.135

Ekstrand, J., Hägglund, M., Waldén, M., 2011. Injury incidence and injury patterns in professional football: the UEFA injury study. Br. J. Sports Med. 45, 553–558. https://doi.org/10.1136/bjsm.2009.060582

Enoka, R.M., Duchateau, J., 2008. Muscle fatigue: what, why and how it influences muscle function. J. Physiol. 586, 11–23. https://doi.org/10.1113/jphysiol.2007.139477

Esteve-Lanao, J., Foster, C., Seiler, S., Lucia, A., 2007. Impact of Training Intensity Distribution on Performance in Endurance Athletes. The Journal of Strength and Conditioning Research 21, 943. https://doi.org/10.1519/R-19725.1

Farina, D., Merletti, R., Enoka, R.M., 2014. The extraction of neural strategies from the surface EMG: an update. J. Appl. Physiol. (1985) 117, 1215–30. https://doi.org/10.1152/japplphysiol.00162.2014

Farina, D., Merletti, R., Enoka, R.M., 2004. The extraction of neural strategies from the surface EMG. J. Appl. Physiol. 96, 1486–1495. https://doi.org/10.1152/japplphysiol.01070.2003

Gao, Z., Xiang, L., Fekete, G., Baker, J.S., Mao, Z., Gu, Y., 2023. A Data-Driven Approach for Fatigue Detection during Running Using Pedobarographic Measurements. Appl. Bionics Biomech. 2023, 1–11. https://doi.org/10.1155/2023/7022513

Garrett, J., Akyildiz, Z., Leduc, C., van den Hoek, D., Manuel Clemente, F., Ardigò, L.P., 2023. Peak running speed can be used to monitor neuromuscular fatigue from a standardized running test in team sport athletes. Research in Sports Medicine 31, 319–330. https://doi.org/10.1080/15438627.2021.1966012

Garrett, J.M., Gunn, R., Eston, R.G., Jakeman, J., Burgess, D.J., Norton, K., 2019. The effects of fatigue on the running profile of elite team sport athletes. A systematic review and meta-analysis. J. Sports Med. Phys. Fitness 59. https://doi.org/10.23736/S0022-4707.19.09356-3

Glover, N.A., Chaudhari, A.M., 2024. Neuromuscular and trunk control mediate factors associated with injury in fatigued runners. J. Biomech. 170, 112176. https://doi.org/10.1016/j.jbiomech.2024.112176

Goodall, S., Charlton, K., Howatson, G., Thomas, K., 2015. Neuromuscular Fatigability during Repeated-Sprint Exercise in Male Athletes. Med. Sci. Sports Exerc. 47, 528–536. https://doi.org/10.1249/MSS.0000000000000443

Grood, E.S., Suntay, W.J., 1983. A Joint Coordinate System for the Clinical Description of Three-Dimensional Motions: Application to the Knee. J. Biomech. Eng. 105, 136–144. https://doi.org/10.1115/1.3138397

Hawkins, M.N., Raven, P.B., Snell, P.G., Stray-Gundersen, J., Levine, B.D., 2007. Maximal oxygen uptake as a parametric measure of cardiorespiratory capacity. Med. Sci. Sports Exerc. 39, 103–7. https://doi.org/10.1249/01.mss.0000241641.75101.64

Hermens, H.J., Freriks, B., Disselhorst-Klug, C., Rau, G., 2000. Development of recommendations for SEMG sensors and sensor placement procedures. Journal of Electromyography and Kinesiology 10, 361–374. https://doi.org/10.1016/S1050-6411(00)00027-4

Hespanhol Junior, L.C., Pena Costa, L.O., Lopes, A.D., 2013. Previous injuries and some training characteristics predict running-related injuries in recreational runners: a prospective cohort study. J. Physiother. 59, 263–269. https://doi.org/10.1016/S1836-9553(13)70203-0

Jewell, C., Hamill, J., von Tscharner, V., Boyer, K.A., 2019. Altered multi-muscle coordination patterns in habitual forefoot runners during a prolonged, exhaustive run. Eur. J. Sport Sci. 19, 1062–1071. https://doi.org/10.1080/17461391.2019.1575912

Joyner, M.J., Coyle, E.F., 2008. Endurance exercise performance: the physiology of champions. J. Physiol. 586, 35–44. https://doi.org/10.1113/jphysiol.2007.143834

Lee, D., Pate, R.R., Lavie, C.J., Sui, X., Church, T.S., Blair, S.N., 2014. Leisure-Time Running Reduces All-Cause and Cardiovascular Mortality Risk. J. Am. Coll. Cardiol. 64, 472–481. https://doi.org/10.1016/j.jacc.2014.04.058

Luo, Z., Zhang, X., Wang, J., Yang, Y., Xu, Y., Fu, W., 2019. Changes in Ground Reaction Forces, Joint Mechanics, and Stiffness during Treadmill Running to Fatigue. Applied Sciences 9, 5493. https://doi.org/10.3390/app9245493

Merletti, R., Parker, P., 2004. Electromyography: Physiology, Engineering, and Non-Invasive Applications. Wiley-IEEE Press.

Miller, M.S., Callahan, D.M., Toth, M.J., 2014. Skeletal muscle myofilament adaptations to aging, disease, and disuse and their effects on whole muscle performance in older adult humans. Front. Physiol. 5. https://doi.org/10.3389/fphys.2014.00369

Millet, G.Y., 2011. Can Neuromuscular Fatigue Explain Running Strategies and Performance in Ultra-Marathons? Sports Medicine 41, 489–506. https://doi.org/10.2165/11588760-000000000-00000

Nicol, C., Avela, J., Komi, P. V, 2006. The stretch-shortening cycle : a model to study naturally occurring neuromuscular fatigue. Sports Medicine 36, 977–999. https://doi.org/10.2165/00007256-200636110-00004

Pangrazio, O., 2016. Epidemiology of soccer players traumatic injuries during the 2015 America Cup. Muscles Ligaments Tendons J. https://doi.org/10.11138/mltj/2016.6.1.124

Paquette, M.R., Melcher, D.A., 2017. Impact of a Long Run on Injury-Related Biomechanics with Relation to Weekly Mileage in Trained Male Runners. J. Appl. Biomech. 33, 216–221. https://doi.org/10.1123/jab.2016-0170

Place, N., Lepers, R., Deley, G., Millet, G.Y., 2004. Time Course of Neuromuscular Alterations during a Prolonged Running Exercise. Med. Sci. Sports Exerc. 36, 1347–1356. https://doi.org/10.1249/01.MSS.0000135786.22996.77

Pollock, M.L., Gaesser, G.A., Butcher, J.D., Despres, J.-P., Dishman, R.K., Franklin, B.A., Garber, C.E., 1998. ACSM Position Stand: The Recommended Quantity and Quality of Exercise for Developing and Maintaining Cardiorespiratory and Muscular Fitness, and Flexibility in Healthy Adults. Med. Sci. Sports Exerc. 30, 975–991. https://doi.org/10.1097/00005768-199806000-00032

Quammen, D., Cortes, N., Van Lunen, B.L., Lucci, S., Ringleb, S.I., Onate, J., 2012. Two different fatigue protocols and lower extremity motion patterns during a stop-jump task. J. Athl. Train. 47, 32–41. https://doi.org/10.4085/1062-6050-47.1.32

Rimmer, E., Verheul, J., Lake, M., 2020. Effect of Fatigue from Repeated Sprints on Hamstring Muscle Activation Patterns During Running, in: 38th International Society of Biomechanics in Sport Conference. Online.

Schlink, B.R., Nordin, A.D., Brooks, C.N., Ferris, D.P., 2021. Fatigue induces altered spatial myoelectric activation patterns in the medial gastrocnemius during locomotion. J. Neurophysiol. 125, 2013–2023. https://doi.org/10.1152/jn.00602.2020

Wilke, J., Fleckenstein, J., Krause, F., Vogt, L., Banzer, W., 2016. Sport-specific functional movement can simulate aspects of neuromuscular fatigue occurring in team sports. Sports Biomech. 15, 151–161. https://doi.org/10.1080/14763141.2016.1159322

Willer, J., Allen, S.J., Burden, R.J., Folland, J.P., 2021. Neuromechanics of Middle-Distance Running Fatigue: A Key Role of the Plantarflexors? Med. Sci. Sports Exerc. 53, 2119–2130. https://doi.org/10.1249/MSS.0000000000002695

Willwacher, S., Kurz, M., Robbin, J., Thelen, M., Hamill, J., Kelly, L., Mai, P., 2022. Running-Related Biomechanical Risk Factors for Overuse Injuries in Distance Runners: A Systematic Review Considering Injury Specificity and the Potentials for Future Research. Sports Medicine 52, 1863–1877. https://doi.org/10.1007/s40279-022-01666-3

Winter, D.A., 2009. Biomechanics and Motor Control of Human Movement. Wiley. https://doi.org/10.1002/9780470549148

Wu, G., Siegler, S., Allard, P., Kirtley, C., Leardini, A., Rosenbaum, D., Whittle, M., D'Lima, D.D., Cristofolini, L., Witte, H., Schmid, O., Stokes, I., 2002. ISB recommendation on definitions of joint coordinate system of various joints for the reporting of human joint motion—part I: ankle, hip, and spine. J. Biomech. 35, 543–548. https://doi.org/10.1016/S0021-9290(01)00222-6

Zebis, M.K., Bencke, J., Andersen, L.L., Alkjær, T., Suetta, C., Mortensen, P., Kjær, M., Aagaard, P., 2011. Acute fatigue impairs neuromuscular activity of anterior cruciate ligament-agonist muscles in female team handball players. Scand. J. Med. Sci. Sports 21, 833–840. https://doi.org/10.1111/j.1600-0838.2010.01052.x

Chapter 5: Manuscript 2

Title: Same Pace, Different Price: OpenSim Metabolic Models vs Indirect Calorimetry for Cost of Transport in High-Intensity Running

Zachary A. Flahaut[1, 2], Nicholas S. Ryan[3], Pär Halje[3], Allison L. Clouthier[1, 4], Daniel L. Benoit[3]

[1] Ottawa-Carleton Institute for Biomedical Engineering, University of Ottawa, Canada

[2]Department of Mechanical Engineering, University of Ottawa, Canada

[3] MoRe-Lab, Department of Health Sciences, Faculty of Medicine, Lund University, Lund, Sweden

[4]School of Human Kinetics, University of Ottawa, Ottawa, Ontario, Canada

8160 words

5.1 Abstract

Background: Static-optimization (SO) musculoskeletal energy models are widely used to estimate running cost of transport (CoT), but their validity during fatiguing, high-intensity running is uncertain.

Purpose: Quantify agreement, bias, and fatigue sensitivity of three musculoskeletal metabolic energy models (*Bhargava2004*, *Umberger2003*, Umberger2010), driven by muscle activations and forces estimated via static optimization, versus indirect calorimetry during constant-speed running, and describe muscle-group energetics and limb asymmetry.

Methods: Seven recreationally trained adults completed ~30 min of treadmill running at ~85% VO2 max on a 1% grade. Whole-body kinematics and kinetics were recorded, and scaled generic OpenSim 3.3 models were used with static optimization (SO) to estimate muscle forces and muscle metabolic power. Cost of transport ($J \cdot kg^{-1} \cdot m^{-1}$) was computed in 30-s windows at pre- (0th minute), mid- (15th minute), and post- (30th minute) fatigue; indirect calorimetry provided reference CoT. Methods and stages were compared with repeated-measures ANOVA; agreement (Bland–Altman), associations (Pearson r), stage-wise slopes, muscle-group contributions, and inter-limb differences were assessed ($\alpha = 0.05$).

Results: CoT differed by estimation method and increased with stage, with no method×stage interaction. Relative to calorimetry, *Bhargava2004* and *Umberger2003* underestimated CoT, *Umberger2010* showed moderate overestimation. Only *Bhargava2004* correlated significantly with calorimetry across stages (r=0.46, p=0.04). Only the *Umberger2010* model reproduced the within-session rise in CoT (stage-wise slopes: calorimetry = 0.4349; *Bhargava2004* = −0.0034; *Umberger2010* = 0.0554; *Umberger2003* =−0.0011). Muscle-level metabolic cost estimates indicated that the quadriceps and hamstrings contributed the largest proportion of total lower-limb metabolic power across all fatigue stages. When comparing limbs, quadriceps metabolic cost was

significantly greater in the right leg than the left when averaged across stages ($p = 0.01$), whereas no significant left–right differences were observed for the remaining muscle groups.

Conclusion: Static optimization–driven energy models showed substantial systematic bias in absolute cost of transport relative to indirect calorimetry and demonstrated limited sensitivity to fatigue-related changes during high-intensity running. These findings indicate that while such models differentiate between estimation methods, their ability to capture within-session metabolic dynamics remains limited.

322 words

Keywords: cost of transport; indirect calorimetry; static optimization; musculoskeletal modelling; running fatigue; OpenSim

5.2 Introduction

The metabolic cost of human locomotion, particularly during running, is a key metric for understanding energy efficiency, performance, and functional capacity (Barnes and Kilding, 2015; di Prampero, 1986; di Prampero et al., 1986; Fletcher et al., 2009). A widely used measure of this cost is the Cost of Transport, defined as the amount of metabolic energy required to move a unit of body mass over a unit distance (Donelan et al., 2002). This parameter serves as a physiological benchmark across a wide array of applications, from gait retraining and prosthetic optimization to sports science and neurological rehabilitation (Collins et al., 2015; Galle et al., 2017; Malcolm et al., 2013).

To quantify energy expenditure during dynamic tasks, indirect calorimetry remains the gold standard. By measuring oxygen uptake (VO2) and carbon dioxide output (VCO2), researchers can infer metabolic energy consumption using well-established equations (Jeukendrup and Wallis, 2005; Péronnet and Massicotte, 1991). During steady-state submaximal running, indirect calorimetry has demonstrated reproducible CoT values between ~3.5–5.0 J/kg/m depending on speed and incline, with values increasing substantially in higher-intensity or uphill conditions (Farris and Sawicki, 2012; Minetti et al., 2002). For example, at treadmill speeds above 2.5 m/s with moderate incline, values may exceed 6–8 J/kg/m in trained individuals (Bellenger et al., 2016; Biancardi et al., 2023).

While whole-body CoT measurements provide a global picture of energy demand, they offer limited information on the contributions of specific joints or muscles. Musculoskeletal simulation frameworks, such as OpenSim (Delp et al., 2007), may be used to gain insight. OpenSim uses experimentally derived motion capture and ground reaction force data to estimate joint kinematics, kinetics, and muscle activations. Within OpenSim, estimates of muscle forces can be derived through static optimization (SO) by minimizing a cost function (often the sum of squared

activations) under biomechanical constraints (Anderson and Pandy, 2001). These muscle activation and force estimates can subsequently be used as inputs for musculoskeletal energy models to estimate metabolic cost during dynamic tasks.

Several musculoskeletal energy models have been proposed to estimate metabolic energy expenditure at the muscle level, including formulations developed by Bhargava et al. (2004), Umberger (2010), and Umberger et al., (2003), which differ in their treatment of muscle activation dynamics, fiber-type composition, and heat production. Despite their increasing use, these energy models have demonstrated mixed agreement with empirically measured CoT values. For instance, Koelewijn et al. (2019) reported systematic underestimation of CoT using the Bhargava model during walking, whereas Umberger-based models have been shown to overestimate CoT, particularly during high-intensity tasks (Luis et al., 2023; Uchida et al., 2016a). Model validation is further limited by heterogeneity in input data quality and processing (e.g., marker/GRF filtering, calorimetry equations) (Hicks et al., 2015) and variability in model personalization/calibration (e.g., scaling, tendon stiffness, EMG use) that measurably shifts CoT estimates (Arones et al., 2020; Luis et al., 2023). Additionally, differences in experimental task design (e.g., speed, grade, steady-state vs. transitions) that change the direction and magnitude of model-to-data agreement tend to cause underestimates at higher metabolic demands during walking (Koelewijn et al., 2019), while predicted costs are also method-dependent across modelling approaches (Mohammadzadeh Gonabadi et al., 2020).

Recent comparative studies reveal that simulation-derived CoT values are highly sensitive to modelling parameters such as muscle-tendon compliance, segment scaling, and joint axis definitions (Gambietz et al., 2024; Modenese et al., 2016). Moreover, fatigue a key modulator of muscle function can alter joint kinetics, motor unit recruitment, and metabolic cost, yet remains

largely unmodeled in most simulations. This introduces uncertainty in the utility of SO-based models for estimating metabolic demand during prolonged or fatigue-inducing protocols.

To date, few studies have directly compared static optimization-based CoT estimates to participant-specific indirect calorimetry data, especially during high-intensity running protocols designed to elicit fatigue. In contrast, many prior validations have relied on published CoT norms or low-intensity walking data (Arones et al., 2020), limiting their applicability to sports or clinical populations undergoing high-load tasks.

The present study therefore adopts a validation-oriented approach, where the suitability of the OpenSim static optimization framework for estimating cost of transport under fatigue is probed by examining conditions in which neuromuscular and physiological changes occur without corresponding kinematic alterations. Specifically, the study evaluates whether the modelling framework can capture divergences between internal load (e.g., EMG and metabolic cost) and external movement patterns, thereby identifying potential gaps in its ability to represent fatigue-related adaptations.

To address these inconsistencies, we evaluated CoT predicted by three musculoskeletal energy models (Bhargava et al., 2004; Umberger, 2010; Umberger et al., 2003) applied post hoc to static-optimization outputs, to answer three questions: (1) Between models: how do CoT estimates differ among *Bhargava2004*, *Umberger2003*, and *Umberger2010* when applied post hoc to static-optimization outputs, (2) Against empirical data: how closely does each model's CoT agree with participant-specific indirect calorimetry across the session and (3) Sensitivity to change: does each model capture within-session changes in metabolic demand as fatigue develops?

We hypothesized that *Bhargava2004* would underestimate cost of transport relative to indirect calorimetry, whereas *Umberger2003* and *Umberger2010* would overestimate it, based on prior

reports showing systematic model-specific biases in simulated metabolic cost (Koelewijn et al., 2019; Luis et al., 2023; Uchida et al., 2016b).

We further hypothesized that these models would show limited sensitivity to changes in metabolic demand across fatigue stages. Given that static optimization does not incorporate fatigue-related mechanisms and that the running task was performed at a constant speed with minimal changes in kinematics, there is no a priori reason to expect model-derived CoT to vary substantially with increasing physiological strain.

Accordingly, this study was designed to evaluate whether static optimization–driven musculoskeletal energy models, which do not incorporate EMG or fatigue dynamics, are sufficient to capture fatigue-related changes in metabolic cost, thereby providing a basis for the development of more physiologically informed modelling approaches.

5.3 Methods

5.3.1 Participants

Seven uninjured (6 males, 1 female) active adults (age = 24.29 ± 3.2 years, height = 173.54 ± 5.89 cm, mass = 71.59 ± 6.51 kg, BMI = 23.73 ± 1.26 kg/m^2, Tegner scale = 6.29 ± 1.7). All participants were right-leg dominant. Leg dominance was based upon the foot they would use to kick a football (soccer ball) the farthest. Participants were included if they reached a minimum score of 5 on the Tegner scale, had not sustained an injury to their lower extremities within the past six months that resulted in missed training sessions or competitive events, and did not suffer from any form of cardiovascular or neurological conditions. All participants read and signed a letter of informed consent approved by the local Ethics Review Authority. The diary number for the review at the Ethics Review Authority is 2024-04208-1.

5.3.2 Experimental Protocol

Participants completed a standardized warm-up on a motorized treadmill consisting of 3 minutes of walking at 5 km/h, followed by 2 minutes of running at 8 km/h, both performed at a 1% incline. Participants were instructed to maintain a natural gait during the warm-up and were not permitted to stretch during this period. Immediately following the warm-up, treadmill speed was increased to a participant-specific running speed corresponding to 85% of estimated VO2 max, and the high-intensity protocol commenced without an additional rest period.

The participant-specific running speed corresponding to 85% VO2 max was established during a prior laboratory visit that included treadmill familiarization and an incremental VO2 max test performed to volitional exhaustion. During this test, treadmill speed was increased in a stepwise manner until exhaustion, and VO2 max was identified using standard physiological criteria, including attainment of at least two of the following: a respiratory exchange ratio ≥ 1.10, heart rate ≥ 90% of age-predicted maximum, and a plateau in VO_2 despite further increases in running speed. The treadmill speed associated with 85% of the measured VO2 max was subsequently used for the submaximal threshold protocol.

Participants then completed a continuous 30-minute high-intensity running bout at this fixed speed, with treadmill incline maintained at 1% throughout the protocol to better approximate the energetic cost of outdoor running (Jones and Doust, 1998; Nicholson and Sleivert, 2001). The run was segmented into three predefined 30-second data collection intervals to assess fatigue progression: pre-fatigue (0 min), mid-fatiguing (15 min), and post-fatigue (30 min).

5.3.3 Data Collection

Synchronized 3D motion capture and ground reaction force data were acquired using a 10-camera motion analysis system (Arqus A9, Qualisys, Sweden) and a force-instrumented treadmill (Arsalis, HP Cosmos, Germany). A custom marker set derived from the Qualysis Sports Marker set

and the convention used by Mantovani and Lamontagne (2017). Kinematic and ground reaction force signals were filtered using a fourth-order, zero-lag Butterworth low-pass filter with a cutoff frequency of 6 Hz, prior to further processing in OpenSim version 3.3 (Delp et al., 2007).

Simultaneously, indirect calorimetry data were collected using a K5 metabolic cart (Cosmed, Italy) operating in breath-by-breath mode to yield a per-breath VO2 and VCO2. These were synchronized and averaged over 30-second windows corresponding to the same three treadmill fatigue stages. Oxygen consumption (VO2) and respiratory exchange ratio (RQ) were used to estimate gross metabolic energy expenditure using the Péronnet and Massicotte (1991) caloric equivalent table, with calibration and processing consistent with CPET best-practice guidance ("ATS/ACCP Statement on Cardiopulmonary Exercise Testing," 2003).

5.3.4 Musculoskeletal Modelling and Energy Estimation

Musculoskeletal modelling was implemented in OpenSim 3.3 using the model from Catelli et al. (2019). Each model was scaled to participant anthropometrics using a static trial. Inverse kinematics (IK) and inverse dynamics (ID) tools were used to estimate joint angles and net joint moments, respectively.

IK joint angles obtained from OpenSim were cross-checked against an independent MATLAB-based inverse kinematics pipeline using the same reflective marker set, joint definitions, and coordinate system. Joint-angle waveforms generated by both pipelines were compared across joints, limbs, and fatigue stages to verify consistency in temporal patterns, phase behaviour, and stride-to-stride continuity prior to downstream analyses. For each run and limb, mean ± standard deviation time-normalized gait-cycle waveforms were generated for hip flexion–extension, hip abduction–adduction, knee flexion–extension, and ankle joint angles.

For each participant, limb, and fatigue stage, joint kinematics and kinetics were time-normalized and averaged across gait cycles prior to static optimization, such that simulations were based on mean stride representations rather than stride-by-stride inputs.

The OpenSim Static Optimization (SO) tool was applied to estimate muscle activation patterns, with muscle forces constrained to reproduce observed joint moments under a minimum-squared activation cost criterion (Anderson and Pandy, 2001; Delp et al., 2007).

To estimate energy expenditure from the simulated activations, we applied three published metabolic energy models: Bhargava et al. (2004) (hereafter *Bhargava2004*), Umberger (2010) (*Umberger2010*). and Umberger et al. (2003b) (*Umberger2003*). Each model estimated the instantaneous metabolic power of individual muscles based on force, activation, fiber length, and contraction velocity. The metabolic energy models (Bhargava 2004; Umberger 2003; Umberger 2010) were implemented using OpenSim probe formulations. Key model components and parameter settings used in the present study are summarized in Appendix Table A.5.6. Muscle metabolic power was summed across all model actuators and integrated over each 30-second interval to compute the total energy expenditure per trial.

This energy was normalized to body mass and the distance covered on the treadmill to yield cost of transport (Donelan et al., 2002, 2001), calculated as

$$CoT = \frac{E_{total}}{m * d} \tag{8}$$

where E_{total} is total energy (J), m is body mass (kg), and d is treadmill distance (m) over 30 seconds.

For the calorimetry-based CoT, energy expenditure was computed using

$$CoT = \frac{VO_2 * EE_{eq}(RQ) * t}{m * d} \tag{9}$$

where EE_{eq} is the energy equivalent in kJ/L O_2, t is the trial duration (30 seconds), and all other terms are as defined above (Donelan et al., 2001; Jeukendrup and Wallis, 2005).

5.3.5 Quality Control: Kinematic Cross-Platform Verification

To verify the validity of IK outputs used as inputs for subsequent musculoskeletal and metabolic analyses, joint-angle waveforms obtained from OpenSim were compared against joint kinematics derived from an independent, MATLAB-based direct kinematics (direct-K) pipeline. The direct-K implementation used the same experimental marker trajectories, joint definitions, and coordinate system conventions, and served as the reference standard for this comparison.

This comparison was performed within each trial to confirm that OpenSim IK accurately reproduced experimentally derived joint kinematics and was not intended to assess fatigue- or stage-related changes in kinematics. Rather, this step served solely as a validity check to ensure that no numerical drift, waveform distortion, or artefacts were introduced by the OpenSim processing pipeline prior to downstream analyses.

For each participant, limb, and trial, joint-angle waveforms from OpenSim IK and direct-K were segmented into individual gait cycles, time-normalized to 0–100% of the gait cycle, and summarized as mean ± standard deviation for hip flexion–extension, hip abduction–adduction, knee flexion–extension, and ankle plantarflexion–dorsiflexion. Statistical parametric mapping (SPM) was used to identify any phase-dependent differences between OpenSim IK and direct-K waveforms. No comparisons were performed across fatigue stages within this quality-control step.

5.3.6 EMG–Model Timing Verification

An auxiliary analysis was conducted to characterize the temporal relationship between experimentally measured surface electromyography (EMG) and muscle activation time series estimated via OpenSim static optimization (SO). This analysis was intended as a descriptive

verification of timing consistency, rather than a validation of activation magnitude or neuromuscular control strategies.

The purpose of this check was to confirm that any temporal offsets between EMG and model-derived activations were systematic and stable across fatigue stages, and therefore unlikely to confound comparisons of model-based metabolic cost. This approach has been previously reported in the literature and is included here to ensure internal consistency of the modeling pipeline rather than to provide novel insight into EMG–model agreement (Arnold et al., 2013; Hamner and Delp, 2013).

For each muscle, EMG linear envelopes and corresponding SO activations were time-normalized to the gait cycle and analyzed on a per-stride basis. The temporal lag between EMG onset and SO activation onset was quantified as a percentage of the gait cycle. This analysis was performed independently for each trial to assess whether timing offsets remained consistent across the session. No attempt was made to modify, align, or correct SO activations based on EMG timing; the results of this verification were used solely to contextualize the interpretation of model-based energy estimates.

5.3.7 Residual and Model Consistency Analysis

To assess the dynamic consistency of the musculoskeletal simulations, a residual actuator analysis was performed following the recommendations of Hicks et al. (2015). Residual forces and moments represent artificial forces and torques applied to the pelvis and joints to compensate for inconsistencies between model kinematics, measured ground reaction forces, and inverse dynamics solutions.

Residual force magnitude was calculated from the pelvis translational residual components, and residual moment magnitude was calculated from the pelvis rotational residual components. These residuals were normalized according to the Hicks approach, with residual force expressed

as a percentage of the peak net external force recorded during the trial and residual moment expressed as a percentage of the product of center-of-mass height and peak net external force. Recommended thresholds of <5% for residual forces and <1% for residual moments were used as reference criteria for simulation quality (Hicks et al., 2015).

For each participant, trial, and fatigue stage (Pre, Mid, Post), both peak and root-mean-square (RMS) normalized residual values were computed. In addition, time-series profiles of normalized residual force and moment magnitudes were generated to assess whether deviations from recommended thresholds were concentrated within specific phases of the running cycle.

This analysis served as a quality-control step to evaluate whether the simulations were sufficiently dynamically consistent to support interpretation of model-derived muscle forces and metabolic cost estimates.

5.3.8 Outcomes and Comparisons

The primary outcome was cost of transport ($J \cdot kg^{-1} \cdot m^{-1}$) computed at three fatigue stages (Pre, Mid, Post) for each estimation approach: indirect calorimetry, *Bhargava2004*, *Umberger2003*, and *Umberger2010*. Planned comparisons examined (i) agreement between each musculoskeletal (MSK) model and indirect calorimetry at each stage, (ii) between-model differences at each stage, and (iii) stage-wise changes within each method across the session. In addition to trial-wide CoT, muscle-level metabolic energy was summarized separately for the left and right limbs and by major muscle groups (e.g., quadriceps, hamstrings, plantarflexors); these side-specific profiles were used to test for between-side differences and to describe group patterns across stages.

5.3.9 Statistical Analysis

For each method and stage, CoT was summarized as mean ± SD. Inferential testing used a two-way repeated-measures ANOVA with factors Method (calorimetry, *Bhargava2004*, *Umberger2003*, *Umberger2010*) and Stage (Pre, Mid, Post); Greenhouse–Geisser corrections were

applied when sphericity was violated. When indicated, post hoc paired t-tests were conducted for the planned model-vs-calorimetry and between-model comparisons at each stage, as well as for within-method stage contrasts (Pre vs Mid; Pre vs Post), with familywise error controlled using Bonferroni/Holm adjustments; exact p-values, effect sizes (Cohen's d), and 95% confidence intervals are reported. Agreement between model-based and calorimetry CoT at each stage was assessed using Bland–Altman bias and 95% limits of agreement, and Pearson's r. For the left–right muscle-energy breakdown, per-leg muscle-group energies were compared with paired (left vs right) t-tests with multiplicity control across groups. Because repeated observations within participants can inflate standard Pearson correlations, we emphasize within-session change metrics (stage-wise slopes) and interpret r values as associations rather than agreement.

All statistical analyses described above relate to metabolic and muscle-level outcomes; kinematic cross-platform comparisons were performed solely as a quality-control verification and were not used for hypothesis testing.

5.4 Results

Results are presented for cost of transport across methods (indirect calorimetry, *Bhargava2004*, *Umberger2003*, *Umberger2010*) and fatigue stages (Pre, Mid, Post), followed by agreement analyses and the left–right muscle-energy breakdown.

5.4.1 Kinematic quality check

A cross-platform comparison between OpenSim inverse kinematics and direct-K joint-angle waveforms was performed as a validity check to confirm that OpenSim IK accurately reproduced experimentally derived kinematics within each trial. This analysis was not intended to evaluate fatigue-related changes in joint motion.

Across all joints and limbs, OpenSim IK waveforms closely matched direct-K waveforms in temporal structure and phase behaviour (Appendix Figures A 5.1–A 5.8). SPM repeated-measures

analyses identified only small, phase-limited differences between methods. A method effect was observed for left hip abduction during mid-stance (~58–66% gait cycle), while isolated phase-specific effects were detected for hip flexion near early stance and terminal swing, and for right knee flexion during early stance. Method × stage interaction terms reached threshold in narrow regions for left ankle and right hip abduction; however, these effects were limited in duration and magnitude.

Representative paired SPM t-tests comparing OpenSim IK and direct-K within individual trials revealed no clusters exceeding the critical threshold across most joints, indicating strong waveform agreement. No evidence of numerical drift, discontinuities, or trial-dependent artefacts was observed. These estimates verify that OpenSim IK provided joint-angle trajectories in agreement with direct kinematics calculations for subsequent musculoskeletal and metabolic analyses.

5.4.2 EMG–Model Timing Check

An auxiliary EMG analysis was performed to evaluate the temporal correspondence between experimentally measured muscle activity and the static optimization (SO) activation time series. Group mean EMG–model lags ranged from approximately −5% to −15% of the gait cycle across muscles and stages, with substantial inter-muscle and inter-stride variability (Figure A 5.9–A 5.12). Boxplots of per-stride lags showed broad distributions for all muscles, and no systematic drift across the three runs was observed. These results indicate that SO activations consistently occurred later than experimental EMG onsets, but the timing offsets were stable across stages, supporting their use in downstream energy-model comparisons. Full summaries for each muscle are provided in Appendix Tables A 5.2–A 5.4.

5.4.3 Main Effects of Method and Fatigue Stage

A two-way repeated-measures ANOVA revealed a significant main effect of estimation method on CoT ($F(3,18) = 116.80$, $p < 0.001$), indicating that the CoT values differed significantly across

the four estimation approaches. In contrast, the main effect of fatigue stage was not statistically significant ($F(2,12) = 2.46$, $p = 0.127$)), showing that CoT did not increase as the fatigue protocol progressed. Importantly, no significant interaction effect was found between estimation method and fatigue stage ($F(6,36) = 1.53$, $p = 0.196$) as seen in Figure 5.1.

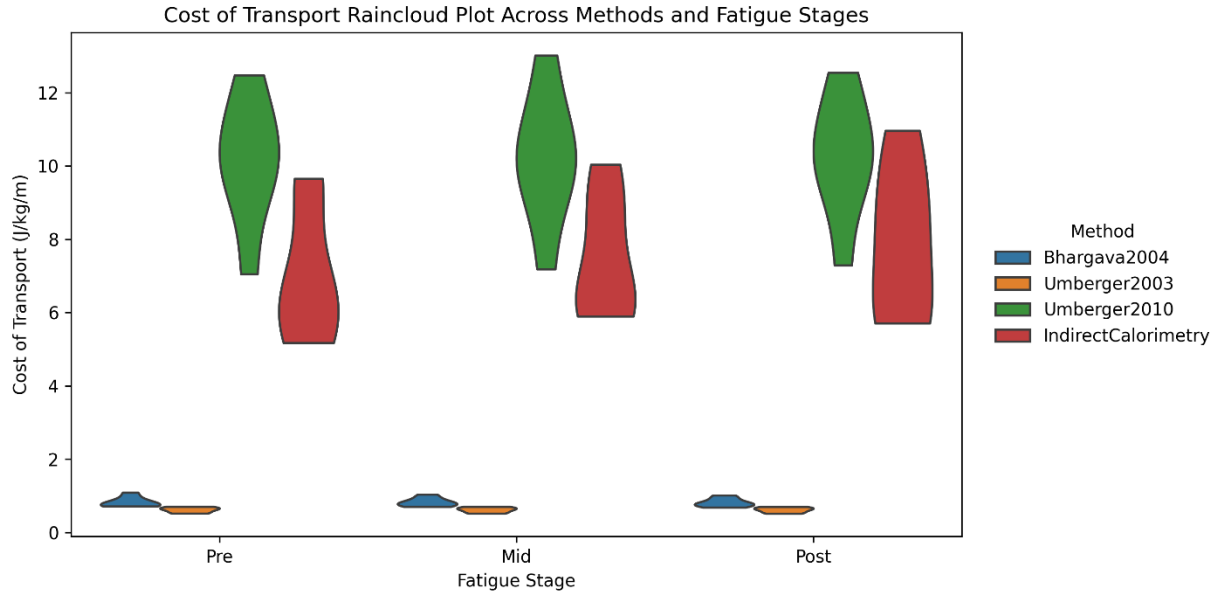

Figure 5.1: Cost of transport ($J \cdot kg^{-1} \cdot m^{-1}$) across three fatigue stages (pre-fatigue, mid-fatiguing, and post-fatigue) estimated using three OpenSim metabolic models (Bhargava2004, Umberger2003, Umberger2010) and indirect calorimetry. Distributions across participants are shown for each method and stage.

5.4.4 Pairwise Model Comparisons

Post hoc pairwise comparisons showed that all three musculoskeletal model-based methods differed from indirect calorimetry. The *Bhargava2004* model (Figure 5.2) produced lower CoT values than indirect calorimetry, with a mean bias of −6.62 J/kg/m. The *Umberger2003* model (Figure 5.3) also underestimated CoT, with a mean bias of −6.82 J· J/kg/m. In contrast, the *Umberger2010* model (Figure 5.4) produced slightly higher CoT values than indirect calorimetry, with a mean bias of +2.75 J/kg/m.

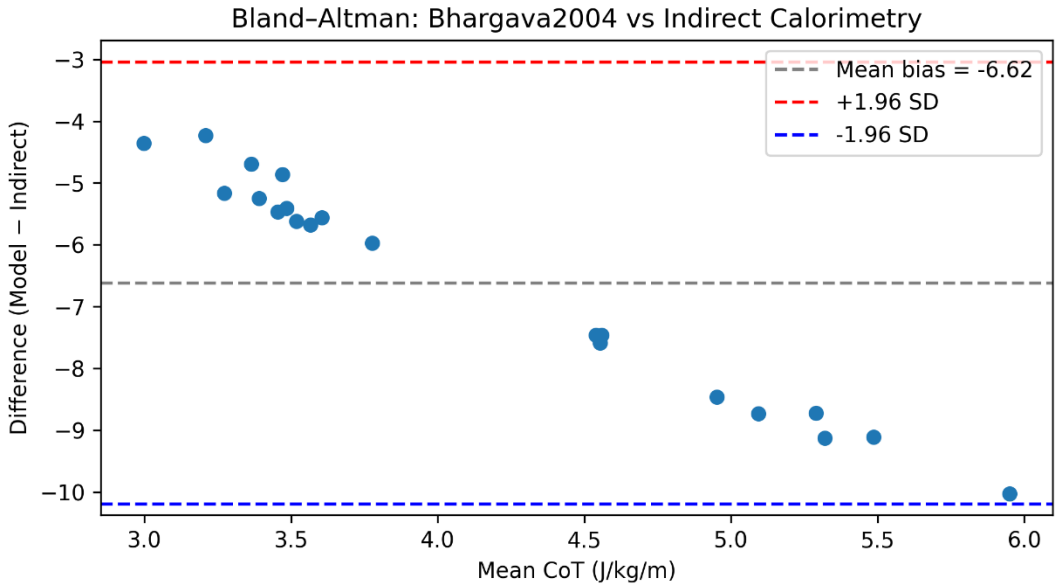

Figure 5.2: Bland–Altman analysis comparing CoT ($J \cdot kg^{-1} \cdot m^{-1}$) estimated using the Bhargava2004 metabolic energy model and indirect calorimetry. Each point represents one participant at one fatigue stage (pre-fatigue, mid-fatigue, or post-fatigue). The x-axis shows the mean CoT of the two methods, and the y-axis shows the difference between methods (Bhargava2004 − indirect calorimetry). Negative values indicate that the model underestimated CoT relative to indirect calorimetry. The grey dashed line represents the mean bias, and the red and blue dashed lines indicate the upper and lower 95% limits of agreement (mean bias ± 1.96 SD).

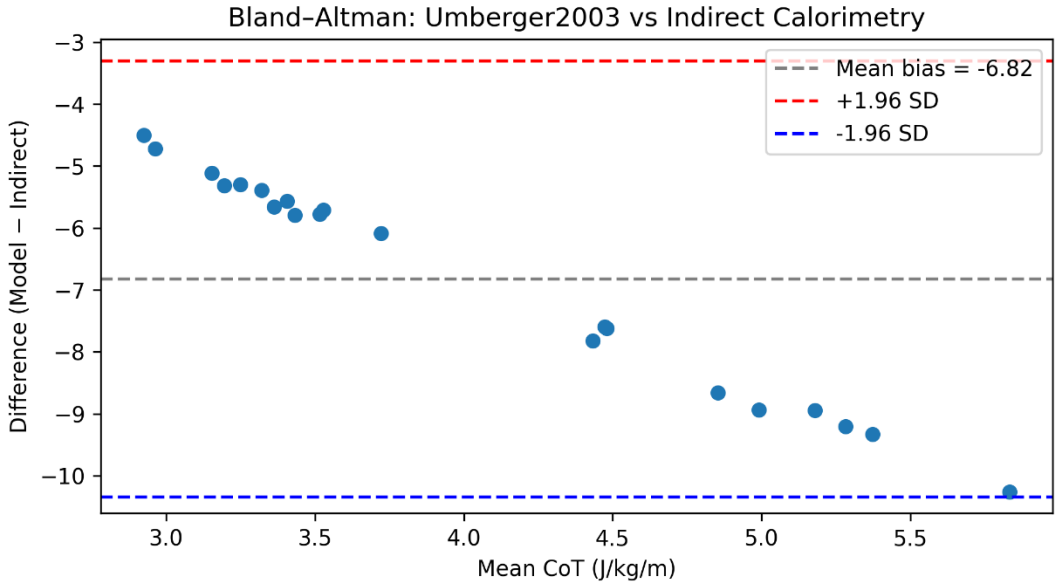

Figure 5.3: Bland–Altman analysis comparing CoT ($J \cdot kg^{-1} \cdot m^{-1}$) estimated using the Umberger2003 metabolic energy model and indirect calorimetry. Each point represents one participant at one fatigue stage (pre-fatigue, mid-fatigue, or post-fatigue). The x-axis shows the mean CoT of the two methods, and the y-axis shows the difference between methods (Umberger2003 − indirect calorimetry). Negative values indicate that the model underestimated CoT relative to indirect calorimetry. The grey dashed line represents the mean bias, and the red and blue dashed lines indicate the upper and lower 95% limits of agreement (mean bias ± 1.96 SD).

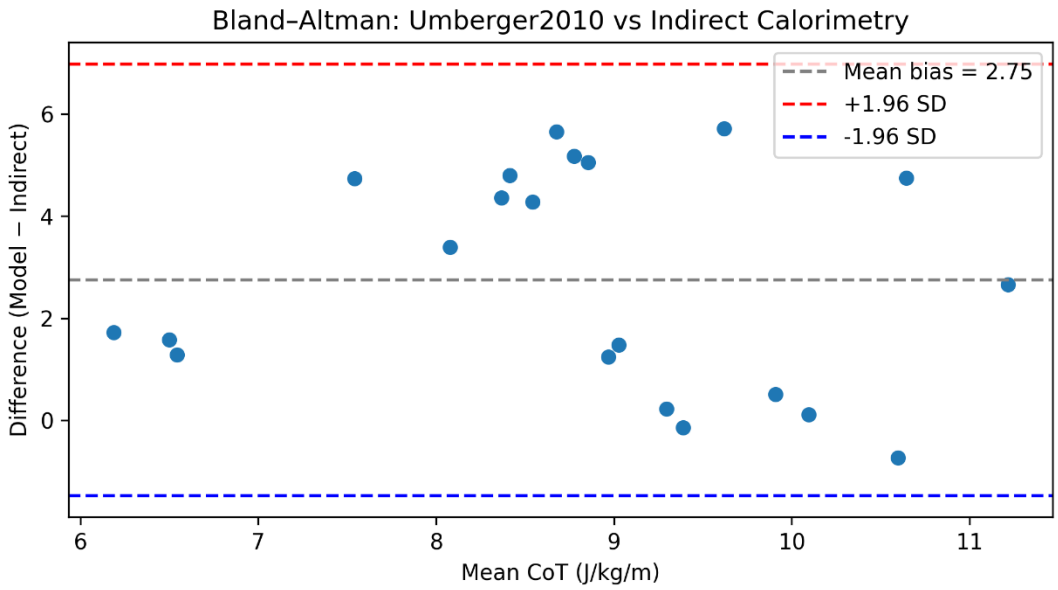

Figure 5.4: Bland–Altman analysis comparing CoT ($J \cdot kg^{-1} \cdot m^{-1}$) estimated using the Umberger2010 metabolic energy model and indirect calorimetry. Each point represents one participant at one fatigue stage (pre-fatigue, mid-fatigue, or post-fatigue). The x-axis shows the mean CoT of the two methods, and the y-axis shows the difference between methods (Umberger2010 − indirect calorimetry). Positive values indicate that the model overestimated CoT relative to indirect calorimetry. The grey dashed line represents the mean bias, and the red and blue dashed lines indicate the upper and lower 95% limits of agreement (mean bias ± 1.96 SD).

5.4.5 Correlation with Indirect Calorimetry

The *Bhargava2004* model (Figure 5.5) showed no significant correlation with indirect calorimetry ($r = -0.05$, $p = 0.8461$). Similarly, the *Umberger2003* model (Figure 5.6) demonstrated a weak, non-significant correlation ($r = 0.27$, $p = 0.2328$). The *Umberger2010* model (Figure 5.7) also showed a weak, non-significant correlation with indirect calorimetry ($r = 0.22$, $p = 0.3339$).

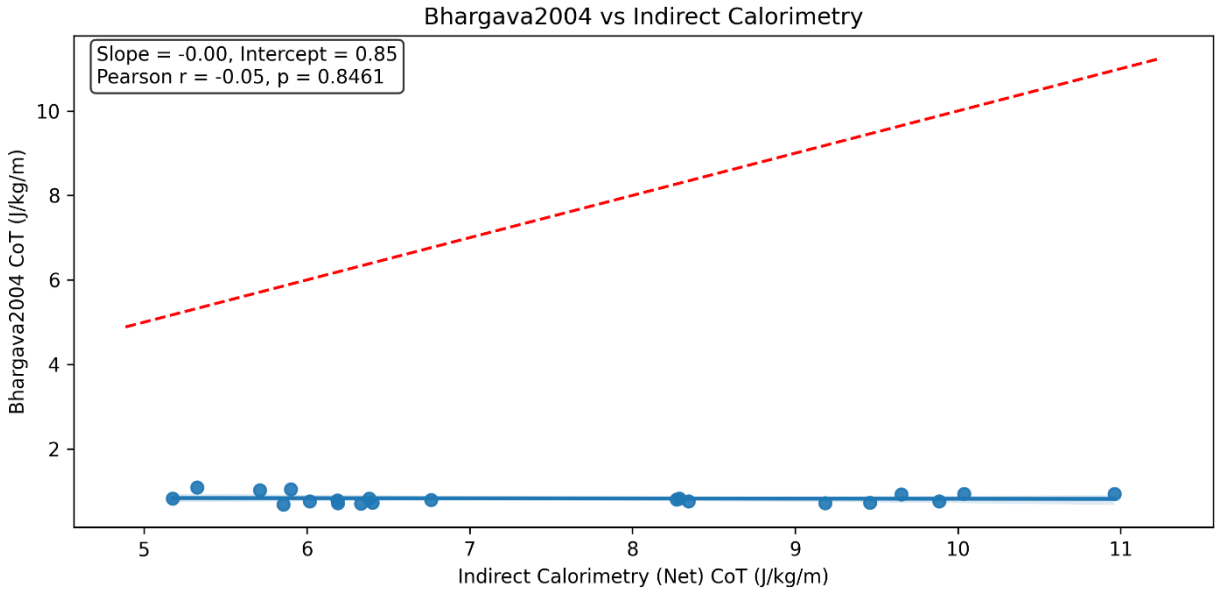

Figure 5.5: Correlation between CoT ($J \cdot kg^{-1} \cdot m^{-1}$) estimated using the Bhargava2004 metabolic energy model and measured by indirect calorimetry. Each point represents one participant at one fatigue stage (pre-fatigue, mid-fatigue, or post-fatigue). The x-axis shows CoT measured by indirect calorimetry, and the y-axis shows CoT estimated by the Bhargava2004 model. The solid blue line represents the linear regression fit, and the red dashed line represents the line of identity (y = x), indicating perfect agreement between methods.

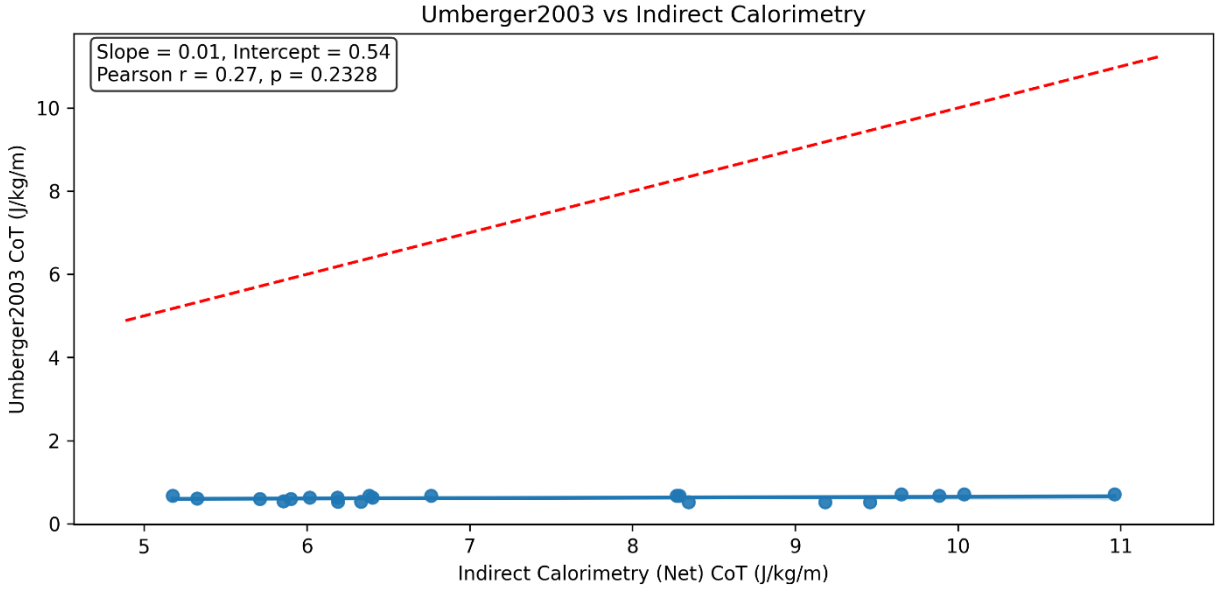

Figure 5.6: Correlation between CoT ($J \cdot kg^{-1} \cdot m^{-1}$) estimated using the Umberger2003 metabolic energy model and measured by indirect calorimetry. Each point represents one participant at one fatigue stage (pre-fatigue, mid-fatigue, or post-fatigue). The x-axis shows CoT measured by indirect calorimetry, and the y-axis shows CoT estimated by the Umberger2003 model. The solid blue line represents the linear regression fit, and the red dashed line represents the line of identity (y = x), indicating perfect agreement between methods.

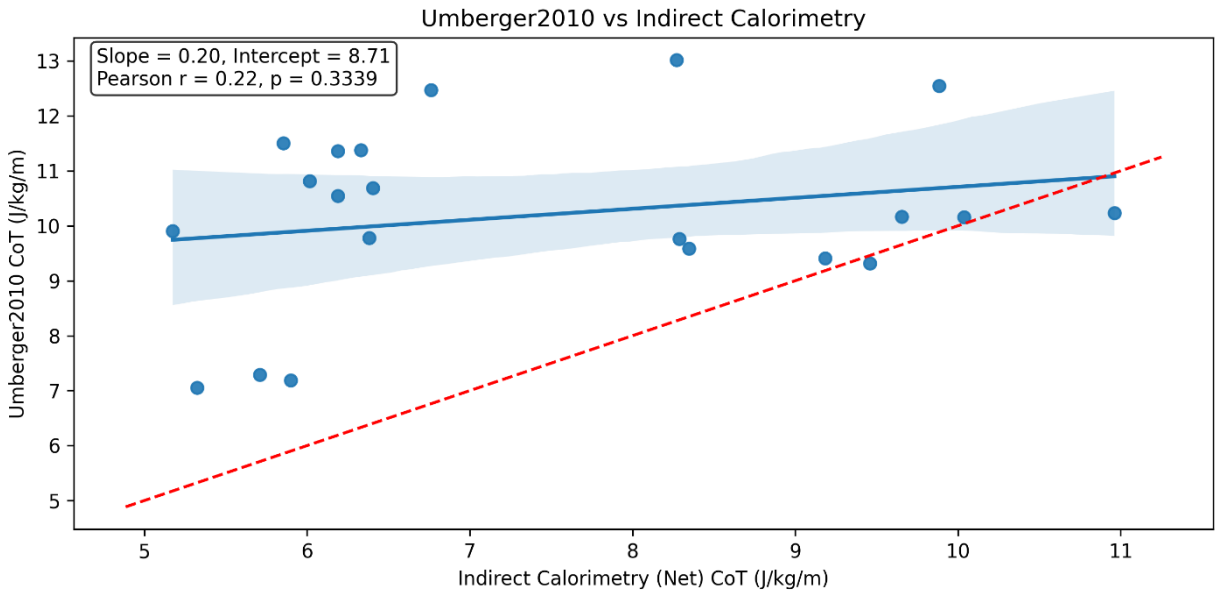

Figure 5.7: Correlation between CoT ($J \cdot kg^{-1} \cdot m^{-1}$) estimated using the Umberger2010 metabolic energy model and measured by indirect calorimetry. Each point represents one participant at one fatigue stage (pre-fatigue, mid-fatigue, or post-fatigue). The x-axis shows CoT measured by indirect calorimetry, and the y-axis shows CoT estimated by the Umberger2010 model. The solid blue line represents the linear regression fit with its 95% confidence interval, and the red dashed line represents the line of identity (y = x), indicating perfect agreement between methods.

5.4.6 CoT Directional Changes Across Fatigue Stages

All four methods were evaluated for their ability to capture changes in CoT across fatigue stages (Figure 5.8). The *Bhargava2004* model showed a negligible change across time, with a slope of −0.0034. The *Umberger2003* model demonstrated a similarly minimal change, with a slope of −0.0011. The *Umberger2010* model produced a modest positive slope of 0.0554, indicating a small increase in CoT from pre- to post-fatigue. In comparison, indirect calorimetry showed the largest change across stages, with a slope of 0.4349. Overall, model-based estimates demonstrated negligible changes across fatigue stages compared to indirect calorimetry.

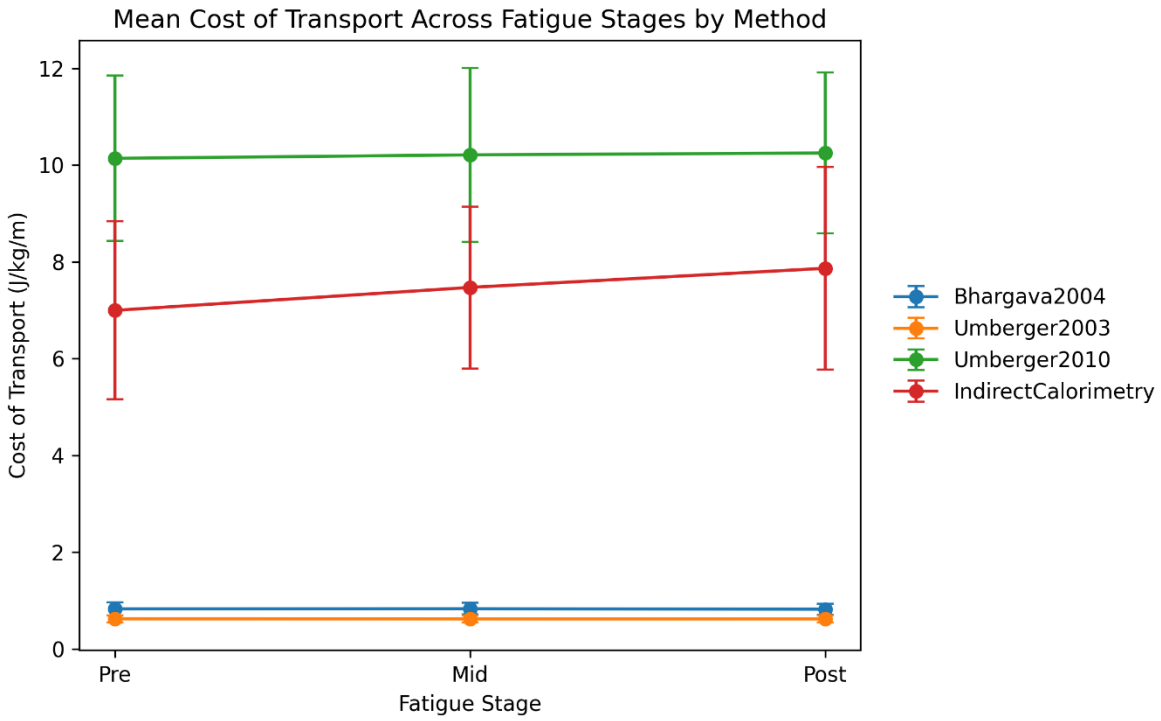

Figure 5.8: Mean cost of transport across fatigue stages (Pre: 02, Mid: 05, Post: 08) for four estimation methods: Bhargava2004, Umberger2003, Umberger2010, and indirect calorimetry. Each point represents the group mean CoT (J/kg/m) at a given fatigue stage, with vertical error bars indicating ±1 standard deviation. Bhargava 2004 consistently produced the lowest CoT estimates, while Umberger2003 yielded the highest across all stages. Indirect calorimetry served as the empirical reference.

5.4.7 Muscle-Level Energy Contributions

The distribution of metabolic energy expenditure across muscle groups was evaluated separately for the left and right legs using the *Umberger2010* metabolic energy model (Figure 5.9-5.10). Across participants, the quadriceps exhibited the highest mean energy expenditure for both limbs (Left: 7.16 ± 2.15 J, Right: 6.86 ± 1.84 J), followed by the hamstrings (Left: 4.80 ± 0.87 J, Right: 4.77 ± 0.97 J). The adductors showed intermediate values (Left: 2.31 ± 0.31 J, Right: 2.21 ± 0.49 J), while the gluteal muscles demonstrated low energy expenditure with similar magnitudes between sides (Left: 0.29 ± 0.04 J, Right: 0.29 ± 0.04 J). The hip flexors, plantarflexors (two subdivisions), and dorsiflexors produced the smallest energy contributions, with mean values

below 0.20 J for all groups on both limbs. These results were consistent across all participants and fatigue stages.

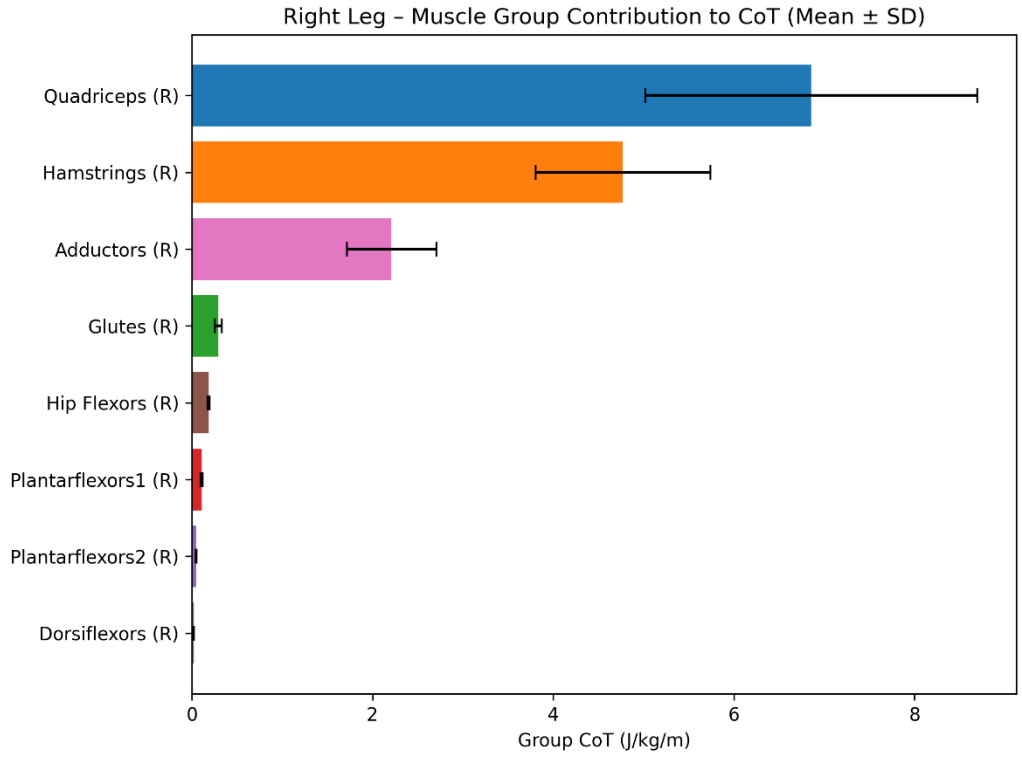

Figure 5.9: Mean cost of transport ($J \cdot kg^{-1} \cdot m^{-1}$) attributed to individual muscle groups using the *Umberger2010* of the right leg, presented as mean ± SD across participants.

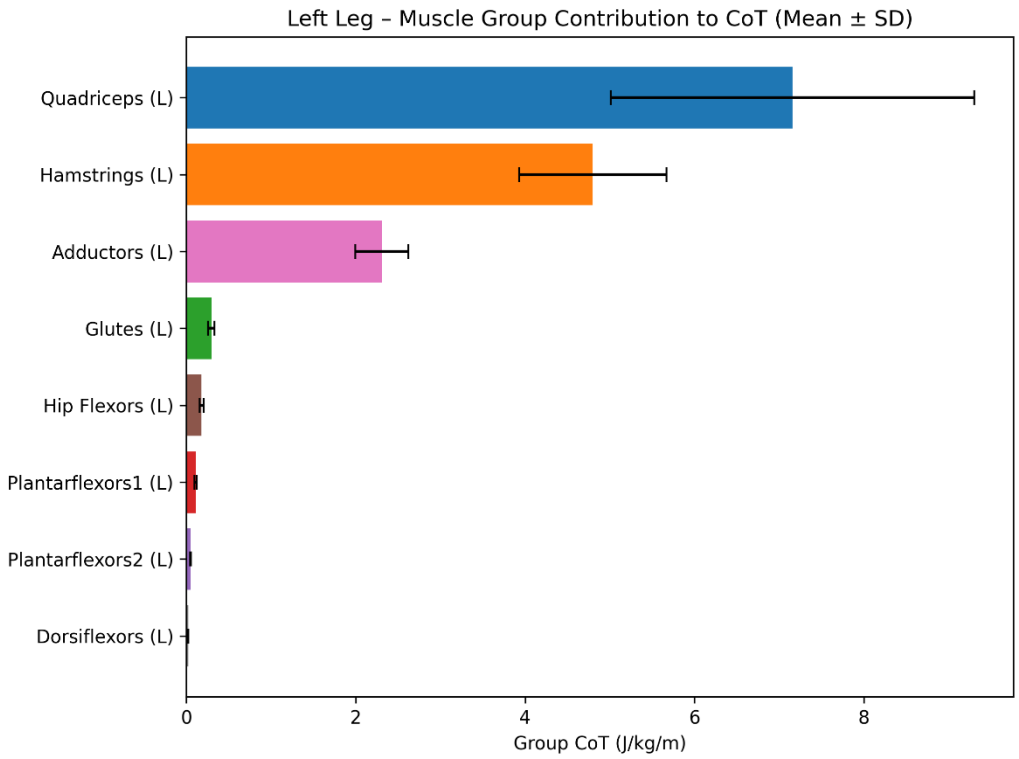

Figure 5.10: Mean cost of transport ($J \cdot kg^{-1} \cdot m^{-1}$) attributed to individual muscle groups using the *Umberger2010* of the left leg, presented as mean ± SD across participants.

Paired t-tests comparing left and right muscle-group energy expenditure revealed no statistically significant side differences for any muscle group (all $p > 0.05$; see Table A 5.2).

5.4.8 Residual Actuator Analysis

Residual actuator magnitudes were evaluated using the criteria proposed by Hicks et al. (2015), with residual forces expressed as a percentage of peak net external force and residual moments expressed as a percentage of the product of center-of-mass height and peak net external force.

Across all fatigue stages (Pre, Mid, Post), both residual force and residual moment values exceeded recommended thresholds. Residual force analysis revealed that the anteroposterior component (FY) was consistently elevated, with mean peak values ranging from approximately 16% to 25% of peak net external force. In contrast, mediolateral (FX) and vertical (FZ) components

remained closer to recommended limits, generally within 3–5%. RMS residual force values demonstrated similar trends, with FY remaining substantially elevated across all stages.

Residual moments also exceeded the recommended 1% threshold across all components. Peak residual moments ranged from approximately 1–3%, while RMS values were notably higher, particularly for the MX component during the post-fatigue stage.

Across the fatigue protocol, residual force magnitudes showed a modest reduction from Pre to Post for FY, while residual moments demonstrated increased variability, with some components (e.g., MX) increasing in magnitude during the post-fatigue stage.

Time-series analysis demonstrated that these elevated residuals were characterized by large transient spikes, particularly during stance phases of running, with peak deviations occurring near initial contact.

Detailed group-level summaries of peak and RMS residual forces and moments are presented in Figure A 5.13, and corresponding time-series profiles are shown in Figure A 5.17.

5.5 Discussion

This study examined the accuracy, bias, and fatigue responsiveness of three musculoskeletal energy models, *Bhargava2004*, *Umberger2003*, and *Umberger2010*, implemented within a static optimization (SO) framework, using indirect calorimetry as the empirical reference during high-intensity running. A central finding of this work is the clear dissociation between physiological fatigue, which was robustly captured by indirect calorimetry, and model-derived energetics, which were largely insensitive to fatigue progression. This indicates that the observed discrepancies primarily reflect limitations inherent to the modelling frameworks rather than deficiencies in the experimental protocol or kinematic (Koelewijn et al., 2019; Luis et al., 2023; Mohammadzadeh Gonabadi et al., 2020; Uchida et al., 2016a, 2016b).

Importantly, the experimental design successfully elicited progressive fatigue, as evidenced by a clear stage-dependent increase in CoT measured via indirect calorimetry. This confirms that participants transitioned through distinct fatigued states over the course of the protocol. In contrast, the musculoskeletal energy models exhibited substantial and systematic bias in absolute CoT and limited responsiveness to fatigue, highlighting fundamental challenges in applying SO to estimate energetics to prolonged, high-demand locomotor tasks.

5.5.1 Evaluation of Hypotheses

The first hypothesis, that *Bhargava2004* would underestimate CoT relative to indirect calorimetry, was supported, as this model consistently produced lower CoT estimates with a systematic negative bias across all fatigue stages.

The second hypothesis, that *Umberger2003* and *Umberger2010* would overestimate CoT, was partially supported. While *Umberger2010* consistently overestimated CoT relative to calorimetry, *Umberger2003* underestimated CoT in the present dataset, contrary to prior reports.

The hypothesis that static optimization–driven models would show limited sensitivity to fatigue-related changes in metabolic demand was supported. Across all models, CoT remained largely unchanged despite increasing physiological strain, and no significant Method × Stage interaction was detected. Although *Umberger2010* was the only model to reproduce the direction of the empirically observed increase in CoT with fatigue, this response was limited and substantially attenuated relative to indirect calorimetry, indicating a lack of meaningful sensitivity.

Collectively, these findings support the premise that static optimization–driven musculoskeletal energy models, which do not incorporate EMG or fatigue dynamics, are insufficient to capture fatigue-related changes in metabolic cost under conditions where kinematics remain stable.

5.5.2 Kinematic Integrity

Supplementary kinematic checks indicated high concordance between OpenSim and an independent MATLAB pipeline across joints, stages, and limbs (Appendix Figures A.1-A.8). Statistical parametric mapping (SPM) repeated-measures ANOVA with random field theory (RFT) correction identified only localized differences (Pataky, 2010; Pataky et al., 2013), including a Method effect for left hip abduction during mid-stance (~58–66% of the gait cycle), Stage effects for hip flexion (right: ~18–33%; left: ~96–100%) and right knee flexion (~10–18%), and small Method × Stage interactions at the left ankle (~72–78%) and right hip abduction (~26–31%).

Across all identified regions, waveform deviations were small, on the order of a few degrees and within typical motion-capture measurement error, indicating limited biomechanical relevance (Benoit et al., 2015, 2006; Kadaba et al., 1989; Leardini et al., 2005; McGinley et al., 2009). No run-dependent drift was observed. Collectively, these results support the validity of the IK inputs and indicate that the observed CoT biases and responsiveness patterns are unlikely to be artefacts of kinematic preprocessing or pipeline choice.

5.5.3 Model Accuracy and Systematic Error

A consistent pattern of systematic error emerged across the three musculoskeletal energy models when compared with indirect calorimetry. Both *Bhargava2004* and *Umberger2003* produced lower CoT values than the empirical reference, whereas *Umberger2010* persistently overestimated CoT. This ordering aligns with the theoretical basis of each approach but also reveals important model-specific limitations under conditions of incline and high-intensity running.

The underestimation observed in *Bhargava2004* reflects its foundational design. The model emphasizes activation and maintenance heat and does not explicitly represent mechanical work or fiber-type dependence (Bhargava et al., 2004). Bhargava et al. (2004) originally developed their model for EMG-informed analysis during static and quasi-static tasks, emphasizing activation cost

over contraction dynamics. As a result, it tends to produce lower metabolic estimates during dynamic locomotor tasks where positive mechanical work and force–velocity effects contribute substantially to energetic demand (Koelewijn et al., 2019; Pizzolato et al., 2017). The consistent negative bias and relatively tight limits of agreement found in the Bland–Altman plots suggest that *Bhargava2004* is systematic and predictable in its behaviour, but insufficient for capturing absolute metabolic cost in high-intensity running.

Umberger2003 also underestimated calorimetry values in this dataset, albeit to a lesser extent than *Bhargava2004*. This contrasts with reports in the literature in which *Umberger2003* frequently overestimates cost, particularly during walking or level-ground running (Luis et al., 2023; Uchida et al., 2016a). In the present study, the use of a 1% treadmill incline, commonly employed to approximate overground running, reflects the mechanical demands of typical running rather than an atypical or exaggerated condition (Kipp et al., 2018; Minetti et al., 2002). Under these conditions, which involve reduced reliance on elastic energy storage and greater concentric muscle work, static optimization may bias force production toward energetically favourable muscles, yielding artificially low CoT estimates. Additionally, in the absence of EMG-informed calibration, SO-derived activations may depart from physiological recruitment patterns, attenuating shortening and lengthening heat contributions central to the *Umberger2003* formulation (Koelewijn et al., 2019; Lloyd and Besier, 2003; Sartori et al., 2012b).

Conversely, *Umberger2010* consistently overestimated CoT relative to indirect calorimetry. This is expected given its enhanced sensitivity to fiber-type composition, shortening–lengthening efficiency, and activation–relaxation heat (Umberger, 2010). In high-intensity running, where Type II fibers are recruited more heavily and force–velocity effects are amplified, these model components can elevate metabolic estimates more than is observed empirically (Silder et al., 2012). The broader limits of agreement observed in the Bland–Altman analyses suggest additional inter-

individual variability, potentially linked to unmodelled differences in tendon elasticity, muscle–tendon architecture, and neuromuscular fatigue.

Importantly, because supplementary kinematic analyses confirmed the integrity of the motion input data, these systematic discrepancies are unlikely to arise from pipeline artefacts. Rather, they reflect the inherent assumptions and mechanical simplifications embedded within each metabolic model, as well as the limitations of the static optimization framework used to estimate muscle activations. In particular, the time-independent nature of static optimization and its lack of fatigue-related dynamics constrain the ability of these models to capture evolving neuromuscular states. The findings emphasize that model–data bias should not be interpreted uniformly across all locomotor contexts; instead, task-specific mechanical demands interact with model structure in ways that can meaningfully alter absolute CoT estimates (Gambietz et al., 2024; Modenese et al., 2016).

5.5.4 Residual and Reserve Actuator Analysis

Residual and reserve actuator analysis indicated that the musculoskeletal simulations did not meet established dynamic consistency criteria (Hicks et al., 2015). Both residual forces and moments exceeded recommended thresholds across all fatigue stages, with the largest deviations observed in the vertical force component (FY) and across all moment components.

Elevated residuals are indicative of inconsistencies between model kinematics, ground reaction forces, and inverse dynamics solutions. These discrepancies are commonly attributed to a combination of factors, including soft tissue artefacts affecting marker trajectories (Benoit et al., 2006), limitations in scaling generic musculoskeletal models to participant-specific anatomy, and measurement noise in experimental data (Hicks et al., 2015; Reinbolt et al., 2005). Additionally, the absence of residual reduction algorithms (RRA) in the present workflow likely contributed to the magnitude of residual forces and moments, as RRA is specifically designed to improve dynamic

consistency by minimizing residual loads while preserving kinematics (Delp et al., 2007; Dembia et al., 2020; Hicks et al., 2015).

The predominance of residuals in the vertical direction suggests inconsistencies in vertical force balance and bodyweight support, rather than forward propulsion. During running, the vertical ground reaction force represents the largest component of external loading and is primarily responsible for supporting body mass and regulating center-of-mass motion throughout stance. As a result, even small discrepancies between measured ground reaction forces and model-derived kinematics can produce substantial vertical residuals. These inconsistencies are particularly sensitive to errors in ground reaction force measurements, treadmill dynamics, and segmental kinematics (Hamner and Delp, 2013; Hicks et al., 2015; Ingen Schenau and Cavanagh, 1990; Reinbolt et al., 2005). In contrast, forward propulsion is governed by the anteroposterior force component, indicating that the observed vertical residuals more likely reflect challenges in accurately capturing vertical loading dynamics rather than errors in propulsive mechanics. Residual moments were also consistently elevated, with increased variability observed under fatigued conditions, indicating challenges in accurately resolving rotational dynamics during prolonged running.

The use of static optimization further contributes to these discrepancies, as the approach resolves muscle redundancy through a cost function that minimizes activation without accounting for activation dynamics, co-contraction, or fatigue-related neuromuscular adaptations (Anderson and Pandy, 2001; Lloyd and Besier, 2003). As a result, the simulated muscle forces represent mechanically optimal solutions rather than physiologically constrained behaviour, which may exacerbate inconsistencies between muscle-generated and inverse dynamics joint moments, particularly under fatigued conditions.

In addition to residual forces and moments, elevated reserve actuator torques were observed, indicating that non-physiological actuators were required to supplement joint moments not adequately produced by the modelled musculature (Hicks et al., 2015). High reserve actuator contributions suggest that the simulated muscle forces were insufficient to reproduce inverse dynamics demands, particularly during phases of the gait cycle associated with high loading or rapid force production. This may reflect limitations in model strength scaling, activation constraints, or the inability of static optimization to capture fatigue-related reductions in force-generating capacity.

These modelling inconsistencies have important implications for the interpretation of metabolic cost estimates. Because reserve actuators do not incur a metabolic penalty within the modelling framework, their use can lead to an underestimation of muscle-driven energy expenditure (Uchida et al., 2016a; Umberger, 2010). As metabolic energy models rely on muscle force predictions derived from inverse dynamics, elevated residuals may further contribute to discrepancies between model-estimated and experimentally measured cost of transport.

Despite these limitations, residual and reserve actuator magnitudes remained relatively consistent across Pre, Mid, and Post stages, with a general reduction observed over time. This consistency suggests that, while absolute simulation accuracy is limited, the modelling framework remains appropriate for relative comparisons across fatigue conditions, which was the primary objective of this study.

Taken together, the elevated residual forces, moments, and reserve actuator contributions indicate that full dynamic consistency was not achieved within the present simulations. While such discrepancies are not uncommon in running analyses, their magnitude suggests that the modelling framework may not fully capture the underlying biomechanics of prolonged high-intensity running, particularly under fatigued conditions. Consequently, metabolic cost estimates derived from the

simulations should be interpreted with caution in absolute terms, as these modelling limitations may contribute to discrepancies between model-estimated and experimentally measured cost of transport. Nevertheless, the framework remains informative for evaluating within-subject and between-stage trends.

Future work should incorporate residual reduction procedures, improved model personalization (e.g., muscle strength scaling and tendon properties), and EMG-informed neuromusculoskeletal modelling approaches to enhance dynamic consistency and physiological realism (Lloyd and Besier, 2003; Sartori et al., 2012a).

5.5.5 Sensitivity to Fatigue Progression

When evaluating how CoT changed across fatigue stages, only the *Umberger2010* model demonstrated a stage-dependent pattern that aligned with the metabolic progression observed in indirect calorimetry. Calorimetry showed a clear rise in CoT from pre- to post-fatigue (slope ≈ +0.435 $J \cdot kg^{-1} \cdot m^{-1}$ per stage), consistent with the increased energetic demands of prolonged high-intensity running. In contrast, both *Bhargava2004* and *Umberger2003* produced slight negative slopes (–0.0034 and –0.0011, respectively), failing to capture even the direction of the physiological response.

The *Umberger2010* model yielded a positive slope (+0.0554), indicating a modest increase across stages that paralleled the calorimetry trend, albeit with an attenuated magnitude. While this suggests improved directional sensitivity compared to the other models, this behaviour should not be interpreted as reflecting fatigue-related physiological mechanisms. All models were driven by kinematic and ground reaction force inputs, which remained largely unchanged across stages, and muscle activations were estimated using static optimization. As such, the modelling framework does not account for fatigue-induced changes in neuromuscular control, recruitment strategies, or muscle efficiency.

The limited sensitivity of model-based CoT estimates to fatigue-related changes therefore reflects constraints inherent to the overall modelling framework rather than the static optimization solver alone. In the present study, the estimated activations remained closely tied to mechanical demands, as dictated by the input kinematics and external forces. While static optimization resolves the muscle redundancy problem under an economy-based objective, the broader musculoskeletal modelling approach does not incorporate fatigue-dependent activation dynamics, muscle-history effects, or individualized muscle–tendon properties. Consequently, changes in neuromuscular control and metabolic efficiency that occur with fatigue are not reflected in the model outputs.

Although the *Umberger2010* formulation includes additional energetic components compared to earlier models, these mechanisms are not explicitly modulated by fatigue within the current framework. Furthermore, assumptions such as rigid tendon behaviour and the absence of fatigue-dependent activation dynamics limit the ability of the model to accurately represent changes in shortening–lengthening energetics under fatigued conditions. This likely contributes to the attenuated CoT response observed across all models (Silder et al., 2008).

Importantly, although the repeated-measures ANOVA detected a significant main effect of stage, this effect was driven primarily by the calorimetry data. The absence of a Method × Stage interaction indicates that the models did not differ statistically in their stage-wise modulation of CoT, despite differences in directional trends.

These findings are consistent with prior work showing that, in the absence of EMG-informed or physiologically constrained activation dynamics, model-based energetics may under-represent fatigue-driven increases in metabolic cost (Arones et al. 2020 and Koelewijn et al. 2019). The present results extend this observation to prolonged, high-intensity running with verified physiological fatigue and stable kinematic inputs, demonstrating that substantial fatigue-related

energetic and neuromuscular changes can occur in the absence of detectable alterations in joint kinematics.

Despite these limitations, the use of a kinematically driven musculoskeletal model was appropriate for the aims of this study. Specifically, the objective was to evaluate whether commonly used modelling approaches are capable of capturing fatigue-related changes in metabolic cost under controlled mechanical conditions. The observed discrepancy between model-based estimates and indirect calorimetry therefore represents a meaningful outcome, highlighting the current limitations of such models when applied to fatigued states rather than a limitation of the study design itself

Taken together, these results suggest that while the *Umberger2010* model demonstrates improved directional alignment with experimental data, all models exhibit limited sensitivity to fatigue-related changes in CoT. This underscores the need for incorporating fatigue-dependent mechanisms or EMG-informed approaches when estimating metabolic cost in prolonged locomotor tasks.

5.5.6 Implications for Musculoskeletal Energy Modelling

The present findings have important implications for the use of musculoskeletal energy models in research contexts where fatigue progression is of interest. While using SO estimates of muscle activation with metabolic models is frequently applied to estimate absolute energetic cost or compare task conditions, the current results demonstrate that their sensitivity to physiological fatigue during prolonged high-intensity locomotion is limited. This is particularly relevant for studies aiming to quantify fatigue accumulation, training load, or performance degradation over time.

The lack of fatigue responsiveness observed in *Bhargava2004* and *Umberger2003* suggests that these models may be appropriate for steady-state or short-duration tasks but are less suitable for investigations in which time-dependent physiological changes are central to the research

question. Even *Umberger2010*, which demonstrated partial directional alignment, substantially underestimated the magnitude of fatigue-related increases in CoT. Without incorporating fatigue-aware activation dynamics, personalized muscle–tendon properties, or EMG-informed constraints, SO-based frameworks are likely to reflect mechanically economical solutions rather than evolving neuromuscular strategies (Lloyd and Besier, 2003; Sartori et al., 2012b).

Compared to forward dynamics approaches such as Computed Muscle Control (CMC), static optimization offers improved computational efficiency and numerical stability, but at the cost of reduced physiological realism (Anderson and Pandy, 2001; Delp et al., 2007). CMC incorporates activation dynamics and temporal constraints, enabling closer tracking of experimentally observed movement patterns (Thelen et al., 2003), whereas static optimization solves each time step independently without accounting for activation history or fatigue-related processes (Lloyd and Besier, 2003; Sartori et al., 2012b). As a result, while static optimization is appropriate for estimating general muscle force patterns, it may be less suitable for capturing time-dependent neuromuscular adaptations under fatigue, as observed in the present study (De Groote et al., 2016).

Another important modelling consideration relates to the representation of musculotendon dynamics within the static optimization framework. The static optimization approach typically assumes simplified musculotendon behaviour, often treating tendon dynamics as rigid or quasi-static (Millard et al., 2013; Zajac, 1989). However, tendon compliance plays a critical role in energy storage and return during running, influencing muscle fiber operating lengths, contraction velocities, and overall metabolic cost (Fukunaga et al., 2001; Lichtwark and Wilson, 2005). Previous work has demonstrated that incorporating compliant tendon dynamics can substantially alter predicted muscle energetics and force distributions compared to rigid tendon assumptions, particularly in cyclic tasks such as gait (Arnold et al., 2013; Uchida et al., 2016a). The absence of explicit tendon compliance modelling in the present simulations may therefore contribute to

discrepancies between model-estimated and experimentally measured cost of transport, especially under fatigue conditions where musculotendon behaviour may be altered.

5.5.7 Protocol Design and Elevated CoT Values

The empirical CoT values observed in this study (6–10 J/kg/m) exceed typical treadmill running estimates at moderate speeds (~3.5–5.0 J/kg/m). These elevated values are attributable to two key factors: the use of a 1% treadmill incline and a workload targeting ~85% of VO2 max. Both conditions are known to elevate energetic demands. Incline running, in particular, increases vertical mechanical work and suppresses elastic energy return, resulting in higher oxygen uptake (Kipp et al., 2018; Minetti et al., 2002). Studies by Bellenger et al. (2019) and Biancardi et al. (2023) confirm that even trained runners show substantial increases in CoT during inclined or prolonged high-speed running.

Beyond confirming physiological plausibility, these elevated CoT values provide a robust benchmark for evaluating musculoskeletal energy models under demanding conditions. Most validation studies of musculoskeletal metabolic models have focused on level walking or low-intensity running, where energetic demands and fatigue effects are relatively modest (Ortiz et al., 2017; Silder et al., 2012). Consequently, there is limited evidence regarding model behaviour during prolonged, high-cost locomotor tasks in which fatigue is expected to play a meaningful role. By eliciting a sustained yet physiologically realistic metabolic load, the present protocol offers a meaningful test of model robustness in a more challenging and ecologically relevant context. That the empirical CoT values map well onto established physiological expectations strengthens confidence in the calorimetry data as a reference standard and supports the interpretation that discrepancies between model-based estimates and calorimetry arise from model formulation and activation assumptions rather than atypical metabolic responses to the task itself.

5.5.8 Muscle-level energy contributions and side differences

Across all musculoskeletal energy models, the quadriceps and hamstrings accounted for the greatest proportion of simulated metabolic energy expenditure. This distribution is mechanically plausible given the dominant role of knee and hip extensors in body-weight support and propulsion during running. However, it is important to emphasize that these muscle-level energy contributions arise from static optimization (SO) solutions and should be interpreted as model-derived, mechanically economical estimates rather than direct representations of neuromuscular recruitment or physiological effort.

Static optimization is known to concentrate force production within larger muscle groups that minimize the objective function (Crowninshield and Brand, 1981), which can bias energetic estimates toward prime movers while underrepresenting the contributions of stabilizing or synergistic musculature. As such, the prominence of the quadriceps and hamstrings in the present results likely reflects optimization behaviour imposed by the modelling framework rather than a comprehensive physiological account of how metabolic demand is distributed across muscles during prolonged high-intensity running.

Paired comparisons revealed no statistically significant bilateral asymmetries in muscle-level metabolic cost across any muscle group. The gluteal muscles demonstrated the largest effect size (Cohen's $d \approx -0.91$) and a trend toward asymmetry ($p = 0.053$), but this did not reach statistical significance. Given that all participants were right-leg dominant, the absence of consistent or statistically meaningful right–left differences suggests that habitual limb dominance did not materially influence the distribution of simulated metabolic work under the present modelling assumptions. This finding is consistent with prior work indicating that running asymmetries are typically subtle and context-dependent, and may only emerge under specific mechanical or fatigue-related conditions (D'Hondt et al., 2024; Helme et al., 2021; Maloney, 2019).

Importantly, these muscle-level energetics should not be interpreted as evidence of symmetrical or asymmetrical neuromuscular control. Because the simulations were not EMG-informed, the estimated muscle contributions reflect how SO partitions mechanical demand based on kinematics and net joint moments rather than how motor units are recruited physiologically. Complementary EMG analyses from a related dataset demonstrated that substantial neuromuscular changes can occur during prolonged running even in the absence of detectable kinematic alterations (see Chapter 4). This dissociation reinforces the known limitation that SO-based approaches capture mechanically optimal solutions rather than fatigue-related adaptations in neuromuscular strategy (Lloyd and Besier, 2003; Sartori et al., 2012a).

Accordingly, the muscle-level energy distributions reported here should be interpreted as descriptive indicators of how energy models using SO muscle activation allocate metabolic cost across muscles under high-intensity running conditions. Within the constraints of the modelling framework, these results provide valuable context for understanding model behaviour and complement the primary analyses of cost of transport accuracy, bias, and fatigue sensitivity. Interpreted in this way, muscle-level energetics help situate the observed model–calorimetry discrepancies without implying direct physiological inference regarding neuromuscular recruitment or fatigue adaptation.

5.5.9 Limitations

First, SO-based activations are not physiologically constrained by fatigue, meaning muscle recruitment changes over time were indirectly inferred from kinematics rather than derived from motor control strategies. None of the models integrate fatigue-related declines in force-generating capacity or shifts in muscle efficiency, both of which are known to influence metabolic cost (Potvin and Fuglevand, 2017).

Second, stride-to-stride variability was not captured in simulations, as each model trial was based on averaged motion data. Prior work suggests this may underestimate true metabolic variability by up to 15% (Alwan and Srinivasan, 2025). Future modelling pipelines should incorporate trial-specific or probabilistic simulation frameworks to better capture intra-individual variability.

Third, protein oxidation was assumed negligible in calorimetry calculations. While this is standard for short, non-fasted trials in healthy individuals (Jeukendrup and Wallis, 2005), it introduces a small degree of error under intense or prolonged exertion. The 30-second averaging window likely mitigates this effect.

It is also important to note that indirect calorimetry reflects whole-body metabolism whereas our MSK estimates include primarily lower-limb musculature; this domain mismatch likely contributes to absolute CoT bias, even if within-session trends are captured.

Finally, our small sample size (n = 7) limits generalizability (Button et al., 2013), though it aligns with precedent in biomechanics validation studies. Larger-scale efforts with broader age, sex, and skill-level representation are needed to establish normative ranges and validate clinical or performance thresholds.

5.6 Conclusion

This study evaluated the performance of three musculoskeletal energy models, *Bhargava2004*, *Umberger2003*, and *Umberger2010*, against indirect calorimetry during sustained high-intensity treadmill running. Kinematic quality checks confirmed high concordance between independent processing pipelines, with only small, phase-limited differences and no evidence of drift, supporting the validity of the inverse kinematics used as model inputs. Despite this, all three models demonstrated systematic bias when compared with calorimetry. *Bhargava 2004* and *Umberger2003* consistently underestimated CoT, whereas *Umberger2010* produced modest

overestimations. Only *Umberger2010* reproduced the physiological direction of within-session CoT increase, though with an attenuated slope relative to calorimetry. The other two models failed to track the empirical rise in metabolic cost across stages.

Across all models, simulated muscle-level energy expenditure was dominated by the quadriceps and hamstrings, reflecting consistent static-optimization solutions across participants and fatigue stages. No statistically significant bilateral asymmetries were observed, although the gluteal muscles showed the largest non-significant trend toward side differences. An auxiliary EMG–model timing analysis revealed substantial negative lags between experimental EMG onsets and SO-derived activation profiles, indicating that model activations occurred later than physiological activation. These timing discrepancies, which were stable across runs, reinforce the known limitation that SO activations reflect mechanically optimal not neurologically driven recruitment patterns (Lloyd and Besier, 2003; Sartori et al., 2013, 2012a). This limitation likely contributes to mismatches between simulated and empirical metabolic behaviour, particularly in stabilizing musculature and under fatigued conditions.

Collectively, these findings demonstrate that using static optimization with musculoskeletal energy models shows limited validity for estimating metabolic cost during prolonged high-intensity running. Despite clear physiological evidence of fatigue from indirect calorimetry, none of the models reliably captured within-session changes in cost of transport. *Umberger 2010* reproduced the direction of the empirical fatigue response but substantially underestimated its magnitude, while *Bhargava2004* and *Umberger2003* failed to reflect fatigue-related increases altogether.

As a result, these models should not be considered substitutes for indirect calorimetry when accurate estimation or tracking of metabolic cost is required. Their outputs reflect mechanically optimal solutions constrained by kinematic inputs and static cost functions rather than physiological adaptations to fatigue. Improving the utility of such models for fatigue-related

applications will likely require task-specific calibration and the integration of fatigue-aware or EMG-informed activation dynamics. Caution is therefore warranted when interpreting metabolic estimates derived from static-optimization pipelines, particularly under high-intensity or fatiguing conditions where neuromuscular behaviour diverges most strongly from model assumptions.

5.7 Appendix

Table A 5.1: Summary of Cost of Transport and Metabolic Power Across Gait Speeds, Models, and Exercise Types

Source	Speed (m/s)	incline (%)	Type	CoT (J/kg/m)	Exercise Type	Notes
(Umberger, 2010)	0.25	0	Simulation	9.5	Treadmill walking	Low-speed inefficiency
(Umberger, 2010)	0.5	0	Simulation	7.2	Treadmill walking	Approaching optimal
(Farris and Sawicki, 2012)	0.75	0	Exp. Indirect Calorimetry	~5.0	Treadmill walking	Walking dataset (scitepress.org)
(Weyand et al., 2010)	1	0	Exp. Indirect Calorimetry	1.64 ± 0.50	Overground walking	Optimum walk speed
(Umberger, 2010)	1	0	Simulation	~4.0	Treadmill walking	Near optimum walking
(Farris and Sawicki, 2012)	1.25	0	Exp. Indirect Calorimetry	~4.2	Treadmill walking	Slight rise above optimum
(Bhargava et al., 2004)	1.5	0	Simulation (EMG-informed)	3.8	Treadmill running	EMG-driven model
(Farris and Sawicki, 2012)	2	1.7	Exp. Indirect Calorimetry	~3.6	Treadmill running	Running onset
(Farris and Sawicki, 2012)	2.25	1.7	Exp. Indirect Calorimetry	~3.5	Treadmill running	Running dataset
(Umberger et al., 2003)	2.5	0	Simulation	3.6	Treadmill running	Steady treadmill running
(Bellenger et al., 2016)	3	0	Experimental	3.7 ± 0.2	Treadmill running	Consistent across studies (Meta-analysis (trained runners))
(Biancardi et al., 2023)	3	0	Experimental	4.20 (track)/4.35 (treadmill)	Track vs treadmill running	Comparison study
(Umberger et al., 2003)	3.5	0	Simulation	3.4	Treadmill running	Faster treadmill running
(Batliner et al., 2018)	1.78–5.14	0	Experimental Indirect	3.82-4.46	Running - developmental athletes	Broad developmental range (Average vs Sub-elite runners)
Energy cost of running (J/kg/m)	n/a	n/a	Direct Calorimetry (modus)	~1.0 kcal/kg/km = 4.18 J/kg/m	n/a	Classic physiology

Table A 5.2: Paired t-test results comparing left and right muscle-group energy expenditure

Group	n_pairs	t	p	Cohen_d
Adductors	7	-1,15547	0,291828	-0,43673
Dorsiflexors	7	-0,99666	0,357409	-0,3767
Glutes	7	-2,39983	0,053307	-0,90705
Hamstrings	7	-0,52781	0,616572	-0,19949
Hip Flexors	7	1,15036	0,293771	0,434795
Plantarflexors1	7	No variability		
Plantarflexors 2	7	-1,66529	0,146908	-0,62942
Quadriceps	7	-1,37284	0,218902	-0,51888

Table A 5.3: Group-Level EMG–Model Lag Summary

This table presents group-level mean ± standard deviation values of EMG–OpenSim activation lags across all recorded muscles and fatigue stages. The complete stride-level dataset used to generate these summaries is provided in the digital appendix (EMG_PerStrideLag_GroupSummary.xlsx).

Table A 5.4: Per-Stride Lag Distributions by Muscle

This table summarizes stride-level EMG–OpenSim activation lag distributions for each muscle and fatigue stage, visualized using boxplots. Complete per-stride numerical values are available in the digital appendix (EMG_PerStrideLag_Summary.xlsx).

Table A 5.5: Aggregate Lag Values

This table reports aggregate lag metrics, including median values, interquartile ranges, and muscle-specific summary statistics. The full numerical dataset supporting these aggregates is provided in the digital appendix (EMG_vs_Activation_GroupSummary.xlsx).

Table A 5.6: Summary of key metabolic energy model parameters and components implemented in the Bhargava (2004), Umberger (2003), and Umberger (2010) formulations. Checkmarks indicate inclusion of specific components within each model, while numerical values represent parameter settings used in the implementations.

Parameter	Bhargava 2004	Umberger 2003	Umberger 2010
Activation Maintenance Rate	✓	✓	✓
Activation Rate	✓	n/a	n/a
Maintenance Rate	✓	n/a	n/a
Shortening Rate	✓	✓	✓
Basal Rate	✓	✓	✓
Mechanical Work Rate	✓	✓	✓
Enforce Minimum Heat Rate per Muscle	✓	✓	✓
Use Bhargava Recruitment Model	n/a	✓	—
Include Negative Mechanical Work	✓	✓	—
Forbid Negative Total Power	✓	✓	—
Basal Coefficient	1.2	1.2	1.2
Basal Exponent	1.0	1.0	1.0
Muscle Effort Scaling	1.0	1.0	1.0
Aerobic Factor	—	1.5	1.5

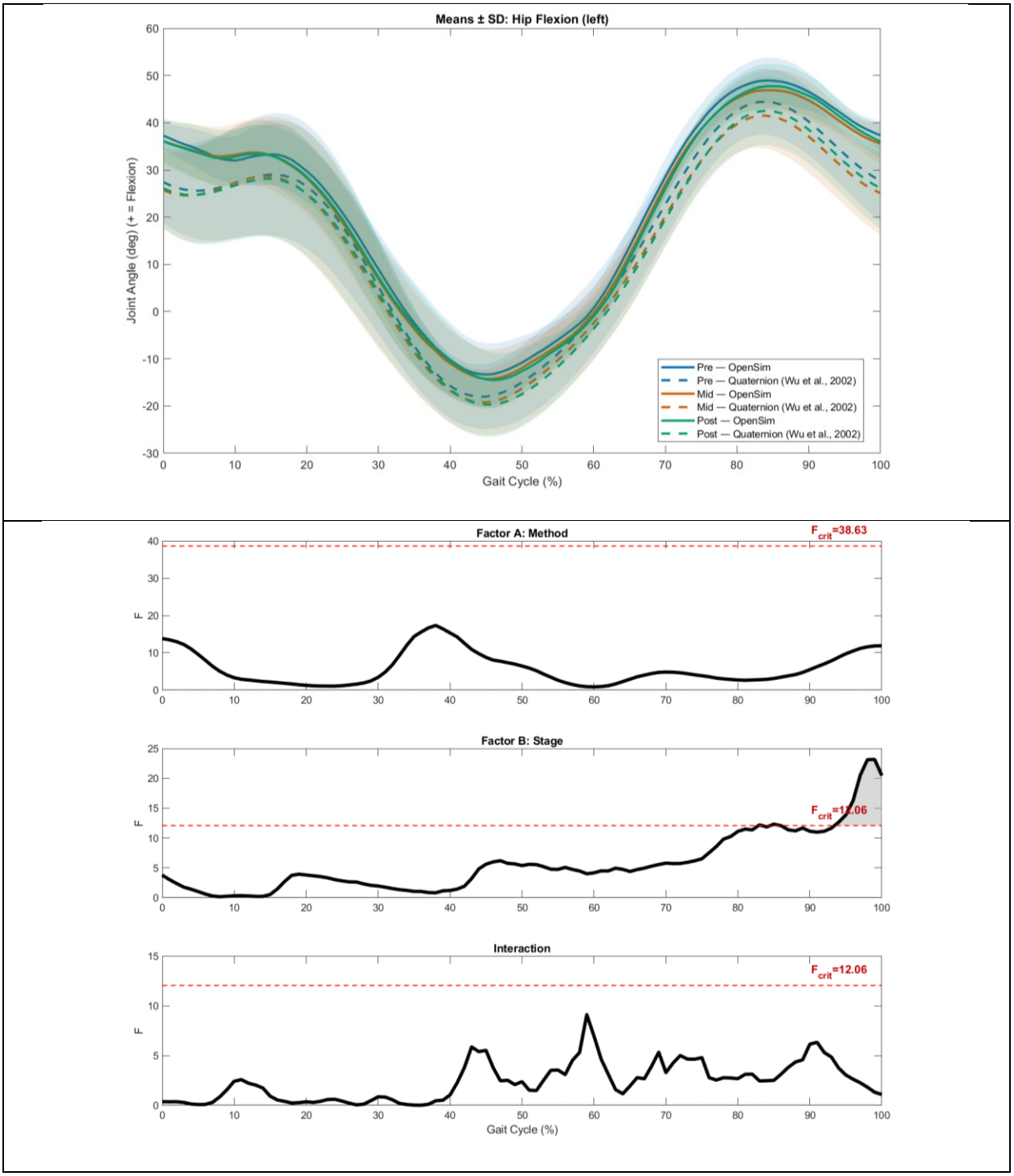

Figure A 5.1: Left-leg hip flexion–extension kinematics and SPM across the gait cycle for both OpenSim IK and MATLAB-derived Euler-angle joint coordinate system (JCS) kinematics. Top panel: Mean ± SD waveforms. Time-normalized gait-cycle waveforms (0–100%) of left hip flexion for three runs (Run 2, Run 5, Run 8). OpenSim curves are solid; MATLAB JCS curves (derived using ISB-recommended conventions; Wu et al., 2005; Grood & Suntay, 1983) are dashed. Shaded bands indicate ±1 SD across strides. Bottom panel: SPM repeated-measures 2-way ANOVA over the gait cycle. F-curves for the main effects of Method (OpenSim vs MATLAB JCS), Stage (Pre, Mid, Post), and their Interaction. The red dashed line denotes the random-field-theory critical threshold at $\alpha = 0.05$; grey shading marks supra-threshold clusters.

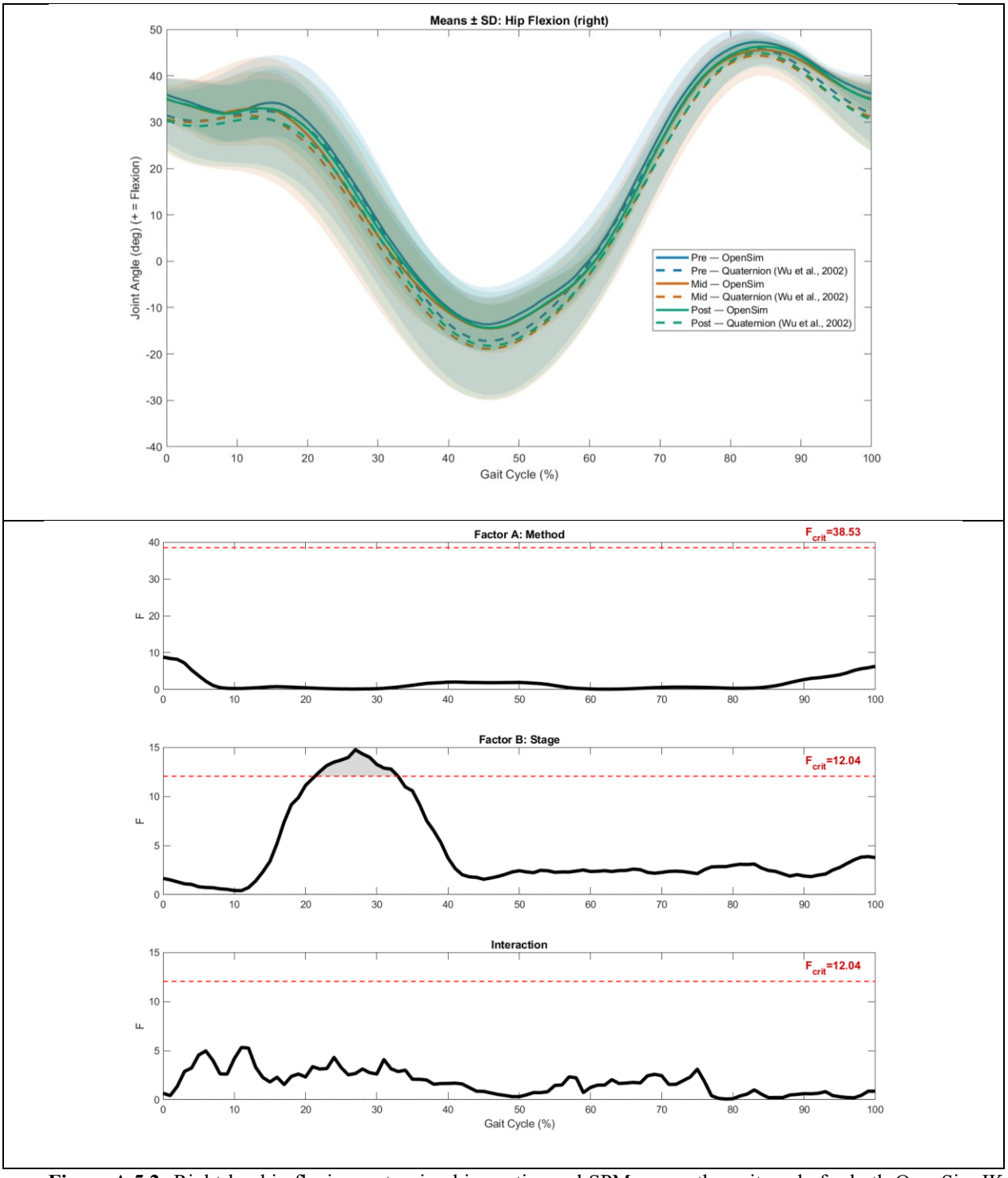

Figure A 5.2: Right-leg hip flexion–extension kinematics and SPM across the gait cycle for both OpenSim IK and MATLAB-derived Euler-angle joint coordinate system (JCS) kinematics. Top panel: Mean ± SD waveforms. Time-normalized gait-cycle waveforms (0–100%) of left hip flexion for three runs (Run 2, Run 5, Run 8). OpenSim curves are solid; MATLAB JCS curves (derived using ISB-recommended conventions; Wu et al., 2005; Grood & Suntay, 1983) are dashed. Shaded bands indicate ±1 SD across strides. Bottom panel: SPM repeated-measures 2-way ANOVA over the gait cycle. F-curves for the main effects of Method (OpenSim vs MATLAB JCS), Stage (Pre, Mid, Post), and their Interaction. The red dashed line denotes the random-field-theory critical threshold at $\alpha = 0.05$; grey shading marks supra-threshold clusters.

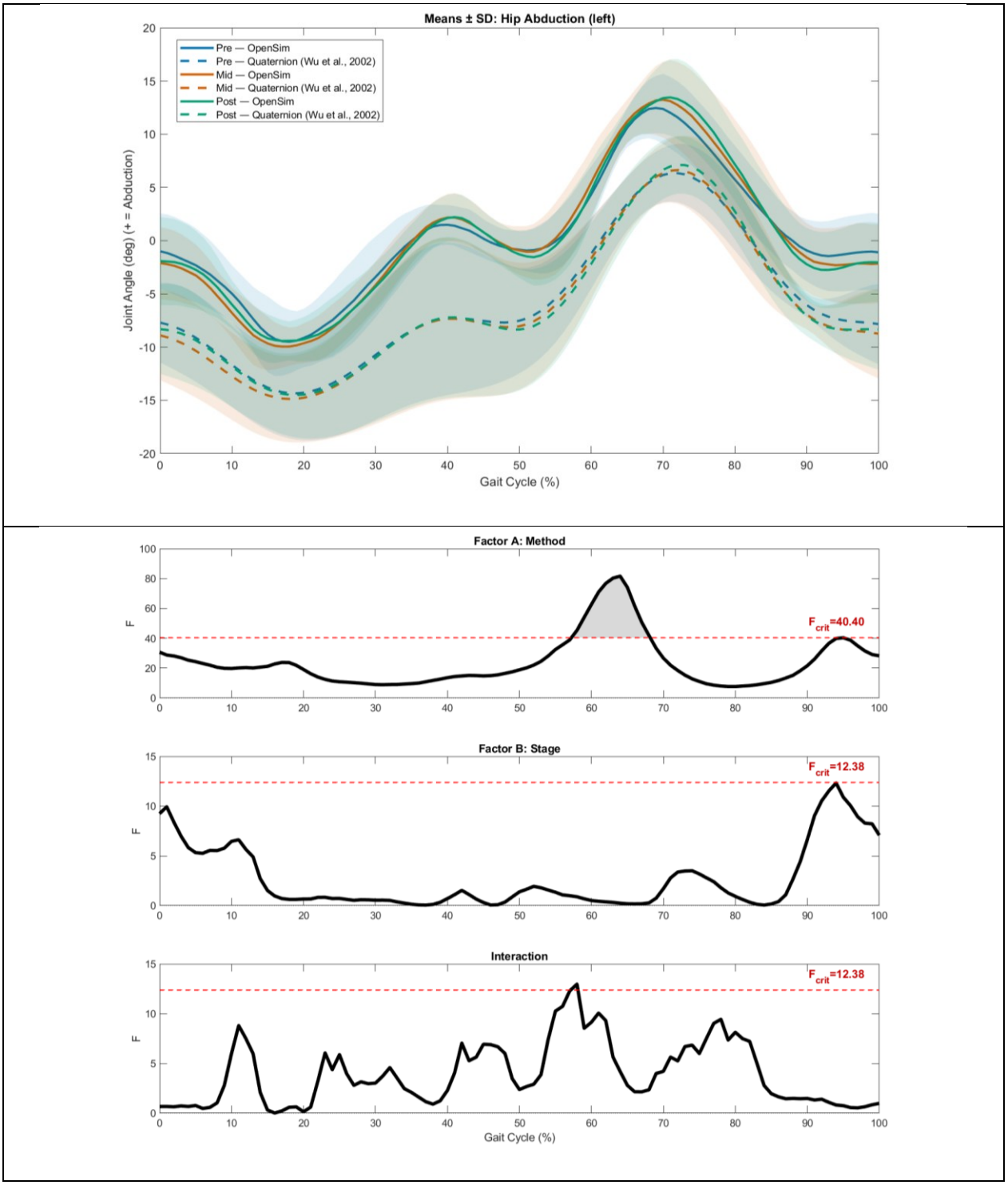

Figure A 5.3: Left-leg hip abduction–adduction kinematics and SPM across the gait cycle for both OpenSim IK and MATLAB-derived Euler-angle joint coordinate system (JCS) kinematics. Top panel: Mean ± SD waveforms. Time-normalized gait-cycle waveforms (0–100%) of left hip flexion for three runs (Run 2, Run 5, Run 8). OpenSim curves are solid; MATLAB JCS curves (derived using ISB-recommended conventions; Wu et al., 2005; Grood & Suntay, 1983) are dashed. Shaded bands indicate ±1 SD across strides. Bottom panel: SPM repeated-measures 2-way ANOVA over the gait cycle. F-curves for the main effects of Method (OpenSim vs MATLAB JCS), Stage (Pre, Mid, Post), and their Interaction. The red dashed line denotes the random-field-theory critical threshold at $\alpha = 0.05$; grey shading marks supra-threshold clusters.

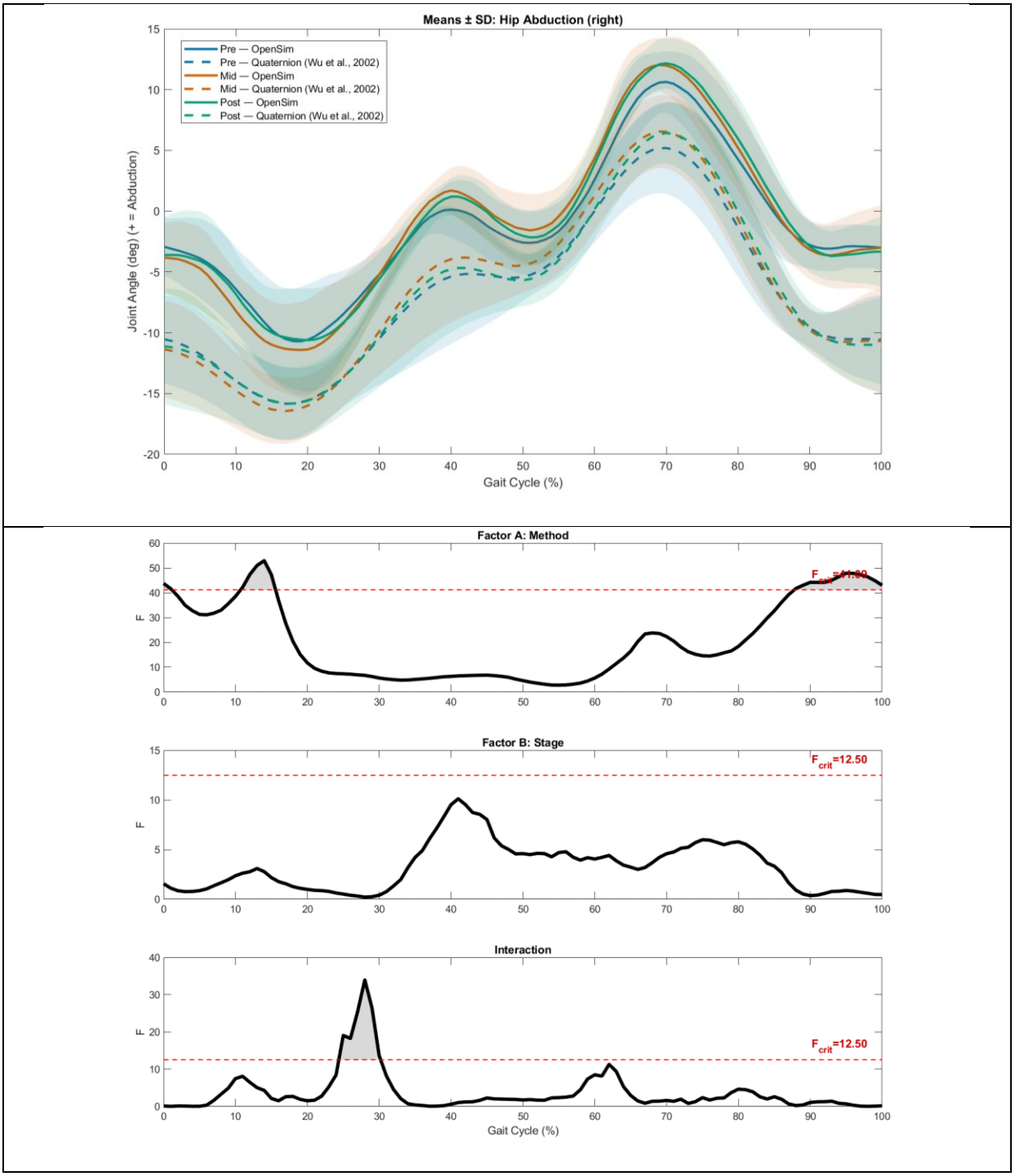

Figure A 5.4: Right-leg hip abduction–adduction kinematics and SPM across the gait cycle for both OpenSim IK and MATLAB-derived Euler-angle joint coordinate system (JCS) kinematics. Top panel: Mean ± SD waveforms. Time-normalized gait-cycle waveforms (0–100%) of left hip flexion for three runs (Run 2, Run 5, Run 8). OpenSim curves are solid; MATLAB JCS curves (derived using ISB-recommended conventions; Wu et al., 2005; Grood & Suntay, 1983) are dashed. Shaded bands indicate ±1 SD across strides. Bottom panel: SPM repeated-measures 2-way ANOVA over the gait cycle. F-curves for the main effects of Method (OpenSim vs MATLAB JCS), Stage (Pre, Mid, Post), and their Interaction. The red dashed line denotes the random-field-theory critical threshold at $\alpha = 0.05$; grey shading marks supra-threshold clusters.

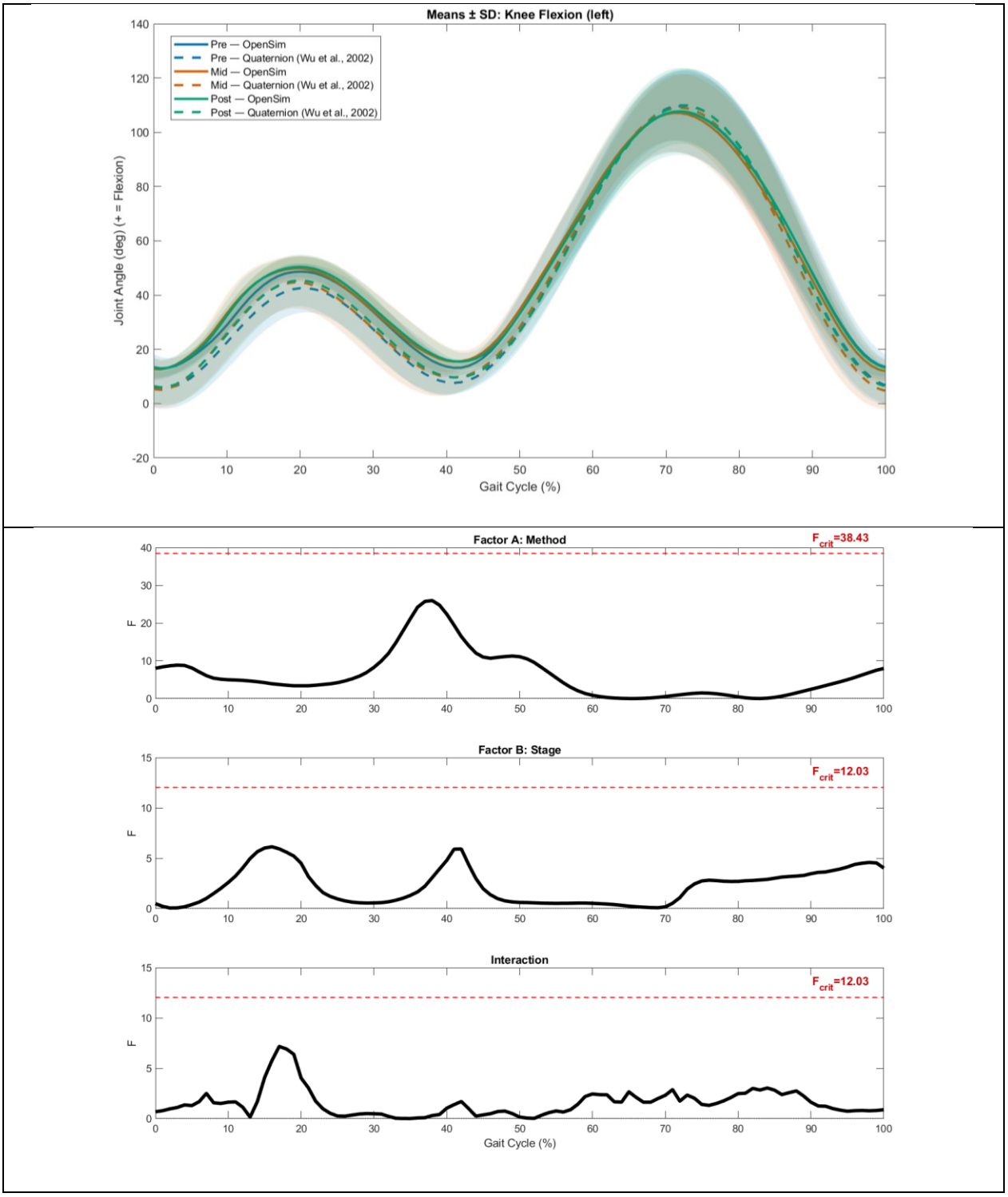

Figure A 5.5: Left-leg knee flexion–extension kinematics and SPM across the gait cycle for both OpenSim IK and MATLAB-derived Euler-angle joint coordinate system (JCS) kinematics. Top panel: Mean ± SD waveforms. Time-normalized gait-cycle waveforms (0–100%) of left hip flexion for three runs (Run 2, Run 5, Run 8). OpenSim curves are solid; MATLAB JCS curves (derived using ISB-recommended conventions; Wu et al., 2005; Grood & Suntay, 1983) are dashed. Shaded bands indicate ±1 SD across strides. Bottom panel: SPM repeated-measures 2-way ANOVA over the gait cycle. F-curves for the main effects of Method (OpenSim vs MATLAB JCS), Stage (Pre, Mid, Post), and their Interaction. The red dashed line denotes the random-field-theory critical threshold at $\alpha = 0.05$; grey shading marks supra-threshold clusters.

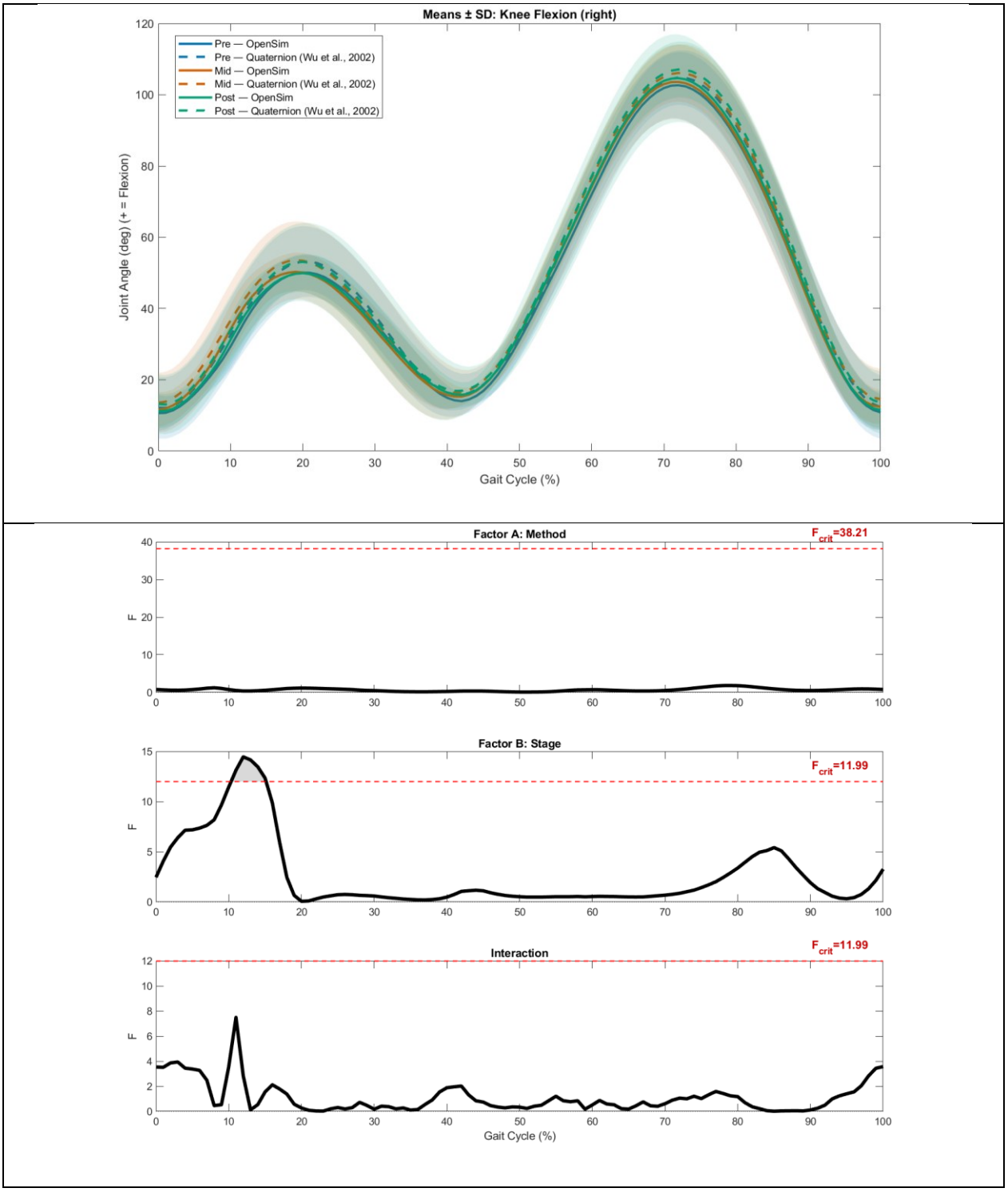

Figure A 5.6: Right-leg knee flexion–extension kinematics and SPM across the gait cycle for both OpenSim IK and MATLAB-derived Euler-angle joint coordinate system (JCS) kinematics. Top panel: Mean ± SD waveforms. Time-normalized gait-cycle waveforms (0–100%) of left hip flexion for three runs (Run 2, Run 5, Run 8). OpenSim curves are solid; MATLAB JCS curves (derived using ISB-recommended conventions; Wu et al., 2005; Grood & Suntay, 1983) are dashed. Shaded bands indicate ±1 SD across strides. Bottom panel: SPM repeated-measures 2-way ANOVA over the gait cycle. F-curves for the main effects of Method (OpenSim vs MATLAB JCS), Stage (Pre, Mid, Post), and their Interaction. The red dashed line denotes the random-field-theory critical threshold at $\alpha = 0.05$; grey shading marks supra-threshold clusters.

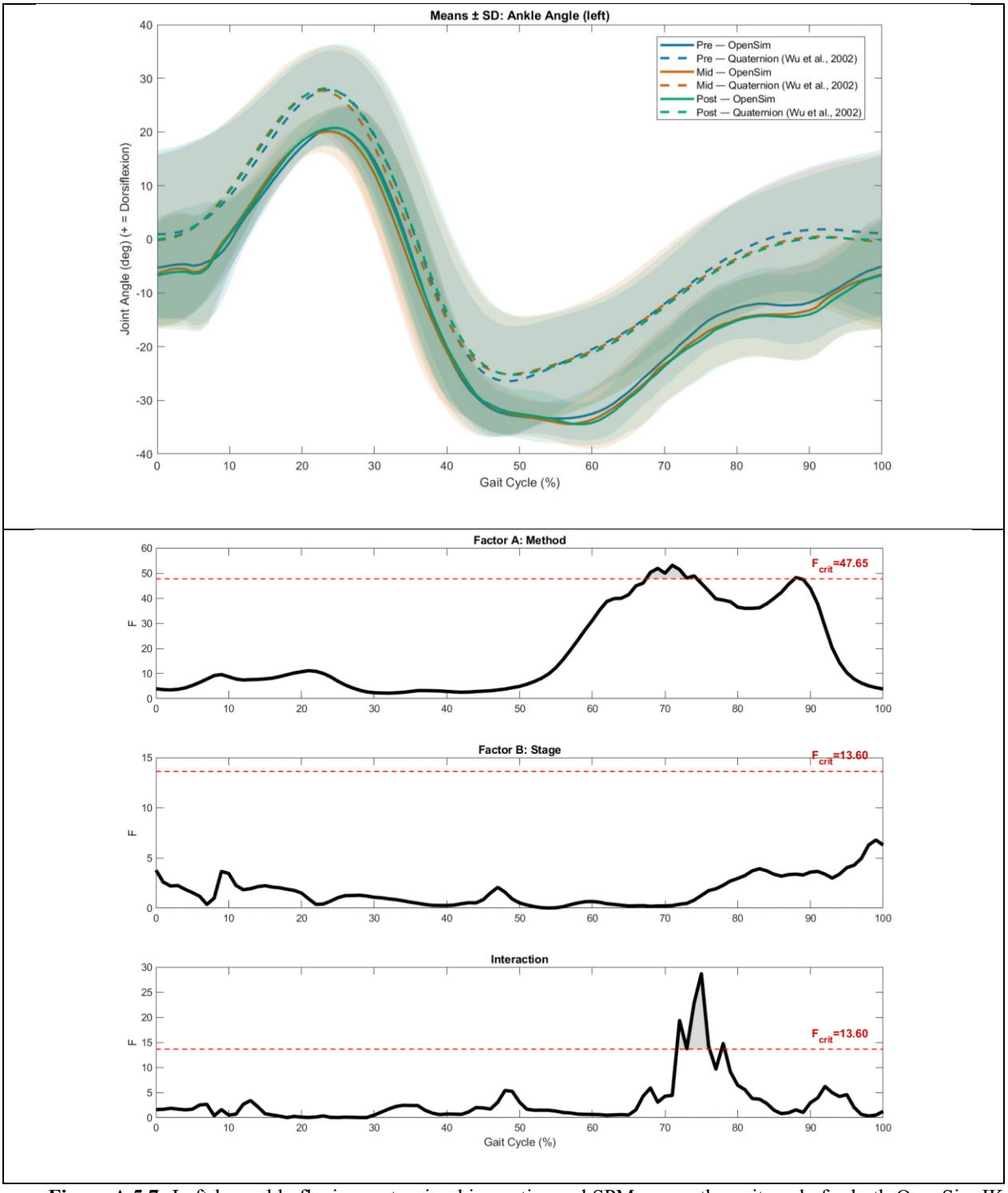

Figure A 5.7: Left-leg ankle flexion–extension kinematics and SPM across the gait cycle for both OpenSim IK and MATLAB-derived Euler-angle joint coordinate system (JCS) kinematics. Top panel: Mean ± SD waveforms. Time-normalized gait-cycle waveforms (0–100%) of left hip flexion for three runs (Run 2, Run 5, Run 8). OpenSim curves are solid; MATLAB JCS curves (derived using ISB-recommended conventions; Wu et al., 2005; Grood & Suntay, 1983) are dashed. Shaded bands indicate ±1 SD across strides. Bottom panel: SPM repeated-measures 2-way ANOVA over the gait cycle. F-curves for the main effects of Method (OpenSim vs MATLAB JCS), Stage (Pre, Mid, Post), and their Interaction. The red dashed line denotes the random-field-theory critical threshold at $\alpha = 0.05$; grey shading marks supra-threshold clusters.

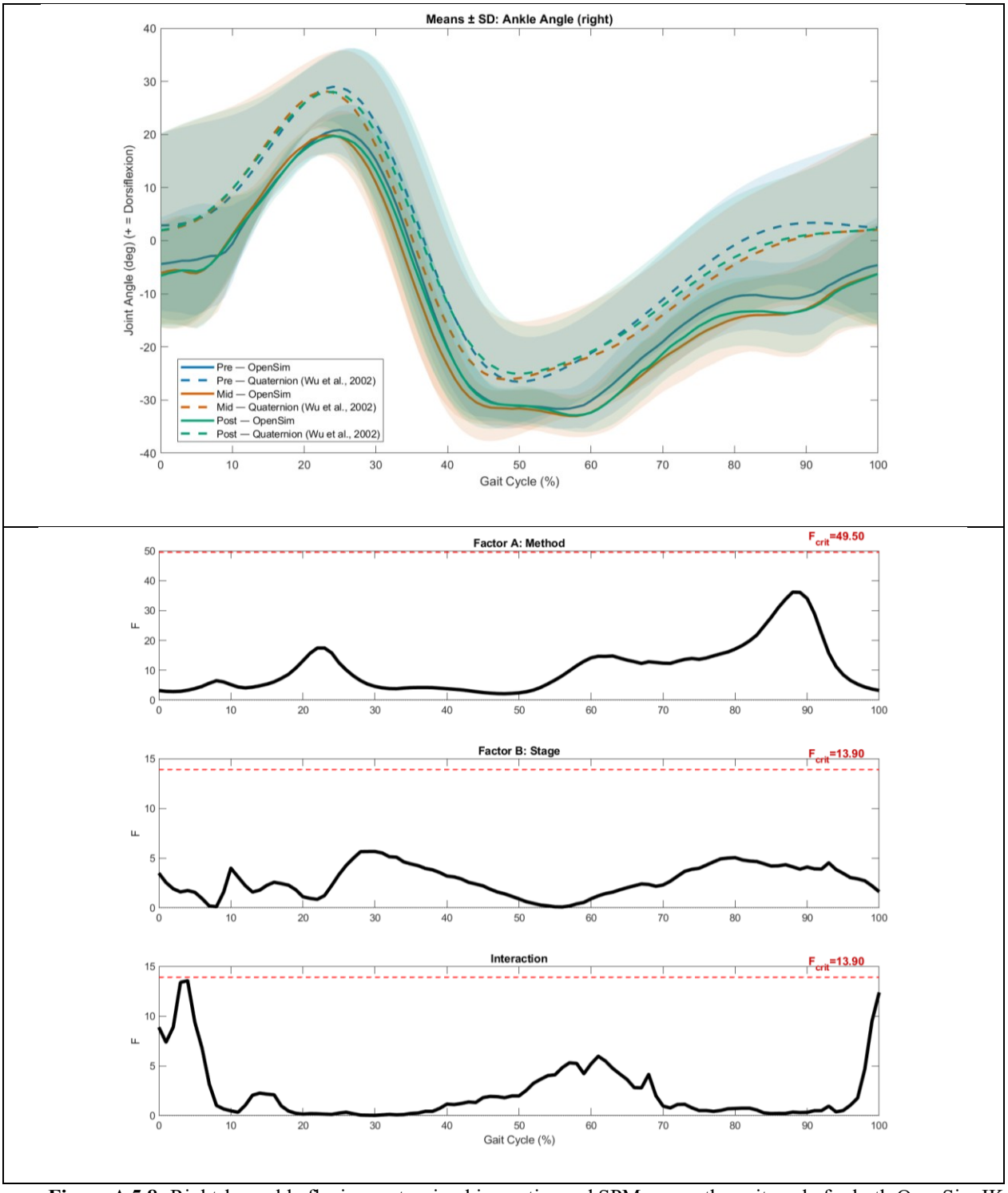

Figure A 5.8: Right-leg ankle flexion–extension kinematics and SPM across the gait cycle for both OpenSim IK and MATLAB-derived Euler-angle joint coordinate system (JCS) kinematics. Top panel: Mean ± SD waveforms. Time-normalized gait-cycle waveforms (0–100%) of left hip flexion for three runs (Run 2, Run 5, Run 8). OpenSim curves are solid; MATLAB JCS curves (derived using ISB-recommended conventions; Wu et al., 2005; Grood & Suntay, 1983) are dashed. Shaded bands indicate ±1 SD across strides. Bottom panel: SPM repeated-measures 2-way ANOVA over the gait cycle. F-curves for the main effects of Method (OpenSim vs MATLAB JCS), Stage (Pre, Mid, Post), and their Interaction. The red dashed line denotes the random-field-theory critical threshold at $\alpha = 0.05$; grey shading marks supra-threshold clusters.

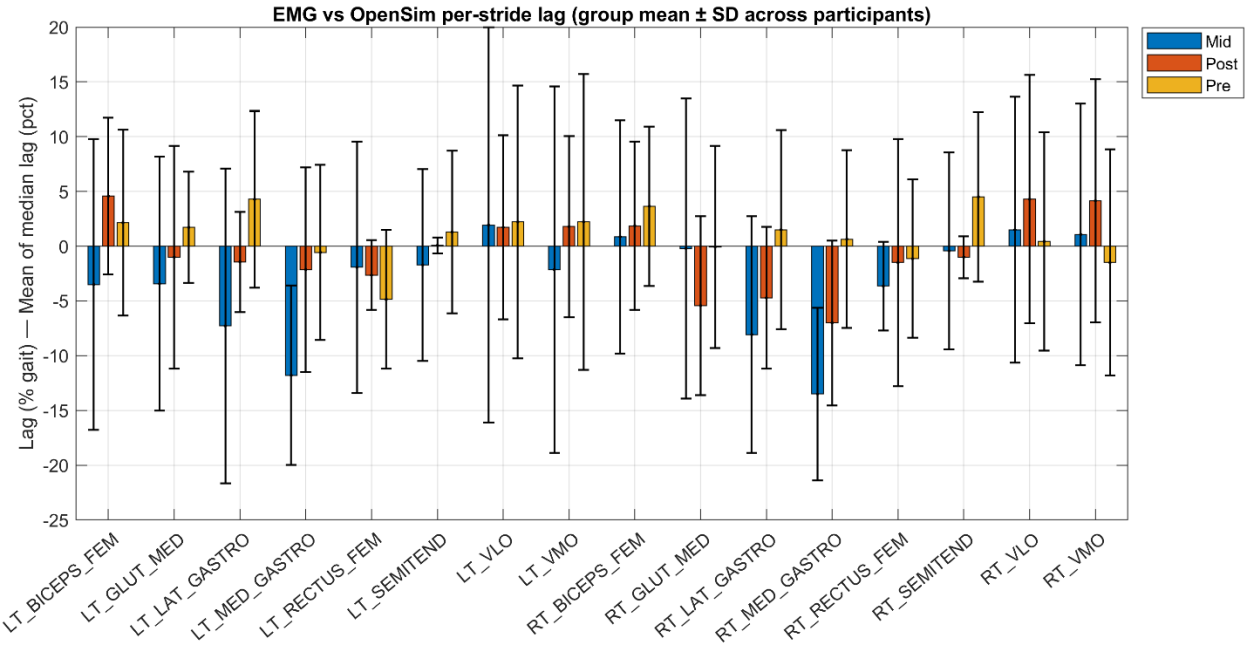

Figure A 5.9: Group-level EMG–OpenSim activation lag for all muscles across the gait cycle (Run2, Run5, Run8). op panel (bars): Mean EMG–model lag (±1 SD) per muscle for each run. Negative values indicate that the SO-derived activation onset occurred later than the corresponding EMG onset; positive values indicate earlier model activation. Muscles are grouped by functional categories (quadriceps, hamstrings, plantarflexors, dorsiflexors, and gluteal muscles). Colours represent fatigue stage (Run_2 = Pre, Run_5 = Mid, Run_8 = Post). Error bars reflect inter-participant variability. These results summarise the central tendency and variability of temporal offsets between experimental EMG and modelled muscle activations, consistent across runs.

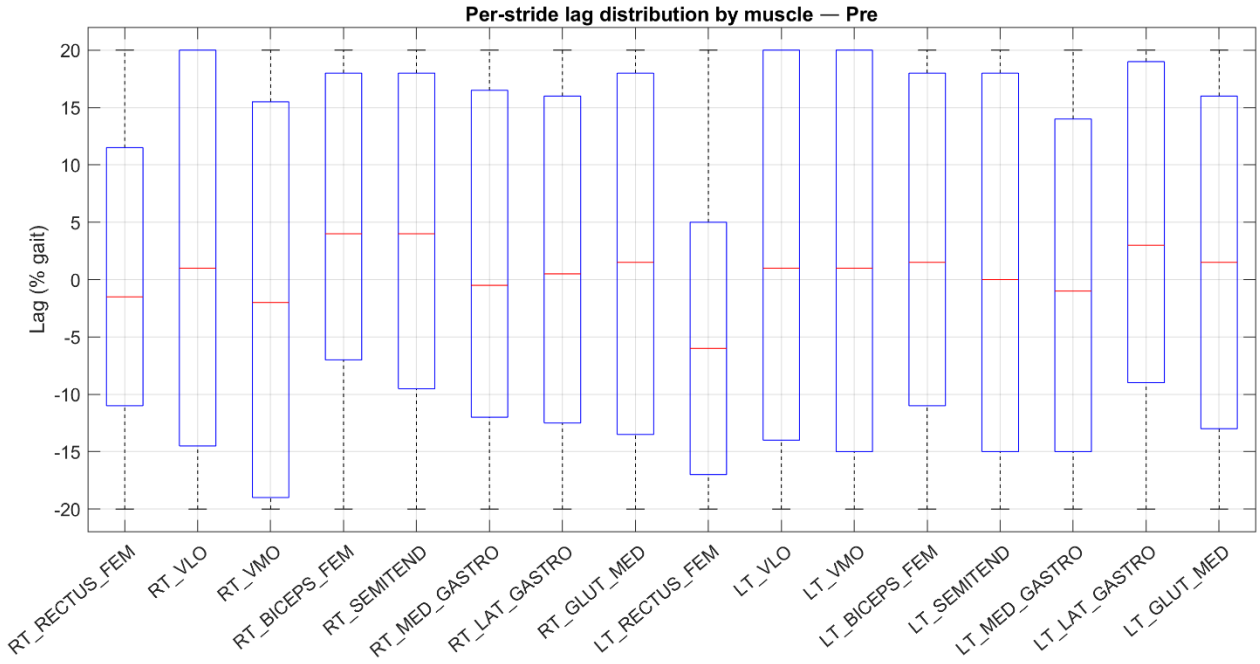

Figure A 5.10: Per-stride EMG–OpenSim activation lag distributions for all recorded muscles during Run$_2$ (Pre-fatigue). Each boxplot represents the stride-level distribution of EMG–model lags for a single muscle. The red line denotes the median offset; box boundaries indicate the interquartile range (IQR); whiskers show 1.5 × IQR, and individual points represent outliers. Negative lags indicate delayed SO activation relative to EMG onset. These distributions illustrate substantial stride-to-stride variability in temporal alignment between EMG and modelled muscle activity at the beginning of the session.

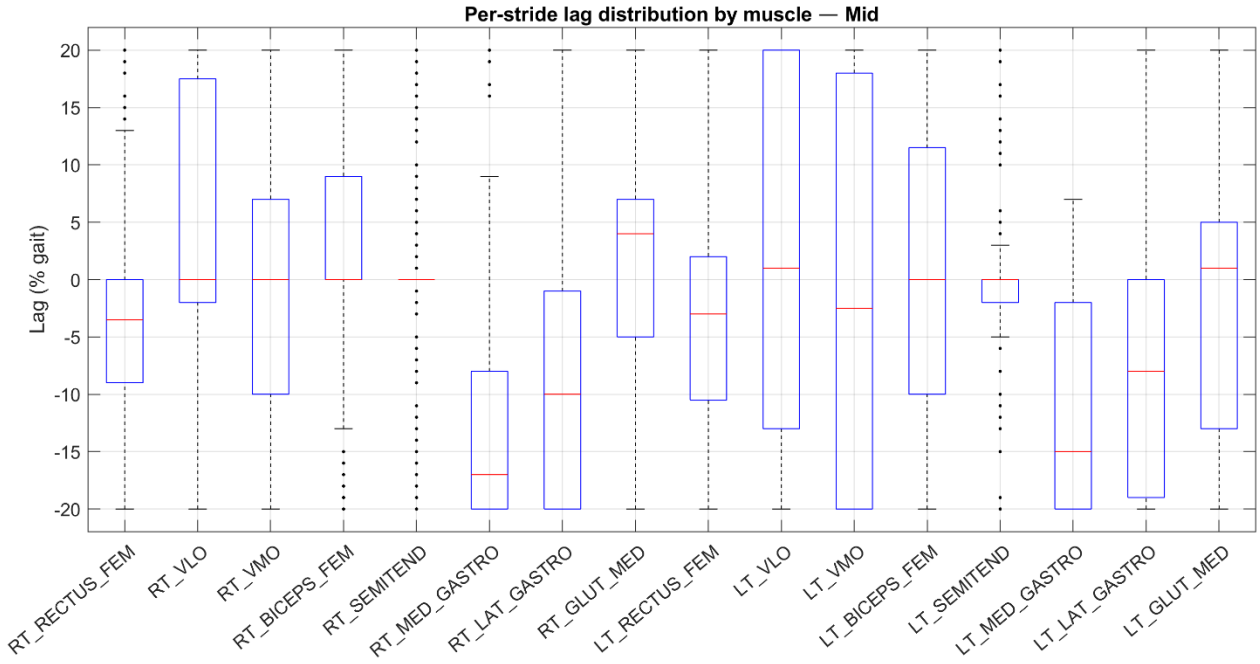

Figure A 5.11: Per-stride EMG–OpenSim activation lag distributions for all recorded muscles during Run$_5$ (Mid-fatigue). Boxplots show stride-level EMG–model lags for each muscle, using the same conventions as Run$_2$. The distribution shapes highlight broad inter-stride variability and largely negative offsets, with no consistent shift in lag magnitude relative to the pre-fatigue stage. These results indicate that activation timing discrepancies remain relatively stable at mid-session despite physiological fatigue.

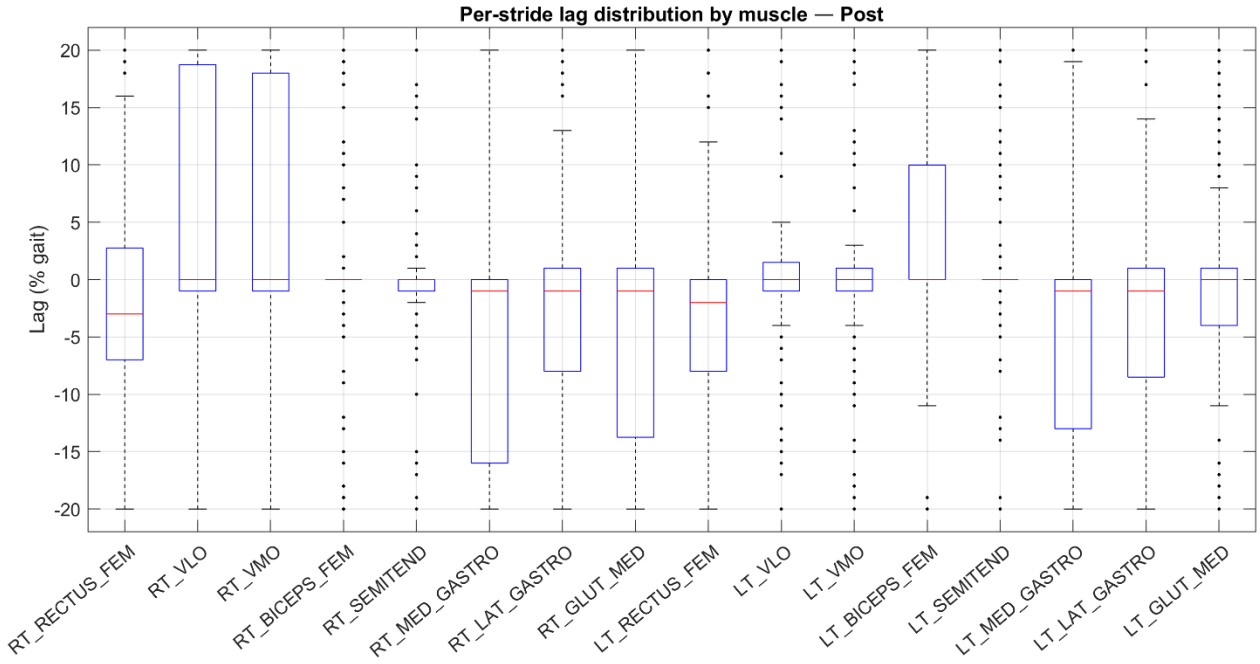

Figure A 5.12: Per-stride EMG–OpenSim activation lag distributions for all recorded muscles during Run$_8$ (Post-fatigue). This figure presents stride-level lag distributions for each muscle at the end of the session. As in previous runs, SO activations generally occurred later than EMG onsets, reflected in predominantly negative lags. The persistence of distribution shape and range across runs suggests that the temporal offset between EMG and SO activations is a structural property of the optimization pipeline rather than an effect of fatigue.

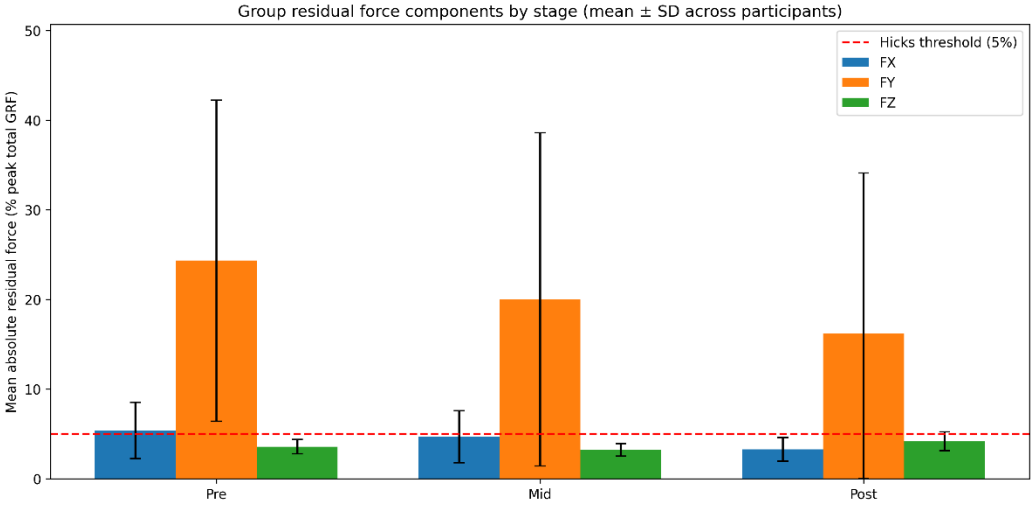

Figure A 5.13: Group-averaged mean absolute residual force components (FX, FY, FZ) across fatigue stages (Pre, Mid, Post), expressed as a percentage of peak net external force (mean ± SD across participants). The dashed line represents the recommended threshold of 5% for acceptable simulation quality (Hicks et al., 2015).

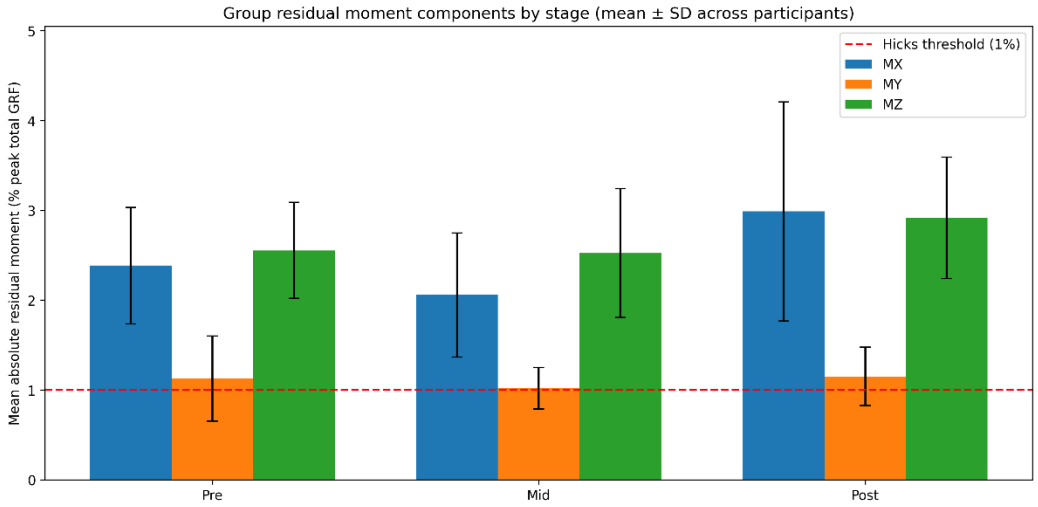

Figure A 5.14: Group-averaged mean absolute residual moment components (MX, MY, MZ) across fatigue stages (Pre, Mid, Post), expressed as a percentage of the product of center-of-mass height and peak net external force (mean ± SD across participants). The dashed line represents the recommended threshold of 1% (Hicks et al., 2015).

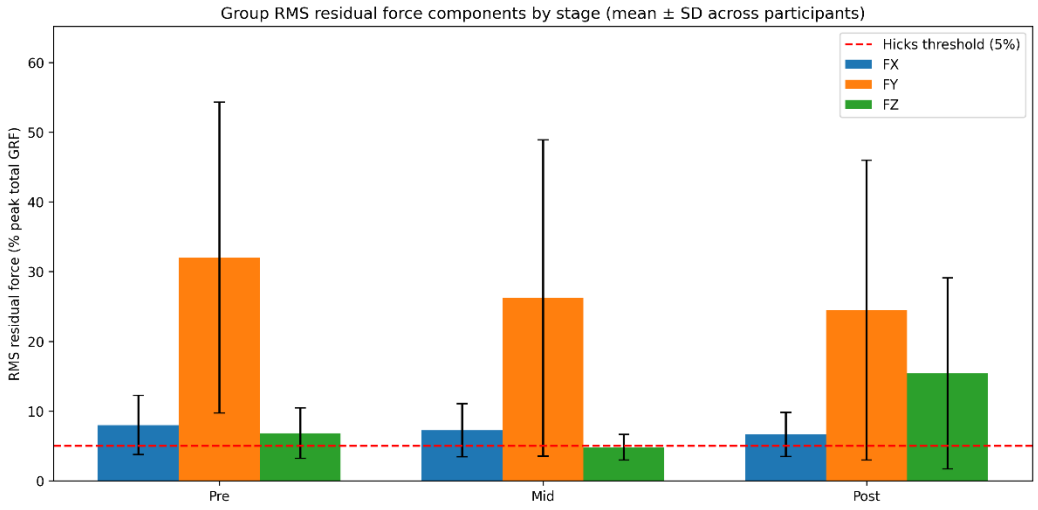

Figure A 5.15: Group-averaged RMS residual force components (FX, FY, FZ) across fatigue stages (Pre, Mid, Post), expressed as a percentage of peak net external force (mean ± SD across participants). The dashed line represents the recommended threshold of 5% (Hicks et al., 2015).

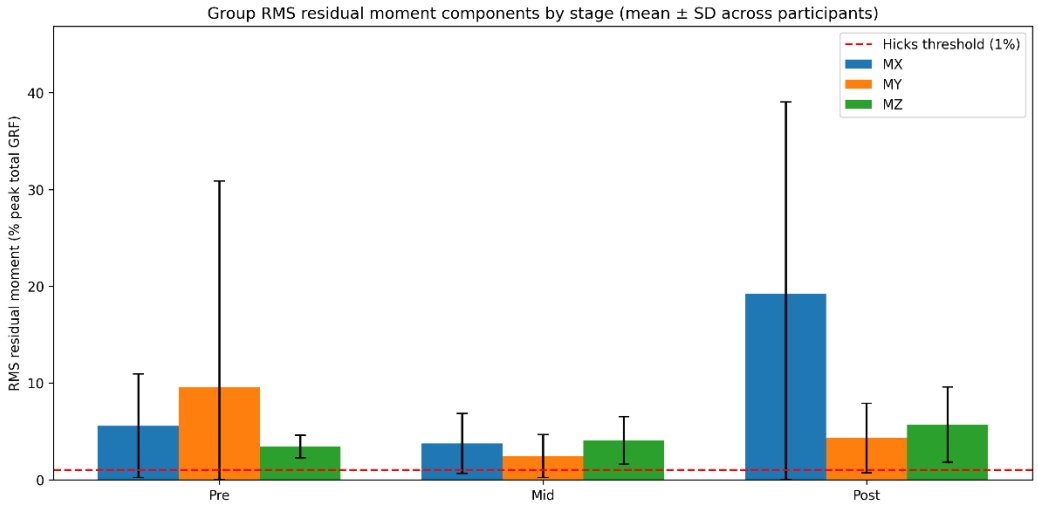

Figure A 5.16: Group-averaged RMS residual moment components (MX, MY, MZ) across fatigue stages (Pre, Mid, Post), expressed as a percentage of the product of center-of-mass height and peak net external force (mean ± SD across participants). The dashed line represents the recommended threshold of 1% (Hicks et al., 2015).

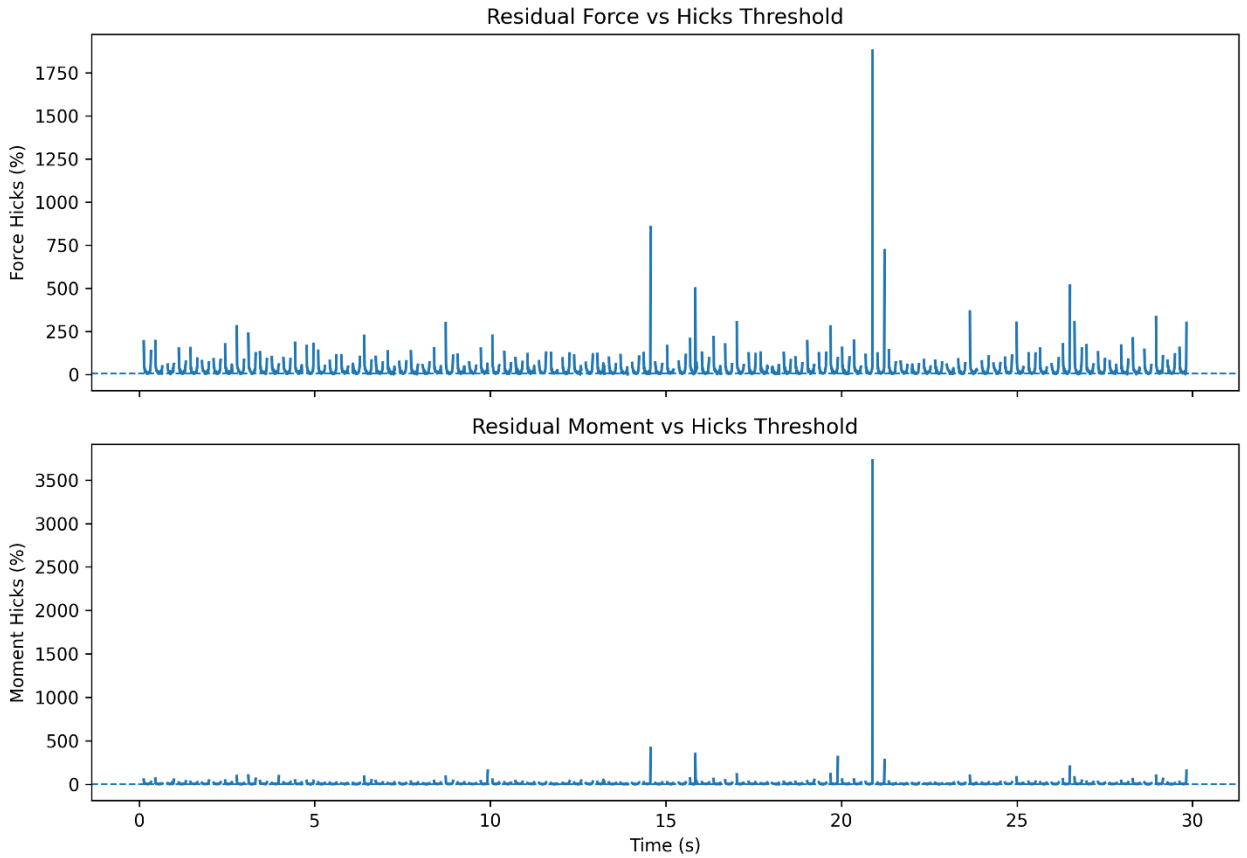

Figure A 5.17: Time-series profiles of residual forces and moments for a representative participant (P005, pre-fatigue trial), expressed as percentages of peak net external force and center-of-mass height–scaled external force. Peaks occur primarily during stance phase events and are representative of the transient residual patterns observed across participants.

5.7.1 Sensitivity Analysis of Residual Reduction Algorithm (RRA)

To assess the sensitivity of metabolic cost estimates to dynamic consistency, a subset of simulations was reprocessed using a residual reduction algorithm (RRA). This analysis was conducted for both the Catelli and LaiUlrich musculoskeletal models for a single trial.

The RRA procedure was applied using the same kinematic and ground reaction force inputs, with adjustments to model mass properties and kinematics to reduce residual forces and moments. Following RRA implementation, cost of transport was recalculated using the Umberger (2003), Umberger (2010), and Bhargava (2004) metabolic energy models.

The implementation of RRA resulted in negligible changes in estimated cost of transport across all models. For the Catelli model, cost of transport values changed from 9.321 $J \cdot kg^{-1} \cdot m^{-1}$ to 9.318 $J \cdot kg^{-1} \cdot m^{-1}$ (Umberger2010), 0.523 $J \cdot kg^{-1} \cdot m^{-1}$ to 0.520 $J \cdot kg^{-1} \cdot m^{-1}$ (Umberger2003), and 0.726 $J \cdot kg^{-1} \cdot m^{-1}$ to 0.721 $J \cdot kg^{-1} \cdot m^{-1}$ (Bhargava2004). For the LaiUlrich model, values changed from 6.306 $J \cdot kg^{-1} \cdot m^{-1}$ to 6.324 $J \cdot kg^{-1} \cdot m^{-1}$ (Umberger2010), 2.487 $J \cdot kg^{-1} \cdot m^{-1}$ to 2.502 $J \cdot kg^{-1} \cdot m^{-1}$ (Umberger2003), and 0.439 $J \cdot kg^{-1} \cdot m^{-1}$ to 0.447 $J \cdot kg^{-1} \cdot m^{-1}$ (Bhargava2004).

Across both musculoskeletal models and all metabolic formulations, changes in cost of transport remained below 1%. These findings indicate that improving dynamic consistency through RRA had minimal influence on the primary outcome measures.

5.8 References

Alwan, A., Srinivasan, M., 2025. Natural variability increases human walking metabolic costs and its implications to simulation-based metabolic estimation. https://doi.org/10.1101/2025.03.13.643096

Anderson, F.C., Pandy, M.G., 2001. Dynamic Optimization of Human Walking. J. Biomech. Eng. 123, 381–390. https://doi.org/10.1115/1.1392310

Arnold, E.M., Hamner, S.R., Seth, A., Millard, M., Delp, S.L., 2013. How muscle fiber lengths and velocities affect muscle force generation as humans walk and run at different speeds. Journal of Experimental Biology. https://doi.org/10.1242/jeb.075697

Arones, M.M., Shourijeh, M.S., Patten, C., Fregly, B.J., 2020. Musculoskeletal Model Personalization Affects Metabolic Cost Estimates for Walking. Front. Bioeng. Biotechnol. 8. https://doi.org/10.3389/fbioe.2020.588925

ATS/ACCP Statement on Cardiopulmonary Exercise Testing, 2003. . Am. J. Respir. Crit. Care Med. 167, 211–277. https://doi.org/10.1164/rccm.167.2.211

Barnes, K.R., Kilding, A.E., 2015. Running economy: measurement, norms, and determining factors. Sports Med. Open 1, 8. https://doi.org/10.1186/s40798-015-0007-y

Bellenger, C.R., Arnold, J.B., Buckley, J.D., Thewlis, D., Fuller, J.T., 2019. Detrended fluctuation analysis detects altered coordination of running gait in athletes following a heavy period of training. J. Sci. Med. Sport 22, 294–299. https://doi.org/10.1016/j.jsams.2018.09.002

Bellenger, C.R., Fuller, J.T., Thomson, R.L., Davison, K., Robertson, E.Y., Buckley, J.D., 2016. Monitoring Athletic Training Status Through Autonomic Heart Rate Regulation: A Systematic Review and Meta-Analysis. Sports Medicine 46, 1461–1486. https://doi.org/10.1007/s40279-016-0484-2

Benoit, D.L., Damsgaard, M., Andersen, M.S., 2015. Surface marker cluster translation, rotation, scaling and deformation: Their contribution to soft tissue artefact and impact on knee joint kinematics. J. Biomech. 48, 2124–2129. https://doi.org/10.1016/j.jbiomech.2015.02.050

Benoit, D.L., Ramsey, D.K., Lamontagne, M., Xu, L., Wretenberg, P., Renström, P., 2006. Effect of skin movement artifact on knee kinematics during gait and cutting motions measured in vivo. Gait Posture 24, 152–164. https://doi.org/10.1016/j.gaitpost.2005.04.012

Bhargava, L.J., Pandy, M.G., Anderson, F.C., 2004. A phenomenological model for estimating metabolic energy consumption in muscle contraction. J. Biomech. 37, 81–88. https://doi.org/10.1016/S0021-9290(03)00239-2

Biancardi, C., Lagos-Hausheer, L., Pequera, G., Castroman, E., Cazot, F., Martinez, E., Bona, R., 2023. Energetic Cost of Running in Track and Treadmill, in: Proceedings of the 11th International Conference on Sport Sciences Research and Technology Support. SCITEPRESS - Science and Technology Publications, pp. 173–178. https://doi.org/10.5220/0012202300003587

Button, K.S., Ioannidis, J.P.A., Mokrysz, C., Nosek, B.A., Flint, J., Robinson, E.S.J., Munafò, M.R., 2013. Power failure: why small sample size undermines the reliability of neuroscience. Nat. Rev. Neurosci. 14, 365–376. https://doi.org/10.1038/nrn3475

Catelli, D.S., Wesseling, M., Jonkers, I., Lamontagne, M., 2019. A musculoskeletal model customized for squatting task. Comput. Methods Biomech. Biomed. Engin. 22, 21–24. https://doi.org/10.1080/10255842.2018.1523396

Collins, S.H., Wiggin, M.B., Sawicki, G.S., 2015. Reducing the energy cost of human walking using an unpowered exoskeleton. Nature 522, 212–215. https://doi.org/10.1038/nature14288

Crowninshield, R.D., Brand, R.A., 1981. A physiologically based criterion of muscle force prediction in locomotion. J. Biomech. 14, 793–801. https://doi.org/10.1016/0021-9290(81)90035-X

De Groote, F., Kinney, A.L., Rao, A. V., Fregly, B.J., 2016. Evaluation of Direct Collocation Optimal Control Problem Formulations for Solving the Muscle Redundancy Problem. Ann. Biomed. Eng. 44, 2922–2936. https://doi.org/10.1007/s10439-016-1591-9

Delp, S.L., Anderson, F.C., Arnold, A.S., Loan, P., Habib, A., John, C.T., Guendelman, E., Thelen, D.G., 2007. OpenSim: Open-Source Software to Create and Analyze Dynamic Simulations of Movement. IEEE Trans. Biomed. Eng. 54, 1940–1950. https://doi.org/10.1109/TBME.2007.901024

Dembia, C.L., Bianco, N.A., Falisse, A., Hicks, J.L., Delp, S.L., 2020. OpenSim Moco: Musculoskeletal optimal control. PLoS Comput. Biol. 16, e1008493. https://doi.org/10.1371/journal.pcbi.1008493

D'Hondt, J., Chapelle, L., Bishop, C., Aerenhouts, D., De Pauw, K., Clarys, P., D'Hondt, E., 2024. Association Between Inter-Limb Asymmetry and Determinants of Middle- and Long-distance Running Performance in Healthy Populations: A Systematic Review. Sports Med. Open 10, 127. https://doi.org/10.1186/s40798-024-00790-w

di Prampero, P., 1986. The Energy Cost of Human Locomotion on Land and in Water*. Int. J. Sports Med. 07, 55–72. https://doi.org/10.1055/s-2008-1025736

di Prampero, P.E., Atchou, G., Brückner, J.-C., Moia, C., 1986. The energetics of endurance running. Eur. J. Appl. Physiol. Occup. Physiol. 55, 259–266. https://doi.org/10.1007/BF02343797

Donelan, J.M., Kram, R., Arthur D., K., 2001. Mechanical and metabolic determinants of the preferred step width in human walking. Proc. R. Soc. Lond. B Biol. Sci. 268, 1985–1992. https://doi.org/10.1098/rspb.2001.1761

Donelan, J.M., Kram, R., Kuo, A.D., 2002. Mechanical work for step-to-step transitions is a major determinant of the metabolic cost of human walking. Journal of Experimental Biology 205, 3717–3727. https://doi.org/10.1242/jeb.205.23.3717

Farris, D.J., Sawicki, G.S., 2012. The mechanics and energetics of human walking and running: a joint level perspective. J. R. Soc. Interface 9, 110–118. https://doi.org/10.1098/rsif.2011.0182

Fletcher, J.R., Esau, S.P., MacIntosh, B.R., 2009. Economy of running: beyond the measurement of oxygen uptake. J. Appl. Physiol. 107, 1918–1922. https://doi.org/10.1152/japplphysiol.00307.2009

Fukunaga, T., Miyatani, M., Tachi, M., Kouzaki, M., Kawakami, Y., Kanehisa, H., 2001. Muscle volume is a major determinant of joint torque in humans. Acta Physiol. Scand. 172, 249–255. https://doi.org/10.1046/j.1365-201x.2001.00867.x

Galle, S., Malcolm, P., Collins, S.H., De Clercq, D., 2017. Reducing the metabolic cost of walking with an ankle exoskeleton: interaction between actuation timing and power. J. Neuroeng. Rehabil. 14, 35. https://doi.org/10.1186/s12984-017-0235-0

Gambietz, M., Nitschke, M., Miehling, J., Koelewijn, A.D., 2024. Contributing Components of Metabolic Energy Models to Metabolic Cost Estimations in Gait. IEEE Trans. Biomed. Eng. 71, 1228–1236. https://doi.org/10.1109/TBME.2023.3331271

Hamner, S.R., Delp, S.L., 2013. Muscle contributions to fore-aft and vertical body mass center accelerations over a range of running speeds. J. Biomech. 46, 780–787. https://doi.org/10.1016/j.jbiomech.2012.11.024

Helme, M., Tee, J., Emmonds, S., Low, C., 2021. Does lower-limb asymmetry increase injury risk in sport? A systematic review. Physical Therapy in Sport 49, 204–213. https://doi.org/10.1016/j.ptsp.2021.03.001

Hicks, J.L., Uchida, T.K., Seth, A., Rajagopal, A., Delp, S.L., 2015. Is My Model Good Enough? Best Practices for Verification and Validation of Musculoskeletal Models and Simulations of Movement. J. Biomech. Eng. 137. https://doi.org/10.1115/1.4029304

Jeukendrup, A.E., Wallis, G.A., 2005. Measurement of Substrate Oxidation During Exercise by Means of Gas Exchange Measurements. Int. J. Sports Med. 26, S28–S37. https://doi.org/10.1055/s-2004-830512

Jones, A.M., Doust, J.H., 1998. The validity of the lactate minimum test for determination of the maximal lactate steady state. Medicine& Science in Sports & Exercise 30, 1304–1313. https://doi.org/10.1097/00005768-199808000-00020

Kadaba, M.P., Ramakrishnan, H.K., Wootten, M.E., Gainey, J., Gorton, G., Cochran, G.V.B., 1989. Repeatability of kinematic, kinetic, and electromyographic data in normal adult gait. Journal of Orthopaedic Research 7, 849–860. https://doi.org/10.1002/jor.1100070611

Kipp, S., Grabowski, A.M., Kram, R., 2018. What determines the metabolic cost of human running across a wide range of velocities? Journal of Experimental Biology. https://doi.org/10.1242/jeb.184218

Koelewijn, A.D., Heinrich, D., van den Bogert, A.J., 2019. Metabolic cost calculations of gait using musculoskeletal energy models, a comparison study. PLoS One 14, e0222037. https://doi.org/10.1371/journal.pone.0222037

Leardini, A., Chiari, L., Croce, U. Della, Cappozzo, A., 2005. Human movement analysis using stereophotogrammetry. Gait Posture 21, 212–225. https://doi.org/10.1016/j.gaitpost.2004.05.002

Lichtwark, G.A., Wilson, A.M., 2005. Effects of series elasticity and activation conditions on muscle power output and efficiency. Journal of Experimental Biology 208, 2845–2853. https://doi.org/10.1242/jeb.01710

Lloyd, D.G., Besier, T.F., 2003. An EMG-driven musculoskeletal model to estimate muscle forces and knee joint moments in vivo. J. Biomech. 36, 765–776. https://doi.org/10.1016/S0021-9290(03)00010-1

Luis, I., Afschrift, M., De Groote, F., Gutierrez-Farewik, E.M., 2023. Insights into muscle metabolic energetics: Modelling muscle-tendon mechanics and metabolic rates during walking across speeds. KTH Royal Institute of Technology, Stockholm.

Malcolm, P., Derave, W., Galle, S., De Clercq, D., 2013. A Simple Exoskeleton That Assists Plantarflexion Can Reduce the Metabolic Cost of Human Walking. PLoS One 8, e56137. https://doi.org/10.1371/journal.pone.0056137

Maloney, S.J., 2019. The Relationship Between Asymmetry and Athletic Performance: A Critical Review. J. Strength Cond. Res. 33, 2579–2593. https://doi.org/10.1519/JSC.0000000000002608

Mantovani, G., Lamontagne, M., 2017. How Different Marker Sets Affect Joint Angles in Inverse Kinematics Framework. J. Biomech. Eng. 139. https://doi.org/10.1115/1.4034708

McGinley, J.L., Baker, R., Wolfe, R., Morris, M.E., 2009. The reliability of three-dimensional kinematic gait measurements: A systematic review. Gait Posture 29, 360–369. https://doi.org/10.1016/j.gaitpost.2008.09.003

Millard, M., Uchida, T., Seth, A., Delp, S.L., 2013. Flexing Computational Muscle: Modeling and Simulation of Musculotendon Dynamics. J. Biomech. Eng. 135. https://doi.org/10.1115/1.4023390

Minetti, A.E., Moia, C., Roi, G.S., Susta, D., Ferretti, G., 2002. Energy cost of walking and running at extreme uphill and downhill slopes. J. Appl. Physiol. 93, 1039–1046. https://doi.org/10.1152/japplphysiol.01177.2001

Modenese, L., Ceseracciu, E., Reggiani, M., Lloyd, D.G., 2016. Estimation of musculotendon parameters for scaled and subject specific musculoskeletal models using an optimization technique. J. Biomech. 49, 141–148. https://doi.org/10.1016/j.jbiomech.2015.11.006

Mohammadzadeh Gonabadi, A., Antonellis, P., Malcolm, P., 2020. Differences between joint-space and musculoskeletal estimations of metabolic rate time profiles. PLoS Comput. Biol. 16, e1008280. https://doi.org/10.1371/journal.pcbi.1008280

Nicholson, R.M., Sleivert, G.G., 2001. Indices of lactate threshold and their relationship with 10-km running velocity. Med. Sci. Sports Exerc. 33, 339–343. https://doi.org/10.1097/00005768-200102000-00026

Ortiz, A.L.R., Giovanelli, N., Kram, R., 2017. The metabolic costs of walking and running up a 30-degree incline: implications for vertical kilometer foot races. Eur. J. Appl. Physiol. 117, 1869–1876. https://doi.org/10.1007/s00421-017-3677-y

Pataky, T.C., 2010. Generalized n-dimensional biomechanical field analysis using statistical parametric mapping. J. Biomech. 43, 1976–1982. https://doi.org/10.1016/j.jbiomech.2010.03.008

Pataky, T.C., Robinson, M.A., Vanrenterghem, J., 2013. Vector field statistical analysis of kinematic and force trajectories. J. Biomech. 46, 2394–2401. https://doi.org/10.1016/j.jbiomech.2013.07.031

Péronnet, F., Massicotte, D., 1991. Table of nonprotein respiratory quotient: an update. Can. J. Sport Sci. 16, 23–9.

Pizzolato, C., Reggiani, M., Saxby, D.J., Ceseracciu, E., Modenese, L., Lloyd, D.G., 2017. Biofeedback for Gait Retraining Based on Real-Time Estimation of Tibiofemoral Joint Contact Forces. IEEE Transactions on Neural Systems and Rehabilitation Engineering 25, 1612–1621. https://doi.org/10.1109/TNSRE.2017.2683488

Potvin, J.R., Fuglevand, A.J., 2017. A motor unit-based model of muscle fatigue. PLoS Comput. Biol. 13, e1005581. https://doi.org/10.1371/journal.pcbi.1005581

Reinbolt, J.A., Schutte, J.F., Fregly, B.J., Koh, B. Il, Haftka, R.T., George, A.D., Mitchell, K.H., 2005. Determination of patient-specific multi-joint kinematic models through two-level optimization. J. Biomech. 38, 621–626. https://doi.org/10.1016/j.jbiomech.2004.03.031

Sartori, M., Reggiani, M., Farina, D., Lloyd, D.G., 2012a. EMG-Driven Forward-Dynamic Estimation of Muscle Force and Joint Moment about Multiple Degrees of Freedom in the Human Lower Extremity. PLoS One 7, e52618. https://doi.org/10.1371/journal.pone.0052618

Sartori, M., Reggiani, M., van den Bogert, A.J., Lloyd, D.G., 2012b. Estimation of musculotendon kinematics in large musculoskeletal models using multidimensional B-splines. J. Biomech. 45, 595–601. https://doi.org/10.1016/j.jbiomech.2011.10.040

Silder, A., Besier, T., Delp, S.L., 2012. Predicting the metabolic cost of incline walking from muscle activity and walking mechanics. J. Biomech. 45, 1842–1849. https://doi.org/10.1016/j.jbiomech.2012.03.032

Silder, A., Heiderscheit, B.C., Thelen, D.G., Enright, T., Tuite, M.J., 2008. MR observations of long-term musculotendon remodeling following a hamstring strain injury. Skeletal Radiol. 37, 1101–9. https://doi.org/10.1007/s00256-008-0546-0

Thelen, D.G., Anderson, F.C., Delp, S.L., 2003. Generating dynamic simulations of movement using computed muscle control. J. Biomech. 36, 321–328. https://doi.org/10.1016/S0021-9290(02)00432-3

Uchida, T.K., Hicks, J.L., Dembia, C.L., Delp, S.L., 2016a. Stretching Your Energetic Budget: How Tendon Compliance Affects the Metabolic Cost of Running. PLoS One 11, e0150378. https://doi.org/10.1371/journal.pone.0150378

Uchida, T.K., Seth, A., Pouya, S., Dembia, C.L., Hicks, J.L., Delp, S.L., 2016b. Simulating Ideal Assistive Devices to Reduce the Metabolic Cost of Running. PLoS One 11, e0163417. https://doi.org/10.1371/journal.pone.0163417

Umberger, B.R., 2010. Stance and swing phase costs in human walking. J. R. Soc. Interface 7, 1329–1340. https://doi.org/10.1098/rsif.2010.0084

Umberger, B.R., Gerritsen, K.G.M., Martin, P.E., 2003. A Model of Human Muscle Energy Expenditure. Comput. Methods Biomech. Biomed. Engin. 6, 99–111. https://doi.org/10.1080/1025584031000091678

Zajac, F.E., 1989. Muscle and tendon: properties, models, scaling, and application to biomechanics and motor control. Crit. Rev. Biomed. Eng. 17, 359–411.

Chapter 6: General Discussion

This thesis explored how physiological fatigue reshapes neuromuscular control and whole-body energetics during steady-state running, and how well these adaptations are captured by commonly used musculoskeletal energy models. Across two complementary studies, one centred on neuromuscular and perceptual indicators (Study 1), and the other on metabolic and simulation-based energetics (Study 2), a convergent picture emerged: fatigue progressively increases internal workload even when the external appearance of running remains remarkably stable. Given this kinematic stability and the heavy reliance on kinematics in OpenSim modelling, it is no surprise that static optimization (SO)–based musculoskeletal models only partially register this internal load, with systematic biases and limited responsiveness to fatigue, except for modest directional sensitivity in the *Umberger2010* formulation. Together, these findings highlight a critical gap between how running looks, how it feels, and how simulation pipelines currently interpret it, underscoring the need for more fatigue-aware frameworks, potentially through EMG-informed modelling.

6.1 Fatigue Without Visible Kinematic Change

Study 1 demonstrated a clear dissociation between running kinematics and the internal neuromuscular processes required to produce them. Across the fatiguing session, runners exhibited rising physiological strain and steadily increasing perceived exertion, along with EMG-derived signatures consistent with neuromuscular fatigue (decreased amplitude, shifts in frequency content, and widening variability). These changes indicate adjustments in motor unit recruitment, altered firing thresholds, and increased neural drive.

Yet the sagittal-plane kinematics remained stable with limited deviations across the gait cycle. The most parsimonious interpretation is that the central nervous system reorganized internal control

by introducing co-contraction, modulating stiffness, and redistributing load across muscles to preserve task-level outputs such as limb trajectories, step timing, and overall form (Bernstein, 1967; Latash, 2012).

Within this framework, fatigue-related neuromuscular changes are accommodated through mechanisms such as increased co-contraction, modulation of joint stiffness, and redistribution of load across synergistic muscles to stabilize movement (Granata and Orishimo, 2001; Hortobágyi et al., 2011; Hug et al., 2015). These compensatory strategies are advantageous for task success, allowing runners to maintain speed and externally visible kinematics even as neuromuscular fatigue develops.

However, both experimental and theoretical work suggests that maintaining stable kinematics through increased co-activation and stiffness comes at the cost of reduced motor flexibility and diminished control reserve (Dingwell et al., 2010; Hamill et al., 2012; Stergiou et al., 2006). As fatigue progresses, the system's ability to respond to perturbations, adapt coordination patterns, or redistribute forces efficiently may be compromised, even when mean joint kinematics remain unchanged. In this context, stable movement patterns may mask increasing vulnerability to coordination errors, altered force transmission, or breakdowns in inter-muscle timing near the end of a bout.

Consequently, a gait pattern that "looks the same" is not synonymous with "moving the same way internally." The present findings highlight that kinematic stability can coexist with substantial neuromuscular reorganization, underscoring the limitations of relying solely on joint kinematics or visual assessment to infer fatigue state. For clinicians and coaches, this distinction is critical: assessments based exclusively on observable technique may overlook the phase in which the margin for error is smallest and the capacity to absorb perturbations is most reduced. Taken together, these results support our Study 1 hypotheses: neuromuscular fatigue increased EMG

amplitude variability and altered spectral characteristics, while sagittal-plane kinematics remained stable across stages. Thus, the expected dissociation between internal neuromuscular changes and externally visible running mechanics was confirmed.

6.2 Model-Based Energetics Divergence from Calorimetry

Study 2 extended this perspective by examining whole-body metabolic demand using indirect calorimetry and comparing it with energy estimates from three standard metabolic energy models (*Bhargava2004*, *Umberger2003*, and *Umberger2010*). The protocol successfully elicited physiological fatigue, as evidenced by a progressive increase in cost of transport measured via indirect calorimetry from pre- to post-fatigue (Figure 5.1). This stage-dependent rise confirms that participants transitioned through increasingly fatigued states during the session.

In contrast, the metabolic energy models diverged substantially from the empirical metabolic response. Both *Bhargava2004* and *Umberger2003* underestimated cost of transport at all stages and, importantly, neither model reproduced the physiological increase in metabolic cost observed with indirect calorimetry; instead, each exhibited slight negative slopes across the session (Figure 5.1). By comparison, the *Umberger2010* model, although modestly overestimating absolute CoT, was the only formulation to track the upward progression observed experimentally. However, this increase was substantially attenuated relative to calorimetry, indicating limited sensitivity to the underlying physiological changes rather than full agreement. These discrepancies reflect the interaction of model scope, optimization assumptions, and metabolic formulation structure. When joint kinematics remain largely unchanged, as observed in the present protocol, SO-derived activations are constrained to similar patterns across stages, limiting the model's capacity to reflect fatigue-related increases in energetic demand. This likely contributes more strongly to the muted model response than a deliberate prioritization of stability over efficiency.

Additionally, the models estimate lower-limb muscle energetics only, whereas calorimetry captures arm swing, trunk stabilization, ventilatory work, and thermoregulatory cost. These components are expected to increase with prolonged high-intensity exercise and may contribute to the widening discrepancy between calorimetry and model-based estimates across stages. Further insight was provided by the EMG–model timing analysis. On average, SO-derived muscle activations occurred later than experimental EMG onsets, resulting in a negative EMG–model lag across muscles and runs (approximately −5% to −15% of the gait cycle). While individual muscles exhibited both positive and negative lags, the mean lag across conditions was negative. Importantly, these average timing offsets did not change systematically across fatigue stages, suggesting that the limited responsiveness of model-based CoT is not attributable to fatigue-related shifts in activation timing. Instead, the stable timing differences are more consistent with how OpenSim estimates activations within the static optimization framework.

Taken together, Study 2 demonstrates that whole-body metabolic cost increases reliably with fatigue under the present protocol, whereas simulation-based energy estimates remain muted or directionally incorrect unless the model incorporates more detailed physiological mechanisms, as in *Umberger2010*. These findings support the Study 2 hypotheses. As expected, *Bhargava2004* underestimated CoT relative to indirect calorimetry, while *Umberger2010* overestimated it. In contrast, *Umberger2003* underestimated CoT in the present dataset, contrary to prior reports.

Consistent with the hypothesis that static optimization–driven models would show limited sensitivity to fatigue-related changes in metabolic demand, none of the models reproduced the magnitude of the experimentally observed increase in CoT. Although *Umberger2010* captured the direction of this increase, the response was substantially attenuated and does not reflect meaningful sensitivity to fatigue. Together, these results indicate that musculoskeletal energy models driven by

static optimization, which do not incorporate EMG or fatigue dynamics, are insufficient to capture fatigue-related changes in metabolic cost.

6.3 Integration of Findings

Taken together, Studies 1 and 2 demonstrate that fatigue during prolonged running manifests primarily as internal neuromuscular and metabolic change rather than as overt alterations in joint kinematics. Across both investigations, externally observable running mechanics remained largely stable, even as physiological strain increased and internal control strategies were substantially reorganized. This dissociation highlights a fundamental limitation of relying on kinematics alone to infer fatigue state.

Study 1 established that neuromuscular fatigue can progress under conditions of apparent biomechanical stability, confirming that preserved joint trajectories do not imply preserved internal control. Study 2 extended this finding by showing that the metabolic consequences of this internal reorganization are reliably captured by indirect calorimetry but are not adequately reproduced by musculoskeletal energy models. In particular, most models failed to reflect within-session increases in metabolic cost despite verified fatigue, underscoring their limited sensitivity to time-dependent physiological change.

Collectively, these findings indicate that static-optimization pipelines reconstruct mechanically economical solutions constrained by kinematics rather than the evolving neuromuscular and energetic demands of fatigued running. As a result, both visible technique and model-derived energetics may underestimate the true physiological burden experienced during prolonged exercise. Addressing this gap will require modelling approaches that move beyond kinematic fidelity alone and incorporate fatigue-aware dynamics, individualized muscle properties, and neuromuscular constraints.

Overall, the thesis hypotheses were partially supported. For Study 1, the expected dissociation between neuromuscular fatigue and kinematic stability was confirmed; however, the anticipated increase in EMG amplitude and consistent spectral shifts were not uniformly observed, indicating more complex and muscle-specific adaptations than initially hypothesized.

For Study 2, the hypothesis that static optimization–based musculoskeletal models would underestimate metabolic cost and fail to capture fatigue-related changes was partially supported. While *Bhargava2004* consistently underestimated cost of transport and the models showed limited sensitivity to fatigue progression, the behaviour of the Umberger models was model-dependent, with *Umberger2010* overestimating cost and demonstrating only modest directional sensitivity to fatigue. Contrary to expectations, discrepancies between model-based estimates and indirect calorimetry did not increase substantially with fatigue, suggesting that these differences are primarily driven by structural limitations of the modelling framework rather than fatigue-dependent effects.

Furthermore, residual actuator analysis indicated that the simulations did not fully satisfy recommended dynamic consistency criteria, reinforcing that discrepancies between model-based energetics and experimental measurements arise from both model formulation and simulation-level constraints.

Taken together, these findings indicate that static optimization–based frameworks are more suitable for relative comparisons under controlled mechanical conditions than for accurately capturing absolute metabolic cost or fatigue-driven physiological adaptations during prolonged high-intensity running.

6.4 Implications for Sports Medicine, Coaching, and Return-to-Play

The decoupling of kinematics from internal load cautions against using visual technique alone to make decisions about training termination or return-to-play readiness. When EMG indices

decline and perceptual strain rises without visible form breakdown, the athlete may be operating near the edge of controllability. This is exactly the context in which slips, missteps, and injurious joint excursions are most likely to occur. Pragmatically, the results argue for integrating simple internal-load indicators, heart rate drift, self-reported exertion levels, and where feasible, wearable EMG proxies into late-session decision rules. For endurance and team-sport contexts, coaches can schedule micro-recoveries or modulate intensity when internal-load signals cross athlete-specific thresholds even if movement quality appears steady. Rehabilitation programs may also benefit from emphasizing fatigue-resistant function in stabilizers such as the gluteus medius and triceps surae, as these muscles play outsized roles in frontal-plane control and propulsion that may be compromised under accumulating fatigue

6.5 Implications for Modelling and Simulation Practice

For researchers who rely on simulation to inform design, intervention, or performance-related decisions, the present findings underscore a consistent requirement: fatigue must be represented explicitly within musculoskeletal modelling frameworks. Static-optimization pipelines are insufficient for modelling fatigued running, because model-derived energetics are determined by a fixed set of inputs, primarily joint kinematics, joint kinetics, muscle–tendon geometry, and activation patterns derived from an economy-based cost function. When kinematics and joint moments remain largely unchanged across a session, as observed here, static optimization produces similar activation solutions, and metabolic estimates remain correspondingly stable.

In addition, key physiological properties within these models, such as maximal force-generating capacity, recruitment thresholds, fiber-type behaviour, tendon compliance, and activation–relaxation dynamics, do not update as a function of accumulated work or fatigue. As a result, SO-based energetics reflect mechanically economical solutions under fixed physiological assumptions rather than the evolving neuromuscular state of a fatigued runner.

To address these limitations, future models should incorporate EMG-informed activation patterns that reflect subject-specific excitation timing, individualized muscle–tendon parameters that capture anatomical and mechanical variability, and fatigue-aware activation and efficiency states capable of representing dynamic reductions in force-generating capacity and shifts in motor unit recruitment. Including upper-body dynamics would allow models to account for arm-swing and trunk-stabilization energetics, while the integration of stability- or robustness-related costs would capture the increased co-contraction and control demands observed under fatigue. Together, these enhancements determine whether simulations can reproduce the upward drift in energetic cost observed experimentally and thereby influence their utility for footwear optimization, clinical decision support, and performance analysis.

6.6 Limitations

Several limitations frame the interpretation of this work. The cohort comprised healthy young adults with recreational training backgrounds; responses may differ in elite athletes, older adults, or clinical populations with distinct neuromuscular capacities and fatigue profiles. The study also required synchronization of multiple measurement systems (motion capture, force platforms, surface electromyography, and indirect calorimetry). Although synchronization procedures were carefully implemented and verified, small timing offsets between modalities can influence the alignment of physiological, neuromuscular, and biomechanical events, thereby contributing additional uncertainty to integrated analyses.

The study was also constrained by a small sample size. Only seven participants were included in the final analyses, well below the sample size estimated in the a-priori power analysis and therefore limiting statistical power, particularly for detecting within-subject fatigue effects or between-method differences. As a result, some true effects may not have reached statistical significance, and the stability of several estimates, especially variability measures and slope

coefficients, should be interpreted cautiously. In addition, the sample was strongly sex-imbalanced, with only one female participant. Given known sex-related differences in muscle fatigue resistance, biomechanics, and metabolic responses to exercise, this limits generalizability and prevents any examination of potential sex-specific patterns.

The indirect calorimetry measurements relied on relatively short 30 second steady-state windows; although consistent with established practice, longer windows can attenuate breath-by-breath noise and better accommodate VO2 kinetics and slow-component behaviour, thereby narrowing uncertainty bounds. Surface electromyography is vulnerable to cross-talk, placement variability, and changes in electrode–skin impedance with sweating; furthermore, it samples superficial portions of muscles and cannot directly capture deeper musculature, which can bias inferences about muscle-group contributions to control (De Luca, 1997).

Standard marker-based motion capture introduces additional sources of error that can obscure small but functionally meaningful changes in kinematics. Soft-tissue artefact causes skin-mounted markers to move relative to the underlying bone, with errors that can exceed several millimetres and vary across segments and phases of gait; these errors are amplified during high-impact tasks and in regions with substantial muscle mass (e.g., thigh and shank). Marker placement inconsistency, cluster deformation, occlusion, and camera calibration inaccuracies further contribute to kinematic uncertainty, while choices in filtering (cutoff frequency and algorithm) can either attenuate true signal or introduce phase shifts that distort joint angle and velocity estimates (Cappozzo et al., 2005; Leardini et al., 2005; Reinschmidt et al., 1997; Winter, 2009).

The treadmill environment, although controlled, is not equivalent to overground locomotion; differences in belt dynamics, visual flow, and air resistance can subtly alter mechanics and energetic cost, even when speed and grade are matched (Jones and Doust, 1998; Riley et al., 2008). On the modelling side, the pipelines were lower-limb only and did not include upper-body degrees of

freedom, arm-swing energetics, or thermoregulatory costs captured by whole-body calorimetry; arm swing alone can measurably influence metabolic cost (Arellano and Kram, 2011).

Static optimization objectives favour economical control strategies that may diverge from the human solutions that emerge under fatigue, where stability and robustness can take precedence over metabolic economy; model verification, validation, and sensitivity analyses remain essential to quantify such gaps (Hicks et al., 2015).

Finally, musculoskeletal and metabolic parameters were not fully individualized, and no explicit fatigue states were implemented; both factors limit the ability of the simulations to express subject-specific adaptations in activation, efficiency, and tendon compliance as sessions progress. These limitations do not overturn the main conclusions but delineate specific targets for improvement in future protocols, including the use of longer calorimetry windows, enhanced EMG procedures, motion-capture approaches that mitigate soft-tissue artefact (e.g., cluster-based tracking, functional joint calibration, or model-based STA compensation), incorporation of upper-body dynamics, and EMG-informed or fatigue-aware modelling frameworks.

6.7 Future Work

The most immediate extension is to implement the EMG-informed neuromusculoskeletal pipeline planned for this program. By driving the muscle model with measured excitations and calibrating metabolic parameters to the individual, we can test directly whether fatigue trends in cost of transport are more faithfully reproduced than with static optimization. Parallel work should estimate or bound fiber-type distributions, tendon compliance, and maximum forces using non-invasive surrogates or optimization-based identification. Incorporating arms and trunk will permit closer energy accounting against whole-body calorimetry and adding explicit stability costs can represent the co-contraction observed under fatigue. Field validation under thermal stress, overground running, and sport-specific tasks will probe generalizability beyond laboratory

constraints. Finally, linking stride-by-stride energy estimates to time-resolved EMG changes may clarify how local muscle fatigue shapes whole-body energetics within a single session.

An additional and complementary direction for future work is the incorporation of explicit muscle fatigue models within the musculoskeletal framework. While EMG-driven approaches provide subject-specific neural input, they do not inherently account for the time-dependent decline in force-generating capacity associated with fatigue. Fatigue models, such as those based on motor unit recruitment dynamics or phenomenological fatigue-recovery formulations (Chang et al., 2017; Michaud et al., 2023), could be integrated to simulate reductions in maximal force production, altered activation–force relationships, and changes in metabolic efficiency over time.

Incorporating fatigue-dependent muscle properties would enable the model to represent the progressive physiological state changes observed during prolonged exercise, rather than relying solely on externally driven kinematics and instantaneous activations. This may improve the ability of musculoskeletal simulations to capture fatigue-related increases in metabolic cost and provide a more mechanistic link between neuromuscular activity and whole-body energetics. Recent work has demonstrated the feasibility of integrating fatigue models within EMG-driven or optimization-based frameworks, suggesting a promising avenue for extending current modeling approaches beyond steady-state assumptions.

6.7.1 Planned EMG-Driven Musculoskeletal Modelling Workflow (Future Work; Not Executed)

The following section documents a pre-registered and fully specified EMG-driven musculoskeletal modelling workflow that was planned as a subsequent phase of this project but was not executed within the timeframe of the present thesis. It is included for transparency, reproducibility, and to outline a clear pathway for future work that builds directly on the findings of Studies 1 and 2. No EMG-driven calibration or forward simulations were performed for the

present thesis, and all results reported herein are based exclusively on static optimization–based modelling and indirect calorimetry.

6.7.1.1 Planned Aim and Scope

The planned aim of this future work is to calibrate participant-specific EMG-driven lower-limb musculoskeletal models to estimate muscle forces and energetic cost during running, and to compare these estimates with (i) static-optimization–based energy models and (ii) indirect calorimetry. This approach was motivated by the observation that static optimization does not adequately capture fatigue-related neuromuscular and metabolic changes under conditions of stable kinematics.

6.7.1.2 Input & Software

The planned EMG-driven pipeline would use OpenSim 3.3 and MATLAB (R2023b). Required inputs would include marker trajectories, synchronised ground-reaction forces and moments, treadmill speed, stride events, and bilateral surface EMG recordings from primary lower-limb muscles.

Preprocessing steps already executed as part of the present thesis include inverse kinematics to compute joint angles, inverse dynamics to compute net joint moments, EMG band-pass filtering, rectification, low-pass envelope extraction, normalization to maximal voluntary isometric contraction (%MVIC), and stride-time normalization.

6.7.1.3 Planned modelling pipeline

Participant-specific musculoskeletal geometry would be parameterized using a surrogate modelling approach following Meyer et al. (2016). Joint space for the lower extremity would be sampled using a Latin hypercube design spanning relevant hip, knee, and ankle angles. At each sampled configuration, musculotendon (MT) lengths and moment arms would be extracted from OpenSim. Least-squares regression would then be used to fit MT lengths as multivariate

polynomial functions of joint angles, with moment arms defined as the partial derivatives of the corresponding length functions with respect to joint angle to enforce derivative consistency (An et al., 1984; Zajac, 1989). Musculotendon velocities would be obtained as the time derivative of the fitted length functions.

EMG-driven calibration would then be performed using the CEINMS framework (Pizzolato et al., 2015). Calibration targets would include excitation-to-activation dynamics and musculotendon parameters such as optimal fiber length, tendon slack length, and maximal isometric force. These parameters would be identified by minimizing the error between model-predicted joint moments and inverse-dynamics moments, subject to physiological bounds and regularization for unmeasured muscles. Joint axis calibration could optionally be applied to refine joint mechanics prior to EMG-informed force estimation (Sartori et al., 2012a).

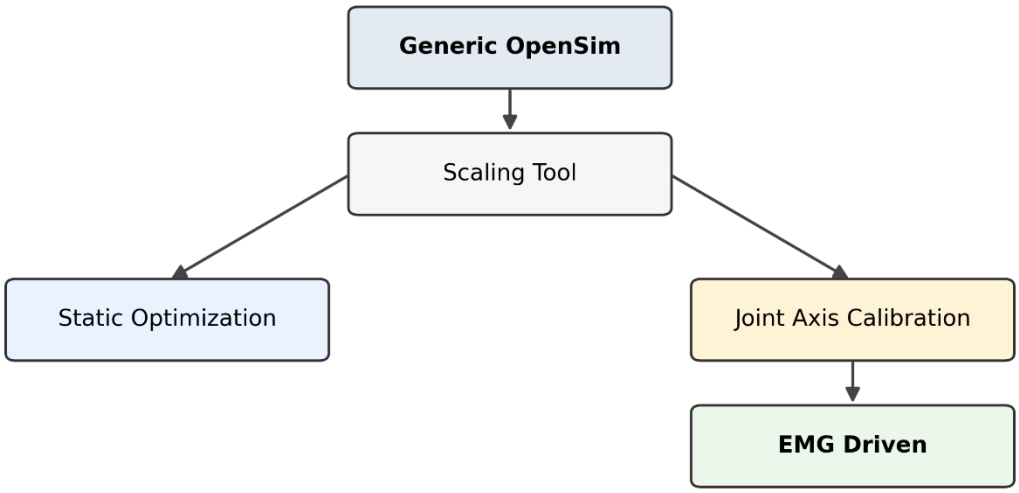

Figure 6.1: Flowchart of the two different approaches used to obtain estimation of muscle activation.

6.7.1.4 Planned Forward Simulation and Energetics Analysis

Following calibration, the EMG-driven model would be executed over pre-fatigue, mid-fatigue, and post-fatigue stages to estimate muscle activations, forces, and instantaneous metabolic

power. Metabolic cost would be computed using established energy models (e.g., *Umberger2003/2010*; *Bhargava 2004*) and aggregated to cost of transport ($J \cdot kg^{-1} \cdot m^{-1}$). These estimates would be compared stage-by-stage against static-optimization results and indirect calorimetry.

6.7.1.5 Planned Outcomes and hypotheses

The primary planned outcome would be stage-wise cost of transport derived from EMG-driven simulations. Secondary outcomes would include muscle-group energy contributions and stride-resolved activation and force profiles. The working hypothesis is that EMG-driven energetics would more closely track fatigue-related changes than static optimization due to the inclusion of measured neural drive and activation dynamics.

6.7.1.1 Planned Validation & statistics Analysis

Planned validation steps include checks on inverse-kinematics marker residuals, inverse-dynamics residual forces and moments, and surrogate model fitting errors for musculotendon lengths and moment arms. Model generalization would be assessed by calibrating on a subset of strides (e.g., pre- and mid-fatigue) and validating on held-out strides (e.g., post-fatigue). Agreement between EMG-driven energetics, static optimization, and indirect calorimetry would be evaluated using repeated-measures analyses (Method × Stage), along with Bland–Altman and correlation analyses.

6.7.1.1 Risks, constraints, and reason for deferral

The computational cost and time required for CEINMS calibration, surrogate fitting, and validation exceeded the available thesis timeline. To preserve methodological rigour, this EMG-driven workflow was deferred and is presented here as a fully specified plan for future work rather than as a partially executed analysis.

6.8 General Conclusion

Across two complementary studies, this thesis demonstrates that fatigue reorganizes the internal dynamics of running without necessarily altering its outward appearance. Neuromuscular indicators, perceptual strain, and whole-body metabolic measurements reveal a clear and progressive internal burden as exercise continues, even though joint kinematics remain stable. This dissociation underscores a key insight: stability of form does not equate to stability of effort. The central nervous system adapts by reshaping recruitment strategies, adjusting co-contraction, and increasing stabilization demands to preserve the global structure of movement, yet these internal adaptations come at a metabolic and neuromechanical cost that becomes increasingly pronounced under sustained high intensity.

Study 2 further shows that commonly used musculoskeletal energy models, despite their utility and widespread adoption, capture only part of this internal transformation. While indirect calorimetry reliably detected the rise in cost of transport with fatigue, only the *Umberger2010* model reproduced this upward progression, and even then, with attenuated sensitivity. The systematic biases and limited responsiveness of the models reflect the fact that their activations are mechanically optimal rather than physiologically driven, as confirmed by the consistent EMG–model timing offsets observed across the session. These findings collectively emphasize that accurate representation of fatigue requires simulations that incorporate the same information the nervous system uses to navigate it, including EMG-derived excitations, personalized muscle–tendon properties, and explicit fatigue mechanisms that evolve with work history.

In relation to the original aims, the results confirmed our Study 1 hypothesis that neuromuscular markers of fatigue would increase while kinematics remained stable. Study 2 hypotheses were supported in part: *Bhargava2004* underestimated CoT relative to indirect calorimetry, while *Umberger2010* overestimated it, with *Umberger2003* underestimating CoT in

the present dataset, contrary to prior reports. Consistent with our hypothesis, simulation-based estimates showed limited sensitivity to fatigue-related metabolic progression, with none of the models reproducing the magnitude of the experimentally observed increase in CoT.

Looking forward, the convergence of empirical and modelling evidence presented here points toward a new generation of neuromusculoskeletal simulations, capable of tracing not only how runners move, but how hard the neuromuscular system must work to maintain that movement as fatigue accumulates. By embedding richer physiological detail and modelling fatigue as a dynamic state rather than an afterthought, we can construct tools that more faithfully reflect real-world running demands. Such models will better support training decisions, rehabilitation planning, and technology design that remain effective past the first few thousand step.

References

Alba-Jiménez, C., Moreno-Doutres, D., Peña, J., 2022. Trends Assessing Neuromuscular Fatigue in Team Sports: A Narrative Review. Sports 10, 33. https://doi.org/10.3390/sports10030033

Allen, D.G., Lamb, G.D., Westerblad, H., 2008. Skeletal Muscle Fatigue: Cellular Mechanisms. Physiol. Rev. 88, 287–332. https://doi.org/10.1152/physrev.00015.2007

Allison, G.T., Fujiwara, T., 2002. The relationship between EMG median frequency and low frequency band amplitude changes at different levels of muscle capacity. Clinical Biomechanics 17, 464–469. https://doi.org/10.1016/S0268-0033(02)00033-5

Alwan, A., Srinivasan, M., 2025. Natural variability increases human walking metabolic costs and its implications to simulation-based metabolic estimation. BioRxiv. https://doi.org/10.1101/2025.03.13.643096

Amann, M., Calbet, J.A.L., 2008. Convective oxygen transport and fatigue. J. Appl. Physiol. 104, 861–870. https://doi.org/10.1152/japplphysiol.01008.2007

An, K.N., Takahashi, K., Harrigan, T.P., Chao, E.Y., 1984. Determination of Muscle Orientations and Moment Arms. J. Biomech. Eng. 106, 280–282. https://doi.org/10.1115/1.3138494

Anderson, F.C., Pandy, M.G., 2001. Dynamic Optimization of Human Walking. J. Biomech. Eng. 123, 381–390. https://doi.org/10.1115/1.1392310

Andersson, E.A., Nilsson, J., Thorstensson, A., 1997. Intramuscular EMG from the hip flexor muscles during human locomotion. Acta Physiol. Scand. 161, 361–70. https://doi.org/10.1046/j.1365-201X.1997.00225.x

Antonopoulos, C., Patikas, D., Koutlianos, N., Papadopoulou, S.D., Chatzopoulos, D., Hatzikotoulas, K., Bassa, E., Kotzamanidis, C., 2014. The Effect of Fatigue on

Electromyographic Characteristics during Obstacle Crossing of Different Heights in Young Adults. J. Sports Sci. Med. 13, 724–30.

Aquino, M.R.C., Liddy, J.J., Napoli, C.D., Fonseca, S.T., van Emmerik, R.E.A., Busa, M.A., 2023. Changes to balance dynamics following a high-intensity run are associated with future injury occurrence in recreational runners. Frontiers in Network Physiology 3. https://doi.org/10.3389/fnetp.2023.1227861

Arellano, C.J., Kram, R., 2011. The effects of step width and arm swing on energetic cost and lateral balance during running. J. Biomech. 44, 1291–1295. https://doi.org/10.1016/j.jbiomech.2011.01.002

Arnold, E.M., Hamner, S.R., Seth, A., Millard, M., Delp, S.L., 2013. How muscle fiber lengths and velocities affect muscle force generation as humans walk and run at different speeds. Journal of Experimental Biology. https://doi.org/10.1242/jeb.075697

Arones, M.M., Shourijeh, M.S., Patten, C., Fregly, B.J., 2020. Musculoskeletal Model Personalization Affects Metabolic Cost Estimates for Walking. Front. Bioeng. Biotechnol. 8. https://doi.org/10.3389/fbioe.2020.588925

Ashcraft, C.M., Frankenfield, D.C., 2015. Validity Test of a New Open-Circuit Indirect Calorimeter. Journal of Parenteral and Enteral Nutrition 39, 738–742. https://doi.org/10.1177/0148607114526242

Assila, N., Begon, M., Duprey, S., 2024. Finite Element Model of the Shoulder with Active Rotator Cuff Muscles: Application to Wheelchair Propulsion. Ann. Biomed. Eng. 52, 1240–1254. https://doi.org/10.1007/s10439-024-03449-5

Åstrand, P.-O., Ryhming, I., 1954. A Nomogram for Calculation of Aerobic Capacity (Physical Fitness) From Pulse Rate During Submaximal Work. J. Appl. Physiol. 7, 218–221. https://doi.org/10.1152/jappl.1954.7.2.218

Astur, D.C., Oliveira, S.G., Badra, R., Arliani, G.G., Kaleka, C.C., Jalikjian, W., Golanó, P., Cohen, M., 2011. Updating of the anatomy of the extensor mechanism of the knee using a three-dimensional technique. Rev. Bras. Ortop. (Sao. Paulo). 46, 490–4. https://doi.org/10.1016/S2255-4971(15)30401-8

ATS/ACCP Statement on Cardiopulmonary Exercise Testing, 2003. . Am. J. Respir. Crit. Care Med. 167, 211–277. https://doi.org/10.1164/rccm.167.2.211

Bacon, A.P., Carter, R.E., Ogle, E.A., Joyner, M.J., 2013. VO2max trainability and high intensity interval training in humans: a meta-analysis. PLoS One 8, e73182. https://doi.org/10.1371/journal.pone.0073182

Barnes, K.R., Kilding, A.E., 2015. Running economy: measurement, norms, and determining factors. Sports Med. Open 1, 8. https://doi.org/10.1186/s40798-015-0007-y

Barstow, T.J., Buchthal, S., Zanconato, S., Cooper, D.M., 1994. Muscle energetics and pulmonary oxygen uptake kinetics during moderate exercise. J. Appl. Physiol. 77, 1742–1749. https://doi.org/10.1152/jappl.1994.77.4.1742

Barstow, T.J., Jones, A.M., Nguyen, P.H., Casaburi, R., 1996. Influence of muscle fiber type and pedal frequency on oxygen uptake kinetics of heavy exercise. J. Appl. Physiol. 81, 1642–1650. https://doi.org/10.1152/jappl.1996.81.4.1642

Bassett, D.R., Howley, E.T., 2000. Limiting factors for maximum oxygen uptake and determinants of endurance performance. Med. Sci. Sports Exerc. 70. https://doi.org/10.1097/00005768-200001000-00012

Batliner, M., Kipp, S., Grabowski, A., Kram, R., Byrnes, W., 2018. Does Metabolic Rate Increase Linearly with Running Speed in all Distance Runners? Sports Med. Int. Open 02, E1–E8. https://doi.org/10.1055/s-0043-122068

Bavil, A.Y., Eghan-Acquah, E., Diamond, L.E., Barrett, R., Carty, C.P., Barzan, M., Nasseri, A., Lloyd, D.G., Saxby, D.J., Feih, S., 2024. Effect of different constraining boundary conditions on simulated femoral stresses and strains during gait. Sci. Rep. 14, 10808. https://doi.org/10.1038/s41598-024-61305-x

Bellenger, C.R., Arnold, J.B., Buckley, J.D., Thewlis, D., Fuller, J.T., 2019. Detrended fluctuation analysis detects altered coordination of running gait in athletes following a heavy period of training. J. Sci. Med. Sport 22, 294–299. https://doi.org/10.1016/j.jsams.2018.09.002

Bellenger, C.R., Fuller, J.T., Thomson, R.L., Davison, K., Robertson, E.Y., Buckley, J.D., 2016. Monitoring Athletic Training Status Through Autonomic Heart Rate Regulation: A Systematic Review and Meta-Analysis. Sports Medicine 46, 1461–1486. https://doi.org/10.1007/s40279-016-0484-2

Benoit, D.L., Damsgaard, M., Andersen, M.S., 2015. Surface marker cluster translation, rotation, scaling and deformation: Their contribution to soft tissue artefact and impact on knee joint kinematics. J. Biomech. 48, 2124–2129. https://doi.org/10.1016/j.jbiomech.2015.02.050

Benoit, D.L., Ramsey, D.K., Lamontagne, M., Xu, L., Wretenberg, P., Renström, P., 2006. Effect of skin movement artifact on knee kinematics during gait and cutting motions measured in vivo. Gait Posture 24, 152–164. https://doi.org/10.1016/j.gaitpost.2005.04.012

Bergh, U., Thorstensson, A., Sjödin, B., Hulten, B., Piehl, K., Karlsson, J., 1978. Maximal oxygen uptake and muscle fiber types in trained and untrained humans. Med. Sci. Sports 10, 151—154.

Bernstein, N.., 1967. Coordinate and Regulation of Movements. Pergamon P.

Besier, T.F., Lloyd, D.G., Ackland, T.R., 2003. Muscle Activation Strategies at the Knee during Running and Cutting Maneuvers. Med. Sci. Sports Exerc. 35, 119–127. https://doi.org/10.1097/00005768-200301000-00019

Bhargava, L.J., Pandy, M.G., Anderson, F.C., 2004. A phenomenological model for estimating metabolic energy consumption in muscle contraction. J. Biomech. 37, 81–88. https://doi.org/10.1016/S0021-9290(03)00239-2

Biancardi, C., Lagos-Hausheer, L., Pequera, G., Castroman, E., Cazot, F., Martinez, E., Bona, R., 2023. Energetic Cost of Running in Track and Treadmill, in: Proceedings of the 11th International Conference on Sport Sciences Research and Technology Support. SCITEPRESS - Science and Technology Publications, pp. 173–178. https://doi.org/10.5220/0012202300003587

Billat, V.L., 2001. Interval Training for Performance: A Scientific and Empirical Practice. Sports Medicine 31, 13–31. https://doi.org/10.2165/00007256-200131010-00002

Blomstrand, E., Rådegran, G., Saltin, B., 1997. Maximum rate of oxygen uptake by human skeletal muscle in relation to maximal activities of enzymes in the Krebs cycle. J. Physiol. 501, 455–460. https://doi.org/10.1111/j.1469-7793.1997.455bn.x

Bogdanis, G.C., 2012. Effects of Physical Activity and Inactivity on Muscle Fatigue. Front. Physiol. 3. https://doi.org/10.3389/fphys.2012.00142

Borotikar, B.S., Newcomer, R., Koppes, R., McLean, S.G., 2008. Combined effects of fatigue and decision making on female lower limb landing postures: Central and peripheral contributions to ACL injury risk. Clinical Biomechanics 23, 81–92. https://doi.org/10.1016/j.clinbiomech.2007.08.008

Boyer, K.A., Hayes, K.L., Umberger, B.R., Adamczyk, P.G., Bean, J.F., Brach, J.S., Clark, B.C., Clark, D.J., Ferrucci, L., Finley, J., Franz, J.R., Golightly, Y.M., Hortobágyi, T., Hunter, S., Narici, M., Nicklas, B., Roberts, T., Sawicki, G., Simonsick, E., Kent, J.A., 2023. Age-related changes in gait biomechanics and their impact on the metabolic cost of walking: Report from

a National Institute on Aging workshop. Exp. Gerontol. 173, 112102. https://doi.org/10.1016/j.exger.2023.112102

Burden, A., 2010. How should we normalize electromyograms obtained from healthy participants? What we have learned from over 25years of research. Journal of Electromyography and Kinesiology 20, 1023–1035. https://doi.org/10.1016/j.jelekin.2010.07.004

Button, K.S., Ioannidis, J.P.A., Mokrysz, C., Nosek, B.A., Flint, J., Robinson, E.S.J., Munafò, M.R., 2013. Power failure: why small sample size undermines the reliability of neuroscience. Nat. Rev. Neurosci. 14, 365–376. https://doi.org/10.1038/nrn3475

Cappozzo, A., Della Croce, U., Leardini, A., Chiari, L., 2005. Human movement analysis using stereophotogrammetry. Gait Posture 21, 186–196. https://doi.org/10.1016/j.gaitpost.2004.01.010

Carvalho, R., Fonseca, S.T., Okai-Nóbrega, L.A., Santos, T.R.T., Araújo, P.A., Quirino, J., Martins, W.R., Prado, L.S., Souza, T.R., 2023. Effects of lower-limb extensors' neuromuscular fatigue on the regularity of running movements: a crossover study. Sports Biomech. 1–18. https://doi.org/10.1080/14763141.2023.2236082

Catelli, D.S., Wesseling, M., Jonkers, I., Lamontagne, M., 2019. A musculoskeletal model customized for squatting task. Comput. Methods Biomech. Biomed. Engin. 22, 21–24. https://doi.org/10.1080/10255842.2018.1523396

Chahla, J., Sherman, B., Cinque, M., Miranda, A., Garrett, W.E., Chiampas, G., O'Malley, H., Gerhardt, M.B., Mandelbaum, B.R., 2018. Epidemiological Findings of Soccer Injuries During the 2017 Gold Cup. Orthop. J. Sports Med. 6. https://doi.org/10.1177/2325967118791754

Chang, J., Chablat, D., Bennis, F., Ma, L., 2017. Muscle Fatigue Analysis Using OpenSim. pp. 95–106. https://doi.org/10.1007/978-3-319-58463-8_9

Chappell, J.D., Herman, D.C., Knight, B.S., Kirkendall, D.T., Garrett, W.E., Yu, B., 2005. Effect of Fatigue on Knee Kinetics and Kinematics in Stop-Jump Tasks. Am. J. Sports Med. 33, 1022–1029. https://doi.org/10.1177/0363546504273047

Clancy, E.A., Hogan, N., 1999. Probability density of the surface electromyogram and its relation to amplitude detectors. IEEE Trans. Biomed. Eng. 46, 730–739. https://doi.org/10.1109/10.764949

Clancy, E.A., Hogan, N., 1997. Relating agonist-antagonist electromyograms to joint torque during isometric, quasi-isotonic, nonfatiguing contractions. IEEE Trans. Biomed. Eng. 44, 1024–1028. https://doi.org/10.1109/10.634654

Coen, P.M., Jubrias, S.A., Distefano, G., Amati, F., Mackey, D.C., Glynn, N.W., Manini, T.M., Wohlgemuth, S.E., Leeuwenburgh, C., Cummings, S.R., Newman, A.B., Ferrucci, L., Toledo, F.G.S., Shankland, E., Conley, K.E., Goodpaster, B.H., 2013. Skeletal Muscle Mitochondrial Energetics Are Associated With Maximal Aerobic Capacity and Walking Speed in Older Adults. The Journals of Gerontology: Series A 68, 447–455. https://doi.org/10.1093/gerona/gls196

Coggan, A.R., Spina, R.J., Rogers, M.A., King, D.S., Brown, M., Nemeth, P.M., Holloszy, J.O., 1990. Histochemical and enzymatic characteristics of skeletal muscle in master athletes. J. Appl. Physiol. 68, 1896–1901. https://doi.org/10.1152/jappl.1990.68.5.1896

Cohen, J., 1992. A power primer. Psychol. Bull. 112, 155–159. https://doi.org/10.1037/0033-2909.112.1.155

Collins, B.W., Pearcey, G.E.P., Buckle, N.C.M., Power, K.E., Button, D.C., 2018. Neuromuscular fatigue during repeated sprint exercise: underlying physiology and methodological considerations. Applied Physiology, Nutrition, and Metabolism 43, 1166–1175. https://doi.org/10.1139/apnm-2018-0080

Collins, S.H., Wiggin, M.B., Sawicki, G.S., 2015. Reducing the energy cost of human walking using an unpowered exoskeleton. Nature 522, 212–215. https://doi.org/10.1038/nature14288

Cortes, N., Onate, J., Morrison, S., 2014. Differential effects of fatigue on movement variability. Gait Posture 39, 888–893. https://doi.org/10.1016/j.gaitpost.2013.11.020

Corvini, G., Conforto, S., 2022. A Simulation Study to Assess the Factors of Influence on Mean and Median Frequency of sEMG Signals during Muscle Fatigue. Sensors 22, 6360. https://doi.org/10.3390/s22176360

Cramer, M.N., Jay, O., 2016. Biophysical aspects of human thermoregulation during heat stress. Autonomic Neuroscience 196, 3–13. https://doi.org/10.1016/j.autneu.2016.03.001

Crouter, S.E., LaMunion, S.R., Hibbing, P.R., Kaplan, A.S., Bassett, D.R., 2019. Accuracy of the Cosmed K5 portable calorimeter. PLoS One 14, e0226290. https://doi.org/10.1371/journal.pone.0226290

Crowninshield, R.D., Brand, R.A., 1981. A physiologically based criterion of muscle force prediction in locomotion. J. Biomech. 14, 793–801. https://doi.org/10.1016/0021-9290(81)90035-X

Davies, W., Atkinson, D., 2013. Risk assessment in anaesthesia. Anaesthesia & Intensive Care Medicine 14, 434–439. https://doi.org/https://doi.org/10.1016/j.mpaic.2013.07.006

De Groote, F., Kinney, A.L., Rao, A. V., Fregly, B.J., 2016. Evaluation of Direct Collocation Optimal Control Problem Formulations for Solving the Muscle Redundancy Problem. Ann. Biomed. Eng. 44, 2922–2936. https://doi.org/10.1007/s10439-016-1591-9

De Luca, C.J., 1997. The Use of Surface Electromyography in Biomechanics. J. Appl. Biomech. 13, 135–163. https://doi.org/10.1123/jab.13.2.135

De Luca, C.J., 1984. Myoelectrical manifestations of localized muscular fatigue in humans. Crit. Rev. Biomed. Eng. 11, 251–79.

De Luca, C.J., Donald Gilmore, L., Kuznetsov, M., Roy, S.H., 2010. Filtering the surface EMG signal: Movement artifact and baseline noise contamination. J. Biomech. 43, 1573–1579. https://doi.org/10.1016/j.jbiomech.2010.01.027

De Luca, C.J., Foley, P.J., Erim, Z., 1996. Motor unit control properties in constant-force isometric contractions. J. Neurophysiol. 76, 1503–16. https://doi.org/10.1152/jn.1996.76.3.1503

De Luca, C.J., Merletti, R., 1988. Surface myoelectric signal cross-talk among muscles of the leg. Electroencephalogr. Clin. Neurophysiol. 69, 568–75. https://doi.org/10.1016/0013-4694(88)90169-1

De Ruiter, C.J., Hamacher, P., Wolfs, B.G.A., 2016. A Short Submaximal Test to Determine the Fatigue Threshold of Knee Extensors in Young Men. Med. Sci. Sports Exerc. 48, 913–919. https://doi.org/10.1249/MSS.0000000000000832

Delp, S.L., Anderson, F.C., Arnold, A.S., Loan, P., Habib, A., John, C.T., Guendelman, E., Thelen, D.G., 2007. OpenSim: Open-Source Software to Create and Analyze Dynamic Simulations of Movement. IEEE Trans. Biomed. Eng. 54, 1940–1950. https://doi.org/10.1109/TBME.2007.901024

Delsoglio, M., Achamrah, N., Berger, M.M., Pichard, C., 2019. Indirect Calorimetry in Clinical Practice. J. Clin. Med. 8, 1387. https://doi.org/10.3390/jcm8091387

Dembia, C.L., Bianco, N.A., Falisse, A., Hicks, J.L., Delp, S.L., 2020. OpenSim Moco: Musculoskeletal optimal control. PLoS Comput. Biol. 16, e1008493. https://doi.org/10.1371/journal.pcbi.1008493

Derrick, T.R., Dereu, D., McLean, S.P., 2002. Impacts and kinematic adjustments during an exhaustive run. Med. Sci. Sports Exerc. 34, 998–1002. https://doi.org/10.1097/00005768-200206000-00015

D'Hondt, J., Chapelle, L., Bishop, C., Aerenhouts, D., De Pauw, K., Clarys, P., D'Hondt, E., 2024. Association Between Inter-Limb Asymmetry and Determinants of Middle- and Long-distance Running Performance in Healthy Populations: A Systematic Review. Sports Med. Open 10, 127. https://doi.org/10.1186/s40798-024-00790-w

di Prampero, P., 1986. The Energy Cost of Human Locomotion on Land and in Water*. Int. J. Sports Med. 07, 55–72. https://doi.org/10.1055/s-2008-1025736

di Prampero, P.E., Atchou, G., Brückner, J.-C., Moia, C., 1986. The energetics of endurance running. Eur. J. Appl. Physiol. Occup. Physiol. 55, 259–266. https://doi.org/10.1007/BF02343797

Dingwell, J.B., John, J., Cusumano, J.P., 2010. Do Humans Optimally Exploit Redundancy to Control Step Variability in Walking? PLoS Comput. Biol. 6, e1000856. https://doi.org/10.1371/journal.pcbi.1000856

Donelan, J.M., Kram, R., Arthur D., K., 2001. Mechanical and metabolic determinants of the preferred step width in human walking. Proc. R. Soc. Lond. B Biol. Sci. 268, 1985–1992. https://doi.org/10.1098/rspb.2001.1761

Donelan, J.M., Kram, R., Kuo, A.D., 2002. Mechanical work for step-to-step transitions is a major determinant of the metabolic cost of human walking. Journal of Experimental Biology 205, 3717–3727. https://doi.org/10.1242/jeb.205.23.3717

Ekblom-Bak, E., Björkman, F., Hellenius, M. -L., Ekblom, B., 2014. A new submaximal cycle ergometer test for prediction of <scp> VO $_{2max}$ </scp>. Scand. J. Med. Sci. Sports 24, 319–326. https://doi.org/10.1111/sms.12014

Ekstrand, J., Hägglund, M., Waldén, M., 2011. Injury incidence and injury patterns in professional football: the UEFA injury study. Br. J. Sports Med. 45, 553–558. https://doi.org/10.1136/bjsm.2009.060582

Encarnación-Martínez, A., Sanchis-Sanchis, R., Pérez-Soriano, P., García-Gallart, A., 2023. Relationship between muscular extensibility, strength and stability and the transmission of impacts during fatigued running. Sports Biomech. 22, 1364–1380. https://doi.org/10.1080/14763141.2020.1797863

Enoka, R.M., Duchateau, J., 2008. Muscle fatigue: what, why and how it influences muscle function. J. Physiol. 586, 11–23. https://doi.org/10.1113/jphysiol.2007.139477

Esteve-Lanao, J., Foster, C., Seiler, S., Lucia, A., 2007. Impact of Training Intensity Distribution on Performance in Endurance Athletes. The Journal of Strength and Conditioning Research 21, 943. https://doi.org/10.1519/R-19725.1

Faber, H., van Soest, A.J., Kistemaker, D.A., 2018. Inverse dynamics of mechanical multibody systems: An improved algorithm that ensures consistency between kinematics and external forces. PLoS One 13, e0204575. https://doi.org/10.1371/journal.pone.0204575

Falconer, K., Winter, D.A., 1985. Quantitative assessment of co-contraction at the ankle joint in walking. Electromyogr. Clin. Neurophysiol. 25, 135–49.

Farina, D., Fattorini, L., Felici, F., Filligoi, G., 2002. Nonlinear surface EMG analysis to detect changes of motor unit conduction velocity and synchronization. J. Appl. Physiol. 93, 1753–1763. https://doi.org/10.1152/japplphysiol.00314.2002

Farina, D., Merletti, R., Enoka, R.M., 2014. The extraction of neural strategies from the surface EMG: an update. J. Appl. Physiol. (1985) 117, 1215–30. https://doi.org/10.1152/japplphysiol.00162.2014

Farina, D., Merletti, R., Enoka, R.M., 2004. The extraction of neural strategies from the surface EMG. J. Appl. Physiol. 96, 1486–1495. https://doi.org/10.1152/japplphysiol.01070.2003

Farris, D.J., Sawicki, G.S., 2012. The mechanics and energetics of human walking and running: a joint level perspective. J. R. Soc. Interface 9, 110–118. https://doi.org/10.1098/rsif.2011.0182

Fick, A.E., 1870. Ueber die Messung des Blutquantums in den Herzventrikeln. Sitzungsberichte der Physikalisch-medizinischen Gesellschaft zu Würzburg 2, 16–28.

Fitchett, M.A., 1985. Predictability of VO2 max from submaximal cycle ergometer and bench stepping tests. Br. J. Sports Med. 19, 85–88. https://doi.org/10.1136/bjsm.19.2.85

Flahaut, Z., Romanick, K.K., Smale, K.B., Flaxman, T.E., Alkjaer, T., Simonsen, E.B., Krosgaard, M.R., Benoit, D.L., 2024. Countermovement jump reveals decreased functional outcome despite subjective improvement after ACL reconstruction. Gait Posture 113, 69–70. https://doi.org/10.1016/j.gaitpost.2024.07.081

Flahaut, Z.A., Ryan, N.S., Halje, P., Clouthier, A.L., Benoit, D.L., 2026. Neuromuscular signatures of fatigue precede kinematic changes in constant-speed treadmill running, in: 10th World Congress of Biomechanics. Vancouver.

Flahaut, Z.A., Ryan, N.S., Halje, P., Clouthier, A.L., Benoit, D.L., 2025. Reliability and Variability of Gait and Running Metrics on the Zebris FDM and HP Cosmos Systems, in: International Society of Biomechanics Conference 2025.

Flaxman, T., Carsen, S., Flahaut, Z., Romanchuk, N., Shourijeh, M., Del Bel, M., Benoit, D., 2024. Using a Musculoskeletal Model to Quantify Voluntary Knee Strength Deficits and Muscular Contribution to Torque in an ACL-injured Paediatric Population, in: Engineering Research Celebration Day 2024. Ottawa, Ontario, Canada.

Flaxman, T.E., Speirs, A.D., Benoit, D.L., 2012. Joint stabilisers or moment actuators: The role of knee joint muscles while weight-bearing. J. Biomech. 45, 2570–2576. https://doi.org/https://doi.org/10.1016/j.jbiomech.2012.07.026

Fletcher, J.R., Esau, S.P., MacIntosh, B.R., 2009. Economy of running: beyond the measurement of oxygen uptake. J. Appl. Physiol. 107, 1918–1922. https://doi.org/10.1152/japplphysiol.00307.2009

Fletcher, J.R., MacIntosh, B.R., 2017. Running Economy from a Muscle Energetics Perspective. Front. Physiol. 8. https://doi.org/10.3389/fphys.2017.00433

Foster, C., 1983. VO2 max and training indices as determinants of competitive running performance. J. Sports Sci. 1, 13–22. https://doi.org/10.1080/02640418308729657

Fregly, B.J., 2021. A Conceptual Blueprint for Making Neuromusculoskeletal Models Clinically Useful. Applied Sciences 11, 2037. https://doi.org/10.3390/app11052037

Fukunaga, T., Miyatani, M., Tachi, M., Kouzaki, M., Kawakami, Y., Kanehisa, H., 2001. Muscle volume is a major determinant of joint torque in humans. Acta Physiol. Scand. 172, 249–255. https://doi.org/10.1046/j.1365-201x.2001.00867.x

Galle, S., Malcolm, P., Collins, S.H., De Clercq, D., 2017. Reducing the metabolic cost of walking with an ankle exoskeleton: interaction between actuation timing and power. J. Neuroeng. Rehabil. 14, 35. https://doi.org/10.1186/s12984-017-0235-0

Gambietz, M., Nitschke, M., Miehling, J., Koelewijn, A.D., 2024. Contributing Components of Metabolic Energy Models to Metabolic Cost Estimations in Gait. IEEE Trans. Biomed. Eng. 71, 1228–1236. https://doi.org/10.1109/TBME.2023.3331271

Gandevia, S.C., 2001. Spinal and Supraspinal Factors in Human Muscle Fatigue. Physiol. Rev. 81, 1725–1789. https://doi.org/10.1152/physrev.2001.81.4.1725

Gao, Z., Xiang, L., Fekete, G., Baker, J.S., Mao, Z., Gu, Y., 2023. A Data-Driven Approach for Fatigue Detection during Running Using Pedobarographic Measurements. Appl. Bionics Biomech. 2023, 1–11. https://doi.org/10.1155/2023/7022513

Garber, C.E., Blissmer, B., Deschenes, M.R., Franklin, B.A., Lamonte, M.J., Lee, I.-M., Nieman, D.C., Swain, D.P., 2011. Quantity and Quality of Exercise for Developing and Maintaining Cardiorespiratory, Musculoskeletal, and Neuromotor Fitness in Apparently Healthy Adults. Med. Sci. Sports Exerc. 43, 1334–1359. https://doi.org/10.1249/MSS.0b013e318213fefb

García-Pérez, J.A., Pérez-Soriano, P., Llana Belloch, S., Lucas-Cuevas, Á.G., Sánchez-Zuriaga, D., 2014. Effects of treadmill running and fatigue on impact acceleration in distance running. Sports Biomech. 13, 259–266. https://doi.org/10.1080/14763141.2014.909527

Garrett, J., Akyildiz, Z., Leduc, C., van den Hoek, D., Manuel Clemente, F., Ardigò, L.P., 2023. Peak running speed can be used to monitor neuromuscular fatigue from a standardized running test in team sport athletes. Research in Sports Medicine 31, 319–330. https://doi.org/10.1080/15438627.2021.1966012

Garrett, J.M., Gunn, R., Eston, R.G., Jakeman, J., Burgess, D.J., Norton, K., 2019. The effects of fatigue on the running profile of elite team sport athletes. A systematic review and meta-analysis. J. Sports Med. Phys. Fitness 59. https://doi.org/10.23736/S0022-4707.19.09356-3

Geijtenbeek, T., 2019. SCONE: Open Source Software for Predictive Simulation of Biological Motion. J. Open Source Softw. 4, 1421. https://doi.org/10.21105/joss.01421

Girard, O., Millet, G.P., Micallef, J.-P., Racinais, S., 2012. Alteration in neuromuscular function after a 5 km running time trial. Eur. J. Appl. Physiol. 112, 2323–2330. https://doi.org/10.1007/s00421-011-2205-8

Glover, N.A., Chaudhari, A.M., 2024. Neuromuscular and trunk control mediate factors associated with injury in fatigued runners. J. Biomech. 170, 112176. https://doi.org/10.1016/j.jbiomech.2024.112176

Goodall, S., Charlton, K., Howatson, G., Thomas, K., 2015. Neuromuscular Fatigability during Repeated-Sprint Exercise in Male Athletes. Med. Sci. Sports Exerc. 47, 528–536. https://doi.org/10.1249/MSS.0000000000000443

Granata, K.P., Orishimo, K.F., 2001. Response of trunk muscle coactivation to changes in spinal stability. J. Biomech. 34, 1117–1123. https://doi.org/10.1016/S0021-9290(01)00081-1

Grood, E.S., Suntay, W.J., 1983. A Joint Coordinate System for the Clinical Description of Three-Dimensional Motions: Application to the Knee. J. Biomech. Eng. 105, 136–144. https://doi.org/10.1115/1.3138397

Guidetti, L., Meucci, M., Bolletta, F., Emerenziani, G. Pietro, Gallotta, M.C., Baldari, C., 2018. Validity, reliability and minimum detectable change of COSMED K5 portable gas exchange system in breath-by-breath mode. PLoS One 13, e0209925. https://doi.org/10.1371/journal.pone.0209925

Gupton, M., Imonugo, O., Black, A.C., Launico, M. V., Terreberry, R.R., 2024. Anatomy, Bony Pelvis and Lower Limb, Knee.

Hall, J.E., Hall, M.E., 2020. Guyton and Hall Textbook of Medical Physiology, 14th ed. Elsevier.

Hamill, J., Palmer, C., Van Emmerik, R.E.A., 2012. Coordinative variability and overuse injury. Sports Medicine, Arthroscopy, Rehabilitation, Therapy & Technology 4, 45. https://doi.org/10.1186/1758-2555-4-45

Hamlin, M., Draper, N., Blackwell, G., Shearman, J., Kimber, N., 2012. Determination of Maximal Oxygen Uptake Using the Bruce or a Novel Athlete-Led Protocol in a Mixed Population. J. Hum. Kinet. 31, 97–104. https://doi.org/10.2478/v10078-012-0010-z

Hamner, S.R., Delp, S.L., 2013. Muscle contributions to fore-aft and vertical body mass center accelerations over a range of running speeds. J. Biomech. 46, 780–787. https://doi.org/10.1016/j.jbiomech.2012.11.024

Harms, S.J., Hickson, R.C., 1983. Skeletal muscle mitochondria and myoglobin, endurance, and intensity of training. J. Appl. Physiol. 54, 798–802. https://doi.org/10.1152/jappl.1983.54.3.798

Hawkins, M.N., Raven, P.B., Snell, P.G., Stray-Gundersen, J., Levine, B.D., 2007. Maximal oxygen uptake as a parametric measure of cardiorespiratory capacity. Med. Sci. Sports Exerc. 39, 103–7. https://doi.org/10.1249/01.mss.0000241641.75101.64

Helme, M., Tee, J., Emmonds, S., Low, C., 2021. Does lower-limb asymmetry increase injury risk in sport? A systematic review. Physical Therapy in Sport 49, 204–213. https://doi.org/10.1016/j.ptsp.2021.03.001

Hepple, R.T., 2002. The role of O2 supply in muscle fatigue. Can. J. Appl. Physiol. 27, 56–69. https://doi.org/10.1139/h02-004

Hermens, H.J., Bruggen, T.A.M. v., Baten, C.T.M., Rutten, W.L.C., Boom, H.B.K., 1992. The median frequency of the surface EMG power spectrum in relation to motor unit firing and action potential properties. Journal of Electromyography and Kinesiology 2, 15–25. https://doi.org/10.1016/1050-6411(92)90004-3

Hermens, H.J., Freriks, B., Disselhorst-Klug, C., Rau, G., 2000. Development of recommendations for SEMG sensors and sensor placement procedures. Journal of Electromyography and Kinesiology 10, 361–374. https://doi.org/10.1016/S1050-6411(00)00027-4

Hespanhol Junior, L.C., Pena Costa, L.O., Lopes, A.D., 2013. Previous injuries and some training characteristics predict running-related injuries in recreational runners: a prospective cohort study. J. Physiother. 59, 263–269. https://doi.org/10.1016/S1836-9553(13)70203-0

Hicks, J.L., Uchida, T.K., Seth, A., Rajagopal, A., Delp, S.L., 2015. Is My Model Good Enough? Best Practices for Verification and Validation of Musculoskeletal Models and Simulations of Movement. J. Biomech. Eng. 137. https://doi.org/10.1115/1.4029304

Hodges, P.W., Bui, B.H., 1996. A comparison of computer-based methods for the determination of onset of muscle contraction using electromyography. Electroencephalography and Clinical

Neurophysiology/Electromyography and Motor Control 101, 511–519. https://doi.org/10.1016/S0921-884X(96)95190-5

Hortobágyi, T., Richardson, S.P., Lomarev, M., Shamim, E., Meunier, S., Russman, H., Dang, N., Hallett, M., 2011. Interhemispheric Plasticity in Humans. Med. Sci. Sports Exerc. 43, 1188–1199. https://doi.org/10.1249/MSS.0b013e31820a94b8

Hug, F., Tucker, K., Gennisson, J.-L., Tanter, M., Nordez, A., 2015. Elastography for Muscle Biomechanics. Exerc. Sport Sci. Rev. 43, 125–133. https://doi.org/10.1249/JES.0000000000000049

Hwang, J., Castelli, D.M., Gonzalez-Lima, F., 2017. The positive cognitive impact of aerobic fitness is associated with peripheral inflammatory and brain-derived neurotrophic biomarkers in young adults. Physiol. Behav. 179, 75–89. https://doi.org/10.1016/j.physbeh.2017.05.011

Impellizzeri, F.M., Rampinini, E., Coutts, A.J., Sassi, A., Marcora, S.M., 2004. Use of RPE-Based Training Load in Soccer. Med. Sci. Sports Exerc. 36, 1042–1047. https://doi.org/10.1249/01.MSS.0000128199.23901.2F

Ingen Schenau, G.J. van, Cavanagh, P.R., 1990. Power equations in endurance sports. J. Biomech. 23, 865–881. https://doi.org/10.1016/0021-9290(90)90352-4

Jacobs, R.A., Siebenmann, C., Hug, M., Toigo, M., Meinild, A., Lundby, C., 2012. Twenty-eight days at 3454-m altitude diminishes respiratory capacity but enhances efficiency in human skeletal muscle mitochondria. The FASEB Journal 26, 5192–5200. https://doi.org/10.1096/fj.12-218206

Jacobson, W.C., Gabel, R.H., Brand, R.A., 1995. Surface vs. fine-wire electrode ensemble-averaged signals during gait. J. Electromyogr. Kinesiol. 5, 37–44. https://doi.org/10.1016/s1050-6411(99)80004-2

Jamnick, N.A., By, S., Pettitt, C.D., Pettitt, R.W., 2016. Comparison of the YMCA and a Custom Submaximal Exercise Test for Determining V˙O2max. Med. Sci. Sports Exerc. 48, 254–259. https://doi.org/10.1249/MSS.0000000000000763

Jeukendrup, A.E., Wallis, G.A., 2005. Measurement of Substrate Oxidation During Exercise by Means of Gas Exchange Measurements. Int. J. Sports Med. 26, S28–S37. https://doi.org/10.1055/s-2004-830512

Jewell, C., Hamill, J., von Tscharner, V., Boyer, K.A., 2019. Altered multi-muscle coordination patterns in habitual forefoot runners during a prolonged, exhaustive run. Eur. J. Sport Sci. 19, 1062–1071. https://doi.org/10.1080/17461391.2019.1575912

Jones, A.M., Doust, J.H., 1998. The validity of the lactate minimum test for determination of the maximal lactate steady state. Medicine& Science in Sports & Exercise 30, 1304–1313. https://doi.org/10.1097/00005768-199808000-00020

Joyner, M.J., Coyle, E.F., 2008. Endurance exercise performance: the physiology of champions. J. Physiol. 586, 35–44. https://doi.org/10.1113/jphysiol.2007.143834

Kadaba, M.P., Ramakrishnan, H.K., Wootten, M.E., Gainey, J., Gorton, G., Cochran, G.V.B., 1989. Repeatability of kinematic, kinetic, and electromyographic data in normal adult gait. Journal of Orthopaedic Research 7, 849–860. https://doi.org/10.1002/jor.1100070611

Kaiyala, K.J., Ramsay, D.S., 2011. Direct animal calorimetry, the underused gold standard for quantifying the fire of life. Comp. Biochem. Physiol. A Mol. Integr. Physiol. 158, 252–264. https://doi.org/10.1016/j.cbpa.2010.04.013

Kaufman, C., Berg, K., Noble, J., Thomas, J., 2006. Ratings of Perceived Exertion of ACSM Exercise Guidelines in Individuals Varying in Aerobic Fitness. Res. Q. Exerc. Sport 77, 122–130. https://doi.org/10.1080/02701367.2006.10599338

Kipp, S., Grabowski, A.M., Kram, R., 2018. What determines the metabolic cost of human running across a wide range of velocities? Journal of Experimental Biology. https://doi.org/10.1242/jeb.184218

Knicker, A.J., Renshaw, I., Oldham, A.R.H., Cairns, S.P., 2011. Interactive Processes Link the Multiple Symptoms of Fatigue in Sport Competition. Sports Medicine 41, 307–328. https://doi.org/10.2165/11586070-000000000-00000

Koelewijn, A.D., Heinrich, D., van den Bogert, A.J., 2019. Metabolic cost calculations of gait using musculoskeletal energy models, a comparison study. PLoS One 14, e0222037. https://doi.org/10.1371/journal.pone.0222037

Konrad, P., 2005. The ABC of EMG: A Practical Introduction to Kinesiological Electromyography, 1st ed.

Kreder, H.J., Hawker, G.A., 2010. 6 - THE KNEE, in: Lawry, G. V, Kreder, H.J., Hawker, G.A., Jerome, D. (Eds.), Fam's Musculoskeletal Examination and Joint Injection Techniques (Second Edition). Mosby, Philadelphia, pp. 65–88. https://doi.org/https://doi.org/10.1016/B978-0-323-06504-7.10006-5

Krishnan, C., Allen, E.J., Williams, G.N., 2011. Effect of knee position on quadriceps muscle force steadiness and activation strategies. Muscle Nerve 43, 563–73. https://doi.org/10.1002/mus.21981

Krosshaug, T., Nakamae, A., Boden, B.P., Engebretsen, L., Smith, G., Slauterbeck, J.R., Hewett, T.E., Bahr, R., 2007. Mechanisms of Anterior Cruciate Ligament Injury in Basketball. Am. J. Sports Med. 35, 359–367. https://doi.org/10.1177/0363546506293899

Kupa, E.J., Roy, S.H., Kandarian, S.C., De Luca, C.J., 1995. Effects of muscle fiber type and size on EMG median frequency and conduction velocity. J. Appl. Physiol. 79, 23–32. https://doi.org/10.1152/jappl.1995.79.1.23

Lakomy, H.K.A., Lakomy, J., 1993. Estimation of maximum oxygen uptake from submaximal exercise on a Concept II rowing ergometer. J. Sports Sci. 11, 227–232. https://doi.org/10.1080/02640419308729989

Latash, M.L., 2012. The bliss (not the problem) of motor abundance (not redundancy). Exp. Brain Res. 217, 1–5. https://doi.org/10.1007/s00221-012-3000-4

Leardini, A., Chiari, L., Croce, U. Della, Cappozzo, A., 2005. Human movement analysis using stereophotogrammetry. Gait Posture 21, 212–225. https://doi.org/10.1016/j.gaitpost.2004.05.002

Lee, D., Pate, R.R., Lavie, C.J., Sui, X., Church, T.S., Blair, S.N., 2014. Leisure-Time Running Reduces All-Cause and Cardiovascular Mortality Risk. J. Am. Coll. Cardiol. 64, 472–481. https://doi.org/10.1016/j.jacc.2014.04.058

Lee, L.-F., Umberger, B.R., 2016. Generating optimal control simulations of musculoskeletal movement using OpenSim and MATLAB. PeerJ 4, e1638. https://doi.org/10.7717/peerj.1638

LeMond, G., Hom, M., 2015. The Science of Fitness: Power, Performance, and Endurance. Elsevier/Academic Press.

Levine, B.D., 2008. VO_2max: what do we know, and what do we still need to know? J. Physiol. 586, 25–34. https://doi.org/10.1113/jphysiol.2007.147629

Li, H., Early, K.S., Zhang, G., Ma, P., Wang, H., 2024. Personalized Hydration Strategy to Improve Fluid Balance and Intermittent Exercise Performance in the Heat. Nutrients 16. https://doi.org/10.3390/nu16091341

Lichtwark, G.A., Wilson, A.M., 2005. Effects of series elasticity and activation conditions on muscle power output and efficiency. Journal of Experimental Biology 208, 2845–2853. https://doi.org/10.1242/jeb.01710

Lindstrom, L., Magnusson, R., Petersén, I., 1970. Muscular fatigue and action potential conduction velocity changes studied with frequency analysis of EMG signals. Electromyography 10, 341–56.

Lloyd, D.G., Besier, T.F., 2003. An EMG-driven musculoskeletal model to estimate muscle forces and knee joint moments in vivo. J. Biomech. 36, 765–776. https://doi.org/10.1016/S0021-9290(03)00010-1

Lourenço, T.F., Martins, L.E.B., Tessutti, L.S., Brenzikofer, R., Macedo, D.V., 2011. Reproducibility of an Incremental Treadmill V̇o2max Test with Gas Exchange Analysis for Runners. J. Strength Cond. Res. 25, 1994–1999. https://doi.org/10.1519/JSC.0b013e3181e501d6

Luis, I., Afschrift, M., De Groote, F., Gutierrez-Farewik, E.M., 2023. Insights into muscle metabolic energetics: Modelling muscle-tendon mechanics and metabolic rates during walking across speeds. KTH Royal Institute of Technology, Stockholm.

Luo, Z., Zhang, X., Wang, J., Yang, Y., Xu, Y., Fu, W., 2019. Changes in Ground Reaction Forces, Joint Mechanics, and Stiffness during Treadmill Running to Fatigue. Applied Sciences 9, 5493. https://doi.org/10.3390/app9245493

Malcolm, P., Derave, W., Galle, S., De Clercq, D., 2013. A Simple Exoskeleton That Assists Plantarflexion Can Reduce the Metabolic Cost of Human Walking. PLoS One 8, e56137. https://doi.org/10.1371/journal.pone.0056137

Maloney, S.J., 2019. The Relationship Between Asymmetry and Athletic Performance: A Critical Review. J. Strength Cond. Res. 33, 2579–2593. https://doi.org/10.1519/JSC.0000000000002608

Mansouri, M., Reinbolt, J.A., 2012. A platform for dynamic simulation and control of movement based on OpenSim and MATLAB. J. Biomech. 45, 1517–1521. https://doi.org/10.1016/j.jbiomech.2012.03.016

Mantovani, G., Lamontagne, M., 2017. How Different Marker Sets Affect Joint Angles in Inverse Kinematics Framework. J. Biomech. Eng. 139. https://doi.org/10.1115/1.4034708

Marcora, S.M., Staiano, W., Manning, V., 2009. Mental fatigue impairs physical performance in humans. J. Appl. Physiol. 106, 857–864. https://doi.org/10.1152/japplphysiol.91324.2008

McGinley, J.L., Baker, R., Wolfe, R., Morris, M.E., 2009. The reliability of three-dimensional kinematic gait measurements: A systematic review. Gait Posture 29, 360–369. https://doi.org/10.1016/j.gaitpost.2008.09.003

McLean, S.G., Felin, R.E., Suedekum, N., Calabrese, G., Passerallo, A., Joy, S., 2007. Impact of Fatigue on Gender-Based High-Risk Landing Strategies. Med. Sci. Sports Exerc. 39, 502–514. https://doi.org/10.1249/mss.0b013e3180d47f0

Merletti, R., Parker, P., 2004. Electromyography: Physiology, Engineering, and Non-Invasive Applications. Wiley-IEEE Press.

Mero, A., Jaakkola, L., Komi, P. V., 1991. Relationships between muscle fibre characteristics and physical performance capacity in trained athletic boys. J. Sports Sci. 9, 161–171. https://doi.org/10.1080/02640419108729877

Meyer, A.J., Eskinazi, I., Jackson, J.N., Rao, A. V., Patten, C., Fregly, B.J., 2016. Muscle Synergies Facilitate Computational Prediction of Subject-Specific Walking Motions. Front. Bioeng. Biotechnol. 4. https://doi.org/10.3389/fbioe.2016.00077

Michaud, F., Frey-Law, L.A., Lugrís, U., Cuadrado, L., Figueroa-Rodríguez, J., Cuadrado, J., 2023. Applying a muscle fatigue model when optimizing load-sharing between muscles for short-

duration high-intensity exercise: A preliminary study. Front. Physiol. 14, 1167748. https://doi.org/10.3389/fphys.2023.1167748

Millard, M., Uchida, T., Seth, A., Delp, S.L., 2013. Flexing Computational Muscle: Modeling and Simulation of Musculotendon Dynamics. J. Biomech. Eng. 135. https://doi.org/10.1115/1.4023390

Miller, M.S., Callahan, D.M., Toth, M.J., 2014. Skeletal muscle myofilament adaptations to aging, disease, and disuse and their effects on whole muscle performance in older adult humans. Front. Physiol. 5. https://doi.org/10.3389/fphys.2014.00369

Miller, R.H., 2014. A comparison of muscle energy models for simulating human walking in three dimensions. J. Biomech. 47, 1373–1381. https://doi.org/10.1016/j.jbiomech.2014.01.049

Millet, G.Y., 2011. Can Neuromuscular Fatigue Explain Running Strategies and Performance in Ultra-Marathons? Sports Medicine 41, 489–506. https://doi.org/10.2165/11588760-000000000-00000

Millet, G.Y., Lepers, R., 2004. Alterations of Neuromuscular Function After Prolonged Running, Cycling and Skiing Exercises. Sports Medicine 34, 105–116. https://doi.org/10.2165/00007256-200434020-00004

Minetti, A.E., Moia, C., Roi, G.S., Susta, D., Ferretti, G., 2002. Energy cost of walking and running at extreme uphill and downhill slopes. J. Appl. Physiol. 93, 1039–1046. https://doi.org/10.1152/japplphysiol.01177.2001

Modenese, L., Ceseracciu, E., Reggiani, M., Lloyd, D.G., 2016. Estimation of musculotendon parameters for scaled and subject specific musculoskeletal models using an optimization technique. J. Biomech. 49, 141–148. https://doi.org/10.1016/j.jbiomech.2015.11.006

Mohammadzadeh Gonabadi, A., Antonellis, P., Malcolm, P., 2020. Differences between joint-space and musculoskeletal estimations of metabolic rate time profiles. PLoS Comput. Biol. 16, e1008280. https://doi.org/10.1371/journal.pcbi.1008280

Mtaweh, H., Tuira, L., Floh, A.A., Parshuram, C.S., 2018. Indirect Calorimetry: History, Technology, and Application. Front. Pediatr. 6. https://doi.org/10.3389/fped.2018.00257

Mu, D., Li, F., Yu, L., Du, C., Ge, L., Sun, T., 2022. Study on exercise muscle fatigue based on sEMG and ECG data fusion and temporal convolutional network. PLoS One 17, e0276921. https://doi.org/10.1371/journal.pone.0276921

Muñoz-Pepi, I., Garcia-Hernandez, N., Parra-Vega, V., 2023. Forward Neuromusculoskeletal Dynamics With Continuous Muscle Wrapping. IEEE Robot. Autom. Lett. 8, 5942–5949. https://doi.org/10.1109/LRA.2023.3300277

Muscle Fiber Types, 2012. , in: Encyclopedia of Exercise Medicine in Health and Disease. Springer Berlin Heidelberg, Berlin, Heidelberg, pp. 611–611. https://doi.org/10.1007/978-3-540-29807-6_2707

Nicholson, R.M., Sleivert, G.G., 2001. Indices of lactate threshold and their relationship with 10-km running velocity. Med. Sci. Sports Exerc. 33, 339–343. https://doi.org/10.1097/00005768-200102000-00026

Nicol, C., Avela, J., Komi, P. V, 2006. The stretch-shortening cycle : a model to study naturally occurring neuromuscular fatigue. Sports Medicine 36, 977–999. https://doi.org/10.2165/00007256-200636110-00004

Olivo, G., Nilsson, J., Garzón, B., Lebedev, A., Wåhlin, A., Tarassova, O., Ekblom, M.M., Lövdén, M., 2021. Higher VO2max is associated with thicker cortex and lower grey matter blood flow in older adults. Sci. Rep. 11, 16724. https://doi.org/10.1038/s41598-021-96138-5

Onishi, H., Yagi, R., Akasaka, K., Momose, K., Ihashi, K., Handa, Y., 2000. Relationship between EMG signals and force in human vastus lateralis muscle using multiple bipolar wire electrodes. J. Electromyogr. Kinesiol. 10, 59–67. https://doi.org/10.1016/s1050-6411(99)00020-6

Oppenheim, A. V., Schafer, R.W., 2010. Discrete-Time Signal Processing, 3rd ed. Prentice Hall, Upper Saddle River.

Ortiz, A.L.R., Giovanelli, N., Kram, R., 2017. The metabolic costs of walking and running up a 30-degree incline: implications for vertical kilometer foot races. Eur. J. Appl. Physiol. 117, 1869–1876. https://doi.org/10.1007/s00421-017-3677-y

Pangrazio, O., 2016. Epidemiology of soccer players traumatic injuries during the 2015 America Cup. Muscles Ligaments Tendons J. https://doi.org/10.11138/mltj/2016.6.1.124

Paquette, M.R., Melcher, D.A., 2017. Impact of a Long Run on Injury-Related Biomechanics with Relation to Weekly Mileage in Trained Male Runners. J. Appl. Biomech. 33, 216–221. https://doi.org/10.1123/jab.2016-0170

Park, J.H., Brown, R.L., Park, C.R., McCully, K., Cohn, M., Haselgrove, J., Chance, B., 1987. Functional pools of oxidative and glycolytic fibers in human muscle observed by 31P magnetic resonance spectroscopy during exercise. Proceedings of the National Academy of Sciences 84, 8976–8980. https://doi.org/10.1073/pnas.84.24.8976

Pataky, T.C., 2010. Generalized n-dimensional biomechanical field analysis using statistical parametric mapping. J. Biomech. 43, 1976–1982. https://doi.org/10.1016/j.jbiomech.2010.03.008

Pataky, T.C., Robinson, M.A., Vanrenterghem, J., 2013. Vector field statistical analysis of kinematic and force trajectories. J. Biomech. 46, 2394–2401. https://doi.org/10.1016/j.jbiomech.2013.07.031

Pedersen, P.K., Bak Sørensen, J., Jensen, K., Johansen, L., Levin, K., 2002. Muscle fiber type distribution and nonlinear VO2-power output relationship in cycling. Med. Sci. Sports Exerc. 34, 655–661. https://doi.org/10.1097/00005768-200204000-00015

Perez-Suarez, I., Martin-Rincon, M., Gonzalez-Henriquez, J.J., Fezzardi, C., Perez-Regalado, S., Galvan-Alvarez, V., Juan-Habib, J.W., Morales-Alamo, D., Calbet, J.A.L., 2018. Accuracy and Precision of the COSMED K5 Portable Analyser. Front. Physiol. 9. https://doi.org/10.3389/fphys.2018.01764

Péronnet, F., Massicotte, D., 1991. Table of nonprotein respiratory quotient: an update. Can. J. Sport Sci. 16, 23–9.

Perry, J., Easterday, C.S., Antonelli, D.J., 1981. Surface versus intramuscular electrodes for electromyography of superficial and deep muscles. Phys. Ther. 61, 7–15. https://doi.org/10.1093/ptj/61.1.7

Pizzolato, C., Lloyd, D.G., Sartori, M., Ceseracciu, E., Besier, T.F., Fregly, B.J., Reggiani, M., 2015. CEINMS: A toolbox to investigate the influence of different neural control solutions on the prediction of muscle excitation and joint moments during dynamic motor tasks. J. Biomech. 48, 3929–3936. https://doi.org/10.1016/j.jbiomech.2015.09.021

Pizzolato, C., Reggiani, M., Saxby, D.J., Ceseracciu, E., Modenese, L., Lloyd, D.G., 2017. Biofeedback for Gait Retraining Based on Real-Time Estimation of Tibiofemoral Joint Contact Forces. IEEE Transactions on Neural Systems and Rehabilitation Engineering 25, 1612–1621. https://doi.org/10.1109/TNSRE.2017.2683488

Place, N., Lepers, R., Deley, G., Millet, G.Y., 2004. Time Course of Neuromuscular Alterations during a Prolonged Running Exercise. Med. Sci. Sports Exerc. 36, 1347–1356. https://doi.org/10.1249/01.MSS.0000135786.22996.77

Plini, E.R.G., Melnychuk, M.C., Andrews, R., Boyle, R., Whelan, R., Spence, J.S., Chapman, S.B., Robertson, I.H., Dockree, P.M., 2024. Greater physical fitness (VO 2 max) in healthy older adults associated with increased integrity of the locus coeruleus-noradrenergic system. Acta Physiol. (Oxf). 240, e14191. https://doi.org/10.1111/apha.14191

Pollock, M.L., Gaesser, G.A., Butcher, J.D., Despres, J.-P., Dishman, R.K., Franklin, B.A., Garber, C.E., 1998. ACSM Position Stand: The Recommended Quantity and Quality of Exercise for Developing and Maintaining Cardiorespiratory and Muscular Fitness, and Flexibility in Healthy Adults. Med. Sci. Sports Exerc. 30, 975–991. https://doi.org/10.1097/00005768-199806000-00032

Poole, D.C., Jones, A.M., 2017. Measurement of the maximum oxygen uptake V̇o2max: V̇o2peak is no longer acceptable. J. Appl. Physiol. 122, 997–1002. https://doi.org/10.1152/japplphysiol.01063.2016

Potvin, J.R., Fuglevand, A.J., 2017. A motor unit-based model of muscle fatigue. PLoS Comput. Biol. 13, e1005581. https://doi.org/10.1371/journal.pcbi.1005581

Quammen, D., Cortes, N., Van Lunen, B.L., Lucci, S., Ringleb, S.I., Onate, J., 2012. Two different fatigue protocols and lower extremity motion patterns during a stop-jump task. J. Athl. Train. 47, 32–41. https://doi.org/10.4085/1062-6050-47.1.32

Quatman, C.E., Hewett, T.E., 2009. The anterior cruciate ligament injury controversy: is "valgus collapse" a sex-specific mechanism? Br. J. Sports Med. 43, 328–335. https://doi.org/10.1136/bjsm.2009.059139

Quesada, P.M., Mengelkoch, L.J., Hale, R.C., Simon, S.R., 2000. Biomechanical and metabolic effects of varying backpack loading on simulated marching. Ergonomics 43, 293–309. https://doi.org/10.1080/001401300184413

Reinbolt, J.A., Schutte, J.F., Fregly, B.J., Koh, B. Il, Haftka, R.T., George, A.D., Mitchell, K.H., 2005. Determination of patient-specific multi-joint kinematic models through two-level optimization. J. Biomech. 38, 621–626. https://doi.org/10.1016/j.jbiomech.2004.03.031

Reinschmidt, C., van den Bogert, A.J., Nigg, B.M., Lundberg, A., Murphy, N., 1997. Effect of skin movement on the analysis of skeletal knee joint motion during running. J. Biomech. 30, 729–732. https://doi.org/10.1016/S0021-9290(97)00001-8

Riemer, R., Hsiao-Wecksler, E.T., 2009. Improving Net Joint Torque Calculations Through a Two-Step Optimization Method for Estimating Body Segment Parameters. J. Biomech. Eng. 131. https://doi.org/10.1115/1.3005155

Riemer, R., Hsiao-Wecksler, E.T., 2008. Improving joint torque calculations: Optimization-based inverse dynamics to reduce the effect of motion errors. J. Biomech. 41, 1503–1509. https://doi.org/10.1016/j.jbiomech.2008.02.011

Riley, P.O., Dicharry, J., Franz, J., Croce, U. Della, Wilder, R.P., Kerrigan, D.C., 2008. A Kinematics and Kinetic Comparison of Overground and Treadmill Running. Med. Sci. Sports Exerc. 40, 1093–1100. https://doi.org/10.1249/MSS.0b013e3181677530

Rimmer, E., Verheul, J., Lake, M., 2020. Effect of Fatigue from Repeated Sprints on Hamstring Muscle Activation Patterns During Running, in: 38th International Society of Biomechanics in Sport Conference. Online.

Romagnoli, M., Alis, R., Sanchis-Gomar, F., Lippi, G., Arduini, A., 2018. An Eighteen-Minute Submaximal Exercise Test to Assess Cardiac Fitness in Response to Aerobic Training. J. Strength Cond. Res. 32, 2846–2852. https://doi.org/10.1519/JSC.0000000000000685

Romanato, M., Meggiorin, E., Sawacha, Z., 2022. Toward the definition of a minimum input model for an EMG analysis in clinics. Gait Posture 97, 19. https://doi.org/10.1016/j.gaitpost.2022.09.036

Romanchuk, N.J., Livock, H., Lukas, K.J., Del Bel, M.J., Benoit, D.L., Carsen, S., 2023. Criteria Used to Determine Unrestricted Return to Activity After ACL Reconstruction in Pediatric and Adolescent Patients: A Systematic Review. Orthop. J. Sports Med. 11. https://doi.org/10.1177/23259671231154540

Roy, S.H., De Luca, C.J., Schneider, J., 1986. Effects of electrode location on myoelectric conduction velocity and median frequency estimates. J. Appl. Physiol. (1985) 61, 1510–7. https://doi.org/10.1152/jappl.1986.61.4.1510

Runge, C.F., Zajac, F.E., Allum, J.H.J., Risher, D.W., Bryson, A.E., Honegger, F., 1995. Estimating net joint torques from kinesiological data using optimal linear system theory. IEEE Trans. Biomed. Eng. 42, 1158–1164. https://doi.org/10.1109/10.476122

S. Shourijeh, M., Smale, K.B., Potvin, B.M., Benoit, D.L., 2016. A forward-muscular inverse-skeletal dynamics framework for human musculoskeletal simulations. J. Biomech. 49, 1718–1723. https://doi.org/10.1016/j.jbiomech.2016.04.007

Sartori, M., Gizzi, L., Lloyd, D.G., Farina, D., 2013. A musculoskeletal model of human locomotion driven by a low dimensional set of impulsive excitation primitives. Front. Comput. Neurosci. 7. https://doi.org/10.3389/fncom.2013.00079

Sartori, M., Reggiani, M., Farina, D., Lloyd, D.G., 2012a. EMG-Driven Forward-Dynamic Estimation of Muscle Force and Joint Moment about Multiple Degrees of Freedom in the Human Lower Extremity. PLoS One 7, e52618. https://doi.org/10.1371/journal.pone.0052618

Sartori, M., Reggiani, M., van den Bogert, A.J., Lloyd, D.G., 2012b. Estimation of musculotendon kinematics in large musculoskeletal models using multidimensional B-splines. J. Biomech. 45, 595–601. https://doi.org/10.1016/j.jbiomech.2011.10.040

Schiaffino, S., Reggiani, C., 2011. Fiber Types in Mammalian Skeletal Muscles. Physiol. Rev. 91, 1447–1531. https://doi.org/10.1152/physrev.00031.2010

Schlink, B.R., Nordin, A.D., Brooks, C.N., Ferris, D.P., 2021. Fatigue induces altered spatial myoelectric activation patterns in the medial gastrocnemius during locomotion. J. Neurophysiol. 125, 2013–2023. https://doi.org/10.1152/jn.00602.2020

Schneider, J., Schlüter, K., Sprave, T., Wiskemann, J., Rosenberger, F., 2020. Exercise intensity prescription in cancer survivors: ventilatory and lactate thresholds are useful submaximal alternatives to VO2peak. Supportive Care in Cancer 28, 5521–5528. https://doi.org/10.1007/s00520-020-05407-y

Scribbans, T.D., Vecsey, S., Hankinson, P.B., Foster, W.S., Gurd, B.J., 2016. The Effect of Training Intensity on VO2max in Young Healthy Adults: A Meta-Regression and Meta-Analysis. Int. J. Exerc. Sci. 9, 230–247.

Seale, J.L., Rumpler, W. V., 1997. Synchronous direct gradient layer and indirect room calorimetry. J. Appl. Physiol. 83, 1775–1775. https://doi.org/10.1152/jappl.1997.83.5.1775

Seth, A., Hicks, J.L., Uchida, T.K., Habib, A., Dembia, C.L., Dunne, J.J., Ong, C.F., DeMers, M.S., Rajagopal, A., Millard, M., Hamner, S.R., Arnold, E.M., Yong, J.R., Lakshmikanth, S.K., Sherman, M.A., Ku, J.P., Delp, S.L., 2018. OpenSim: Simulating musculoskeletal dynamics and neuromuscular control to study human and animal movement. PLoS Comput. Biol. 14, e1006223. https://doi.org/10.1371/journal.pcbi.1006223

Silder, A., Besier, T., Delp, S.L., 2012. Predicting the metabolic cost of incline walking from muscle activity and walking mechanics. J. Biomech. 45, 1842–1849. https://doi.org/10.1016/j.jbiomech.2012.03.032

Silder, A., Heiderscheit, B.C., Thelen, D.G., Enright, T., Tuite, M.J., 2008. MR observations of long-term musculotendon remodeling following a hamstring strain injury. Skeletal Radiol. 37, 1101–9. https://doi.org/10.1007/s00256-008-0546-0

Silverman, J.D., Balbinot, G., Masani, K., Zariffa, J., Eng, P., 2021. Validity and Reliability of Surface Electromyography Features in Lower Extremity Muscle Contraction in Healthy and Spinal Cord-Injured Participants. Top. Spinal Cord Inj. Rehabil. 27, 14–27. https://doi.org/10.46292/sci20-00001

Simoneau, M., Bégin, F., Teasdale, N., 2006. The effects of moderate fatigue on dynamic balance control and attentional demands. J. Neuroeng. Rehabil. 3, 22. https://doi.org/10.1186/1743-0003-3-22

Solomonow, M., Baratta, R., Zhou, B.H., Shoji, H., Bose, W., Beck, C., D'Ambrosia, R., 1987. The synergistic action of the anterior cruciate ligament and thigh muscles in maintaining joint stability. Am. J. Sports Med. 15, 207–213. https://doi.org/10.1177/036354658701500302

Stergiou, N., Harbourne, R.T., Cavanaugh, J.T., 2006. Optimal Movement Variability. Journal of Neurologic Physical Therapy 30, 120–129. https://doi.org/10.1097/01.NPT.0000281949.48193.d9

Sun, J., Liu, G., Sun, Y., Lin, K., Zhou, Z., Cai, J., 2022. Application of Surface Electromyography in Exercise Fatigue: A Review. Front. Syst. Neurosci. 16. https://doi.org/10.3389/fnsys.2022.893275

Sushkova, O.S., Morozov, A.A., Gabova, A.V., Karabanov, A.V., Illarioshkin, S.N., 2021. A Statistical Method for Exploratory Data Analysis Based on 2D and 3D Area under Curve Diagrams: Parkinson's Disease Investigation. Sensors 21, 4700. https://doi.org/10.3390/s21144700

Sutherland, D.H., 2001. The evolution of clinical gait analysis part l: kinesiological EMG. Gait Posture 14, 61–70. https://doi.org/10.1016/s0966-6362(01)00100-x

Svantesson, E., Hamrin Senorski, E., Alentorn-Geli, E., Westin, O., Sundemo, D., Grassi, A., Čustović, S., Samuelsson, K., 2019. Increased risk of ACL revision with non-surgical

treatment of a concomitant medial collateral ligament injury: a study on 19,457 patients from the Swedish National Knee Ligament Registry. Knee Surg. Sports Traumatol. Arthrosc. 27, 2450–2459. https://doi.org/10.1007/s00167-018-5237-3

Taylor, J.L., Amann, M., Duchateau, J., Meeusen, R., Rice, C.L., 2016. Neural Contributions to Muscle Fatigue. Med. Sci. Sports Exerc. 48, 2294–2306. https://doi.org/10.1249/MSS.0000000000000923

Tegner, Y., Lysholm, J., 1985. Rating systems in the evaluation of knee ligament injuries. Clin. Orthop. Relat. Res. 43–9.

Thelen, D.G., Anderson, F.C., Delp, S.L., 2003. Generating dynamic simulations of movement using computed muscle control. J. Biomech. 36, 321–328. https://doi.org/10.1016/S0021-9290(02)00432-3

Uchida, T.K., Hicks, J.L., Dembia, C.L., Delp, S.L., 2016a. Stretching Your Energetic Budget: How Tendon Compliance Affects the Metabolic Cost of Running. PLoS One 11, e0150378. https://doi.org/10.1371/journal.pone.0150378

Uchida, T.K., Seth, A., Pouya, S., Dembia, C.L., Hicks, J.L., Delp, S.L., 2016b. Simulating Ideal Assistive Devices to Reduce the Metabolic Cost of Running. PLoS One 11, e0163417. https://doi.org/10.1371/journal.pone.0163417

Umberger, B.R., 2010. Stance and swing phase costs in human walking. J. R. Soc. Interface 7, 1329–1340. https://doi.org/10.1098/rsif.2010.0084

Umberger, B.R., Gerritsen, K.G.M., Martin, P.E., 2003. A Model of Human Muscle Energy Expenditure. Comput. Methods Biomech. Biomed. Engin. 6, 99–111. https://doi.org/10.1080/1025584031000091678

Vaienti, E., Scita, G., Ceccarelli, F., Pogliacomi, F., 2017. Understanding the human knee and its relationship to total knee replacement. Acta Biomed. 88, 6–16. https://doi.org/10.23750/abm.v88i2-S.6507

van der Zee, T.J., Kuo, A.D., 2021. Soft tissue deformations explain most of the mechanical work variations of human walking. Journal of Experimental Biology 224. https://doi.org/10.1242/jeb.239889

van Melick, N., Meddeler, B.M., Hoogeboom, T.J., Nijhuis-van der Sanden, M.W.G., van Cingel, R.E.H., 2017. How to determine leg dominance: The agreement between self-reported and observed performance in healthy adults. PLoS One 12, e0189876. https://doi.org/10.1371/journal.pone.0189876

Vesterinen, V., Nummela, A., Äyrämö, S., Laine, T., Hynynen, E., Mikkola, J., Häkkinen, K., 2016. Monitoring Training Adaptation With a Submaximal Running Test Under Field Conditions. Int. J. Sports Physiol. Perform. 11, 393–399. https://doi.org/10.1123/ijspp.2015-0366

Wan, J.-J., Qin, Z., Wang, P.-Y., Sun, Y., Liu, X., 2017. Muscle fatigue: general understanding and treatment. Exp. Mol. Med. 49, e384. https://doi.org/10.1038/emm.2017.194

Wasserman, K., 2012. Principles of Exercise Testing and Interpretation : Including Pathophysiology and Clinical Applications, 5th ed. Lippincott Williams & Wilkins, Philadelphia.

Weyand, P.G., Sandell, R.F., Prime, D.N.L., Bundle, M.W., 2010. The biological limits to running speed are imposed from the ground up. J. Appl. Physiol. 108, 950–961. https://doi.org/10.1152/japplphysiol.00947.2009

Wilke, J., Fleckenstein, J., Krause, F., Vogt, L., Banzer, W., 2016. Sport-specific functional movement can simulate aspects of neuromuscular fatigue occurring in team sports. Sports Biomech. 15, 151–161. https://doi.org/10.1080/14763141.2016.1159322

Willer, J., Allen, S.J., Burden, R.J., Folland, J.P., 2021. Neuromechanics of Middle-Distance Running Fatigue: A Key Role of the Plantarflexors? Med. Sci. Sports Exerc. 53, 2119–2130. https://doi.org/10.1249/MSS.0000000000002695

Willwacher, S., Kurz, M., Robbin, J., Thelen, M., Hamill, J., Kelly, L., Mai, P., 2022. Running-Related Biomechanical Risk Factors for Overuse Injuries in Distance Runners: A Systematic Review Considering Injury Specificity and the Potentials for Future Research. Sports Medicine 52, 1863–1877. https://doi.org/10.1007/s40279-022-01666-3

Winkert, K., Kirsten, J., Dreyhaupt, J., Steinacker, J.M., Treff, G., 2020. The COSMED K5 in Breath-by-Breath and Mixing Chamber Mode at Low to High Intensities. Med. Sci. Sports Exerc. 52, 1153–1162. https://doi.org/10.1249/MSS.0000000000002241

Winkert, K., Kirsten, J., Kamnig, R., Steinacker, J.M., Treff, G., 2021. Differences in V˙O2max Measurements Between Breath-by-Breath and Mixing-Chamber Mode in the COSMED K5. Int. J. Sports Physiol. Perform. 16, 1335–1340. https://doi.org/10.1123/ijspp.2020-0634

Winter, D.A., 2009. Biomechanics and Motor Control of Human Movement. Wiley. https://doi.org/10.1002/9780470549148

Wu, G., Siegler, S., Allard, P., Kirtley, C., Leardini, A., Rosenbaum, D., Whittle, M., D'Lima, D.D., Cristofolini, L., Witte, H., Schmid, O., Stokes, I., 2002. ISB recommendation on definitions of joint coordinate system of various joints for the reporting of human joint motion—part I: ankle, hip, and spine. J. Biomech. 35, 543–548. https://doi.org/10.1016/S0021-9290(01)00222-6

Xia, R., Zhang, X., Wang, X., Sun, X., Fu, W., 2017. Effects of Two Fatigue Protocols on Impact Forces and Lower Extremity Kinematics during Drop Landings: Implications for Noncontact Anterior Cruciate Ligament Injury. J. Healthc. Eng. 2017, 1–8. https://doi.org/10.1155/2017/5690519

Zajac, F.E., 1989. Muscle and tendon: properties, models, scaling, and application to biomechanics and motor control. Crit. Rev. Biomed. Eng. 17, 359–411.

Zebis, M.K., Bencke, J., Andersen, L.L., Alkjær, T., Suetta, C., Mortensen, P., Kjær, M., Aagaard, P., 2011. Acute fatigue impairs neuromuscular activity of anterior cruciate ligament-agonist muscles in female team handball players. Scand. J. Med. Sci. Sports 21, 833–840. https://doi.org/10.1111/j.1600-0838.2010.01052.x

Appendix

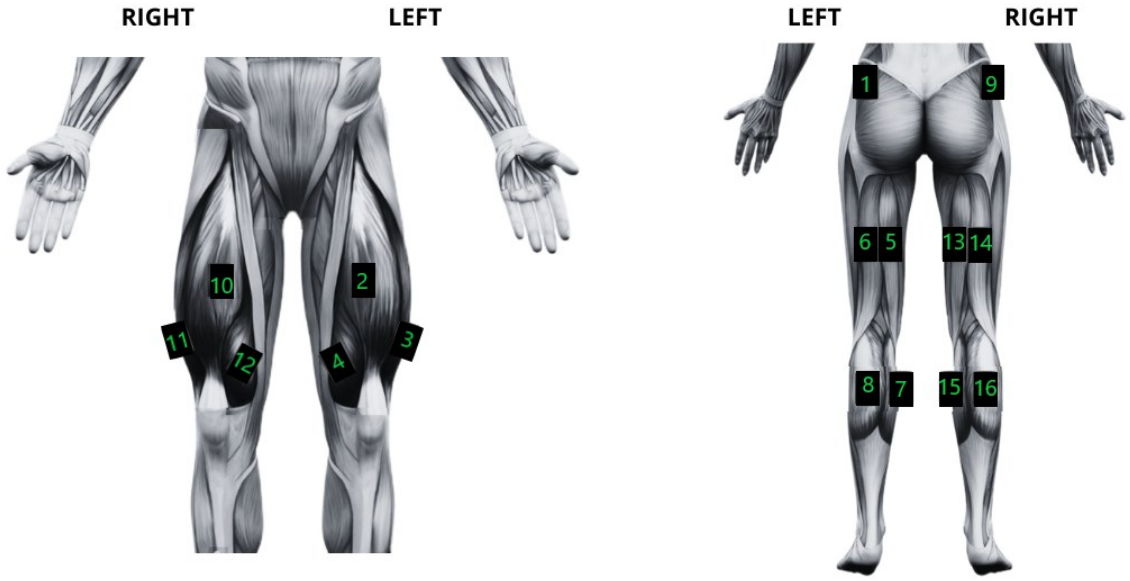

Figure A 9.1: EMG electrode placement

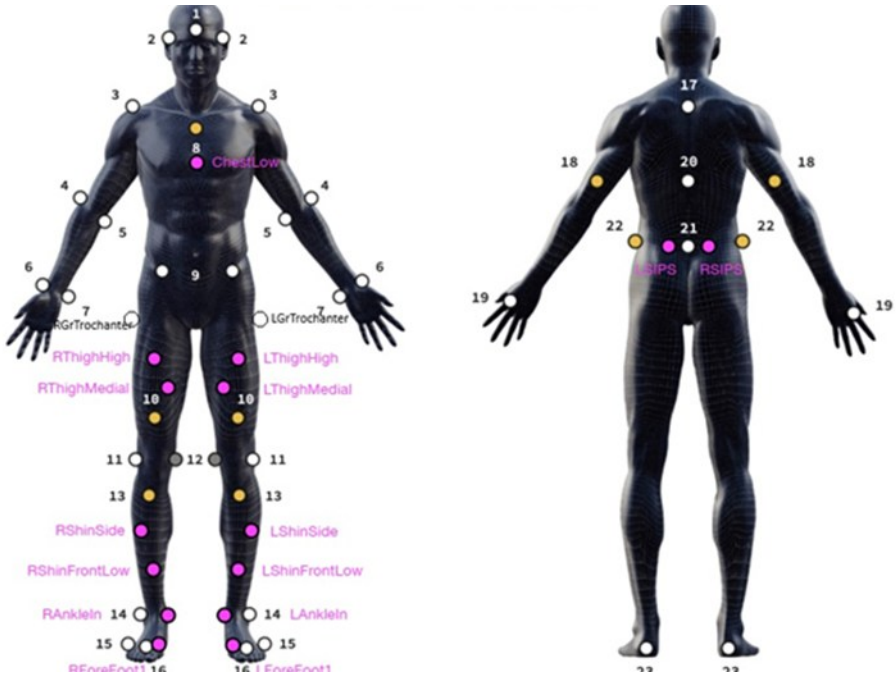

Figure A 9.2: Reflective Marker Placement for Motion Capture

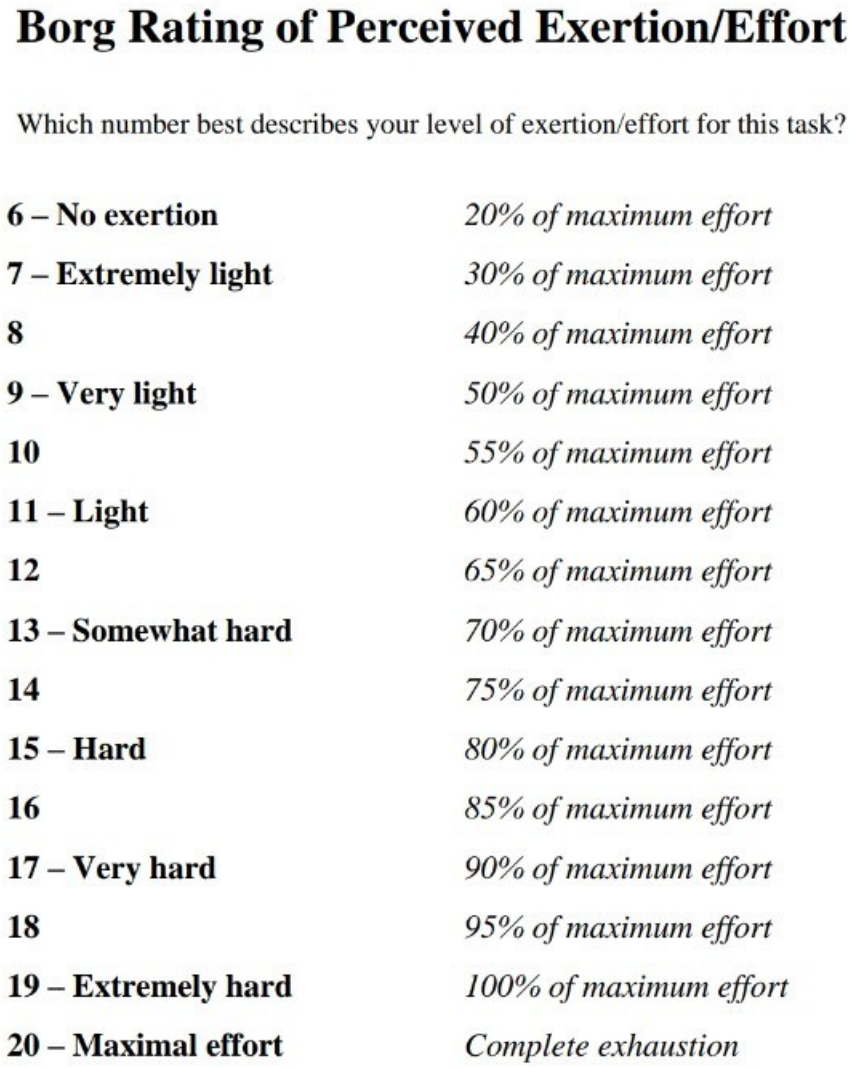

Borg Rating of Perceived Exertion/Effort

Which number best describes your level of exertion/effort for this task?

6 – No exertion	*20% of maximum effort*
7 – Extremely light	*30% of maximum effort*
8	*40% of maximum effort*
9 – Very light	*50% of maximum effort*
10	*55% of maximum effort*
11 – Light	*60% of maximum effort*
12	*65% of maximum effort*
13 – Somewhat hard	*70% of maximum effort*
14	*75% of maximum effort*
15 – Hard	*80% of maximum effort*
16	*85% of maximum effort*
17 – Very hard	*90% of maximum effort*
18	*95% of maximum effort*
19 – Extremely hard	*100% of maximum effort*
20 – Maximal effort	*Complete exhaustion*

Figure A 9.3: Borg scale

Table A 9.1: Participant Running speeds for the visit 2 protocal

Participant	Speed (km/h)
P005	13.5
P006	10.0
P007	10.0
P009	10.5
P011	10.0
P012	12.0
P019	11.5

Swedish version of the Consent form

Betydelsen av funktionell kapacitet, biomekanik och rörelsemönster efter knäskada.

Samtycke till att delta i projektet

Jag har fått muntlig och/eller skriftlig information om studien "Betydelsen av funktionell kapacitet, biomekanik och rörelsemönster efter knäskada" och har haft möjlighet att ställa frågor. Om jag har ytterligare frågor vet jag att jag när som helst kan kontakta de personer som leder studien. Jag förstår hur min medverkan i studien kommer att gå till och bekräftar att mitt deltagande är frivilligt. Jag vet att jag när som helst kan avbryta mitt deltagande i studien utan att ange något skäl. Jag får behålla den skriftliga informationen.

Jag är medveten om att resultaten av studien kommer att publiceras, men att inga data kommer att kunna härledas till min person samt att allt material kommer att bearbetas och förvaras på ett betryggande sätt, allt enligt gällande lagstiftning.

Jag samtycker till att delta i projektet "Betydelsen av funktionell kapacitet, biomekanik och rörelsemönster efter knäskada".

☐ Ja ☐ Nej

English version of the Consent form

The importance of functional capacity, biomechanics and movement patterns after knee injury.

Consent to participate in the project

I have received verbal and/or written information about the study 'The role of functional capacity, biomechanics and movement patterns after knee injury' and have had the opportunity to ask questions. If I have any further questions, I know that I can contact the people conducting the study at any time. I understand how my participation in the study will work and confirm that my participation is voluntary. I know that I can withdraw from the study at any time without giving any reason. I may keep the written information.

I am aware that the results of the study will be published, but that no data will be attributable to me and that all material will be processed and stored in a secure manner, in accordance with current legislation.

I consent to participate in the project " The importance of functional capacity, biomechanics and movement patterns after knee injury.".

☐ Yes ☐ No

Data Collection Form

All data acquisition procedures were documented using the Data Collection Form (Data Collection Form_En_07NOV2024), provided as a separate supplementary file.

Computational Resources

All configuration files used in this thesis (OpenSim tool setup XMLs and related assets) are available in a public repository: OpenSim Configs for Thesis Reproduction. Analyses were performed using OpenSim 3.3 and MATLAB R2023b. The repository contains the exact XML files used and a checksum manifest for integrity verification.